Photo-induced Activation of Metal Complexes in Living Cells for Photodynamic Therapy (PDT) and Photo-activated Chemotherapy (PACT)

Dissertation

zur

Erlangung der naturwissenschaftlichen Doktorwürde

(Dr. sc. nat.)

vorgelegt der

Mathematisch-naturwissenschaftlichen Fakultät

der

Universität Zürich

von

Pierroz Vanessa

aus

Martigny-Combe VS

Promotionskomitee

Prof. Dr. Gilles Gasser (Vorsitz, Leitung der Dissertation)

PD. Dr. Stefano Ferrari (Leitung der Dissertation)

Prof. Dr. Massimo Lopes

Prof. Dr. Bruno Therrien

Zürich, 2015

ALWAYS LAUGH WHEN YOU CAN. IT IS CHEAP MEDICINE.

Lord Byron

TABLE OF CONTENTS

Acknowledgments

I am extremely grateful to my supervisors Prof. Gilles Gasser and PD Stefano Ferrari for the opportunity to work on such rewarding projects, their supervision and constant guiding through the last 4 years and helping me to develop my scientific skills and mind. I wish to thank all my committee members for their invaluable time and advices during the course of my thesis to ensure I was heading to the right direction.

A special thanks to the incomparable technical, scientific and friendly support from all the Institute of Molecular Cancer Research members, especially Farah, Odette and Ippa, who made our work so easier.

A big thanks to all the past and current members of the Gasser group. I will for sure miss the lab's improvised summer night barbecues, Christmas dinners, weekly cakes and papers celebration. My sincere gratitude goes to my friends Tanmaya, Malay, Anna, Cristina, Philipp and Riccardo with who I was daily interacting and whose work made mine possible.

My sincere apologies go to the members of the Ferrari lab, who had to bear with me daily and sometimes with my craziness. A special wink to Giuseppe that on a whim, accompanied me to a phenomenal and memorable USA trip. To him and Murat, who followed me in the emptiness of the sky for an unforgettable skydiving jump in Germany. To Serena, who simply by saying my name put me back in the right track. On daily bases, thanks to all of the Ferrari members for listening to my complains, stories and to your scientific inputs and constant support in the lab or around Italian or Turkish coffee. A special thank to Christiane that I consider as my mentor.

A special thought to inspiring people; Tanmaya, Malay and Tamara.

You all made my stay memorable and fulfilling.

Last but for sure not least, I would like to acknowledge my parent, relatives and friends who always believed in me and were truly supportive, especially in the last months were my presence was missing.

Summary

Elaboration of new generations of more effective and safer metal-based anticancer agents, has been stimulated by the severe side effects encountered by patients undergoing chemotherapeutic treatments. In this search, ruthenium complexes have shown encouraging potential, demonstrating a wide antiproliferative profile against cancer cells. Seminal studies conducted in our labs have resulted in the development of ruthenium(II)-based new anticancer agents, which showed distinct cytotoxicity mechanisms.

First, a substitutionally-inert bis(dppz)-Ru(II) complex has been synthetized that impairs the mitochondrial membrane potential of cells leading to apoptosis. A follow-up structure-activity relationship analysis investigating the impact of lipophilicity, charge and size-based modification revealed the presence of carboxylic acid functionality as indispensable to confer cytotoxicity to the Ru(II) complex. This complex was successfully inactivated by protecting the carboxylate functionality with a photolabile protecting group. The anticancer activity could be regained by UV-A irradiation (2.58 J/cm^2).

Second, a seemingly harmless ruthenium(II) complex was prepared. It targets the cell nucleus and causes significant damage to DNA, such as single-strand breaks (SSBs) and purines oxidation upon UV-A irradiation (1.29 J/cm^2). After 24 h, double-strand breaks (DSBs) are also created that lead overall to cell death.

Collectively, these findings are an important progress towards developing a new class of metal-based anticancer agents, which have the potential to overcome the drawbacks of the current platinum-based drugs.

Zusammenfassung

Die Ausarbeitung einer neuen Generation von effizienteren und sichereren Antikrebswirkstoffen auf Metallbasis wurde von den starken Nebenwirkungen, die Patienten erleiden, welche mit Medikamenten auf Platinbasis behandelt werden, angeregt. In dieser Suche haben sich Rutheniumkomplexe durch ihr grosses Potential hervorgetan und ein weites Spektrum an antiproliferativer Wirkung auf Krebszellen gezeigt. Bahnbrechende Studien unseres Labors haben zur Entwicklung von neuartigen, auf Ruthenium(II) basierenden Antikrebsmitteln geführt, welche ausgeprägte zytotoxische Mechanismen aufweisen, sobald sie durch Licht aktiviert wurden.

Als erstes wurde ein substitutionell-inerter bis(dppz)-Ru(II) Komplex synthetisiert, welcher auf Mitochondrien abzielt und deren Membranpotential beeinträchtigt, was zur Apoptose führt. Eine darauf folgende Struktur-Aktivitätsanalyse, welche die Auswirkung von Lipophilie, Ladung und Grössenmodifikation untersuchte, hat gezeigt, dass das Vorhandensein einer funktionellen Carbonsäure unabdingbar für eine zytotoxische Wirkung des Ru(II) Komplexes ist. Dieser Komplex konnte inaktiviert werden durch das Verdecken des funktionellen Carboxylats mit einer photolabilen Schutzgruppe, wobei die Antikrebswirkung durch Bestrahlung mit UV-A (2.58 J/cm^2) wiederhergestellt werden konnte.

Als zweites wurde ein scheinbar harmloser Ruthenium(II) Komplex konstruiert, welcher den Zellnukleus zum Ziel hat, wo er, nach erfolgter UV-A Bestrahlung (1.29 J/cm^2), signifikanten Schaden an der DNS anrichtet, beispielsweise *"single-strand breaks"* und Purinoxidation. Nach 24h entstehen zusätzlich DNS *"double-strand breaks"*, was schliesslich zum Zelltod führt.

Zusammenfassend sind diese Erkenntnisse ein wichtiger Schritt in Richtung einer neuen Klasse von Antikrebsmitteln auf Metallbasis, welche das Potential haben, die Nachteile der derzeitigen Medikamente auf Platinbasis zu überwinden.

1. Introduction

An overview about the effects of cisplatin on DNA and how cells cope with DNA damages: repair and resistance mechanisms; and highlight on the use of Ruthenium complexes in phototherapy.

1.1. CISPLATIN

1.1.1. SERENDIPITOUS DISCOVERY

The accidental discovery made by Rosenberg and colleagues in the 1960s, that the reaction product of a platinum electrode and ammonium chloride, cisplatin (Figure 1), was able to halt bacterial cell division, revolutionized few years later the field of cancer treatment.[1, 2] While severe side effects encountered by patients almost stopped clinical trials in phase I, the stunning amount of partial and complete remissions reported on patients who previously exhausted all possible treatments in phase I and *inter alia* on early testicular cancer in phase II, led to drug approval in 1978.[3] Cisplatin has a potent effect on treating several types of solid cancers, among which feature testes, ovaries, bladder, head and neck, lung and breast.[4-6] Although actions have been taken to tackle the most common side effects (e.g. anti-nausea drugs and hydration to take care of the kidney),[3, 7] cisplatin treatment remains aggressive for most of the tissues.[8-10] The main goal of anticancer research is now two-pronged: overcoming side effects (i.e. carboplatin)[11, 12] and preventing resistance (i.e. oxaliplatin on colorectal cancer) (structures in Figure 1).[12, 13] Combination therapies are frequently used, but research towards other metal complexes is also ongoing.

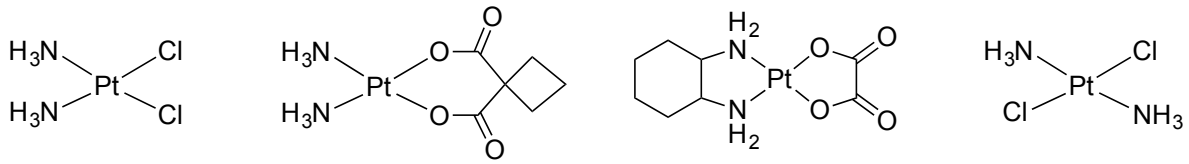

Figure 1. Structures of cisplatin and platinum derivatives.

1.1.2. MECHANISM OF ACTION AND REPAIR: FOCUS ON DNA INTERACTION

A lot of efforts have been invested in order to clearly understand the mechanism of action of cisplatin. Even if the DNA is the undeniable major target of the drug, effects have been reported on protein or mitochondrial function for example.[14, 15] By itself, cisplatin is a neutral compound. To interact with DNA, cisplatin follows spontaneous aquation in cells, corresponding to the replacement of cis-chloro groups with water molecules. The mono- and bi-activated forms are both reactive with purine at position

N7, leading to the formation of DNA-protein crosslink as well as inter-strand and intra-strand DNA crosslinks (Figure 2).[16] However only bi-adduct are responsible for toxicity, since transplatin (Figure 1) lesions on DNA are not cytotoxic.[12]

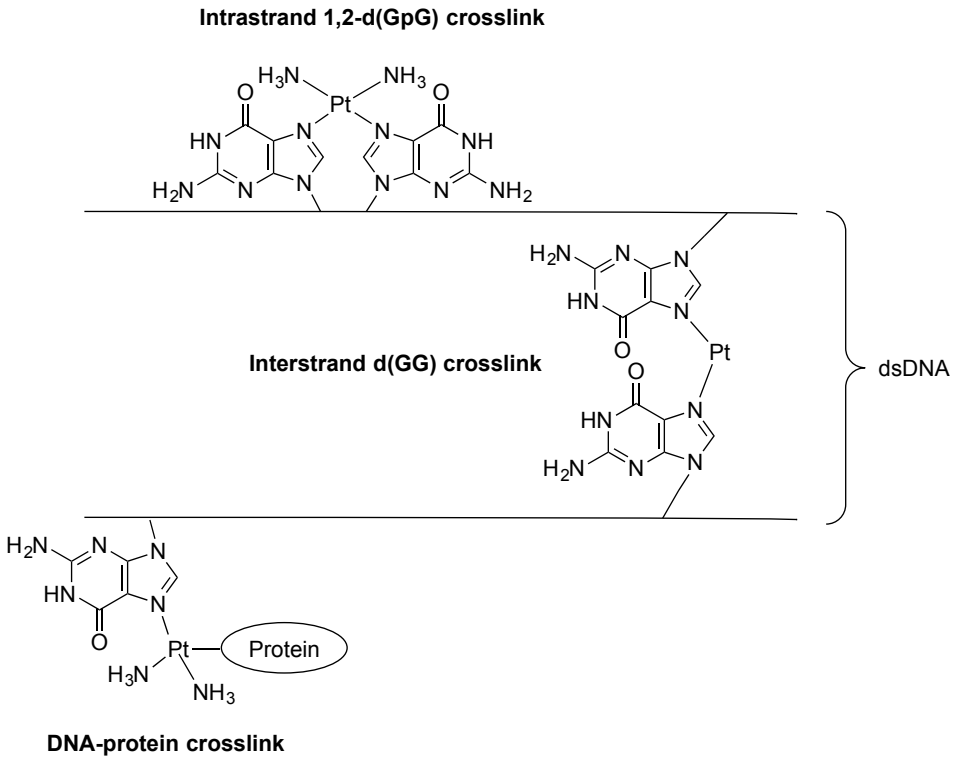

Figure 2. Majors DNA interaction of cisplatin.

Intra-strand DNA crosslinks account for about 90 % of the cisplatin-DNA crosslinks and are mainly repaired by the Nucleotide Excision Repair (NER) machinery.[17] On the other hand, the only 10% remaining inter-strand crosslinks are the most toxic ones, since covalent lesions are formed on both strands of DNA, thereby blocking replication forks.[18] They require the Fanconi Anemia (FA) and Homologous recombination (HR) pathway for repair. Repair mechanisms of cisplatin induced DNA crosslinks are detailed in chapter 1.3. Taken together, these intra- and inter-strand crosslinks represent a massive burden for the cell, in a way that overloads both repair pathways and ultimately leads to cell death.

1.1.3. MECHANISM OF RESISTANCE IN CELL

Resistance to chemotherapeutics results in an insufficiency trigger of apoptosis. The mechanisms observed to play a role in resistance, spontaneously occurring or linked

to chronic drug exposure, include (i) decreased accumulation of the drug in cells, (ii) increased efflux and (iii) increased activation of repair machinery.[12, 16]

Specifically to point (i), once injected in the blood, thiol-containing molecules, such as glutathione (GSH) or cysteinylglycine, play an important role in cisplatin resistance, as high level of metallothioneins correlates with decrease sensitivity to cisplatin. GSH acts as a redox-regulator, inhibiting the pool of the active form of the drug through thiol-conjugation.[19] Therefore, increased production of GSH or thiol-containing molecules in general, for instance by over activation of factors involved in the synthesis, will reduce the pool of functional cisplatin. Decreased accumulation of cisplatin can also arise from decreased amount of drug entering cells. Most of the drug enters the cell by passive diffusion, although a portion of cisplatin enters cells by active transport. Decreased expression of membrane transporters CTR1, reduces the portion of cisplatin.[20]

Regarding point (ii), as cofactor of the multidrug resistance protein 2 (MRP2), GSH also facilitates the efflux of cisplatin. Overexpression of MRP2 has been shown to promote cisplatin insensitivity.

Finally, regarding point (iii), overexpression of members of DNA repair machineries, leading to efficient repair (i.e., as in this case NER and HR), or inhibition of factors involved in apoptosis, such as p53,[21] Bcl members or caspases, will contribute to cell survival and hence resistance.[16]

1.1.4. RUTHENIUM COMPLEXES AS PROMISING PLATINUM SUBSTITUTES IN CANCER

In the quest for anticancer drugs with increased potency and reduced side effects, other metal complexes than platinum have been examined, with ruthenium complexes being one of the best candidates.[22, 23] While the mode of action of platinum derivatives is related to DNA targeting, Ru compounds have been reported to target different cellular organelles such as the nucleus and the mitochondria, for example. The differences in the biological activity of ruthenium compounds lie in the different coordination states and the wide range of ligands that can be coordinated to the metal centre. Ruthenium complexes differ from other metal complexes in the fact that under physiological conditions, ruthenium can reach three oxidation states, namely Ru(II), Ru(III) and Ru(IV). The oxidation potential of Ru complexes in general can be

exploited to target their activity towards cancer or infected areas. Indeed, cancer and diseased tissue in general, produce a reduced environment which is prompt to convert relatively inert Ru(III) into active Ru(II).[24] Such strategy is generally referred to as "activation by reduction". The Ru(III) complex acts therefore as prodrug. In other words, the product injected to the patient is not the active form.

Moreover, the Ru oxidation states (II) and (III) are both prone to ligand exchange. Importantly, it has been now postulated that Ru complexes are mimicking iron in binding to protein that usually bind to iron such as albumin or transferrin.[25] This phenomenon would explain why usually Ru complexes have a lower systemic toxicity compared to platinum drugs. However, it has been established that cancer cells, by continuously dividing, require more iron, and thereby, increase the expression of the transferrin receptor at their cellular membrane. The latest peculiarity will allow for a more specific delivery of the Ru complexes to cancer over healthy cells *via* transferrin transportation.

Worthy of note, two ruthenium compounds namely, NAMI-A and KP1339, are now in phase II clinical trial and a third one, RAPTA-C is proceeding towards clinical trial (structures in Figure 3).[24, 26, 27]

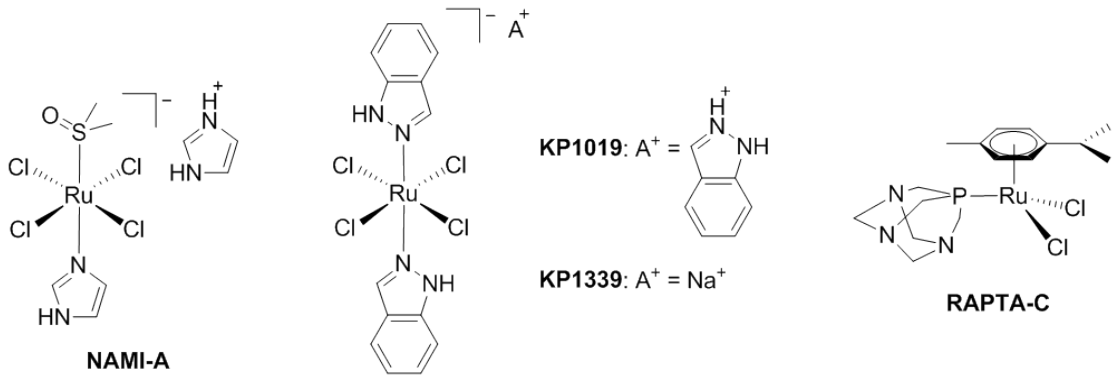

Figure 3. Structures of NAMI-A, KP1019, KP1339 and RAPTA-C.

1.2. Ru(II) complexes and light: targeted therapy

1.2.1. Aim and scope

The severe systemic side effects encountered by patients treated with cisplatin have driven the research to elaborate more targeted strategies.[21] Light-activated therapy has become an attractive strategy in the clinic since temporal and spatial control is possible. In photodynamic therapy (PDT), light, oxygen and innocuous photosensitizers (PS) are combined to produce cytotoxic reactive oxygen species (ROS), which ultimately kill nearby cells. This therapy is currently used in the clinic, especially for the treatment of skin diseases, but is more and more applied for the treatment of cancer, typically for skin, head and neck and cavity-located cancers. Among all the photosensitizers approved, only two bear a metal ion.[28] This is surprising since platinum-based anticancer compounds are the most used drugs in chemotherapy.

Another light-triggered approach using metal complexes, namely photo-activated chemotherapy (PACT), relies on different mechanisms to provoke cell death (e.g. ligand ejection, DNA crosslinking and caging approaches). The advantage of the latter technique is its oxygen independency, fundamental since the internal core of tumor are generally hypoxic.[29]

In the following perspective article, the use of Ru(II) complexes as photosensitizers and photoactivatable prodrugs in the treatment of cancer is presented.

1.2.2. Contributions to the perspective article

V.P.: wrote the Ruthenium complexes in PACT chapter of the first draft. This perspective article as been accepted for publication in *Chem. Sci.* (DOI:10.1039/C4SC03759F).

1.2.3. Perspective article: Combination of Ru(II) complexes and light new frontiers in cancer therapy[30]

Reproduced by permission of The Royal Society of Chemistry.

Chemical Science

PERSPECTIVE

View Article Online
View Journal

Cite this: DOI: 10.1039/c4sc03759f

Combination of Ru(II) complexes and light: new frontiers in cancer therapy

Cristina Mari,†[a] Vanessa Pierroz,†[ab] Stefano Ferrari[b] and Gilles Gasser*[a]

The synergistic action of light, oxygen and a photosensitizer (PS) has found applications for decades in medicine under the name of photodynamic therapy (PDT) for the treatment of skin diseases and, more recently, for the treatment of cancer. However, of the thirteen PSs currently approved for the treatment of cancer over more than 10 countries, only two contain a metal ion. This fact is rather surprising considering that nowadays around 50% of conventional chemotherapies involve the use of cisplatin and other platinum-containing drugs. In this perspective article, we review the opportunities brought by the use of Ru(II) complexes as PSs in PDT. In addition, we also present the recent achievements in the application of Ru(II) complexes in photoactivated chemotherapy (PACT). In this strategy, the presence of oxygen is not required to achieve cell toxicity. This is of significance since tumors are generally hypoxic. Importantly, this perspective article focuses particularly on the Ru(II) complexes for which an *in vitro* biological evaluation has been performed and the mechanism of action (partially) unveiled.

Received 4th December 2014
Accepted 13th January 2015

DOI: 10.1039/c4sc03759f

www.rsc.org/chemicalscience

Introduction

The biological activity of ruthenium (Ru) compounds has been known for decades.[1–3] Two Ru complexes are currently in phase II clinical trials (NAMI-A and KP1339) as anticancer drug candidates and a third one, RAPTA-C, is progressing towards clinical trials (see Fig. 1 for the structures of these compounds).[4–10] The increasing interest in the biological behavior of Ru compounds is due to their appealing physicochemical properties. Among others, such complexes can have different geometries (*e.g.* tetrahedral or octahedral) allowing for the design of compounds with a specific cellular target (*e.g.* proteins). Hence, the rigid and well-defined spatial arrangement of a series of Ru complexes has enabled the preparation of highly potent and selective enzyme inhibitors. The group of Meggers has notably demonstrated such a concept with kinase inhibitors.[2,11,12] Other attractive features of Ru complexes include their generally lower systemic toxicity compared to platinum complexes and their higher cellular uptake, thanks to the specific transport of ruthenium inside cells by transferrin.[13] Of utmost importance, ruthenium complexes can easily be obtained in two oxidation states (II and III) and are prone to ligand exchange. Such properties have been found to play a pivotal role in the mode of action of both NAMI-A and KP1339.[14] Ru(III) complexes are thus prodrugs – meaning that the

[a]*Department of Chemistry, University of Zurich, Winterthurerstrasse 190, CH-8057 Zurich, Switzerland. E-mail: gilles.gasser@chem.uzh.ch; Web: http://www.gassergroup.com; Fax: +41 44 635 6803; Tel: +41 44 635 4630*
[b]*Institute of Molecular Cancer Research, University of Zurich, Winterthurerstrasse 190, CH-8057 Zurich, Switzerland*
† These authors have contributed equally to the work.

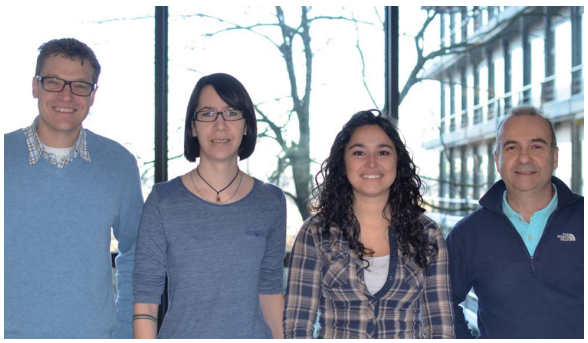

Cristina Mari (third from left) was born in Milan (Italy) where she grew up and completed her education. She obtained a Master's in Chemistry at the University of Milan in 2010, with a one year project on the functionalization of peptide nucleic acids with peptides or a rhenium dye. In 2011, she moved to the group of Prof. Gilles Gasser at the University of Zurich (Switzerland), where she is heading towards the end of her PhD. Her current research focuses on the investigation of new DNA intercalating photoactivatable ruthenium complexes as anticancer drug candidates.

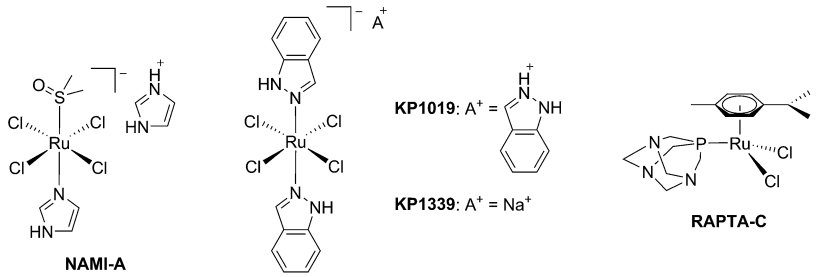

Fig. 1 Structures of NAMI-A, KP1339, KP1019 and RAPTA-C.

compound which is administered to the patient is not the active species. Ru(III) complexes are reduced into a more active Ru(II) form when localized in an hypoxic environment, which is a property characteristic of tumors.[6] This phenomenon is normally referred to as "activation by reduction" and was also exploited for the *in situ* activation of Pt-based anticancer drug candidates, like satraplatin.[15]

Nowadays, the use of the "prodrug approach" is very appealing to reduce the systemic toxicity of a drug candidate.[16] In order to activate the prodrugs, two different kinds of stimuli can be employed, namely an internal stimulus (reducing cellular conditions, hypoxia, enzymatic reactions, *etc.*) or an external stimulus (magnetic field, temperature, light, *etc.*). The first approach, however, presents a significant disadvantage, in that it completely relies on intracellular parameters. In other words, once the prodrug is injected into the patient, physicians have no more control over the fate of the compound. On the contrary, this is exactly the kind of control that can be achieved using an external stimulus. The latter indeed provides complete *spatial and temporal control* over the generation of the toxic molecule. As of today, the most commonly applied technique to induce the formation of active species is *via* light irradiation.[15,17,18]

The light-mediated activation of prodrugs in the field of anticancer research can be generally divided into two categories: photodynamic therapy (PDT) and photoactivated chemotherapy (PACT). PDT relies mainly on the generation of the toxic reactive oxygen species (ROS) singlet oxygen ($^1O_2$). On the other hand, PACT exploits different mechanisms to induce cell death such as ligand ejection, DNA crosslinking and caging approaches. In this perspective article, we intend to give an overview of recent progress in the application of ruthenium

Vanessa Pierroz (second from left) was born and completed her whole education in Switzerland. After completion of her matriculation examination in Saint-Maurice in 2006, she studied biology at the University of Lausanne (Switzerland). After obtaining her Bachelor's degree in biology in 2009, she undertook a Master's in medical biology at the same institution. During these studies, she first completed a pre-Master thesis, under the supervision of Dr Benjamin Boutrel at the Centre of Psychiatric Neurosciences, where she investigated the interindividual vulnerability to develop alcohol abuse in rats. Afterwards, she joined the laboratories of Dr Pascal Schneider at the Department of Biochemistry to perform her Master's thesis, investigating the proteolytic maturation of Tumor Necrosis Factors (TNF) family members. She obtained her Master's degree in 2011. She then moved to Zurich to start her PhD thesis in the groups of Prof. Gilles Gasser and PD Dr Stefano Ferrari, where she is studying the photo-activation of metallodrugs in living cells.

Stefano Ferrari (fourth from left) was born in Trento (Italy) and completed his undergraduate studies in Biology at the Universities of Padua (Italy) and Dundee (Scotland). He received his PhD in Biochemistry from the University of Padua in 1988. After a post-doctoral stage with Prof. George Thomas at the Friedrich Miescher Institute in Basel (Switzerland), he took up a Junior Group Leader position at the Institute of Experimental Cancer Research of the University of Freiburg (Germany) and subsequently a Program-Team Head position at the Department of Oncology of Novartis, Basel (Switzerland). Since 2001 he is a lecturer at the Institute of Molecular Cancer Research of the University of Zurich. Over the years, Stefano's studies have addressed the role of signaling in cell growth and proliferation as well as in the control of cell cycle transitions.

Gilles Gasser (first from left) was born, raised and educated in Switzerland. He received his PhD thesis from the University of Neuchâtel in 2004 after working in the group of Prof. Helen Stoeckli-Evans. After post-doctoral stays at Monash University (Australia) with Prof. Leone Spiccia and at the Ruhr-University Bochum (Germany) with Prof. Nils Metzler-Nolte, Gilles started his independent career at the Department of Chemistry of the University of Zurich (Switzerland) first as a Swiss National Science Foundation (SNSF) Ambizione fellow and then, since 2011, as a SNSF Assistant Professor. Over his career, Gilles has been the recipient of several awards including a SNSF fellowship for prospective researchers, an Alexander von Humboldt fellowship (2007) and the Werner Prize from the Swiss Chemical Society (2015). Gilles's group is currently working on several topics which all involve the use of metal complexes in a medicinal or chemical biology context.

complexes in both PDT and PACT, focusing particularly on those compounds for which an *in vitro* evaluation of the biological activity has been performed and the mechanism of action (partially) unveiled. Notably, these topics have been partially reviewed in the past but an article covering all subjects is, to the best of our knowledge, currently missing.[17–26]

Ruthenium complexes as photosensitizers in PDT

Photodynamic therapy is an approved medical technique, which is applied in dermatology for the treatment of several diseases such as acne or psoriasis and in ophthalmology for age-related macular degeneration. Since relatively recently, this technique has been used for the treatment of some types of cancer. For example, Photofrin® (Fig. 2), the only FDA-approved PDT drug, is employed to treat esophageal and non-small cell lung cancers. In the UK, on the other hand, there are several photoactive agents which are clinically approved (*i.e.* Foscan®, Fig. 2) to treat a wide range of cancer types, from skin to internal organs.[27,28]

More specifically, PDT relies on the synergistic activity of an ideally non-toxic molecule called a photosensitizer (PS), light and molecular oxygen. The PS is administrated to the patient either locally or systemically. Upon light irradiation at a wavelength in its range of absorption, the PS is able to reach its singlet excited state ^{1}PS* (Fig. 3). Very importantly, the PS must then undergo an intersystem crossing (ISC) so that the excited state has a triplet character (^{3}PS*). At this point, PDT relies on two different mechanisms called Type I and Type II. A Type I reaction consists of an electron or proton transfer from the triplet excited state of the PS to the surrounding biological substrates (or the other way around). This leads to the formation of radicals that can further interact with molecular oxygen to form ROS such as superoxide, hydroxyl radicals or peroxides. At the same time, an energy transfer from the triplet excited state of the PS to molecular oxygen in its ground triplet state ($^3O_2$) can occur (a Type II reaction). In this case, singlet oxygen ($^1O_2$) is generated. $^1O_2$ is a very reactive form of oxygen with an estimated half life of 40 ns in a biological environment.[27] Consequently, it will rapidly react just with the surrounding biomolecules, generating topical cellular damage that can ultimately lead to cell death. PSs which are nowadays applied in clinics mainly rely on the Type II mechanism of action.[29]

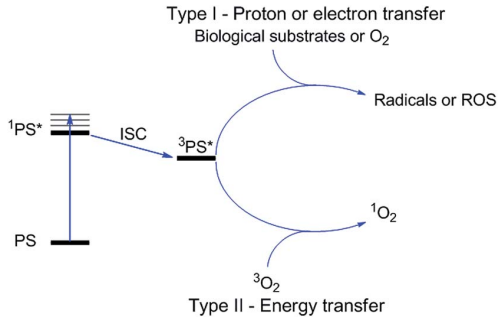

Fig. 3 Mechanisms of action of PDT.

PDT is a very appealing medical technique due to its intrinsic selectivity. The toxic species are generated just at the site of light irradiation, with complete spatial and temporal control. Furthermore, due to the very fast reactivity of $^1O_2$, damage is limited to the irradiated areas. The outcomes of PDT treatment depend on the performance of the PS but also on other very important factors (*e.g.* the light component, the *in vivo* dosimetry or the oxygen tension). To be clinically applicable, a PS should, among other requirements, (i) localize mainly (ideally only) in cancer cells; (ii) should be non-toxic in the absence of light, while displaying strong phototoxicity. This behavior is normally described by the so-called phototoxic index (PI), defined for a compound as the ratio of its IC_{50} in the dark to its IC_{50} upon light irradiation. Finally, the PS (iii) should be excited in the red or near-IR region of the spectrum (>600 nm). This last requirement is very important to avoid cytotoxicity deriving from high energy light irradiation. In addition, the use of long wavelength light allows for a deeper penetration through the human tissues.[21,30]

The great majority of PSs that are currently applied in clinics are based on a cyclic tetrapyrrolic scaffold. The photophysical and biological characteristics of porphyrins, phthalocyanines and chlorins match the requirements for a PDT agent relatively well. On the other hand, their performances are also limited by important side-effects. As an example, treatment with Photofrin® results in light sensitivity for several weeks due to slow clearance of the drug from the body.[31] As a consequence, an

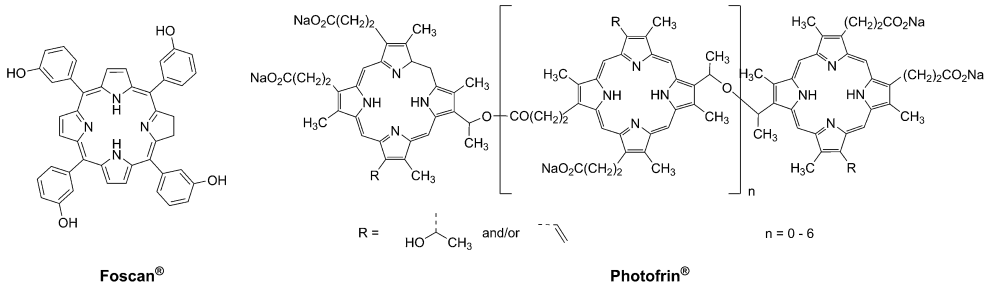

Fig. 2 Structures of porphyrin-based approved PDT agents.

important effort has been undertaken to improve the performances of the current PSs following two approaches: the modification of a conventional porphyrin-based PS or the optimization of entirely new systems that can outperform porphyrins in their PDT activity. In this specific section, we present a description of the influence of the insertion of ruthenium fragments into porphyrin-based PSs, focusing our attention on the works that report on the biological behavior of these new systems. Furthermore, we present the recent achievements in the use of ruthenium polypyridyl complexes as novel PSs in the innovative attempt to move away from the traditional porphyrin-as-PS paradigm.

Ruthenium-containing porphyrin PSs

The derivatization of the porphyrin core with metal complexes is an appealing opportunity to improve the activity of a PS. This functionalization was exploited for the first time fifteen years ago by Brunner and coworkers.[32,33] They synthesized hematoporphyrin–platinum conjugates to combine the strong anticancer activity of platinum-based drugs with the phototoxic effect of porphyrins. The metal derivatization of a porphyrin core can enhance the intrinsic properties of a PS by modifying its physico-chemical characteristics. For example, the metal fragment can change the lipophilicity of the PS, increase its water solubility or improve its cellular uptake. As mentioned above, ruthenium complexes display very promising biological behavior. Consequently, several research groups have recently evaluated the possibility of introducing Ru(II) moieties on the periphery of porphyrins. For instance, Therrien *et al.* synthesized a wide range of Ru-modified porphyrin systems and studied their biological performances.[34] More specifically, they appended a number of Ru-arene fragments to the *meso*-4′-tetrapyridylporphyrin scaffold to evaluate the influence of the different aromatic moieties (**1a–e**, Fig. 4, top). All the compounds were found to induce 60–80% mortality in human Me300 melanoma cells at a 10 μM concentration, using light at 652 nm with a dose of 5 J cm^{-2}. The photoactivity of the metal-functionalized systems was found to be independent of the nature of the arene. This flexibility can give access to the use of arenes which are derivatized with targeting agents or chemotherapeutic compounds. Fig. 5, which shows the phototoxicity evaluation of the compounds synthesized by Therrien *et al.*, demonstrates that the improved behavior of their systems required the presence of the Ru fragment, since the Rh analog **3** was not internalized by cells and was therefore not toxic. In addition, the Os derivative **2** exerted just a weak phototoxic effect (see Fig. 4 for the structures of the latter compounds).

The same authors also studied the influence of tetra- *vs.* mono-metallic derivatization (**4a-b**/**6a–b** *vs.* **5a–b**/**7a–b**, Fig. 6),

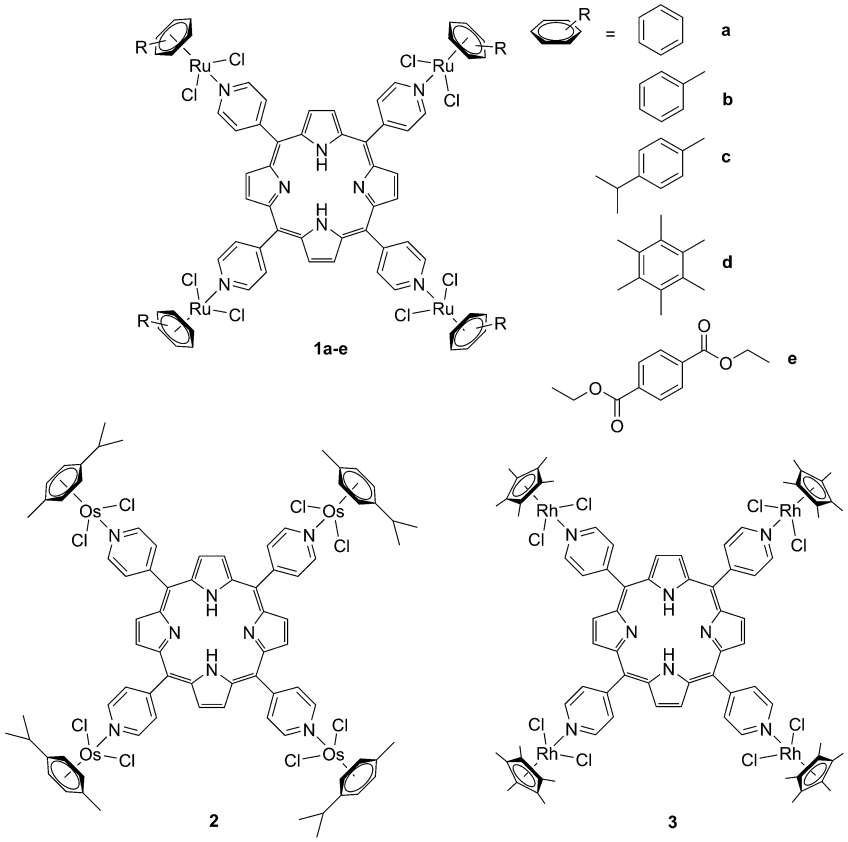

Fig. 4 Structures of Ru–porphyrin conjugates (top, **1a–e**), and Os and Rh analogs (bottom, **2** and **3**).[34]

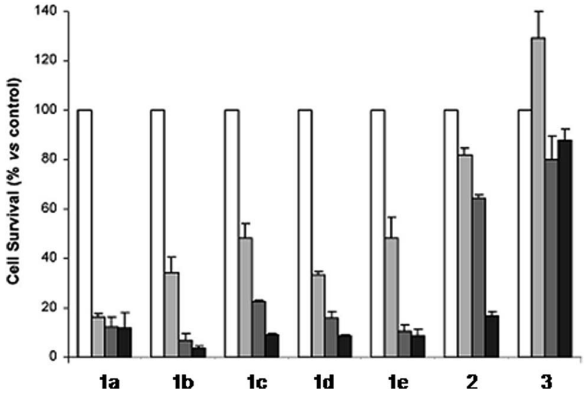

Fig. 5 Phototoxicity evaluation of compounds **1a–e**, **2** and **3** on Me300 melanoma cells. Cells were incubated with 10 μM of the compounds, incubated for 24 h, then irradiated at 652 nm with 0 J cm^{-2} (white bar), 5 J cm^{-2} (light grey bar), 15 J cm^{-2} (dark grey bar) or 30 J cm^{-2} (black bar) light doses. Adapted with permission from ref. 34. Copyright 2008 American Chemical Society.

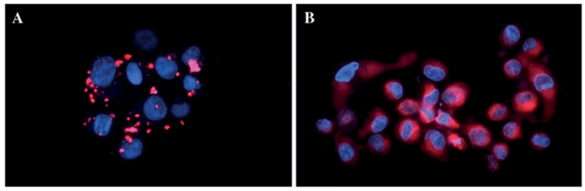

Fig. 7 Fluorescence microscopy images of human Me300 melanoma cells incubated for 24 h with 5 μM of **4a** (A) and **6a** (B), displaying red luminescence. The blue luminescence in the nuclei derives from DAPI co-staining. With kind permission from Springer Science and Business Media.[35]

as well as the nature of the pyridylporphyrin isomers, by comparing 4′-pyridylporphyrin or 3′-pyridylporphyrin derivatives (**4a–b**/**5a–b** *vs.* **6a–b**/**7a–b**, Fig. 6).[35] Several conclusions could be drawn from this small structure–activity relationship (SAR) study. For example, the type of pyridylporphyrin isomer was shown to play a major role in the observed activity, since the 3′-pyridyl substituted compounds showed a greater phototoxic effect than the 4′-pyridyl analogs. On the other hand, the number of Ru atoms or the arene derivatization seemed to have less influence on the biological activity.

In more detail, upon the 652 nm light irradiation of human Me300 melanoma cells, a LD_{50} of 5 μM was reached with a light dose of 0.5 J cm^{-2} for compounds **6a** and **6b** and with a light dose of 2.5 J cm^{-2} for **7a** and **7b**. For the 4-pyridyl derivatives, 5 or even 10 J cm^{-2} were necessary to achieve the same potency. This difference in biological activity was explained by luminescence microscopy studies, where **4a** (more hydrophobic) was shown to form aggregates inside the cytoplasm (Fig. 7A), although the authors did not discuss further about accumulation in a specific organelle. This aggregation could lead to a quenching of the ROS production. On the contrary, compound

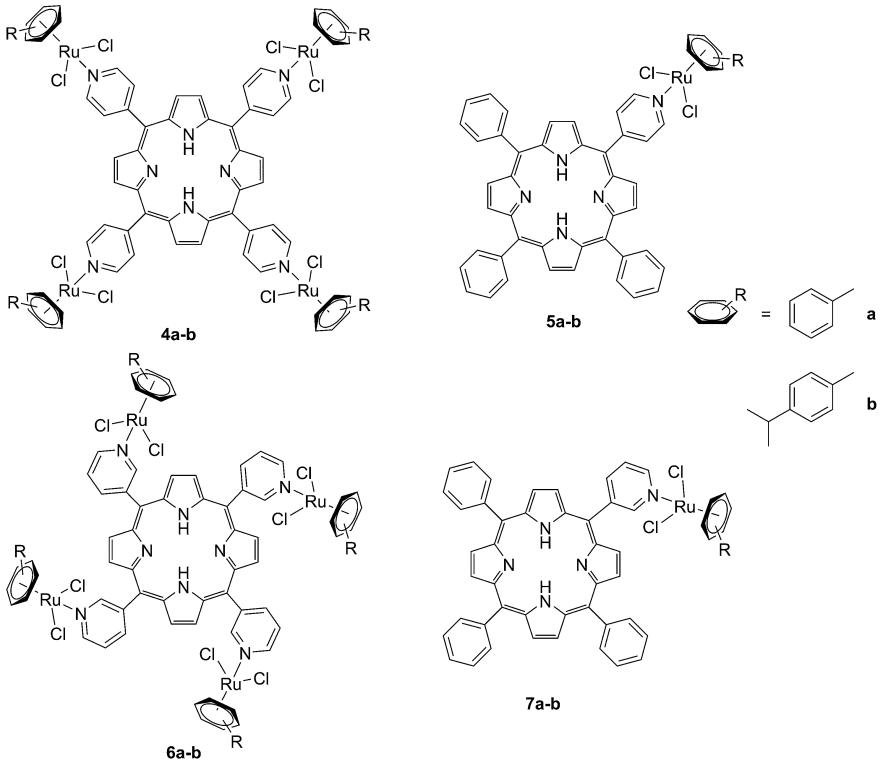

Fig. 6 Structures of the Ru–porphyrin conjugates evaluated in the SAR study by Schmitt *et al.*[35]

6a was shown to be evenly distributed in the cytoplasm, where it could exert its phototoxic activity (Fig. 7B).

The two best compounds in this study, namely [Ru(η^6-*p*-^{i}PrC$_6$H$_4$Me)(PMP)Cl$_2$] (PMP = 5-(3-pyridyl)-10,15,20-triphenylporphyrin) and [Ru$_4$(η^6-*p*-^{i}PrC$_6$H$_4$Me)$_4$(PTP)Cl$_8$] (PTP = 5,10,15,20-tetra(3-pyridyl)porphyrin) (**6b** and **7b**) were evaluated *in vivo* on nude mice xenografted with human head and neck carcinoma KB cells.[36] Since PDT is a synergistic cooperation of different components (PS, light and O_2), the evaluation of its *in vivo* efficacy depends on the combination of a complex system of parameters, which reciprocally affect each other. As a consequence, the authors determined that crucial factors to be optimized during *in vivo* studies were not just the concentration of the drug, but also the interval between PS administration and light treatment (the drug-light interval, DLI), light fluence and the fluence rate.[36] They therefore adopted a statistical approach to find the combination of parameters that would yield the best therapeutic outcomes, thereby reducing as much as possible the number of required experiments. The study showed that, if PS concentration and light fluence were not crucial parameters, a long DLI and the use of the tetranuclear species led to statistically significant tumor growth stabilization up to at least 30 days.

Since the study on these systems highlighted that the number of ruthenium modifications is correlated with an increase in phototoxicity, the authors synthesized two cationic octanuclear metalla-cubes **8** and **9** (Fig. 8). These compounds, thanks to their higher ruthenium content, showed better activities when compared to their tetranuclear analogs.[37] An LD_{50} of 1 μM was reached upon irradiation with 652 nm light and a 2–7 J cm^{-2} light dose for both compounds, whereas for the tetranuclear analogs, a light dose of 5–10 J cm^{-2} at the same wavelength resulted in a LD_{50} of 5 μM.

Another interesting approach used by this group for the combination of Ru complexes and PDT is the application of Ru-cages as carriers for porphyrin photosensitizers inside cancer cells. The authors developed the two cages presented in Fig. 9, namely hexa- (**10**) and octanuclear (**11**), which were characterized by different mechanisms of release.[38] In the case

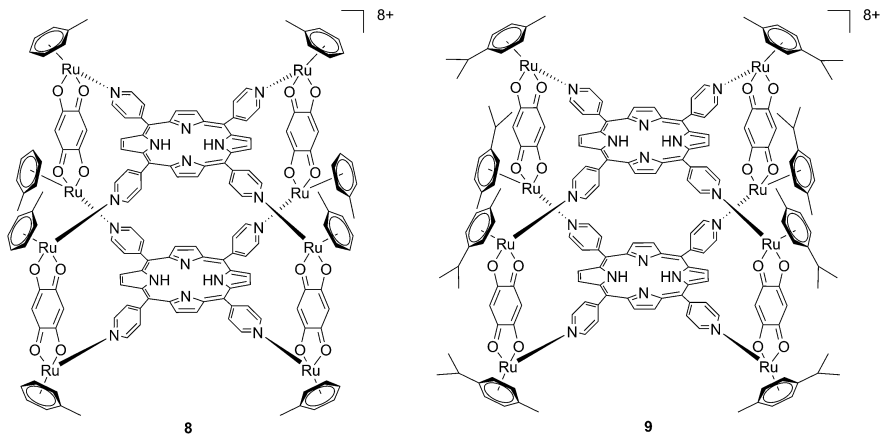

Fig. 8 Polynuclear metalla-cubes **8** and **9** synthesized by Therrien to increase phototoxicity.[37]

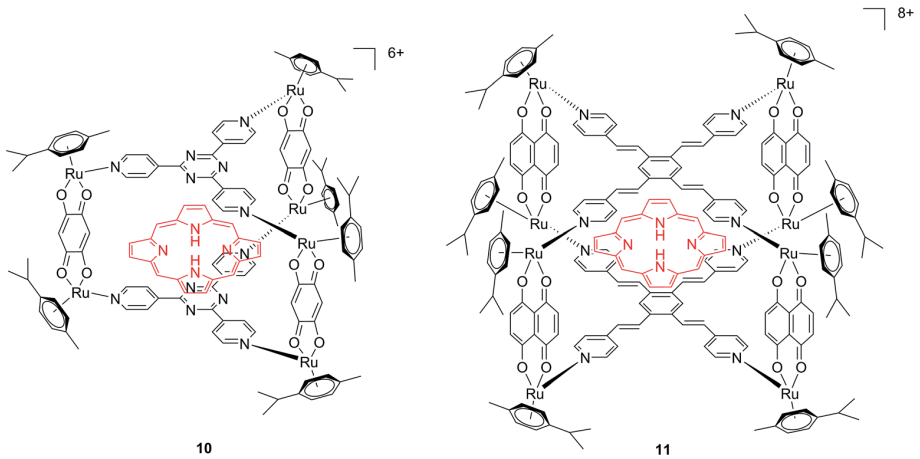

Fig. 9 Ruthenium cages **10** and **11** applied as carriers of a porphyrin PS inside cancer cells.[38]

of **10**, the cage must be disrupted to allow the release of the PS, whereas for **11**, the PS can diffuse through the sides of the cage. As a consequence of this difference, **11** was found to be 10 times more photoactive than **10**. The authors obtained phototoxicity in the submicromolar range and a PI of about 20 for **11** on cervical cancer HeLa cells, upon irradiation at 455 nm with an impressively weak light dose (0.2 J cm^{-2}). This result demonstrated the release of the porphyrin after cellular internalization, as was also shown by luminescence microscopy (Fig. 10). In these pictures, it is possible to notice the red luminescence from the free PS and the blue emission originating from the empty cage. This also indicates that the two systems are localizing in different cellular compartments after release. Furthermore, the internalization of the porphyrin in both cages resulted in a hypochromic effect on the porphyrin. This means that when the PS is trapped, its emission is dramatically reduced and consequently also the phototoxic effect. This phenomenon leads to a safe delivering agent that does not display undesired phototoxicity outside of cells.

With the same idea in mind, namely to obtain a synergistic biological effect owing to the conjugation of porphyrin and ruthenium fragments, Alessio and coworkers synthesized a library of compounds where *meso*-tetraphenylporphyrin or *meso*-4′-tetrapyridylporphyrin cores were modified on their peripheries with Ru complexes.[39] The authors then selected five cationic species for biological evaluation.[40] The most active compounds **13** and **14** (Fig. 11) contain four ruthenium moieties and their coordination sphere is a slight modification of the $[Ru([9]aneS_3)(en)Cl]^+$ complex (**12**, Fig. 11, top left, $[9]aneS_3$ = 1,4,7-trithiacyclononane, en = ethylenediamine), which was already shown by the same group to be characterized by a strong cytotoxicity.[41,42]

As expected, the ruthenium fragments strongly improved the physicochemical behavior of the porphyrin core. This resulted in a clear increase in cytotoxicity of the compounds, most likely, as speculated by the authors, due to higher cellular accumulation. Furthermore, the potency of the systems in human breast cancer cells MDA-MB-231 was improved by one order of magnitude upon exposure to 5 J cm^{-2} of 590–700 nm light, thus reaching the nanomolar range. Following the same strategy, Swavey *et al.* explored a range of possible modifications of porphyrins to improve their activity and selectivity.[43] In particular, they introduced a $Ru(bipy)_2$ moiety (bipy = 2,2′-bipyridine) with a labile Cl ligand to obtain additional DNA binding and light-induced DNA cleavage. Two pentafluoroaryl groups, which are known to increase the excited state lifetime of a PS, were also linked to the porphyrin, to give compound **15** (Fig. 12, left). The authors obtained a very strong affinity for DNA and consequent photocleavage of plasmid supercoiled DNA. Furthermore, they demonstrated that the compound exerted a higher phototoxicity on melanoma cells when compared to normal skin fibroblast cells.

To improve the efficacy and the selectivity of their system, the same authors removed one pentafluoroaryl group and evaluated the effect of the insertion of a metal into the porphyrin ring (**16a–d**, Fig. 12, right).[44] Upon coordination of a metal ion in the porphyrin, the photophysical properties of the system undergo an important change due to the metal perturbing the energy levels of the free ligand. For instance, it was noticed that the complexation of Zn(II) increases the lifetime of the excited state of the porphyrin.[19] In this work, they demonstrated that all three metal-coordinated systems were able to nick plasmid DNA upon induction with light, with the Zn(II) system **16d** also generating double strand breaks. In cellular studies, Ni(II) and Cu(II)–porphyrins were inactive as photosensitizers. On the other hand, the Zn(II) system at a concentration of 5 μM induced cell death very efficiently on a melanoma cell line upon white light irradiation (Fig. 13, bottom). Interestingly, the same treatment did not show any efficacy on normal skin fibroblast cells (Fig. 13, top), providing indications of a very selective system.

Of utmost interest, the authors performed *in vivo* studies with compound **16d** on *Drosophila melanogaster* to assess its general toxicity in the dark as well as biodistribution.[45] The compound was found to be harmless for the larvae and during their development. Cellular localization studies were also performed by feeding the larvae with the compound. Confocal microscopy revealed that the molecule was able to accumulate in the cytosol, but also in the nuclei at higher concentration. This suggests that the compound is not readily metabolized.

Another interesting class of compounds includes the coordinatively saturated ruthenium polypyridyl complexes. These compounds are known to be kinetically inert and substitutionally stable. Therefore, they do not have a labile ligand that can covalently bind DNA. Nevertheless, it was shown that, with the use of appropriate ligands such as dipyrido[3,2-*a*:2′,3′-*c*]-phenazine (dppz) or tetrapyrido[3,2-*a*:2′,3′-*c*:3″,2″-*h*:2‴,3‴-*j*]-phenazine (tpph), these complexes can interact very strongly with double-stranded DNA *via* intercalation or groove binding. Thanks to these interesting characteristics, these compounds were extensively studied as DNA intercalating probes[46,47] or as cytotoxic agents.[48–51] Furthermore, it was demonstrated that these compounds are also able to produce $^1O_2$ (see next paragraph for more information on this topic). To exploit this property, Wong and co-workers conjugated a $[Ru(bipy)_2phen]^{2+}$ (phen = 1,10-phenanthroline) moiety to a porphyrin core *via* three different linkers on the phen (Fig. 14) and evaluated the biochemical behavior of the resulting systems **17a–c**.[52] The ruthenium conjugation was also introduced here to improve the two-photons absorption (TPA) characteristics of the compounds. As a consequence, by virtue of the simultaneous absorption of two photons, the molecule can be excited at 800 nm, a more tissue penetrating and less harmful wavelength. Therefore, this interesting characteristic allows for the development of bifunctional PDT and tumor imaging agents.

Interestingly, the authors could achieve a different cellular localization based on the type of linker used to connect the porphyrin core to the ruthenium moiety. This difference allowed for studying the effects of PDT in different cellular compartments. Compounds **17a** and **17b** were characterized by the best cellular uptake, as demonstrated by flow cytometry analysis. Comparably, they also displayed the best phototoxic behavior with a toxicity of 118 and 175 μM on HeLa cells in the dark and LD_{50} of 1 μM upon yellow light irradiation with doses of 6.5 and

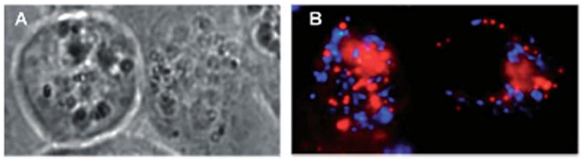

Fig. 10 Fluorescence microscopy of HeLa cells incubated with **11** (2 μM, 2 h): (A) white light and (B) fluorescence. Reprinted with permission from ref. 38. Copyright 2012 American Chemical Society.

2.0 J cm^{-2}, respectively. Compound **17b** also showed its activity as a TPA-PDT agent, causing cell shrinkage upon irradiation at 850 nm. The compound, which localized in the mitochondria before light exposure, was found to relocate in the nuclei after light irradiation. The authors therefore assumed that **17b** induced light-mediated damage to mitochondria, from which it is then released. Once in the cytosol, the compound can damage the nuclear membrane and cause cell death. Interestingly, they also showed that the presence of the Zn atom in their conjugates had a detrimental effect on the emission quantum yields of the systems in DMSO, going from values of 1.93–5.3% for the free base compounds to <1% when Zn(II) was inserted in the porphyrin ring. The authors considered this difference in the photophysical behavior to be related to an energy transfer from the Soret band of Zn–porphyrins to the ruthenium fragment.

Ruthenium complexes as PSs

As discussed above, porphyrins certainly have good characteristics as PSs due to their intrinsic physico-chemical properties. On the other hand, the PSs available on the market still display a number of drawbacks such as their low solubility in biological media, lack of selective cancer accumulation and the frequently encountered photosensitivity in patients undergoing PDT treatments. Over the last few years, several research groups have explored the possibility to move away from tetrapyrrolic systems, studying the potential of metal complexes as PSs themselves. The application of ruthenium complexes as PSs is a reasonable approach due to their tunable photophysics and the aforementioned advantages for biological applications (see Introduction). As an example of this approach, our group synthesized six $[Ru(bipy)_2dppz]^{2+}$ complexes **18a–f** with different functional groups on the dppz ligand (Fig. 15).[53]

As highlighted before, the presence of the dppz intercalative ligand was meant to increase the affinity of the compounds for DNA, so that a targeted delivery of singlet oxygen to the genetic material can be achieved. All Ru complexes were found to be non-toxic (up to 100 μM) to both normal fetal lung fibroblast cells (MRC-5) and cervical cancer HeLa cells in the dark. Nevertheless, the amino- and methoxy-substituted Ru complexes showed impressive photoactivities. When HeLa cells were irradiated with a light dose of 9.27 J cm^{-2} at 420 nm, IC_{50} values in the low micromolar range were obtained for **18a** and **18b**. An impressive PI of 43 for the latter and even >150 for the former were obtained. Cellular distribution studies were performed on both compounds by means of confocal microscopy and high-resolution continuum source atomic absorption spectrometry (HR-CS AAS) and the results are reported in Fig. 16. These techniques indicated a very good cellular uptake of both compounds. Furthermore, HR-CS AAS analysis confirmed the nuclear localization for both complexes after 4 h incubation, allowing for target delivery of $^1O_2$ to DNA. Compounds **18a** and **18b** also showed good efficiency in generating strand breaks of supercoiled plasmid DNA upon light irradiation. This feature strongly suggested the involvement of DNA in the mechanism of phototoxicity. Further studies are ongoing to investigate the interaction of **18b** with DNA, and the exact mechanism of cell death engendered by light activation.

With the similar goal of targeting and photocleaving DNA, Brewer *et al.* studied mono-metallic or supramolecular complexes of Ru, Pt, Rh and their abilities to interact with DNA upon light irradiation in depth (see also the PACT section below). In particular, they demonstrated the ability of three $[(TL)_2Ru(dpp)]^{2+}$ compounds (dpp = 2,3-bis(2-pyridyl)pyrazine, with TL = bipy, phen or Ph_2phen = 4,7-diphenyl-1,10-phenanthroline) to efficiently photocleave supercoiled pUC18 plasmid DNA upon irradiation at $\lambda = 450$ nm thanks to the formation of $^1O_2$.[54] However, the biological activity of compounds of the type $[(TL)_2Ru(dpp)]^{2+}$ in cells was not evaluated. Turro and coworkers are also very active in the field of light-activated ruthenium complexes. They synthesized and characterized many compounds and studied their photophysics, and light-mediated interactions with DNA and proteins due to the formation of singlet oxygen,[55,56] or to other mechanisms (see also the PACT section below). To further highlight the mode of action of these photoactivated compounds, these researchers investigated their light-induced effects on DNA and proteins in fibroblasts.[57] The two complexes, $[Ru(tpy)(pydppn)]^{2+}$ (**19**) and $[Ru(pydppn)_2]^{2+}$ (**20**) reported in Fig. 17, with tpy = [2,2′;6′,2″]-terpyridine and pydppn = 3-(pyrid-2′-yl)-4,5,9,16-tetraaza-dibenzo[*a*,*c*]naphthacene,[56] displayed very long lifetimes of the excited states (20–24 μs), thanks to the pydppn ligand, which allows for singlet oxygen generation with an efficiency of almost 100%.

The authors were then able to demonstrate that **19** and, to a lesser extent, **20** induced photodynamic damage to the tumor suppressor p53 and the DNA polymerase processivity factor PCNA (proliferating cell nuclear antigen), both of them being key components of DNA maintenance and repair pathways. Upon light irradiation of cells and cell lysates (3.15 J cm^{-2} of visible light), the compounds induced covalent crosslinking of the protein subunits, the formation of DNA–protein adducts and, as a consequence, the inhibition of DNA replication. p53 crosslinking was previously demonstrated to correlate with the formation of singlet oxygen,[58] and the work of Turro and colleagues[57] demonstrated a strong reduction in the efficiency of p53 photodamage by the presence of sodium azide, a known singlet oxygen quencher. In addition, protein–DNA crosslinking was demonstrated to depend on singlet oxygen-mediated formation of 8-oxo-7,8-dihydroguanine and its further reaction with amino groups in the protein. Also in this case though, the evaluation of the phototoxic profile of the compounds on cells was not explored.

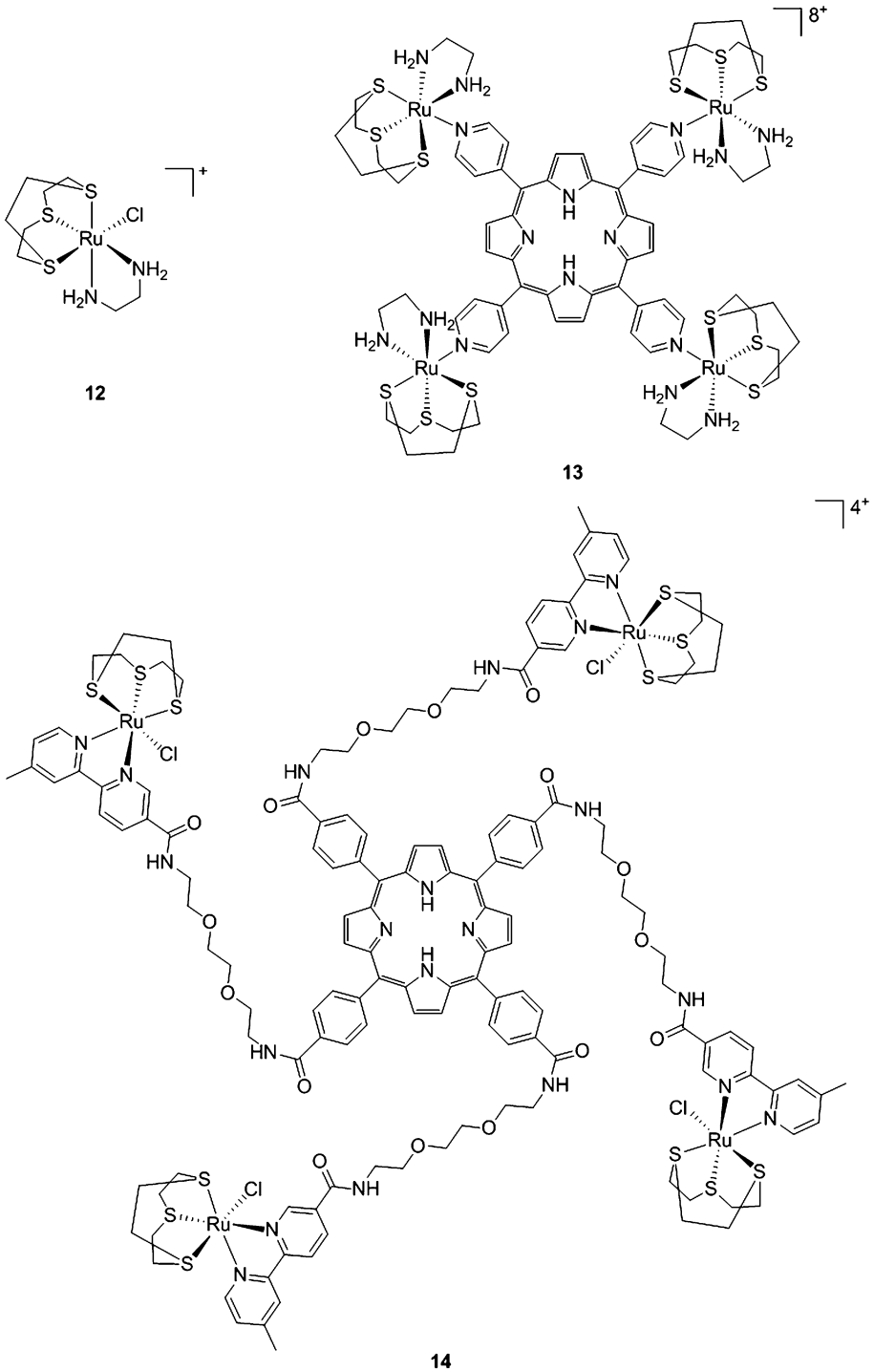

Fig. 11 Structures of $Ru([9]aneS_3)(en)Cl]^+$ (top, left) and of the ruthenium-derivatized porphyrin systems **13** and **14**.[40]

Ruthenium polypyridyl complexes also have an excellent record of performance in the field of dye-sensitized solar cells (DSSCs)[59] due to their absorption in the visible range and very long lifetimes. Interestingly, and as previously noted, these characteristics are also of extreme importance in the field of PDT. Consequently, our group decided to explore the photodynamic behavior of two derivatives of ruthenium complexes bearing a benzenedithiol (**21**) and a tridentate polypyridyl ligand (**22**), respectively (Fig. 18), which were previously employed in the field of DSSCs.[60]

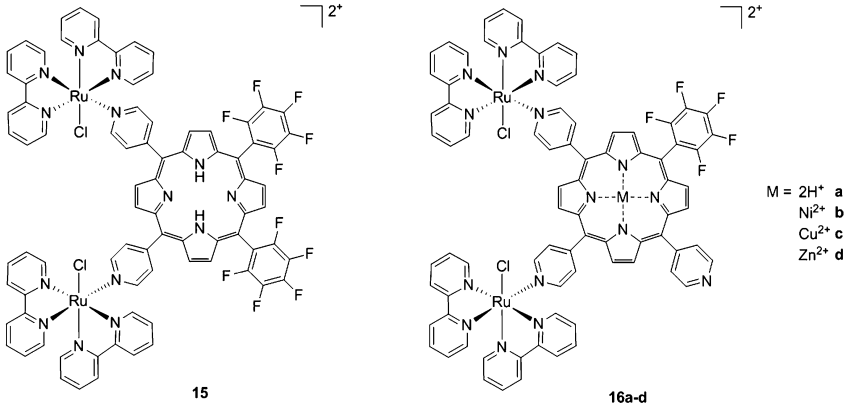

Fig. 12 Porphyrin with pentafluoroaryl and Ru(bipy)$_2$Cl fragments to give **15** (left) and Ru–porphyrin conjugates containing different metals in the ring (**16a–d**, right).[43,44]

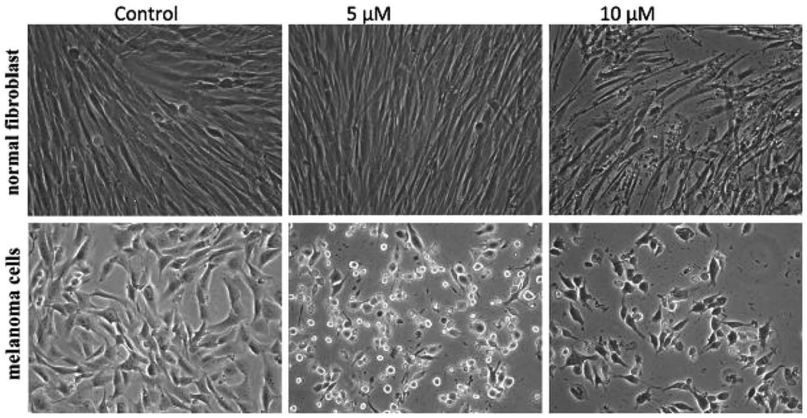

Fig. 13 Phase contrast microscopy images of cells irradiated with a 60 W tungsten lamp for 30 min. Normal fibroblast cells (top) and melanoma cells (bottom) without **16d** (control) and in the presence of 5 and 10 μM concentrations of **16d**. Reproduced from ref. 44 with permission from The Royal Society of Chemistry.

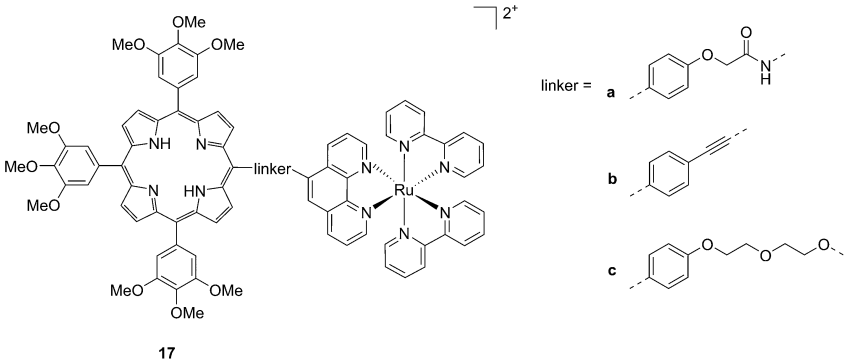

Fig. 14 Structures of Ru–porphyrin conjugates **17a–c**, with three different bridging linkers.[52]

Both compounds were characterized by moderate uptake by HeLa cells, as indicated by inductively coupled plasma mass spectrometry (ICP-MS) analysis performed after 4 h incubation. **21** accumulated preferentially in mitochondria (67% of the entire Ru uptake) as also confirmed by fluorescence confocal microscopy (Fig. 19). **22**, on the other hand, was shown to target

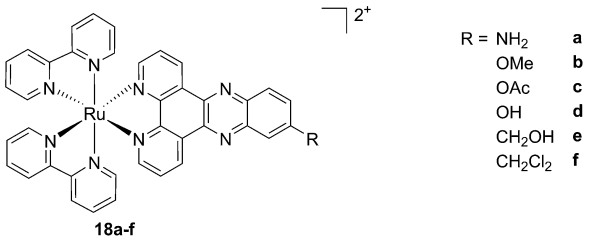

Fig. 15 Structures of the six different DNA intercalating Ru complexes **18a–f**.[53]

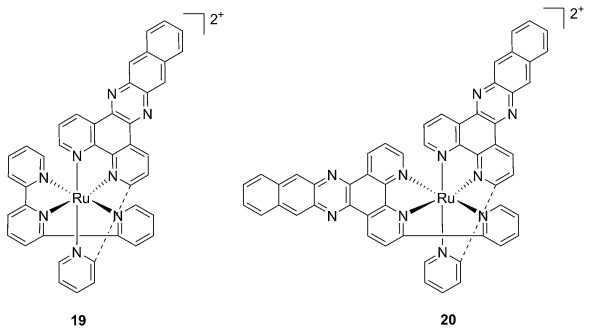

Fig. 17 Structures of the Ru complexes **19** and **20** bearing the tridentate pydppn ligand, which confers very long excited state lifetimes.[57]

the nuclei, where 50% of the total Ru that entered cells was localized.

Phototoxicity was evaluated on HeLa cells. **21** was found to be most active upon irradiation at 420 nm with 6.95 J cm^{-2}. Its PI was equal to 80, with an IC_{50} of 620 nM upon light irradiation. It is important to notice that although the uptake of **21** was not as high as those reported for similar complexes, the amount of compound present in cells was sufficient to produce a strong phototoxic effect. On the contrary, **22** displayed a lower phototoxicity against HeLa with an IC_{50} of 25.3 μM under the same irradiation conditions. Of utmost interest, the compounds were also evaluated for their potential activity as PSs in antibacterial PDT (aPDT). The use of PDT to kill bacteria was recently exploited to overcome the problematic occurrence of resistance to available antibiotics. This is essentially due to the fact that a resistance mechanism is far more difficult to develop for bacteria since PDT does not have a specific target but can affect the entire cell. The antibacterial activities of **21** and **22** were tested on the Gram-(−) *Staphylococcus aureus* and on the Gram-(+) *Escherichia coli*. Surprisingly, **22** was active against both strains, with a reduction of >6 log_{10} of the viability of the *S. aureus* and >4 log_{10} of that of *E. coli* at a concentration of 50 μM and with a dose of 8 J cm^{-2} of light at 420 nm. Under the same

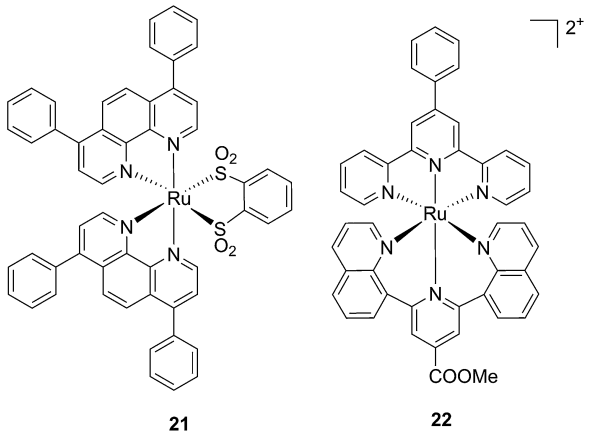

Fig. 18 Structures of the ruthenium complexes **21** and **22** which have PDT and aPDT activity.[60]

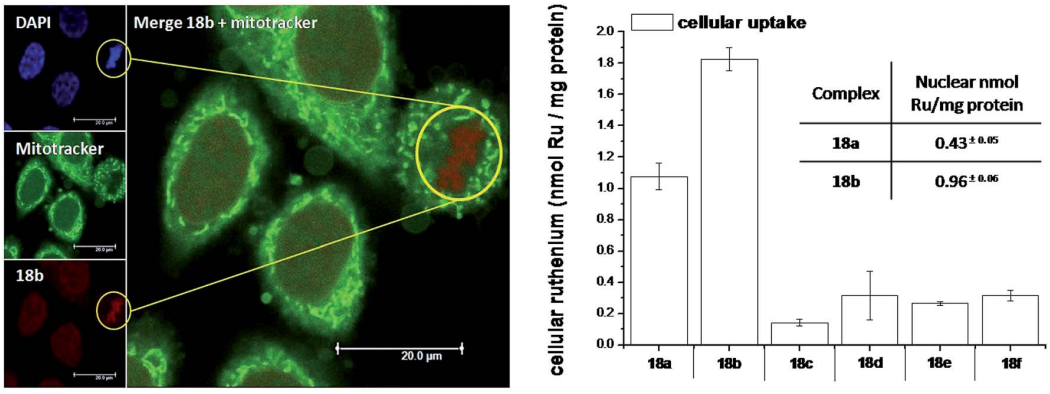

Fig. 16 Left: Confocal microscopy images of HeLa cells treated for 2 h with 100 μM of complex **18b** (excitation at 488 nm, emission above 600 nm, bottom left) and stained with DAPI (nuclear staining, top left) and with Mitotracker green (mitochondrial staining, middle left); in the yellow circle a representative example of the different localization of **18b** and Mitotracker green is found (picture on the right). Right: Cellular uptake into HeLa cells treated for 4 h with 20 μM solutions of the complexes **18a–f**. Results are expressed as the mean ± error of independent experiments. In the inset: nuclear uptake for complexes **18a** and **18b**. Reproduced with permission from ref. 53. © 2014 Wiley-VCH Verlag GmbH & Co. KGaA, Weinheim.

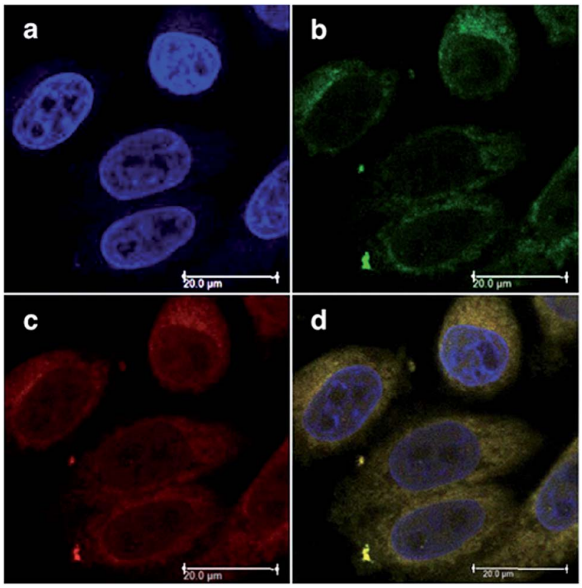

Fig. 19 Fluorescence confocal microscopy images of HeLa cells incubated with 40 μM of **21** for 4 h: (a) DAPI staining, (b) Mitotracker green FM staining, (c) visualization of **21** by excitation at 405 nm, (d) overlay of a–c. Reprinted with permission from ref. 60. Copyright 2014 American Chemical Society.

conditions, **21** displayed the same activity towards *S. aureus*, while being completely non-toxic towards *E. coli*. The very good performance of **22** is particularly promising considering that it is reported that normally Gram-(−) bacteria are less sensitive to PDT treatment.

In the last few years, Glazer and coworkers have thoroughly investigated the application of Ru polypyridyl complexes as PACT agents (see also PACT section). However, they also recently performed an in-depth biological characterization of two potential PDT agents. In particular, they evaluated $[Ru(Ph_2phen)_3]^{2+}$ (**23**) and $[Ru(Ph_2phen\text{-}SO_3)_3]^{4-}$ (**24**) (Fig. 20), which are known dyes for solar cells or biological staining, but which were never investigated as PDT agents.[61] The two compounds have very similar structures but extremely different physical properties, mainly due to their different charges, namely +2 for **23** and −4 for **24**. This, along with the subsequent difference in hydrophilicity of the two molecules, was expected to induce distinct cellular responses. Nonetheless, both molecules were found to be able to produce singlet oxygen when photo-irradiated.

Toxicity experiments were performed on three different cell lines (A549 human non-small lung cancer cells, HL60 human promyelocytic leukemia cells and Jurkat human T lymphoblastoid cells) in the dark and upon irradiation with 7 J cm^{-2} of >400 nm light. **23** showed a very good cytotoxic effect on all cell lines studied. Irradiation brought a further increment in potency, with IC_{50} values ranging from 0.075 μM to 0.35 μM, depending on the cell lines employed. However, the PI was just around 10–20. Surprisingly, **24** appeared to be non-toxic in the dark (up to 300 μM) on all cell lines studied. Nevertheless, irradiation induced strong toxicity with IC_{50} values in the low micromolar range, resulting in a larger therapeutic window compared to **23**. The compounds also displayed a different subcellular localization, with **23** accumulating in mitochondria and lysosomes and **24** displaying a non-specific accumulation in the cytoplasm (Fig. 21). Interestingly, mitochondrial uptake of **23** was proposed by the authors as the cause of toxicity in the dark. Upon light irradiation, **23** relocalized from mitochondria and lysosomes to the nucleus. This phenomenon was explained by the authors as the consequence of damage to the nuclear membrane induced by **23** upon light irradiation. On the other hand, when cells incubated with **24** were irradiated, the compound was mainly observed in lysosomes, suggesting that no damage occurred to the nuclear membrane in this case.

Investigation of the mechanism of cell death using distinct assays and read-outs revealed a role for light-induced apoptotic pathways in the case of **24**. On the other hand, initial necrotic cell death in the dark, followed by a combination of necrotic and apoptotic pathways, was observed for **23** upon light irradiation.

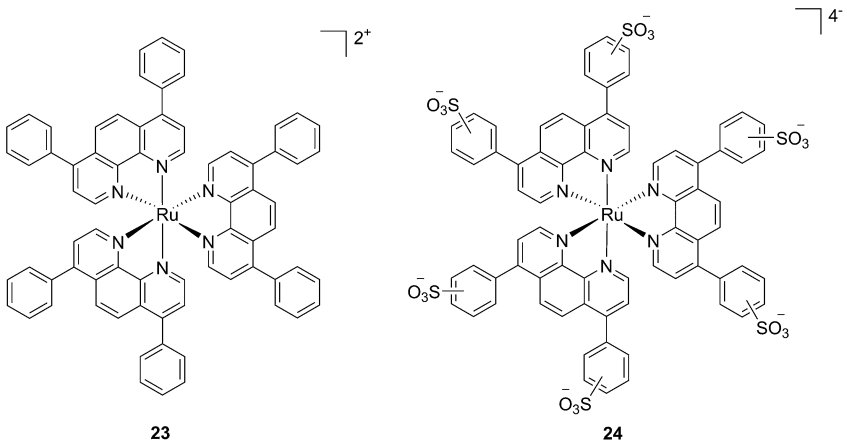

23 **24**

Fig. 20 Structures of the Ph_2phen complexes **23** and **24** with different charges investigated by Glazer and co-workers.[61]

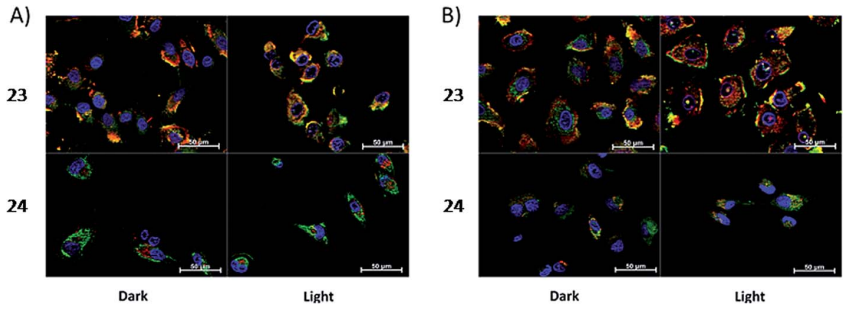

Fig. 21 ApoTome microscopy showing subcellular localization of **23** and **24** at 8 h. Co-localization of **23** and **24** in mitochondria or lysosomes is indicated by the apparent yellow emission. (A) Mitotracker green FM was used to image mitochondria. (B) Lysotracker green DND-26 was used to image lysosomes. Red color denotes intrinsic emission of **23** and **24**, whereas blue color denotes Hoechst staining of the nucleus. The yellow color results from overlap of the red emission from the ruthenium complexes and green emission of the organelle-specific dyes, indicating co-localization. Compound **23** localizes in both the mitochondria and the lysosomes, while **24** was not predominantly found in either organelle. Reprinted with permission from ref. 61. Copyright 2014 American Chemical Society.

While one of the main problems of PDT is its reliance on oxygen, which is often present at low concentrations in the tumor environment (hypoxic conditions), the application of metal complexes as PSs also has its drawbacks, which are due to the need for light at a high energy (blue or green) for the excitation of the PS. McFarland and co-workers addressed both issues by taking advantage of the possibility to fine tune the photophysical characteristics of coordination compounds. More specifically, by modifying the structures of the ligands coordinated to the metal centre, the authors developed Ru polypyridyl PSs characterized by a triplet intraligand (^{3}IL) excited state with remarkably long lifetimes. Oxygen was reported to be able to quench this excited state even when present at very low concentrations (3.5%). Furthermore, the strong photosensitizing ability of this excited state allowed PDT effects to be achieved in the red and NIR regions where compounds have marginal absorptions (ε values in the order of 10 M^{-1} cm^{-1}). The first series of compounds bearing a pyrenylethynyl moiety on the phenathroline ligand was strongly effective on the cell line Malme-3M, a malignant melanoma lung metastasis.[62] Melanoma cells are able to grow at very low oxygen concentrations and have a remarkable ability to resist the outburst of ROS.[63] Nevertheless, compound **25** (Fig. 22, left) could induce cell death in a melanoma cell line, with a toxicity increase of two orders of magnitude upon irradiation with white light at 7 J cm^{-2}. In these conditions, EC_{50} went from 62 μM in the dark to 200 nM upon irradiation.

A second class of compounds studied by the same group contained the extensively conjugated benzo[*i*]dipyrido[3,2-*a*:2′,3′-*c*]phenazine ligand (dppn, Fig. 22, right).[64] The authors could exploit the ^{3}IL excited state of these compounds with very long lifetimes to obtain a remarkable PDT effect. Impressively, EC_{50} values in the low micromolar range were obtained upon irradiation with 100 J cm^{-2} light at 625 nm, where the compounds have marginal absorption. This efficacy demonstrated that it is possible to achieve good photoactivity with compounds that mainly absorb in the blue-green region of the light spectrum. Furthermore, the same authors developed a system where the Ru polypyridyl complexes are connected to polythiophene chains of variable lengths (Fig. 23). This conjugation gave access to a low-lying ^{3}IL excited state and to a strong non covalent DNA association.[65] Gel electrophoresis experiments were performed on the complexes to elucidate the interaction with plasmid DNA. These analyses suggested that compounds bearing more than one thiophene unit are able to induce light-mediated damages to plasmid DNA *via* an oxygen-independent pathway. This was indicated by the fact that compound **27c** was still able to induce single strand breaks when the experiment was performed under argon atmosphere. Therefore, the authors speculated that these thiophene conjugates could act *via* photoinitiated Type II reaction in the case of

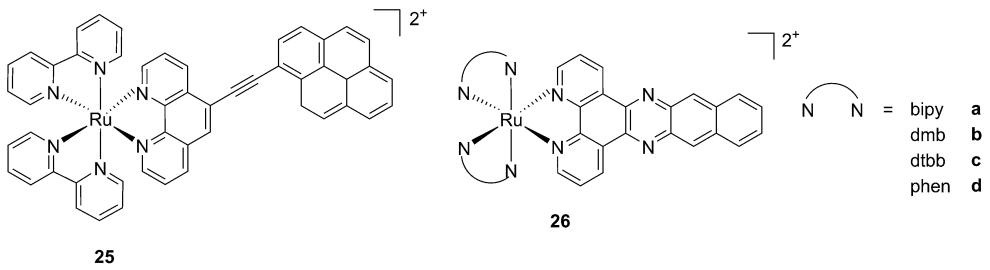

25 26

Fig. 22 Structures of ruthenium complexes **25** and **26** studied by McFarland, characterized by ^{3}IL excited states.[62,64]

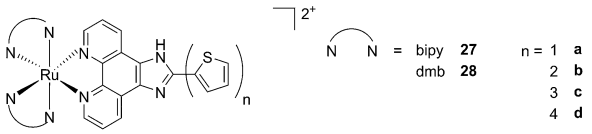

Fig. 23 Structures of Ru polypyridyl complexes conjugated with different polythiophene moieties to achieve dual Type I/II photosensitization.[65]

high oxygen tension. On the contrary, under low oxygen concentration, the compounds induced damage to DNA *via* a Type I pathway. This behavior was already observed for this class of compounds in the photoinactivation of bacteria.[66] A PS with the ability to act *via* a dual Type I/II photosensitization could allow for the treatment of hypoxic tissues, broadening the spectra of applicability of PDT.

The *in vitro* PDT effect of these compounds was found to be directly proportional to the polythiophene chain length, with a PI of > 200 when 4 thiophene units were present in the complex. The two best compounds **27c** and **28c**, bearing three thiophene units, were also tested *in vivo* on mice, which were inoculated with colon carcinoma cells (CT26.WT). In animals treated with compound **28c** (53 mg kg^{-1}), administration of 525 nm continuous wave light (192 J cm^{-2}) resulted in complete tumor regression, with no recurrence up to 52 days after the end of the treatment. These compounds are currently under optimization for clinical phase I trials.[65]

A very elegant approach to effectively increase the selectivity of PDT treatment is the so-called CALI (chromophore-assisted light inactivation). This technique is based on the functionalization of a modest protein inhibitor with a PS, allowing for strong enhancement of the inhibitory properties through photo-triggered $^1O_2$ generation in close proximity to the active site (see the mechanism in Fig. 24). The Kodadek group recently explored this technique using a $[Ru(bipy)_3]^{2+}$ derivative,[67] demonstrating the feasibility of this technique on both membrane and intracellular proteins.

Furthermore, the authors showed selective inhibition of RBBP9 serine hydrolase, which is implicated in pancreatic cancer, in protein-enriched cell lysate.[68] The limitation of this approach is related to the choice of PS, since $[Ru(bipy)_3]^{2+}$ derivatives do not allow efficient photosensitization due to the short wavelengths required for excitation. A careful optimization of the system could provide a very useful tool for future targeted PDT applications.

Ruthenium complexes in PACT

As mentioned above, PDT relies on the presence of oxygen to induce cell death. However, most tumors are hypoxic in their internal core,[69] limiting the efficacy of PDT. Hence, increasing efforts are devoted to the optimization of novel photo-activation strategies that do not rely on an oxygen-dependent mechanism, but which would still allow for spatial and temporal control of the toxicity engendered to cells. Strategies of this type are normally referred to as photoactivated chemotherapy. In this section of the review, we describe the recent efforts in the use of ruthenium complexes for PACT. We have divided this section into two main parts depending on the photo-activation strategy employed. In the first part, we will focus on ruthenium-based DNA photobinders acting (1) in a cisplatin-like mode of action resulting in DNA helix distortion; (2) *via* intercalation yielding DNA cleavage; and (3) *via* conjugated oligodeoxyribonucleotides (ODNs) to allow for gene silencing. In the second part, we will discuss photo-activated release approaches involving Ru(II) complexes. In this part, we will first introduce the use of Ru(II) complexes as caging agents for the selective release of bioactive molecules upon light activation. We will then present a parallel approach consisting of the photorelease of cytotoxic Ru(II) complexes rendered inactive upon caging.

Photo-activated Ru complexes targeting DNA

Cancer cells differ from their original healthy precursor cells by their ability, *inter alia*, to continuously proliferate.[70] This feature, conferred by mutations in tumor suppressor genes or by the altered expression/activity of proto-oncogenes, implies continuous activation of DNA replication, which is not the case in healthy cells, which rather display the ability to enter quiescence after a certain number of cell divisions. This hallmark of cancer has been extensively exploited to selectively target cancer cells by means of chemotherapeutic drugs, inhibiting components of the DNA replication/transcription machineries, such as topoisomerase I (*e.g.* camptothecin)[71] or covalently binding to DNA (*e.g.* cisplatin)[72]. In this section, we will introduce photo-triggered strategies designed to target DNA.

Ligand photo-dissociation and DNA target. The best known metal complex used in cancer treatment is undoubtedly cisplatin, a metal-based drug that targets growing cells by interfering with DNA replication. Cisplatin is a prodrug that first undergoes a process called aquation, by which chloride ligands are displaced by water. The cytotoxic activity of cisplatin

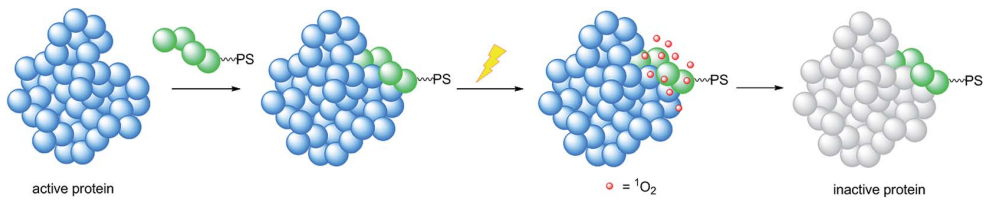

Fig. 24 Mechanism of the CALI strategy to inhibit enzymes, applied by the Kodadek group.

results from interaction of the highly reactive hydrated form of the drug with DNA, preferentially with the N7 atoms of purine residues.[73] The majority of lesions generated by cisplatin consist of intra-strand cross-links at two consecutive purines that are promptly addressed by the Nucleotide Excision Repair pathway. On the other hand, the far smaller proportion of inter-strand crosslinks causes distortions of the double helix and inhibits replication,[74] transcription[74,75] and translation,[76] representing a serious threat to cell survival. Furthermore, although replication fork stalling at inter-strand crosslinks does not compromise the completion of S-phase, as it is compensated for by incoming forks from the opposite site of the lesion, the real threat consists of the persistence of the inter-strand crosslink until mitosis, leading to apoptosis.[77] The broad spectrum of action of cisplatin, as well as its lack of specificity for cancer cells, is evidenced by the severe side effects observed in patients treated with the drug (*e.g.* nephrotoxicity, ototoxicity, *etc.*).[72] Hence, a significant effort has been directed towards more targeted strategies, involving the use of an external trigger such as light to induce cytotoxicity. As an example, Sadler and coworkers have designed and characterized photoactivatable cisplatin derivatives with clear potential for use in PACT.[78–80] In particular, they showed that irradiation of Pt(IV) diazido derivatives with UV-A or blue light induced photoejection of the azido ligands and reduction of the metal to Pt(II). As a consequence, the photoproduct can covalently bind DNA in a similar way to cisplatin, generating a potent cytotoxic effect on cells in culture.[20,81]

In contrast to square planar Pt(II) compounds, Ru(II) complexes offer octahedral conformations. It was shown that complexes with distorted octahedral geometry can undergo ligand dissociation after photo-irradiation,[82,83] which is followed by the formation of an aqua complex that can bind to DNA in a manner similar to cisplatin. To exploit this concept, Glazer and coworkers recently investigated the potential use of methyl substituents on one polypyridyl ligand to obtain highly distorted geometries.[84] To this end, an unstrained $[Ru(bipy)_2$-phen$]^{2+}$ (**29**) and two methylated derivatives of $[Ru(bipy)_2$(2,2′-bypiridyl)$]^{2+}$ (**30**) and $[Ru(bipy)_2$(dipirido[3,2-*f*:2′,3′-*h*]-quinoxaline)$]^{2+}$ (**31**) were synthesized (see Fig. 25 for structures). As expected, after >450 nm light irradiation using a 200 W projector, the authors could monitor the photoejection of the methylated ligand of **30** and **31**, with half-lives ($t_{1/2}$) of 2 and 60 min, respectively. Since photoejection of the latter ligand resulted in the formation of a similar aqua species to cisplatin, the authors naturally explored the activity of the photo-product on biologically relevant molecules. In the presence of plasmid DNA pUC19, only irradiated (>450 nm, 200 W, 1 h) products showed DNA damage. Complex **29** produced DNA photocleavage, **30** showed only DNA photobinding whilst **31** combined both properties. To verify if the DNA damage observed *in vitro* would reflect in decreased viability in cancer cells in culture, the authors treated HL60 leukemia and A549 lung cancer cells for 12 h with the complexes in the dark prior to >450 nm irradiation for 3 min at 410 W, followed by a further 72 h of incubation (see Table 1 for complete IC_{50} values). As a control, they used aminolevulinic acid (ALA) which is a clinically available PS. Complexes **30** and **31** showed no toxicity in the dark with IC_{50} values of > 100 μM. However, a strong effect after irradiation on both cells with IC_{50} on HL60 cells of 1.6 and 2.6 μM, respectively, and of 1.1 and 1.2 μM, respectively, on A549 cells, was observed. In order to efficiently mimic the three-dimensional tumor environment, the authors also assessed the photo-toxicity of the compounds on A549 spheroids. As reported for the monolayer cell culture, complex **30** was confirmed to be efficient with an IC_{50} of 21 μM upon light irradiation, a value that corresponds to twice the potency of cisplatin on the same spheroids. Worthy of note, glutathione (GSH), responsible for cisplatin inhibition in cells, had no deleterious effect on DNA binding or cleavage efficiency nor on the toxicity of the ruthenium complexes **30** and **31**.

More recently, Glazer *et al.* applied the same methylation strategy to a novel strained $Ru(bipy)_2$ complex bearing a 2,3-dihydro-1,4-dioxino[2,3-*f*]-1,10-phenanthroline (dop) (**32**) ligand.[85] The methylated form of **32** is 2,3-dihydro-1,4-dioxino [2,3-*f*]-2,9-dimethyl-1,10-phenanthroline (dmdop) (**33**, Fig. 26). To further increase the straining, the authors also synthesized a $[Ru(dmphen)_2(dop)]^{2+}$ (dmphen = 2,9-dimethyl-1,10-phenanthroline) (**34**, Fig. 26). As anticipated by the authors, after irradiation at >400 nm with a 200 W projector at a distance of 12 inches from the cuvette, both methylated analogs showed photoejection. The process was found to be 10-fold faster for complex **34** ($t_{1/2}$ = 4 min) than for **33** ($t_{1/2}$ = 42 min). The authors further analyzed photo-induced DNA damage. Upon the same irradiation settings, complex **32** created single strand breaks (SSBs) in pUC19, likely *via* $^1O_2$ production. In comparison, complex **34** showed covalent binding while **33** showed a combination of both mechanisms. Regarding cell photo-

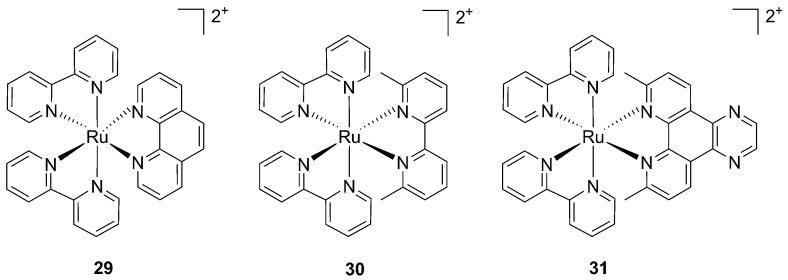

Fig. 25 Structures of the strained Ru complexes **30** and **31** that undergo ligand photoejection and the inert control **29**.[84]

Table 1 Cytotoxicity IC_{50} values in 2D and 3D cellular assays[a]

IC_{50} (μM)								
	Light			Dark			PI	
Compounds	HL60	A549	A549 spheroid	HL60	A549	A549 spheroid	HL60	A549
Cisplatin	3.1 ± 0.2	3.4 ± 0.6	n. d.	3.1 ±0.1	3.5 ± 0.6	42 ± 3.6	1	1
29	8.1 ± 1.9	40 ± 4	>300	240 ± 9	250 ± 5	>300	3	6.3
30	1.6 ± 0.2	1.1 ± 0.3	21.3 ± 2.3	>300	150 ± 7	>300	>188	136
31	2.6 ± 1.0	1.2 ± 0.1	64.6 ± 4.7	108 ± 1.9	250 ± 5	>300	42	208
ALA	16.2 ± 3.2	21 ± 3.5	>300	>300	87.8 ± 5.5	>300	>18	4.2

[a] n. d. = not determined. ALA = aminolevulinic acid.

toxicity, complex **34** exerted the highest toxicity against leukemia cells HL60 with a PI of >1880. The IC_{50} was 300 μM in the dark while the value was 0.16 μM after 12 h incubation, 3 minutes irradiation at >400 nm with 410 W projector and 72 h recovery. This impressive PI was explained by the fact that **34** binds and distorts DNA, whereas the mechanism of action of complex **33** is characterized by a dual mode of action including SSBs formation *via* $^1O_2$ production and DNA distortion, which possibly lowers its distortion efficiency.

Following a similar distortion strategy, the same group studied the coordination of biquinoline (biq) to ruthenium-based complexes. Such a ligand would act as a potent geometry distorter, and at the same time, improve the light activation process by pushing the absorption maximum to higher wavelengths. Indeed, the resulting strained Ru(II) 2,2′-biquinoline complexes (see Fig. 27 for structures) were shown to be active in the PDT therapeutic window. **35**, which bears one biq, and **36**, which contains two biq ligands, can absorb light up to 700 and 800 nm, respectively.[86] Both complexes induced decreased electrophoretic migration of the DNA plasmid pUC19 only upon illumination (samples were placed at 12 inches from a 200 W lamp equipped with either blue, green, red or near-IR cut-off filters and irradiated for 1 h or 3 h). Since the appearance of open circular or linear DNA was not observed, the mechanism involved clearly coincides with photobinding. Maximal activity has been observed with blue light irradiation, which is consistent with the absorption profile of the Ru(II) complex. Cytotoxicity against HL60 leukemia cells followed the same light-dose/-wavelength profile as DNA photo-cleavage. After 12 h incubation followed by 7 J cm^{-2} light irradiation and 72 h recovery, a cell viability assay revealed that complex **36** had the best phototoxicity profile with IC_{50} values of between 2.3 and 5.1 μM among the different wavelengths used, compared to 47.3 μM in the dark (see Table 2 for IC_{50} values). The interesting PIs (blue:

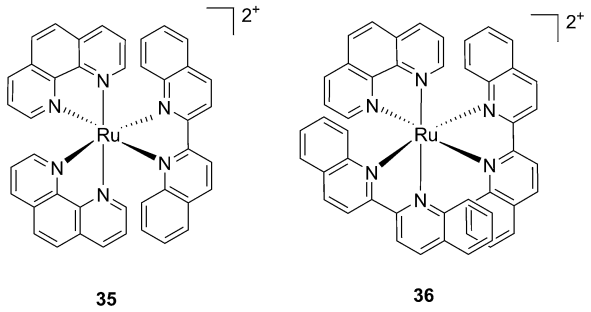

35 36

Fig. 27 Structures of the two Ru(II) complexes **35** and **36** with the biq ligands that are exchanged upon irradiation.[86]

Table 2 Photobiological activities of **35** and **36** on HL-60 cells[a]

IC_{50} (μM)						PI	
Compounds	Dark	Blue (3 min)	Red (3 min)	Red (6 min)	IR (25 min)	Blue	IR
35	52.5	1.2	13.8	7.6	15.8	43.8	3.32
36	47.3	2.4	4.5	2.3	5.1	19.2	9.2
Cisplatin	3.1	3.1	n. d.	n. d.	n. d.	1	

[a] n. d.= not determined.

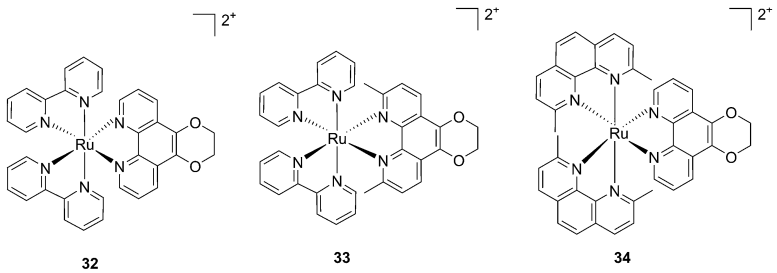

32 33 34

Fig. 26 Structures of the photostable control compound **32** and the strained **33** and **34** that undergo ligand photoejection.[85]

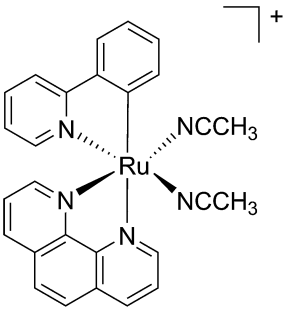

37

Fig. 28 Structure of the Ru(II) complex **37** with labile CH_3CN ligand.[91]

19.7, IR: 9.2) obtained for complex **36** hold great promise for this type of Ru(II) complex, which can be activated with red light or even with near-IR wavelengths. Interestingly, a complex similar to compound **36** but bearing a 2-phenylpyridine (phpy) instead of the phen, had different photophysical properties. Indeed, Dunbar, Turro and coworkers found that the latter complex had enhanced phototoxicity against HeLa cells.[87] Nevertheless, its mode of action remains unclear, since no ligand dissociation was observed. Moreover, the short lifetime of the compound rules out any singlet oxygen mechanism.[88]

Another manner to shift the MLCT absorption of a Ru(II) complex to the red (PDT window) is by insertion of a cyclometallating ligand.[89] For this purpose, Turro and coworkers focused on the ligand phpy. More specifically, they investigated the photo-induced ligand release of *cis*-$[Ru(phpy)(phen)(CH_3CN)_2]^{2+}$ (**37**, Fig. 28), a complex known to decrease tumor growth in mice,[90] but whose photo-induced ligand release potential had never been evaluated. First, they observed that 3 min of irradiation at 690 nm were sufficient to eject one CH_3CN, while 30 min were needed to release the second acetonitrile ligand. They could also observe an enhancement of cytotoxicity upon light irradiation (100 s irradiation at 690 nm, 5 J cm^{-2}). As expected, the compound displayed a potent cytotoxicity on human advanced ovarian epithelial cancer cells (OVCAR-5) in the dark, with an IC_{50} of 1 μM (15 h incubation followed by rinsing and then by 24 h recovery). Upon light irradiation, the IC_{50} reached 70 nM, a 14-fold increase compared to dark conditions. According to agarose gel shift assay, this increase in toxicity upon light illumination is due to photobinding of the complex to DNA. Of note, the authors could demonstrate that GSH enhanced the photo-dissociation process, but still further analyses are needed to fully understand its role.[91]

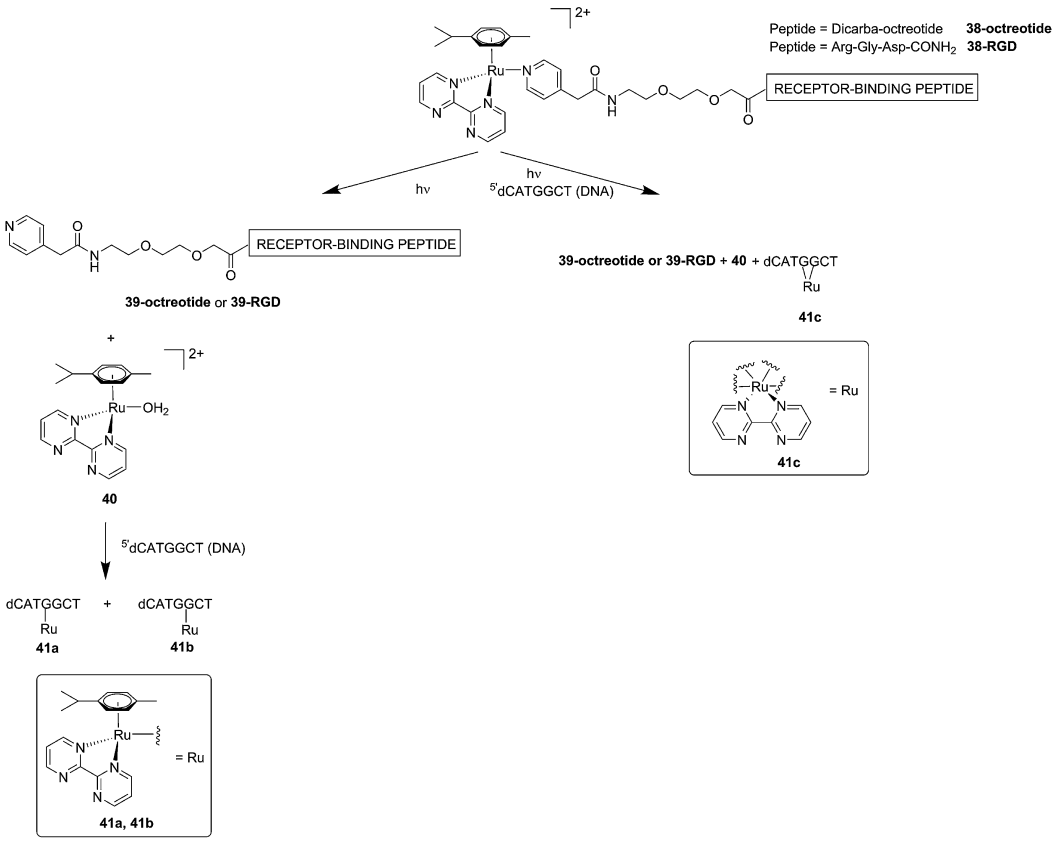

Fig. 29 Schematic representation of the photo-dissociation process. Left branch: pre-irradiated Ru–peptide conjugates followed by addition of the oligonucleotide. Right branch: irradiation of a mixture of peptide-conjugated Ru(II) complex and the oligonucleotide.[94]

Although light-activated prodrugs offer an already high temporal and spatial selectivity *per se*, they still suffer from the recurrent problem of photosensitivity. Despite the fact that Ru complexes may be mimicking Fe uptake and thereby accumulate in cancer cells overexpressing transferrin,[92,93] and assuming an intravenous administration, the light-activatable prodrugs presented above are supposed to be transported everywhere in the body without special selectivity for cancer cells. This implies that surrounding healthy tissues are not free from deleterious effects. To tackle this important drawback, several groups have envisaged coupling a targeting moiety to light-activatable prodrugs. In this perspective, Marchán *et al.* coupled two different receptor-binding peptides, which are known to target receptors overexpressed on the membrane of some cancer cells, to a photoactivated Ru(II) arene complex (Fig. 29).[94] Since tumor endothelial cells overexpress two types of integrins, $\alpha_v\beta_3$ and $\alpha_v\beta_5$, the authors attached the specific targeting peptide sequence Arg-Gly-Asp (RGD). On the other hand, they decided to target the somatostatin receptor sst_2, which is located at the membranes of malignant cells in supernumerary copies, using the peptide octreotide, a somatostatin agonist. The authors reported interesting and promising *in vitro* studies. First, they showed that conjugation to the peptides did not affect the photoactivation process, since the reactive aqua species was formed after pyridine ligand loss upon visible light irradiation (420 nm lamps). Second, they reported that DNA binding of the Ru-conjugates was not compromised by the presence of the peptides. When pre-irradiated (8 h) peptide-conjugated Ru(II) complexes **38-octreotide** or **38-RGD** were incubated overnight with the 9-ethylguanine, monofunctional adducts were formed. The same was true for the incubation with a short oligonucleotide sequence ($^{5'}$dCATGGCT), as shown in Fig. 29, left branch. The formation of monofunctional adducts **41a** and **41b** was due to the release of the pyridyl ligand **39-octreotide** or **39-RGD** (depending on the compound used) upon irradiation, followed by formation of the aqua species $[Ru(\eta^6\text{-}p\text{-cymene})(bpm)(H_2O)]^{2+}$ (bpm = 2,2′-bipyrimidine) **40**. This intermediate then reacted with one guanine present in the sequence, yielding the isomers **41a** and **41b**. On the other hand, when the solution containing the Ru–peptide conjugates and the oligonucleotide was intensively irradiated (9 J cm^{-2}, 9 h irradiation), the bifunctional adduct **41c** appeared, due to consequent arene release (see Fig. 29, right branch). Encouragingly, the authors demonstrated the specificity of the ruthenium complex for guanine over other potential biological ligands present in octreotide such as histidine or methionine, since no interactions between the ruthenium complex and these amino acids were observed. Nevertheless, these promising results and targeted strategy still need to be verified in cell-based assays.

DNA intercalation and photo-cleavage. Covalent binding to guanine is not the only manner by which a (metal-based) drug can interfere with DNA replication. Different compounds have indeed been shown to interact with DNA in a non-covalent fashion. Flat aromatic structures (*e.g.* dppz or PHEHAT = 1,10-phenanthrolino[5,6-*b*]1,4,5,8,9,12-hexaazatriphenylene; TAP = 1,4,5,8-tetraazaphenanthrene; IPPBA = 3-(1*H*-imidazo[4,5-*f*]-[1,10]phenanthrolin-2yl)phenylboronic acid) are known to intercalate between two DNA bases. These DNA intercalative moieties place the metal in close proximity to the bases, facilitating direct photo-induced oxidation of guanines or DNA cleavage, for instance. To this end, de Feyter's group evaluated the effect of flat aromatic ligands on DNA conformation upon intercalation and upon photo-irradiation of $[Ru(TAP)_2\text{-}PHEHAT]^{2+}$ (**42**) (Fig. 30).[95] However, since no biological evaluation in cells or mice has been performed, only the important findings will be mentioned in this section. The authors could demonstrate that the main binding motif of the complex to DNA occurred *via* intercalation of the PHEHAT ligand. They could also highlight the importance of hydrogen bond-mediated TAP intercalation in DNA in the nicking activity upon visible light irradiation, since a decrease in nicking activity was observed when hydrogen bonds were prevented by urea. Nevertheless, urea treatment had no effect on the second type of DNA damage observed upon irradiation, namely adduct formation between the complex and DNA.

Recently, Wang *et al.* succeeded to shift the absorption of a Ru complex to longer wavelengths in order to obtain ligand photorelease in the PDT window. At the same time, the authors achieved an increase of the lifetime of the excited state, which facilitates $^1O_2$ production, thus combining PDT and PACT mechanisms. The authors undertook the latter by introduction of a 2,3-bis(2-pyridyl)-benzoquinoxaline (dpb) ligand into the structure of the Ru(II) complex, whose delocalized π system was able to shift ^{1}MLCT absorption to lower energy.[96] The authors observed the formation of several photoproducts when $[Ru(\eta^6\text{-}p\text{-cymene})(dpb)(py)]^{2+}$ (py = pyridine) (**43**) (Fig. 30) was irradiated with visible light (>400 nm) with the moieties (py) and (dpb) released in a 3.4 : 1 ratio. Moreover, the authors showed that the complex was a modest $^1O_2$ generator with a $^1O_2$ quantum yield of 0.25 in CH_3CN. Further investigation of the direct effects on DNA revealed the photo-binding and photocleaving ability of the complex. These behaviors were subsequently examined in cell-based assays. After 4 h incubation in A549 cells, followed by 1 h irradiation at >400 nm and an additional incubation of 20 h in the dark, the complex showed enhanced toxicity after light irradiation, although with a moderate PI of about 7 (IC_{50} in the dark: 27.6 μM, upon light

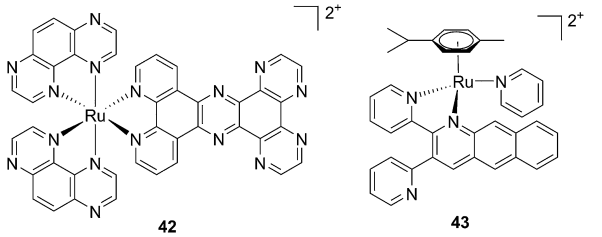

42 43

Fig. 30 Structures of $[Ru(TAP)_2PHEHAT]^{2+}$ **42** studied for DNA intercalation and nicking by de Feyter and $[Ru(\eta^6\text{-}p\text{-cymene})(dpb)(py)]^{2+}$ **43** synthesized by Wang, characterized by high wavelength absorption and ligand release.[95,96]

exposure: 4.0 μM). Brewer and co-workers also aimed to tune the absorption of the Ru(II) complexes to lower energy wavelengths and to not be, at the same time, dependent on the presence of oxygen to achieve cell killing. To this end, they designed a mixed-metal supramolecular complex $[\{(bipy)_2Ru(dpp)\}_2RhCl_2]^{5+}$ (**44**, Fig. 31) containing two Ru(II) centers to absorb visible light and one Rh(III) atom.[97] Complexes containing Rh(III) have previously been shown to photo-cleave DNA.[98] By agarose gel shift assays, the authors were able to characterize the structural requirements for the photo-cleavage process. First, they could show that the presence of rhodium in the molecule is needed for the DNA cleavage to occur. Indeed, when DNA was irradiated for 10 min at >475 nm, no cleavage was observed in the presence of the analog compounds lacking Rh(III), both in the presence and absence of oxygen. Second, they could demonstrate that the process followed metal-to-metal charge transfer (MMCT) and not the ordinary MLCT process. To show this, the authors compared the DNA photo-cleavage efficiency of two analogs with inaccessible Rh(dσ*) and Ir(dσ*) orbitals, namely $[\{(bipy)_2Ru(bpm)\}_2RhCl_2]^{5+}$ and $[\{(bipy)_2Ru(dpp)\}_2IrCl_2]^{5+}$ (**45** and **46** in Fig. 31). As expected, both analogs failed to cleave DNA. The same group then tested the photo-triggered impact of their Ru–Rh mixed-metal complex on African green monkey kidney epithelial cells (vero cells) replication.[99] The authors demonstrated that when cells were pretreated with **44** and exposed to >460 nm light, limited growth was observed up to 12 μM (conditions: 48 h incubation with compounds, then removal of the medium and 4 min irradiation at >460 nm, followed by 48 h recovery). At higher concentrations, cell death was observed. Interestingly, cell death was not observed with cells pretreated with the osmium analog complex **47**, shown in Fig. 31. This last observation highlighted the fundamental role of the Ru atoms in **44** in triggering cell death.

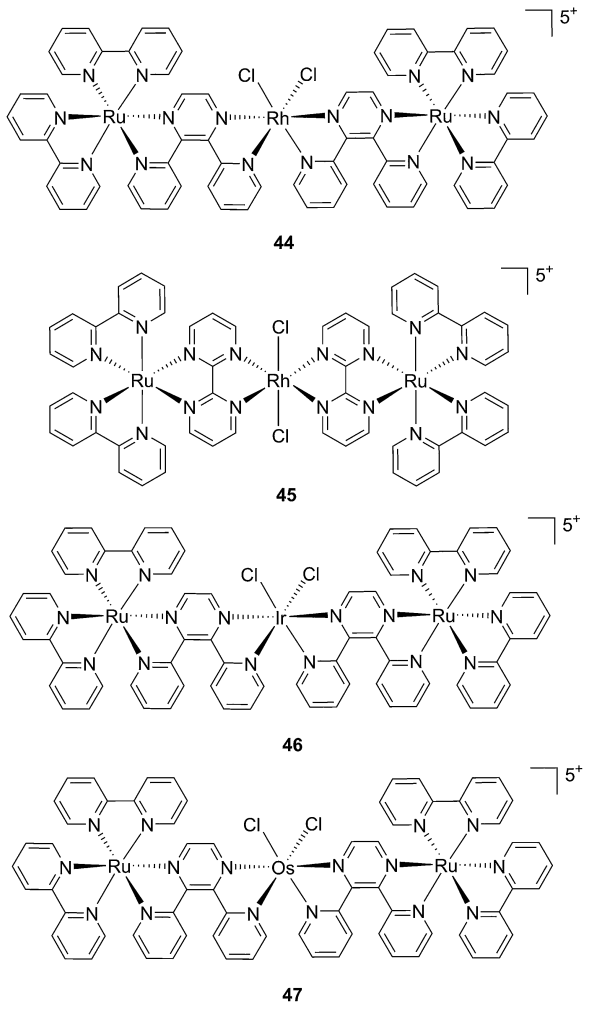

Fig. 31 Structures of the mixed-metal supramolecular complexes; (**44**) $[\{(bipy)_2Ru(dpp)\}_2RhCl_2]^{5+}$, (**45**) $[\{(bipy)_2Ru(bpm)\}_2RhCl_2]^{5+}$, (**46**) $[\{(bipy)_2Ru(dpp)\}_2IrCl_2]^{5+}$, and (**47**) $[\{(bipy)_2Ru(dpp)\}_2OsCl_2]^{5+}$.[97,99]

Gene silencing (ODN strategy)

Another attractive approach to target DNA is the use of oligodeoxyribonucleotides (ODNs) to inhibit gene expression. ODNs can act on different kinds of targets, namely double-stranded DNA by triple helix formation (antigene strategy) or mRNA (antisense strategy). However, these strategies suffer from the low stability of ODNs, their ineffective delivery into cells and from the low affinity of the ODNs for the target sequence. To overcome these drawbacks, chemically modified ODNs have been investigated with different moieties, including ruthenium complexes. In the last few years, the group of Kirsch-De Mesmaeker focused its attention on the detection of nucleic acids using metal complexes.[100] As an example, they employed highly photo-reactive Ru complexes to irreversibly crosslink ODNs to a DNA target sequence. A photoinduced electron transfer (PET) takes place between a Ru complex and the guanine present in close vicinity in the complementary DNA sequence. This results in covalent binding between the Ru complex and the guanine, forming a crosslink (see Fig. 32). The authors first examined the different geometric factors influencing adduct formation using $[Ru(TAP)_2dip]^{2+}$ (dip = 4,7-diphenylphenanthroline) (**48**, Fig. 33). They demonstrated that guanines at the 3′ side of the complementary strand, compared to the ruthenium complex anchoring position, are more favorable for the recombination of radicals formed by PET (irradiation settings: 1 h at 4 °C with a mercury/xenon lamp (200 W) using a filter (2M KNO_3 solution)).[101]

In a follow-up study, the same group explored the importance of the anchoring position of the Ru complex with respect to the ODN sequence. To do so, the photo-reactive polyazaaromatic complex $[Ru(TAP)_2(dppz)]^{2+}$ was coupled to the ODN sequence either *via* the dppz (*alias* Ru(D) (**49**) in Fig. 34) or the TAP moiety (*alias* Ru(T) (**50**) in Fig. 34). Adduct formation efficiencies and DNA interactions were evaluated. The authors found that both versions of anchored Ru complexes had the same DNA photo-ligation efficiency upon light irradiation (442 nm, 50 mW, 60 min) but, interestingly, they interacted with DNA in a different fashion. Whilst Ru(T) interacts by

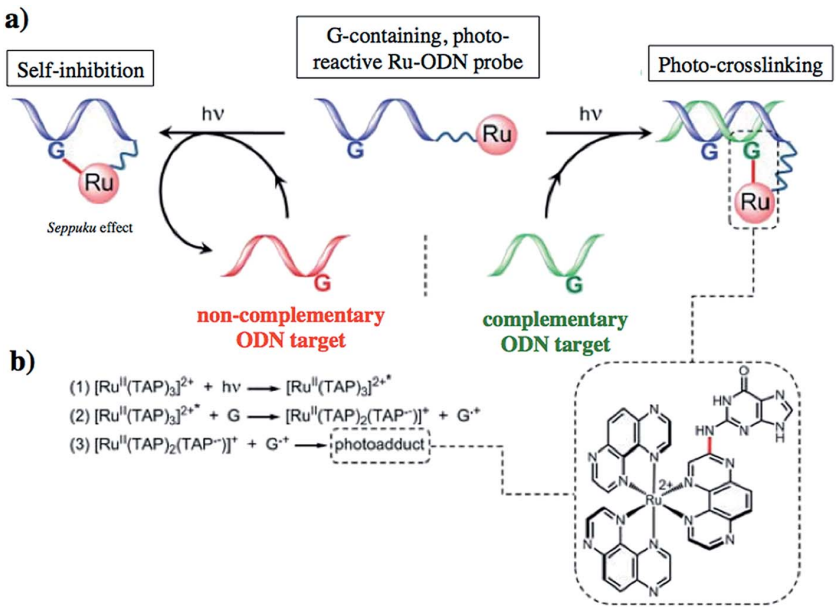

Fig. 32 (a) Schematic representation of the Ru–ODN strategy, (b) explanation of the adduct formation. Adapted from ref. 102.

intercalation with the dppz ligand, Ru(D) interacts *via* TAP without intercalation. On one hand, dppz intercalation places the ruthenium center in direct contact with the guanine, favoring the PET process and back electron transfer. However, this geometrical conformation secludes the reduced $TAP^{\bullet -}$ and oxidized $G^{+\bullet}$, thus reducing the photo-crosslinking efficiency. On the other hand, the TAP interaction puts $TAP^{\bullet -}$ and oxidized guanine in an optimal orientation for the photo-crosslinking reaction.[102]

This Ru–ODN strategy was examined in cell-based assays.[103] In their study, Delvenne and co-authors coupled the complementary sequence of the oncogene E6, stimulated after HPV16 infection and responsible for the silencing of p53, to a poly-azaaromatic complex $[Ru(TAP)_2(phen)]^{2+}$ (**51**, Fig. 35). With this tool in hand, they tested the efficiency of the conjugate for impairing HPV16 positive cervical cancer cell (SiHa) proliferation upon visible illumination. They could demonstrate an irreversible crosslink between the target and the Ru-conjugated probe. The authors could not only show reduced cell proliferation (45–50% growth inhibition on SiHa cells, 24 h post

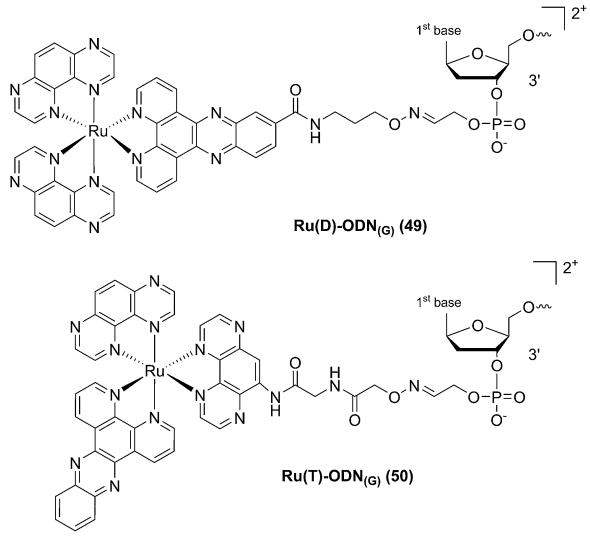

Fig. 34 Structures of the Ru(II) complexes with an ODN sequence coupled either on the dppz (**49**) or on the TAP (**50**) moiety.[102]

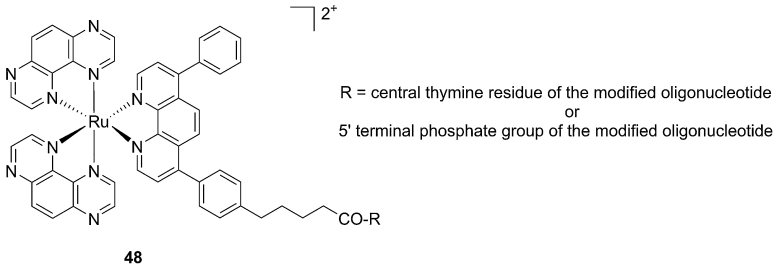

48

Fig. 33 Structure of the $[Ru(TAP)_2dip]^{2+}$ conjugated to the ODN sequences.[101]

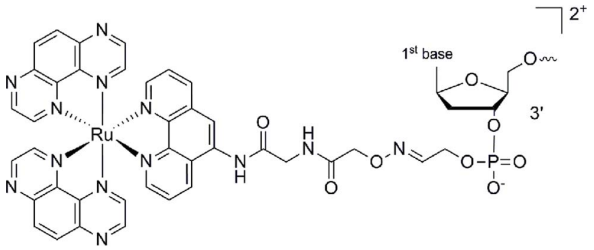

51

Fig. 35 Structure of $[Ru(TAP)_2(phen)]^{2+}$.[103]

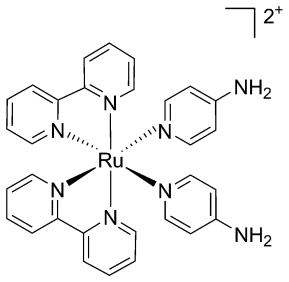

52

Fig. 36 Structure of the Ru(II) caged neuroactive 4-AP.[104]

illumination at 380–480 nm for 2 h 30), but also a restored amount of p53, which is the principal target of E6, as well as a reduced E6 protein level. The use of photo-reactive Ru complexes for conjugation to ODN sequences offers, in light of the studies presented above, an attractive tool in the field of gene silencing. On one hand, the presence of a metal complex can enhance cell delivery of the Ru–ODN due to the positive charge brought by the Ru complex. On the other hand, the affinity of the probe for the target is improved since an irreversible crosslink is induced upon light irradiation. Moreover, undesired non-specific interactions are avoided if the DNA target sequence is not present, since the complex is capable of auto-inhibition (the 'seppuku effect'), thus eliminating any collateral inhibition or crosslink (see Fig. 32).

Photo-release strategy

Modification of the activity of a compound can be achieved by masking the functional groups involved in the toxicity with a cleavable moiety, acting as a cage. The idea of using light-responsive cages to deliver biologically active compounds into living cells or organisms is extremely appealing, offering control over the cytotoxicity and improved cellular uptake thanks to the modulation of the lipophilicity or the insertion of a charge. However, to date, there are only a few examples reported in the literature. Those are described below.

Ruthenium complexes as caging moieties. The first study mentioned in this part of the perspective does not actually deal with cancer therapy, but presents for the first time the concept of using a Ru complex as a suitable cage for molecules bearing nitrogen atoms. Indeed, the $[Ru(II)(bipy)_2]$ fragment was the first ruthenium cage used to release a molecule. Etchenique *et al.* caged the neurocompound 4-aminopyridine (4-AP) (**52**, Fig. 36), which is known to promote neuronal activity by blocking specific K^+ channels.[104] The authors were able to monitor the electrical activity of a neuron within an isolated ganglion after photo-release of 4-AP. First, as expected, they confirmed that the caged 4-AP did not change the electric pulse when kept in the dark. A similar behavior was found for the cage itself. Nevertheless, upon pulsed irradiation (pulsed Xe lamp, 0.5 J per pulse, low pass filter at 480 nm), a signal similar to the one of the free 4-AP was detected, demonstrating the photo-release of the neuro-compound. Of note, Etchenique and coworkers presented the release of other bioactive compounds upon light activation such as GABA,[105–107] glutamate,[108,109] nicotine[110] and dopamine.[111] However, this impressive work is not discussed herein since it is not related to anticancer research.

Kodanko and collaborators, in turn, considered the latter study and the opportunity offered by Ru complexes to act as an effective photo-caging group for nitriles. They synthesized a Ru(II)tris(2-pyridylmethyl)amine complex **53**, functionalized with two molecules of a known cathepsin K inhibitor **54** containing a nitrile group (Cbz-Leu-$NHCH_2CN$) (Fig. 37).[112] In healthy tissue, cathepsin K is a proteinase secreted by osteoclasts to degrade bones. It was shown to be expressed by breast cancer metastasized to bones as well. The authors were able to demonstrate the inhibition of the enzymatic activity of cathepsin K upon light activation (365 nm for 15 min) even if only one molecule of the inhibitor was released (IC_{50} values of 5.6 μM in the dark *vs.* 63 nM upon light irradiation).

Driven by these promising *in vitro* results, the same authors chose a different Ru cage and a second cathepsin K inhibitor **55**, yielding the compounds **56** and **57** reported in Fig. 38.[113]

The new inhibitor **55** was chosen because of its better inhibition potency than **54** (reported IC_{50}: 35 and 9 nM for **54** and **55**, respectively). Moreover, using the $Ru(bipy)_2$ fragment as a cage, they could demonstrate that both nitrile ligands could be photoreleased. However, complex **57** required a longer exposure time to release the inhibitor (up to 60 min of irradiation) than complex **56** (15 min). Using the same experimental conditions (tungsten lamp, 250 W, >395 nm, H_2O filter), **56** and **57** showed significantly enhanced inhibition activities compared to the parent inhibitors **54** and **55** (IC_{50} values are 36 nM and 28 nM,

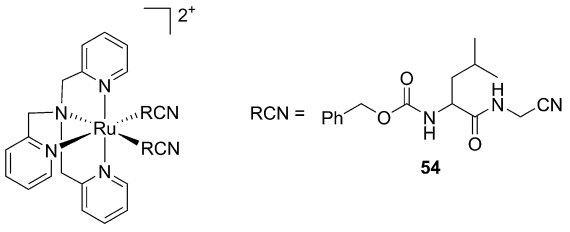

53 54

Fig. 37 Structures of caged cathepsin K inhibitor (Cbz-Leu-$NHCH_2$-CN) (RCN).[112]

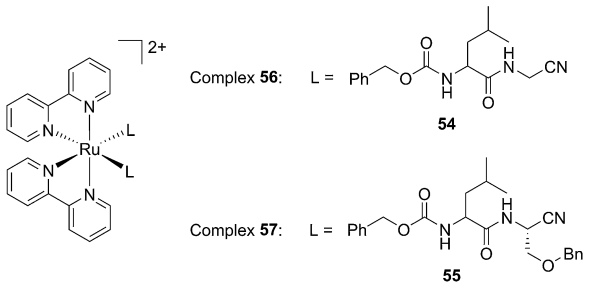

Fig. 38 Structures of the Ru(II) complexes containing cathepsin K inhibitors.[113]

respectively). Complex **56** showed a dark to light IC_{50} improvement from 560 nM to 16 nM (PI = 35). The photo-activated inhibition of cathepsin K is twice as effective as the parent inhibitor alone, correlating with the two molecules of inhibitor released. In the case of complex **57**, the dark to light IC_{50} enhancement was from 2.2 μM to 25 nM (PI = 88). The light-triggered inhibition is in good agreement with the slow release rate of the second inhibitor molecule, reaching a similar value to the free parent molecule **55**. In order to verify that none of the drugs or photoproducts were toxic in cells, the authors tested the viability of Bone Marrow Macrophages (BMM) and PC3 cells after 30 min incubation with the complexes, followed by a dark environment or 15 min irradiation for **56** or 40 min for **57** and 24 h additional incubation. They were able to confirm that no toxicity was found in murine BMM or PC3 cells up to 10 μM for complex **56** and up to 1 μM for **57**. Since **56** showed the most promising features, the authors evaluated its enzymatic inhibition ability in a cell-based assay. Enzymatic activity in osteoclasts decreased by 25% and 50% when treated with 100 nM and 1 μM, respectively, either with **54** or with the photo-activated **56** (see the enzymatic inhibition studies in mouse osteoclasts in Fig. 39 for **54** and Fig. 40 for **56**). These findings suggest that the photo-released enzyme inhibitors can play a potent role in the treatment of diseases where increased enzymatic activity is observed, sparing normal activity in surrounding tissues. These studies widen the perspective on the use of Ru(II) complexes as caging groups for the release of a large variety of biomolecules, from the pioneering $Ru(II)(bipy)_2$ fragment as a neurotransmitter releaser, to nitrile-based protease inhibitors.

Kodanko and colleagues applied the $Ru(bipy)_2$ fragment as a cage. However, compared to this, the Ru(II)tpy fragment offers a lower energy ^{1}MLCT absorption, fitting within the PDT window

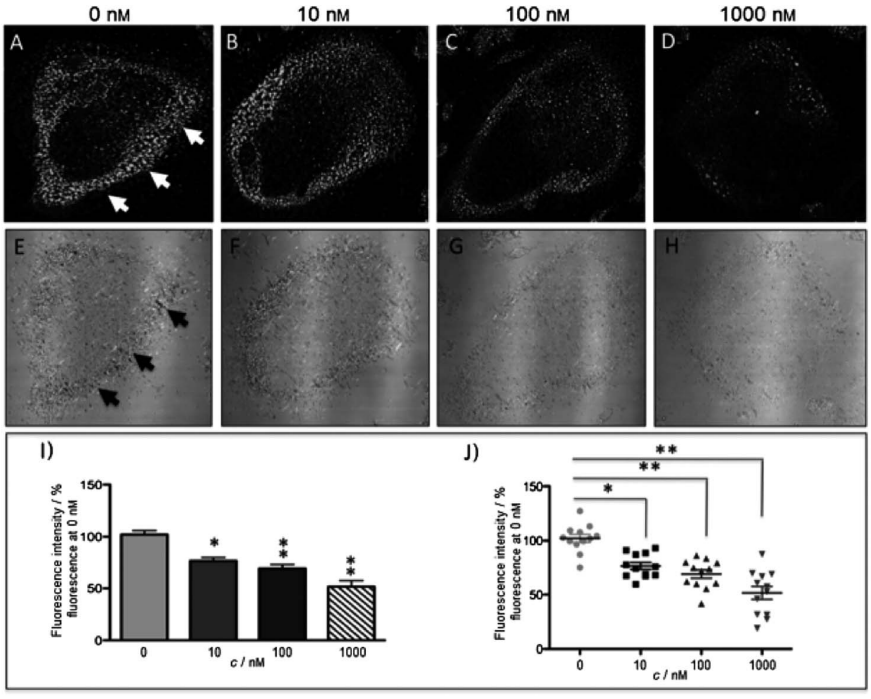

Fig. 39 Confocal microscopy images of mouse osteoclast cells treated with **54**. Cells were pre-incubated with **54** (10–1000 nm) for 30 min at 37 °C in the presence of cathepsin B inhibitor CA074Me (1 mm). Cells were treated with the cathepsin K substrate Z-LR-4MbNA (0.25 mm) and nitrosalicylaldehyde (1.0 mm, a precipitating agent), leading to the release of 4MbNA (green fluorescent precipitate indicative of cathepsin activity, arrows). Cells were fixed and imaged with a confocal laser scanning microscope (Zeiss LSM 780) using a 40× oil immersion lens. For each of the conditions at least six images of individual osteoclast cells were acquired, and fluorescence intensity per osteoclast area was measured and quantified using ImageJ software (NIH). The intensity of green fluorescence is a direct measure of the quantity of hydrolyzed and precipitated substrate (A–D), also visible on DIC images (E–H). The quantified data are shown as column (I) and dot (J) plots; $*p < 0.05$, $**p < 0.001$. Results are representative of at least three experiments. Reproduced with permission from ref. 113. © 2014 Wiley-VCH Verlag GmbH & Co. KGaA, Weinheim.

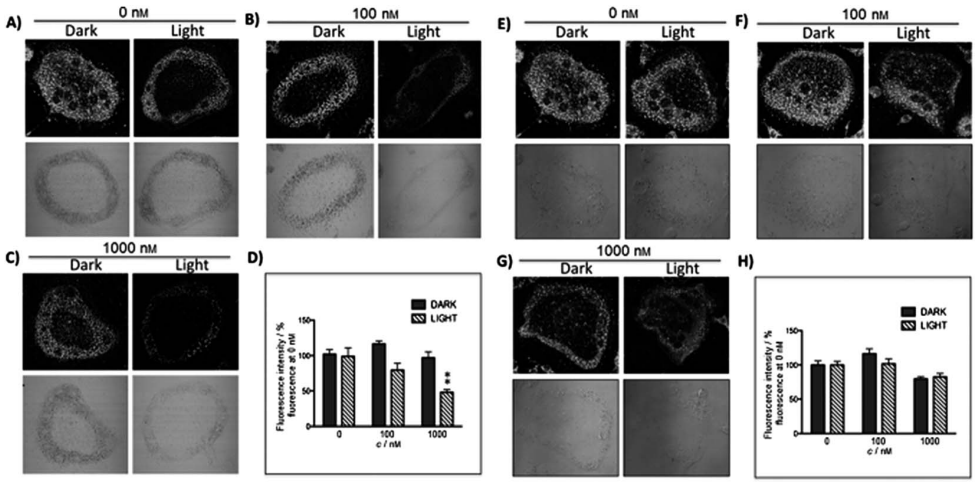

Fig. 40 Confocal microscopy images of mouse osteoclast cells treated with the ruthenium-caged inhibitor **56** (A–D) or *cis*-$[Ru(bpy)_2(MeCN)_2](PF_6)_2$ (E–H). Cells were pre-incubated with either complex (0–1000 nm) for 30 min at 37 °C in the presence of cathepsin B inhibitor CA074Me (1 mm), then exposed to dark (no irradiation) or light (irradiation at 250 W, 395–750 nm) conditions for 15 min. Cells were treated with the cathepsin K substrate Z-LR-4MbNA (0.25 mm) and nitrosalicylaldehyde (1.0 mm, a precipitating agent), leading to the release of 4MbNA (green fluorescent precipitate indicative of cathepsin activity). Cells were fixed and imaged with a confocal laser scanning microscope (Zeiss LSM 780) using a 40× oil immersion lens. For each of the conditions at least six images of individual osteoclast cells were acquired, and fluorescence intensity per osteoclast area was measured and quantified using ImageJ (NIH) software as described for Fig. 39 above; $^{**}p < 0.001$. Results are representative of at least three experiments. Reproduced with permission from ref. 113. © 2014 Wiley-VCH Verlag GmbH & Co. KGaA, Weinheim.

(600–850 nm). Turro *et al.* took this opportunity and designed a Ru(II)tpy complex able to induce the release of 5-cyanouracil (5CNU), a known pyrimidine catabolism inhibitor, upon irradiation with visible light (>400 nm). Since it was shown that the bis-aqua Ru derivative can bind DNA, the following $[Ru(tpy)(5CNU)_3]^{2+}$ complex (**59**, Fig. 41) can potentially be used as a dual-action therapeutic agent.[114]

Indeed, the authors demonstrated that similarly to its analog complex bearing $(CH_3CN)_3$ (**58**, Fig. 41), the complex efficiently released the two axial ligands when irradiated with visible light (150 W Xe lamp housed in a Milliarc compact arc lamp housing), concomitantly producing the bis-aqua species. Only the latter photoproduct was then able to bind to DNA as observed by a reduction in the plasmid pUC19 mobility, when complexes **58** and **59** were irradiated for 5 or 15 min, respectively. However, extending these observations to cellular studies was revealed to be more challenging. Indeed, when human cervical cancer HeLa cells were treated with 100 μM of the Ru complexes for 2 h in the dark, followed by 1 h light irradiation, only complex **59** was shown to be capable of generating damage (no damage was observed in non-irradiated cells for **58** and **59**). Moreover, cells treated with 100 μM of free 5CNU showed the same extent of damage as for complex **59** upon light irradiation, coinciding with only one molecule of 5CNU being released. The latter observation was confirmed when the LC_{50} value of irradiated **59** matched the one of free 5CNU (156 and 151 μM, respectively). In both cases, the mono-aqua photoproduct formed was not able to bind DNA. Accordingly, no decreased mobility was observed in agarose gel shift assay. This was also confirmed by the absence of cytotoxicity upon irradiation in the case of **58** or increased toxicity for **59**.

Ruthenium complexes as photo-released drug candidates. The photo-cleavage of a cage to release bioactive components is not a novel strategy since this method has been successfully used to release small organic molecules.[115] However, to the best of our knowledge, the specific release of a cytotoxic metal complex has never been reported before the work of our group. Indeed, we could recently successfully inactivate a previously characterized cytotoxic ruthenium complex (**61**)[116] by attachment to a photo-labile protecting group (PLPG) (**60**, Fig. 42). UPLC-MS experiments confirmed that, upon UV-A exposure, the original complex was released from the PLPG. As previously suggested by SAR studies,[50] we could demonstrate that caging reduced the toxicity of the Ru complex (IC_{50} > 100 μM in the dark) and that the original toxicity could be regained upon irradiation at 350 nm (2.58 J cm^{-2}) (17 μM). This value coincides with the value of the original non-caged complex (**61**).[51] We also

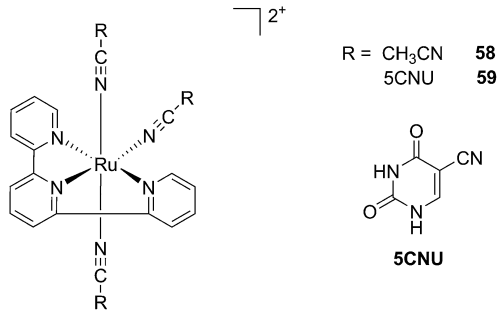

Fig. 41 Structures of the Ru-inhibitor complexes synthesized by Turro.[114]

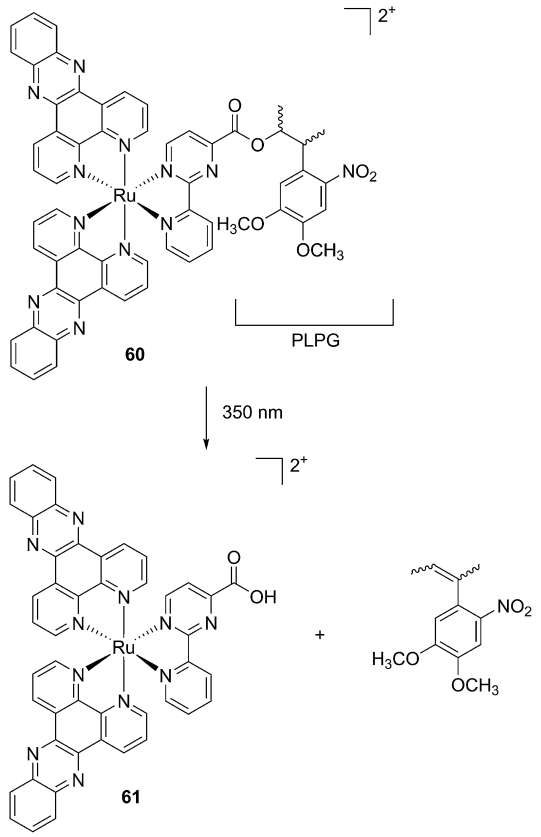

Fig. 42 Structures of the caged Ru(II) complex **60** and of the toxic photoproduct **61** which is released.[51]

investigated the fate of the Ru complexes by confocal microscopy. We could show that the caged complex was probably relocalizing from the cytoplasm and nucleoli (before light irradiation) to mitochondria, which were previously shown to be the preferential target of this complex.[116] Our group recently demonstrated that such a concept could be applied to a rhenium(I) organometallic complex.[51] Although there are a few advantages to use UV-A light as a trigger in the context of light-activated drugs, this type of light is only able to penetrate up to the derma, which protects tissues in the lower layers. Therefore, it would be of high interest to push the light activation of these drug candidates to the PDT or near-IR window.

Conclusions

As shown in this perspective article, Ru(II) complexes offer several opportunities as light-activated drug candidates. Although very promising *in vitro* results have been achieved so far, the lack of *in vivo* studies (to the best of our knowledge, there have only been three reported so far) undoubtedly does not allow for a full assessment of the suitability of such compounds in a clinical context. However, we are confident that more such studies will be reported in the near future, shedding light on the full potential of these compounds.

Abbreviations

[9]aneS_3	1,4,7-Trithiacyclononane
^{3}IL	Triplet intraligand
aPDT	Antibacterial PDT
ALA	Aminolevulinic acid
bipy	2,2′-Bipyridine
biq	2,2′-Biquinoline
bpm	2,2′-Bipyrimidine
CALI	Chromophore-assisted light inactivation
DAPI	4′,6-Diamidino-2-phenylindole
DLI	Drug to light interval
dmb	4,4′-Di-methyl-2,2′-bipyridine
dmdop	2,3-Dihydro-1,4-dioxino[2,3-*f*]-2,9-dimethyl-1,10-phenanthroline
dmphen	2,9-Dimethyl-1,10-phenanthroline
dop	2,3-Dihydro-1,4-dioxino[2,3-*f*]-1,10-phenanthroline
dpb	2,3-Bis(2-pyridyl)-benzoquinoxaline
dpp	2,3-Bis(2-pyridyl)pyrazine
dppn	Benzo[*i*]dipyrido[3,2-*a*:2′,3′-*c*]phenazine
dppz	Dipyrido[3,2-*a*:2′,3′-*c*]phenazine
DSSCs	Dye-sensitized solar cells
dtbb	4,4′-Di-*t*-butyl-2,2′-bipyridine
en	Ethylenediamine
GSH	Glutathione
HR-CS AAS	High-resolution continuum source atomic absorption spectrometry
ICP-MS	Inductively coupled plasma mass spectrometry
IPPBA	3-(1*H*-Imidazo[4,5-*f*][1,10]phenanthrolin-2yl)-phenylboronic acid
ISC	Intersystem crossing
MLCT	Metal to ligand charge transfer
MMCT	Metal to metal charge transfer
ODNs	Oligodeoxyribonucleotides
PACT	Photoactivated chemotherapy
PCNA	Proliferating cell nuclear antigen
PDT	Photodynamic therapy
PET	Photoinduced electron transfer
Ph_2phen	4,7-Diphenyl-1,10-phenanthroline
PHEHAT	1,10-Phenanthrolino[5,6-*b*]1,4,5,8,9,12-hexaazatriphenylene
phen	1,10-Phenanthroline
phpy	2-Phenylpyrydine
PI	Phototoxic index
PMP	5-(3-Pyridyl)-10,15,20-triphenylporphyrin
PS	Photosensitizer
PTP	5,10,15,20-Tetra(3-pyridyl)porphyrin
py	Pyridine
pydppn	3-(Pyrid-2′-yl)-4,5,9,16-tetraaza-dibenzo[*a*,*c*]-naphthacene
ROS	Reactive oxygen species
SAR	Structure activity relationship
SSBs	Single strand breaks
TAP	1,4,5,8-Tetraazaphenanthrene
TPA	Two photon absorption
tpph	Tetrapyrido[3,2-*a*:2′,3′-*c*:3″,2″-*h*:2‴,3‴]phenazine
tpy	[2,2′;6′,2″]-Terpyridine

Acknowledgements

This work was financially supported by the Swiss National Science Foundation (SNSF Professorship PP00P2_133568 to G.G.), the University of Zurich (G.G.), the Stiftung für Wissenschatliche Forschung of the University of Zurich (G.G. and S.F.), the Stiftung zur Krebsbekämpfung (S.F), the Huggenberger-Bischoff Stiftung (S.F) and the Hartmann-Müller Stiftung (S.F.).

References

1 A. Bergamo, C. Gaiddon, J. H. M. Schellens, J. H. Beijnen and G. Sava, *J. Inorg. Biochem.*, 2012, **106**, 90–99.
2 N. L. Kilah and E. Meggers, *Aust. J. Chem.*, 2012, **65**, 1325–1332.
3 L. Salassa, *Eur. J. Inorg. Chem.*, 2011, 4931–4947.
4 G. Sava, S. Zorzet, C. Turrin, F. Vita, M. Soranzo, G. Zabucchi, M. Cocchietto, A. Bergamo, S. DiGiovine, G. Pezzoni, L. Sartor and S. Garbisa, *Clin. Cancer Res.*, 2003, **9**, 1898–1905.
5 J. M. Rademaker-Lakhai, D. van den Bongard, D. Pluim, J. H. Beijnen and J. H. M. Schellens, *Clin. Cancer Res.*, 2004, **10**, 3717–3727.
6 C. G. Hartinger, S. Zorbas-Seifried, M. A. Jakupec, B. Kynast, H. Zorbas and B. K. Keppler, *J. Inorg. Biochem.*, 2006, **100**, 891–904.
7 C. G. Hartinger, M. A. Jakupec, S. Zorbas-Seifried, M. Groessl, A. Egger, W. Berger, H. Zorbas, P. J. Dyson and B. K. Keppler, *Chem. Biodiversity*, 2008, **5**, 2140–2155.
8 N. R. Dickson, S. F. Jones and H. A. Burris, *J. Clin. Oncol.*, 2011, **29**, suppl., abstr 2607.
9 A. Weiss, R. H. Berndsen, M. Dubois, C. Muller, R. Schibli, A. W. Griffioen, P. J. Dyson and P. Nowak-Sliwinska, *Chem. Sci.*, 2014, **5**, 4742–4748.
10 R. Trondl, P. Heffeter, C. R. Kowol, M. A. Jakupec, W. Berger and B. K. Keppler, *Chem. Sci.*, 2014, **5**, 2925–2932.
11 J. Maksimoska, L. Feng, K. Harms, C. Yi, J. Kissil, R. Marmorstein and E. Meggers, *J. Am. Chem. Soc.*, 2008, **130**, 15764–15765.
12 M. Doerr and E. Meggers, *Curr. Opin. Chem. Biol.*, 2014, **19**, 76–81.
13 F. Kratz, M. Hartmann, B. Keppler and L. Messori, *J. Biol. Chem.*, 1994, **269**, 2581–2588.
14 W. H. Ang, A. Casini, G. Sava and P. J. Dyson, *J. Organomet. Chem.*, 2011, **696**, 989–998.
15 P. J. Bednarski, F. S. Mackay and P. J. Sadler, *Anti-Cancer Agents Med. Chem.*, 2007, **7**, 75–93.
16 J. Rautio, H. Kumpulainen, T. Heimbach, R. Oliyai, D. Oh, T. Jarvinen and J. Savolainen, *Nat. Rev. Drug Discovery*, 2008, **7**, 255–270.
17 U. Schatzschneider, *Eur. J. Inorg. Chem.*, 2010, 1451–1467.
18 N. A. Smith and P. J. Sadler, *Philos. Trans. R. Soc., A*, 2013, **371**, 20120519.
19 O. J. Stacey and S. J. A. Pope, *RSC Adv.*, 2013, **3**, 25550–25564.
20 N. J. Farrer, L. Salassa and P. J. Sadler, *Dalton Trans.*, 2009, 10690–10701.
21 S. L. H. Higgins and K. J. Brewer, *Angew. Chem., Int. Ed. Engl.*, 2012, **51**, 11420–11422.
22 S. Swavey, *Ruthenium Complexes as Photosensitizers: New Possibilities in Photodynamic Therapy*, Nova Science Publishers, Inc., New York, 2011.
23 G. S. Smith and B. Therrien, *Dalton Trans.*, 2011, 10793–10800.
24 T. Joshi and G. Gasser, *Synlett*, 2014, DOI: 10.1055/s-0034-1379426.
25 J. Ghesquiere, S. Le Gac, L. Marcelis, C. Moucheron and A. Kirsch-De Mesmaeker, *Curr. Top. Med. Chem.*, 2012, **12**, 185–196.
26 E. C. Glazer, *Isr. J. Chem.*, 2013, **53**, 391–400.
27 A. P. Castano, T. N. Demidova and M. R. Hamblin, *Photodiagn. Photodyn. Ther.*, 2004, **1**, 279–293.
28 Z. Huang, *Technol. Cancer Res. Treat.*, 2005, **4**, 283–293.
29 K. Plaetzer, B. Krammer, J. Berlanda, F. Berr and T. Kiesslich, *Laser. Med. Sci.*, 2009, **24**, 259–268.
30 S. Bonnet, *Comments Inorg. Chem.*, 2014, DOI: 10.1080/02603594.02602014.02979286.
31 R. K. Pandey and C. K. Herman, *Chem. Ind.*, 1998, **18**, 739–743.
32 C. Lottner, K.-C. Bart, G. Bernhardt and H. Brunner, *J. Med. Chem.*, 2002, **45**, 2064–2078.
33 C. Lottner, K.-C. Bart, G. Bernhardt and H. Brunner, *J. Med. Chem.*, 2002, **45**, 2079–2089.
34 F. Schmitt, P. Govindaswamy, G. Süss-Fink, W. H. Ang, P. J. Dyson, L. Juillerat-Jeanneret and B. Therrien, *J. Med. Chem.*, 2008, **51**, 1811–1816.
35 F. Schmitt, P. Govindaswamy, O. Zava, G. Süss-Fink, L. Juillerat-Jeanneret and B. Therrien, *J. Biol. Inorg. Chem.*, 2009, **14**, 101–109.
36 M. Pernot, T. Bastogne, N. P. E. Barry, B. Therrien, G. Koellensperger, S. Hann, V. Reshetov and M. Barberi-Heyob, *J. Photochem. Photobiol., B*, 2012, **117**, 80–89.
37 F. Schmitt, N. P. E. Barry, L. Juillerat-Jeanneret and B. Therrien, *Bioorg. Med. Chem. Lett.*, 2012, **22**, 178–180.
38 F. Schmitt, J. Freudenreich, N. P. E. Barry, L. Juillerat-Jeanneret, G. Süss-Fink and B. Therrien, *J. Am. Chem. Soc.*, 2012, **134**, 754–757.
39 T. Gianferrara, I. Bratsos, E. Iengo, B. Milani, A. Ostric, C. Spagnul, E. Zangrando and E. Alessio, *Dalton Trans.*, 2009, 10742–10756.
40 T. Gianferrara, A. Bergamo, I. Bratsos, B. Milani, C. Spagnul, G. Sava and E. Alessio, *J. Med. Chem.*, 2010, **53**, 4678–4690.
41 B. Serli, E. Zangrando, T. Gianferrara, C. Scolaro, P. J. Dyson, A. Bergamo and E. Alessio, *Eur. J. Inorg. Chem.*, 2005, 3423–3434.
42 I. Bratsos, S. Jedner, A. Bergamo, G. Sava, T. Gianferrara, E. Zangrando and E. Alessio, *J. Inorg. Biochem.*, 2008, **102**, 1120–1133.
43 S. Rani-Beeram, K. Meyer, A. McCrate, Y. Hong, M. Nielsen and S. Swavey, *Inorg. Chem.*, 2008, **47**, 11278–11283.
44 P. Sweigert, Z. Xu, Y. Hong and S. Swavey, *Dalton Trans.*, 2012, 5201–5208.

45 J. Yoho, C. Stroh, S. Swavey and M. Kango-Singh, *Genesis*, 2014, **52**, 309–314.
46 B. M. Zeglis, V. C. Pierre and J. K. Barton, *Chem. Commun.*, 2007, 4565–4579.
47 M. R. Gill, J. Garcia-Lara, S. J. Foster, C. Smythe, G. Battaglia and J. A. Thomas, *Nat. Chem.*, 2009, **1**, 662–667.
48 U. Schatzschneider, J. Niesel, I. Ott, R. Gust, H. Alborzinia and S. Wölfl, *ChemMedChem*, 2008, **3**, 1104–1109.
49 V. Pierroz, T. Joshi, A. Leonidova, C. Mari, J. Schur, I. Ott, L. Spiccia, S. Ferrari and G. Gasser, *J. Am. Chem. Soc.*, 2012, **134**, 20376–20387.
50 T. Joshi, V. Pierroz, S. Ferrari and G. Gasser, *ChemMedChem*, 2014, **9**, 1419–1427.
51 T. Joshi, V. Pierroz, C. Mari, L. Gemperle, S. Ferrari and G. Gasser, *Angew. Chem., Int. Ed. Engl.*, 2014, **53**, 2960–2963.
52 J. X. Zhang, J. W. Zhou, C. F. Chan, T. C. K. Lau, D. W. J. Kwong, H. L. Tam, N. K. Mak, K. L. Wong and W. K. Wong, *Bioconjugate Chem.*, 2012, **23**, 1623–1638.
53 C. Mari, V. Pierroz, R. Rubbiani, M. Patra, J. Hess, B. Spingler, L. Oehninger, J. Schur, I. Ott, L. Salassa, S. Ferrari and G. Gasser, *Chem.–Eur. J.*, 2014, **20**, 14421–14436.
54 M. T. Mongelli, J. Heinecke, S. Mayfield, B. Okyere, B. S. J. Winkel and K. J. Brewer, *J. Inorg. Biochem.*, 2006, **100**, 1983–1987.
55 Y. Sun, L. E. Joyce, N. M. Dickson and C. Turro, *Chem. Commun.*, 2010, **46**, 2426–2428.
56 Y. Liu, R. Hammitt, D. A. Lutterman, L. E. Joyce, R. P. Thummel and C. Turro, *Inorg. Chem.*, 2009, **48**, 375–385.
57 R. Zhao, R. Hammitt, R. P. Thummel, Y. Liu, C. Turro and R. M. Snapka, *Dalton Trans.*, 2009, 10926–10931.
58 S. I. Bae, R. Zhao and R. M. Snapka, *Biochem. Pharmacol.*, 2008, **76**, 1653–1668.
59 G. C. Vougioukalakis, A. I. Philippopoulos, T. Stergiopoulos and P. Falaras, *Coord. Chem. Rev.*, 2011, **255**, 2602–2621.
60 A. Frei, R. Rubbiani, S. Tubafard, O. Blacque, P. Anstaett, A. Felgenträger, T. Maisch, L. Spiccia and G. Gasser, *J. Med. Chem.*, 2014, **57**, 7280–7292.
61 M. Dickerson, Y. Sun, B. Howerton and E. C. Glazer, *Inorg. Chem.*, 2014, **53**, 10370–10377.
62 R. Lincoln, L. Kohler, S. Monro, H. Yin, M. Stephenson, R. Zong, A. Chouai, C. Dorsey, R. Hennigar, R. P. Thummel and S. A. McFarland, *J. Am. Chem. Soc.*, 2013, **135**, 17161–17175.
63 B. Zbytek, J. A. Carlson, J. Granese, J. Ross, M. Mihm and A. Slominski, *Expert Rev. Dermatol.*, 2008, **3**, 569–585.
64 H. Yin, M. Stephenson, J. Gibson, E. Sampson, G. Shi, T. Sainuddin, S. Monro and S. A. McFarland, *Inorg. Chem.*, 2014, **53**, 4548–4559.
65 G. Shi, S. Monro, R. Hennigar, J. Colpitts, J. Fong, K. Kasimova, H. Yin, R. DeCoste, C. Spencer, L. Chamberlain, A. Mandel, L. Lilge and S. A. McFarland, *Coord. Chem. Rev.*, 2014, **282–283**, 127–138.
66 Y. Arenas, S. Monro, G. Shi, A. Mandel, S. McFarland and L. Lilge, *Photodiagn. Photodyn. Ther.*, 2013, **10**, 615–625.
67 J. Lee, D. G. Udugamasooriya, H.-S. Lim and T. Kodadek, *Nat. Chem. Biol.*, 2010, **6**, 258–260.
68 X. Liu, M. Dix, A. E. Speers, D. A. Bachovchin, A. M. Zuhl, B. F. Cravatt and T. J. Kodadek, *ChemBioChem*, 2012, **13**, 2082–2093.
69 A. L. Harris, *Nat. Rev. Cancer*, 2002, **2**, 38–47.
70 D. Hanahan and R. A. Weinberg, *Cell*, 2011, **144**, 646–674.
71 Y. H. Hsiang, R. Hertzberg, S. Hecht and L. F. Liu, *J Biol Chem*, 1985, **260**, 14873–14878.
72 B. Lippert, *Cisplatin, Chemistry and Biochemistry of a Leading Anticancer Drug*, Verlag Helvetica Chimica Acta: Zürich, Wiley_VCH, Weinheim, Germany, 1999, pp. 111–134.
73 Z. H. Siddik, *Oncogene*, 2003, **22**, 7265–7279.
74 K. M. Comess, J. N. Burstyn, J. M. Essigmann and S. J. Lippard, *Biochemistry*, 1992, **31**, 3975–3990.
75 Y. Corda, M. F. Anin, M. Leng and D. Job, *Biochemistry*, 1992, **31**, 1904–1908.
76 J. M. Rosenberg and P. H. Sato, *Mol. Pharmacol.*, 1993, **43**, 491–497.
77 A. J. Deans and S. C. West, *Nat. Rev. Cancer*, 2011, **11**, 467–480.
78 F. S. Mackay, J. A. Woods, H. Moseley, J. Ferguson, A. Dawson, S. Parsons and P. J. Sadler, *Chem.–Eur. J.*, 2006, **12**, 3155–3161.
79 F. S. Mackay, J. A. Woods, P. Heringová, J. Kašpárková, A. M. Pizarro, S. A. Moggach, S. Parsons, V. Brabec and P. J. Sadler, *Proc. Natl. Acad. Sci. U. S. A.*, 2007, **104**, 20743–20748.
80 A. F. Westendorf, J. A. Woods, K. Korpis, N. J. Farrer, L. Salassa, K. Robinson, V. Appleyard, K. Murray, R. Grünert, A. M. Thompson, P. J. Sadler and P. J. Bednarski, *Mol. Cancer Ther.*, 2012, **11**, 1894–1904.
81 Y. Zhao, J. A. Woods, N. J. Farrer, K. S. Robinson, J. Pracharova, J. Kasparkova, O. Novakova, H. Li, L. Salassa, A. M. Pizarro, G. J. Clarkson, L. Song, V. Brabec and P. J. Sadler, *Chem.–Eur. J.*, 2013, **19**, 9578–9591.
82 B. Durham, J. V. Caspar, J. K. Nagle and T. J. Meyer, *J. Am. Chem. Soc.*, 1982, **104**, 4803–4810.
83 P. C. Ford, *Coord. Chem. Rev.*, 1982, **44**, 61–82.
84 B. S. Howerton, D. K. Heidary and E. C. Glazer, *J. Am. Chem. Soc.*, 2012, **134**, 8324–8327.
85 A. N. Hidayatullah, E. Wachter, D. K. Heidary, S. Parkin and E. C. Glazer, *Inorg. Chem.*, 2014, **53**, 10030–10032.
86 E. Wachter, D. K. Heidary, B. S. Howerton, S. Parkin and E. C. Glazer, *Chem. Commun.*, 2012, **48**, 9649–9651.
87 B. Peña, A. David, C. Pavani, M. S. Baptista, J.-P. Pellois, C. Turro and K. R. Dunbar, *Organometallics*, 2014, **33**, 1100–1103.
88 B. A. Albani, B. Peña, K. R. Dunbar and C. Turro, *Photochem. Photobiol. Sci.*, 2014, **13**, 272–280.
89 P. G. Bomben, K. C. D. Robson, P. A. Sedach and C. P. Berlinguette, *Inorg. Chem.*, 2009, **48**, 9631–9643.
90 C. Gaiddon, P. Jeannequin, P. Bischoff, M. Pfeffer, C. Sirlin and J. P. Loeffler, *J. Pharmacol. Exp. Ther.*, 2005, **315**, 1403–1411.

91 A. M. Palmer, B. Peña, R. B. Sears, O. Chen, M. El Ojaimi, R. P. Thummel, K. R. Dunbar and C. Turro, *Philos. Trans. R. Soc., A*, 2013, **371**, 20120135.
92 W. Guo, W. Zheng, Q. Luo, X. Li, Y. Zhao, S. Xiong and F. Wang, *Inorg. Chem.*, 2013, **52**, 5328–5338.
93 M. Pongratz, P. Schluga, M. A. Jakupec, V. B. Arion, C. G. Hartinger, G. Allmaier and B. K. Keppler, *J. Anal. At. Spectrom.*, 2004, **19**, 46–51.
94 F. Barragán, P. López-Senín, L. Salassa, S. Betanzos-Lara, A. Habtemariam, V. Moreno, P. J. Sadler and V. Marchán, *J. Am. Chem. Soc.*, 2011, **133**, 14098–14108.
95 W. Vanderlinden, M. Blunt, C. C. David, C. Moucheron, A. Kirsch-De Mesmaeker and S. De Feyter, *J. Am. Chem. Soc.*, 2012, **134**, 10214–10221.
96 Y. Chen, W. Lei, G. Jiang, Y. Hou, C. Li, B. Zhang, Q. Zhou and X. Wang, *Dalton Trans.*, 2014, 15375–15384.
97 S. Swavey and K. J. Brewer, *Inorg. Chem.*, 2002, **41**, 6196–6198.
98 A. Sitlani, E. C. Long, A. M. Pyle and J. K. Barton, *J. Am. Chem. Soc.*, 1992, **114**, 2303–2312.
99 A. A. Holder, D. F. Zigler, M. T. Tarrago-Trani, B. Storrie and K. J. Brewer, *Inorg. Chem.*, 2007, **46**, 4760–4762.
100 L. Marcélis, W. Vanderlinden and A. Kirsch - De Mesmaeker, in *Inorganic Chemical Biology*, ed. G. Gasser, Wiley-VCH Verlag GmbH & Co. KGaA, 2014.
101 O. Lentzen, J.-F. Constant, E. Defrancq, M. Prévost, S. Schumm, C. Moucheron, P. Dumy and A. Kirsch-De Mesmaeker, *ChemBioChem*, 2003, **4**, 195–202.
102 S. Le Gac, M. Foucart, P. Gerbaux, E. Defrancq, C. Moucheron and A. Kirsch-De Mesmaeker, *Dalton Trans.*, 2010, 9672–9683.
103 A. Reschner, S. Bontems, S. Le Gac, J. Lambermont, L. Marcélis, E. Defrancq, P. Hubert, C. Moucheron, A. Kirsch-De Mesmaeker, M. Raes, J. Piette and P. Delvenne, *Gene Ther.*, 2013, **20**, 435–443.
104 L. Zayat, C. Calero, P. Alborés, L. Baraldo and R. Etchenique, *J. Am. Chem. Soc.*, 2003, **25**, 882–883.
105 L. Zayat, M. G. Noval, J. Campi, C. I. Calero, D. J. Calvo and R. Etchenique, *ChemBioChem*, 2007, **8**, 2035–2038.
106 V. Lopes-dos-Santos, J. Campi, O. Filevich, S. Ribeiro and R. Etchenique, *Braz. J. Med. Biol. Res.*, 2011, **44**, 688–693.
107 O. Filevich and R. Etchenique, *Photochem. Photobiol. Sci.*, 2013, **12**, 1565–1570.
108 E. Fino, R. Araya, D. S. Peterka, M. Salierno, R. Etchenique and R. Yuste, *Front. Neural Circuits*, 2009, **3**, 1–9.
109 M. Salierno, E. Marceca, D. S. Peterka, R. Yuste and R. Etchenique, *J. Inorg. Chem.*, 2010, **104**, 418–422.
110 O. Filevich, M. Salierno and R. Etchenique, *J. Inorg. Biochem.*, 2010, **104**, 1248–1251.
111 R. Araya, V. Andino-Pavlovsky, R. Yuste and R. Etchenique, *ACS Chem. Neurosci.*, 2013, **4**, 1163–1167.
112 R. Sharma, J. D. Knoll, P. D. Martin, I. Podgorski, C. Turro and J. J. Kodanko, *Inorg. Chem.*, 2014, **53**, 3272–3274.
113 T. Respondek, R. Sharma, M. K. Herroon, R. N. Garner, J. D. Knoll, E. Cueny, C. Turro, I. Podgorski and J. J. Kodanko, *ChemMedChem*, 2014, **9**, 1306–1315.
114 M. A. Sgambellone, A. David, R. N. Garner, K. R. Dunbar and C. Turro, *J. Am. Chem. Soc.*, 2013, **135**, 11274–11282.
115 G. Mayer and A. Heckel, *Angew. Chem., Int. Ed. Engl.*, 2006, **45**, 4900–4921.
116 V. Pierroz, T. Joshi, A. Leonidova, C. Mari, J. Schur, I. Ott, L. Spiccia, S. Ferrari and G. Gasser, *J. Am. Chem. Soc.*, 2012, **134**, 20376–20387.

1.3. DNA DAMAGE AND REPAIR

1.3.1. SHORT OVERVIEW OF DNA DAMAGES AND RESPONSE MECHANISMS

The genomic integrity is continuously challenged by endogenous (oxygen radicals, replication errors, etc) and exogenous (UV light, alkylating and crosslinking agents, etc) stresses that cause DNA damage as represented in Figure 4. Each type of DNA lesions is processed by a specific repair pathway according to a common scheme: detection of the lesion, recruitment of the repair machinery to the site of damage and repair of the lesion.[31]

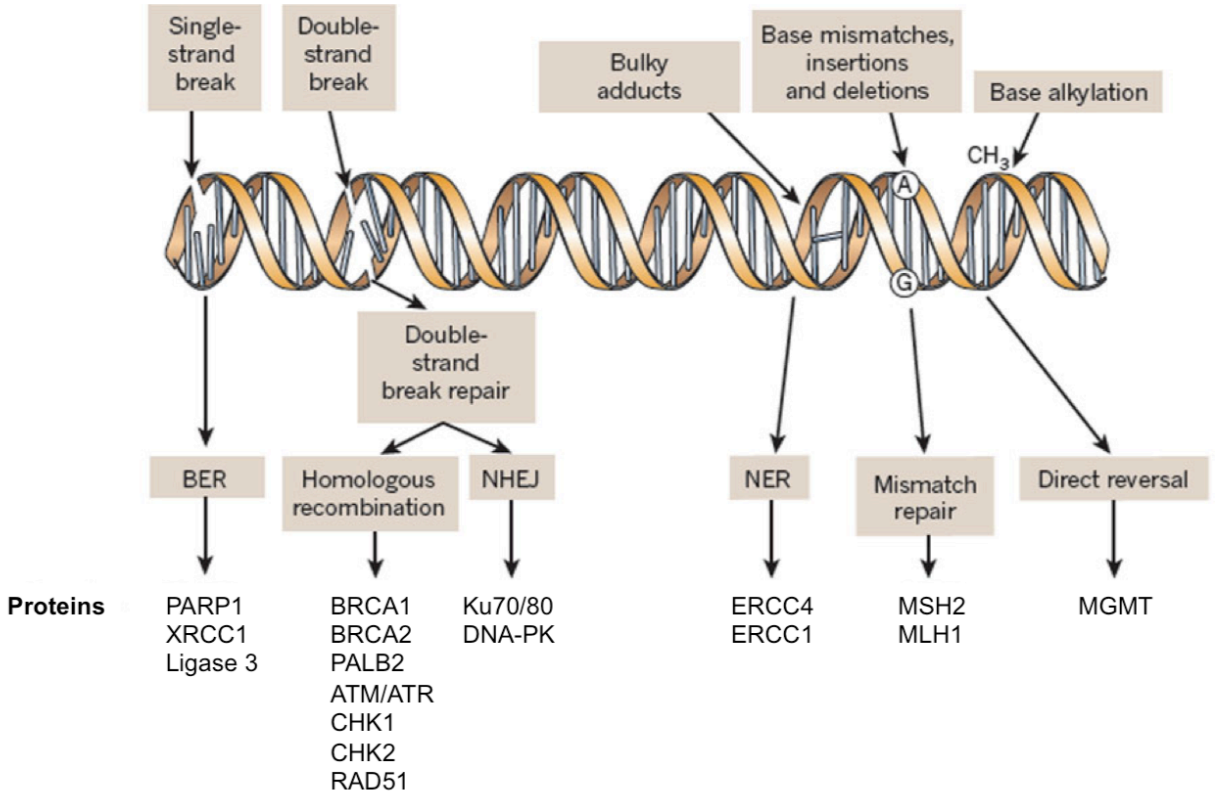

Figure 4. Overview of DNA damage and repair. Adapted from ref [31].

1.3.2. CISPLATIN INDUCED DNA DAMAGES AND REPAIR MECHANISM

1.3.2.1. INTRA-STRAND DNA CROSSLINK

Cisplatin induced intra-strand DNA crosslinks produce a kink in the DNA structure, which is recognized and repaired by the NER pathway.[17] This pathway is also

responsible for the repair of DNA bulky lesions caused by UV damage, mostly thymine dimers and 6-4 PP (Figure 5). Two NER pathways are distinguished, the global genomic NER (GG-NER) and the transcription coupled NER (TC-NER). The principal difference is that in the case of TC-NER, the lesion is recognized by the RNA polymerase, whereas in the GG-NER, XPC-HR23B, XPA and RPA are involved in sensing the lesion. After lesion recognition, the transcription factor TFIIH is recruited to the site of damage. The TFIIH subunits XPB and XPD, two helicases, open the DNA surrounding the lesion. This conformational change allows then the recruitment of other factors, such as XPG. The role of RPA in this context is to protect the single stranded DNA from nucleases, while the endonuclease XPG, make the first 3' incision. The role of XPA in this process is still unclear. The ERCC1-XPF endonuclease is recruited to perform the 5' incision, liberating a 24-32 oligomer. In the presence of PCNA, polymerases δ or ε can then refill the gap, which will be closed by DNA Ligase I.[32, 33] Defects in the NER reaction lead to xeroderma pigmentosum, a disease characterized by severe sensitivity to sunlight with high risk to develop cancer. This is due to the deficiency in the repair of UV-mediated damage.[34]

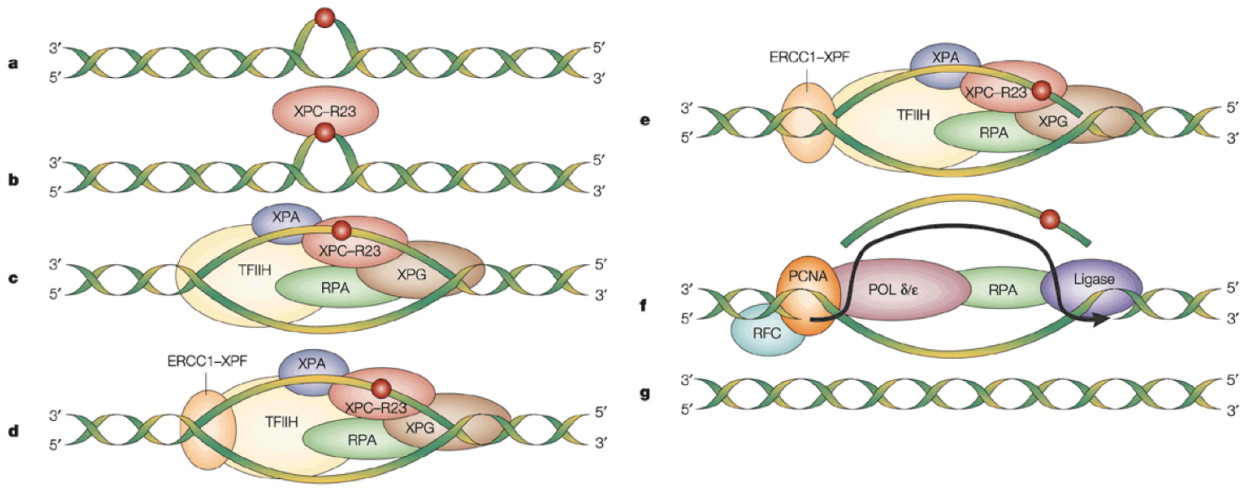

Figure 5. Cisplatin intra-strand DNA crosslink repair by GG-NER. Adapted from ref [32].

1.3.2.2. INTER-STRAND DNA CROSSLINK

The minor in number but major in effect are inter-strand DNA crosslinks. Such lesions require the Fanconi Anemia (FA) protein complex as well as the Homologous recombination (HR) pathway for repair (Figure 6). Inter-strand crosslink are highly

toxic because they interfere with fundamental cellular processes like DNA replication and transcription that necessitate strand separation.[35] The recognition of inter-strand crosslinks is operated by FANCM and associated proteins (FAAP20, FAAP24, FAAP100) and promotes the recruitment and activation of the FA core complex (FANC-A, B, C, E, F, G, L). FANCL, an E3-ligase, monoubiquitinates the FANCI-D2 heterodimer. The latter can then recruit the nuclease FAN1 and with the cooperation of other structure specific nucleases, such as MUS81-EME1, SNM1A, XPF-ERCC1 and SLX1-SLX4, the inter-strand DNA crosslink is incised and unhooked. Fork stabilization and complete repair is now undertaken by Homologous recombination (HR) machinery. Briefly, RPA DNA coating protein is replaced by RAD51 with the help of factor such as BRCA2, which control the search for homology and strand invasion. RAD54, a DNA-dependent ATPase stabilizes the RAD51-ssDNA complex. The polymerase ζ fills the gap and Holiday junctions are resolved by specific endonucleases mentioned above.[36]

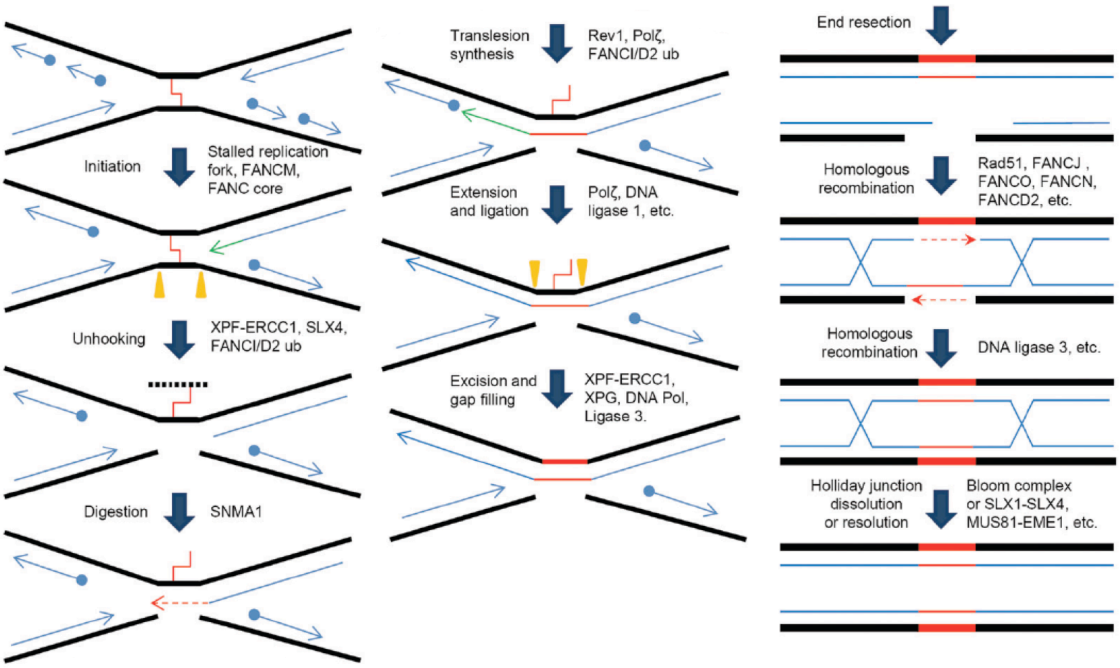

Figure 6. Cisplatin inter-strand DNA crosslink repair during replication. Adapted from ref [36].

1.3.3. Oxidative DNA base lesions: 8-oxo-Guanines

Oxidative stress and resulting base oxidation such as 8-oxo-Guanine, are repaired in cells by the Base Excision Repair (BER) pathway (Figure 7). The key protein in this repair is 8-oxoguanine DNA glycosylase 1 (OGG1) that removes 8-oxo-G lesions, leaving an abasic apurinic/apyrimidinic (AP) site. AP endonuclease 1 (APE1) can then cut at the 5' site of the sugar, leaving either a native or an oxidized 5'-sugar phosphate. In the case of the native sugar, polymerase β will remove the sugar thanks to its 5′-deoxyribose phosphate (dRP) lyase activity and refill the gap before ligation (Single Nucleotide Excision). In the second case, where the sugar is oxidized, two or more nucleotides can be excised. Two nucleotides are removed by the help of the flap endonuclease FEN1, that substitutes for the (dRP) lyase activity deficiency of polymerase β. In this case we talk of long-patch BER. More than two nucleotides are removed by DNA strand-displacement synthesis mediated by polymerase β or δ/ε, FEN1 operates the cleavage and the strand is religated.[37]

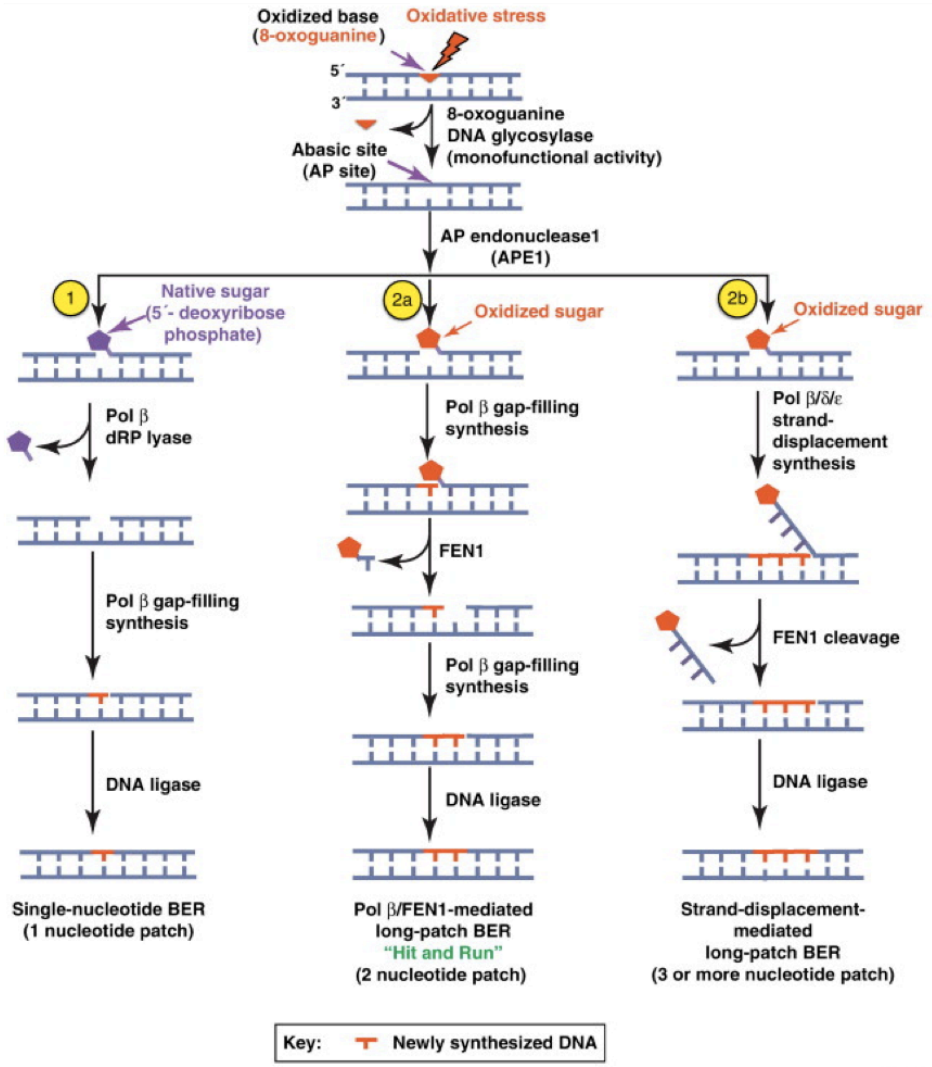

Figure 7. Oxidized base repair by BER pathway. Taken from ref [37].

In the situation of OGG1 overload, non-excised 8-oxo-Gs can persist and are addressed in the next cell cycle (Figure 8). In this case, the Mismatch Repair (MMR) machinery is involved. Indeed, polymerase β will recognize an 8-oxo-G as a thymine (T) and mispairs it with an adenine (A). If this error is not resolved before the next cell cycle, a transversion mutation CG -> AT will occur. The role of MUTYH is then crucial in this process. MUTYH will excise the mismatched A, leaving an apurinic site to be processes by APE1 with the help of FEN1, PCNA, RPA, polymerase λ and the ligase.[38] MUTYH can give then a second chance to OGG1 to remove the oxidized base, but if the latter is still overloaded, it can give rise to a futile cycle, that will lead ultimately to apoptosis.[39] Recently, MutSβ, a protein involved in the mismatch

recognition in MMR, has been found to recognize cisplatin inter-strand DNA crosslinks.[40]

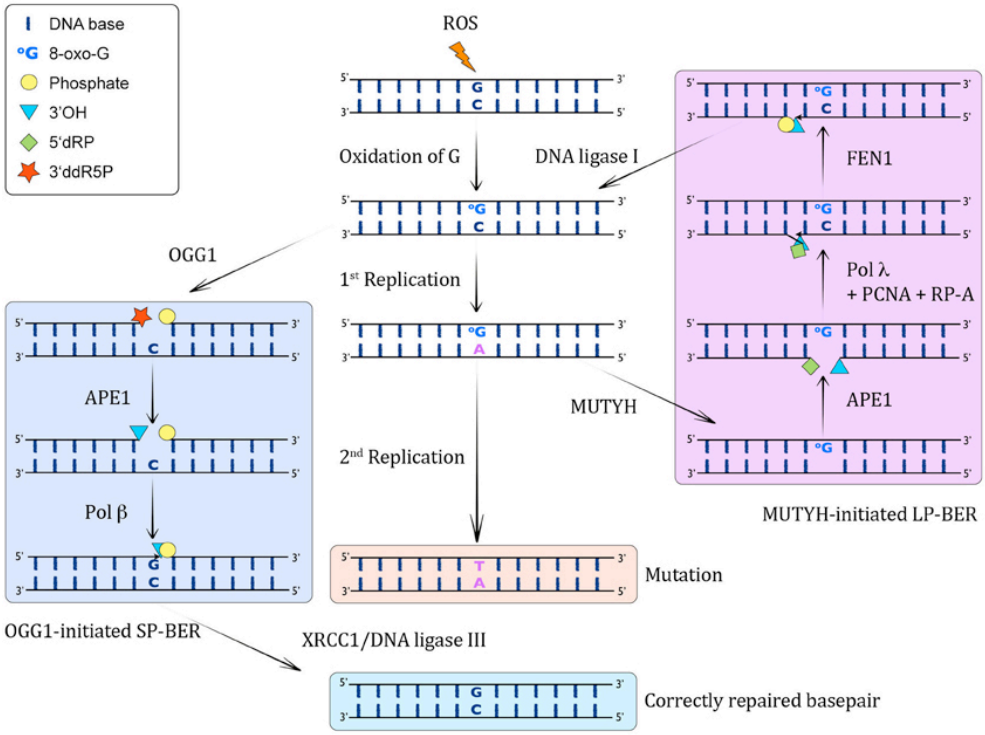

Figure 8. 8-oxo-G repair outcome. Taken from ref [38].

UV-induced SSBs and photosensitization: repair mechanism

It has been reported that SSBs can be produced by UV and visible wavelengths in the 240-546 nm range.[41] It is also possible to induce SSBs by means of intermediate molecules that will act as photosensitizers. These photosensitizing molecules will transfer the energy of the light absorbed via electron transfer or energy transfer to surrounding molecules, such as water or bases, thereby creating SSBs.[42] The case of Ruthenium based photosensitizers is discussed in section 1.2. SSBs will be recognized by PARP1 and repaired by BER excision repair pathway.

2. Results

Project 1: Photo-uncaging of Ru(II) complex in living cells using UV-A irradiation as trigger.

This study is divided into 3 articles. In the first one, the promising biological effects of a Ru(II) complex on cancer cells have been investigated. The following SAR study revealed that the carboxylic function of the complex is crucial for toxicity. Finally, the biological deactivation of this complex by coordination of a photo-protecting group and its efficient release upon light irradiation is depicted in the last study.

Project 2: Investigation of the mechanisms of action and repair of an efficient photosensitizer Ru(II) complex upon UV-A irradiation.

2.1. PHOTO-ACTIVATED UNCAGING OF RU(II) COMPLEXES IN CANCER CELLS (PACT)

The aim of this study is to specifically deliver metal complexes to living cells using light as an external trigger. We could show that such concept is potentially relevant for cancer therapy and PACT in general. We used a substitutionally-inert bis(dppz)-Ru(II) complex as anticancer drug candidate and UV-A light as trigger.

2.1.1. CONTRIBUTIONS TO THE ARTICLES

V.P.: performed all the biological experiments; viability assays, microscopy, MMP assay, FACS, mitochondria extraction.

2.1.2. MOLECULAR AND CELLULAR CHARACTERIZATION OF THE BIOLOGICAL EFFECTS OF RUTHENIUM(II) COMPLEXES INCORPORATING 2-PYRIDYL-2-PYRIMIDINE-4-CARBOXYLIC ACID

After identification of a promising anticancer drug candidate, namely $[Ru(dppz)_2(CppH)]^{2+}$, showing cytotoxic activity in the range of cisplatin, investigation of its behavior in cells and mechanism of action of the complex have been unveiled. Briefly, the complex targets mitochondria, impairs their membrane potential, leading to apoptosis.

This chapter has been published in *J. Am. Chem. Soc.* in 2012. Reused with permission from [43]. Copyright (2012) American Chemical Society.

JACS
JOURNAL OF THE AMERICAN CHEMICAL SOCIETY

Article

pubs.acs.org/JACS

Molecular and Cellular Characterization of the Biological Effects of Ruthenium(II) Complexes Incorporating 2-Pyridyl-2-pyrimidine-4-carboxylic Acid

Vanessa Pierroz,[†,‡] Tanmaya Joshi,[§] Anna Leonidova,[†] Cristina Mari,[†] Julia Schur,[∥] Ingo Ott,[∥] Leone Spiccia,*[,§] Stefano Ferrari,*[,‡] and Gilles Gasser*[,†]

[†]Institute of Inorganic Chemistry, University of Zurich, Winterthurerstrasse 190, CH-8057 Zurich, Switzerland

[‡]Institute of Molecular Cancer Research, University of Zurich, Winterthurestrasse 190, CH-8057 Zurich, Switzerland

[§]ARC Centre of Excellence for Electromaterials Science and School of Chemistry, Monash University, Victoria 3800, Australia

[∥]Institute of Medicinal and Pharmaceutical Chemistry, Technische Universität Braunschweig, Beethovenstrasse 55, 38106 Braunschweig, Germany

Supporting Information

ABSTRACT: A great majority of the Ru complexes currently studied in anticancer research exert their antiproliferative activity, at least partially, through ligand exchange. In recent years, however, coordinatively saturated and substitutionally inert polypyridyl Ru(II) compounds have emerged as potential anticancer drug candidates. In this work, we present the synthesis and detailed characterization of two novel inert Ru(II) complexes, namely, $[Ru(bipy)_2(Cpp\text{-}NH\text{-}Hex\text{-}COOH)]^{2+}$ (**2**) and $[Ru(dppz)_2(CppH)]^{2+}$ (**3**) (bipy = 2,2′-bipyridine; CppH = 2-(2′-pyridyl)pyrimidine-4-carboxylic acid; Cpp-NH-Hex-COOH = 6-(2-(pyridin-2-yl)pyrimidine-4-carboxamido)hexanoic acid; dppz = dipyrido[3,2-*a*:2′,3′-*c*]phenazine). **3** is of particular interest as it was found to have IC_{50} values comparable to cisplatin, a benchmark standard in the field, on three cancer cell lines and a better activity on one cisplatin-resistant cell line than cisplatin itself. The mechanism of action of **3** was then investigated in detail and it could be demonstrated that, although **3** binds to calf-thymus DNA by intercalation, the biological effects that it induces did not involve a nuclear DNA related mode of action. On the contrary, confocal microscopy colocalization studies in HeLa cells showed that **3** specifically targeted mitochondria. This was further correlated by ruthenium quantification using High-resolution atomic absorption spectrometry. Furthermore, as determined by two independent assays, **3** induced apoptosis at a relatively late stage of treatment. The generation of reactive oxygen species could be excluded as the cause of the observed cytotoxicity. It was demonstrated that the mitochondrial membrane potential in HeLa was impaired by **3** as early as 2 h after its introduction and even more with increasing time.

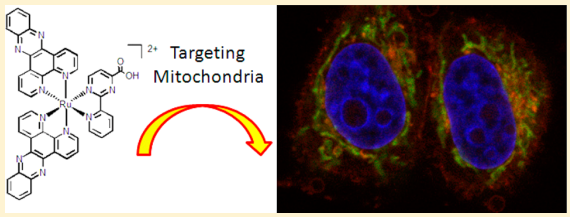

INTRODUCTION

The phenomenal success of the chemotherapeutic drug cisplatin has boosted the research directed at novel metal-based drugs, especially since severe side effects including nephrotoxicity can be encountered during treatment with this compound.[1−7] Among the potential metal-based candidates, ruthenium complexes have emerged as leading players by showing extremely promising results.[8−18] Two Ru(III) candidates, namely, imidazolium *trans*-[tetrachloro-(dimethylsulfoxide)-(1*H*-imidazole)ruthenate(III) (NAMI-A)[19,20] and indazolium *trans*-[tetrachlorobis(1*H*-indazole)-ruthenate(III)] (KP1019),[21] have even entered clinical trials (Figure 1).[22] Despite their structural similarities, these two Ru complexes exert their cytotoxic action differently. While KP1019 exhibits promising effects against a variety of tumor models including colorectal carcinomas and primary explanted human tumors,[23] NAMI-A only has a minor activity against primary tumor cells but an impressive efficacy against the formation of metastases.[23,24] For both NAMI-A and KP1019, and generally speaking for the majority of the Ru complexes investigated for medicinal purposes, the complexes usually undergo ligand exchange to exert their antiproliferative activities, as cisplatin does. There are, however, exceptions such as the Ru(II) based enzyme inhibitors of Meggers et al.[25−27] and the coordinatively saturated and substitutionally inert polypyridyl Ru(II) compounds.[28,29] For the latter, the cytotoxic effects were at least partially attributed to noncovalent interactions with nucleic acids, particularly DNA.[30−37] In recent years, however, several studies have shown that other factors, such as modification of cell membrane and cell adhesion properties,[38] topoisomerase I and II inhibition[39] or mitochondria-mediated apoptosis,[32,33,40−43] could be responsible for cytotoxicity.

Received: July 25, 2012
Published: November 27, 2012

   dx.doi.org/10.1021/ja307288s | *J. Am. Chem. Soc.* 2012, 134, 20376−20387

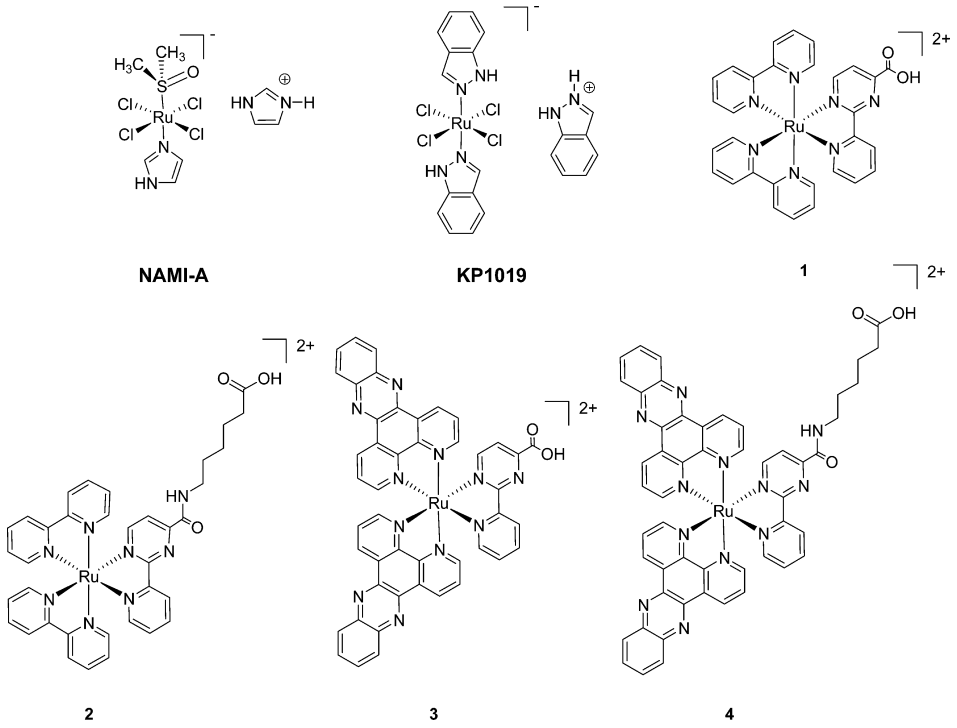

Figure 1. Structures of NAMI-A, KP1019, and the Ru(II) complexes (isolated as hexafluorophosphate salts) studied in this work.

Scheme 1. Syntheses of 2 and 3[a]

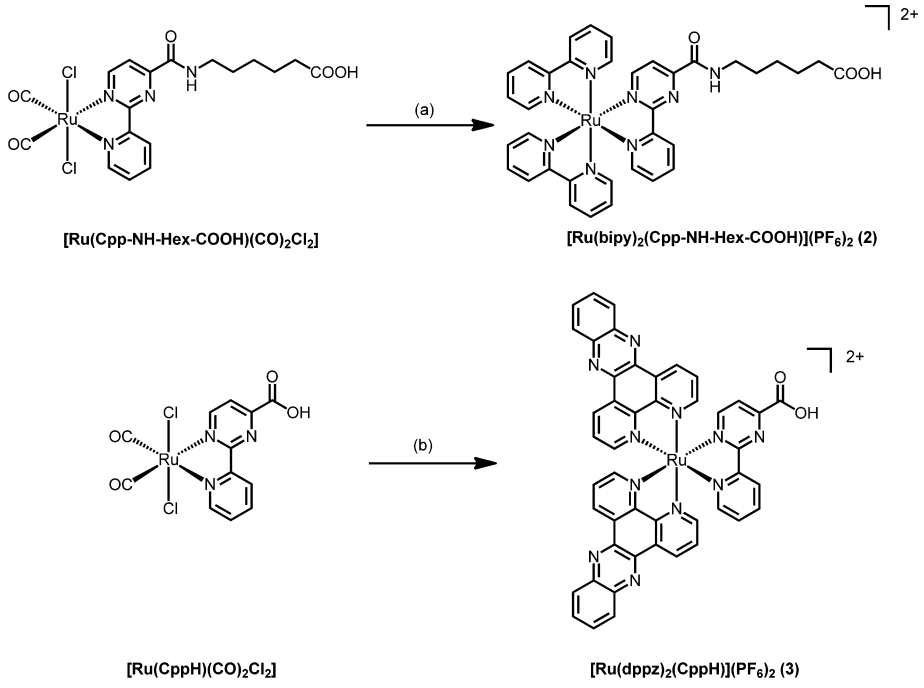

[a]Conditions: (a) (i) bipy, Me_3NO, 2-methoxyethanol, Δ, 4 h; (ii) $CH_3CN/H_2O/H_2SO_4$ (45:45:10), Δ, 24 h, 75%; (b) (i) dppz, Me_3NO, 2-methoxyethanol, Δ, 4 h; (ii) $CH_3CN/H_2O/H_2SO_4$ (45:45:10), Δ, 24 h, 66%.

Inspired by these findings, we have decided to thoroughly investigate the *in vitro* behavior of four Ru(II) complexes bearing a derivative of the 2-(2′-pyridyl)pyrimidine (Cpp) ligand,[44] namely, $[Ru(bipy)_2(CppH)]^{2+}$ (**1**),[44] $[Ru(bipy)_2(Cpp\text{-}NH\text{-}Hex\text{-}COOH)]^{2+}$ (**2**), $[Ru(dppz)_2(CppH)]^{2+}$ (**3**), and $[Ru(dppz)_2(Cpp\text{-}NH\text{-}Hex\text{-}COOH)]^{2+}$ (**4**)[45] (bipy =

dx.doi.org/10.1021/ja307288s | J. Am. Chem. Soc. 2012, 134, 20376−20387

Table 1. Cytotoxicities (IC_{50}) of 1−4 Dequalinium Chloride Hydrate and Cisplatin towards Human (Cancer) Cell Lines[a]

	IC_{50} (μM)					
	HeLa	MCF7	U2OS	A2780	A2780-CP70	MRC-5
1	>100	>100	>100	>100	>100	>100
2	>100	>100	>100	>100	>100	>100
3	10.0 ± 1.3	4.3 ± 0.1	13.5 ± 2.5	2.8 ± 0.1	4.0 ± 1.2	15.1 ± 2.2
4	57.5 ± 4.8	22.0 ± 3.8	83.2 ± 5.6	26.8 ± 7.6	49.6 ± 5.0	66.3 ± 8.1
cisplatin	11.5 ± 2.9	1.8 ± 0.3	11.8 ± 1.7	2.9 ± 0.6	13.8 ± 3.0	7.9 ± 1.2
dequalinium chloride hydrate	21.9 ± 3.6	2.9 ± 0.5	13.4 ± 2.5	1.0 ± 0.1	1.7 ± 0.7	48.9 ± 7.6

[a]Cells were treated with different concentrations of the ruthenium complexes, cisplatin, and dequalinium chloride hydrate for 48 h. The cell viability was determined by using the resazurin reduction test.

2,2′-bipyridine; CppH = 2-(2′-pyridyl)pyrimidine-4-carboxylic acid; Cpp-NH-Hex-COOH = 6-(2-(pyridin-2-yl)pyrimidine-4-carboxamido)hexanoic acid; dppz = dipyrido[3,2-*a*:2′,3′-*c*]-phenazine) (Figure 1). Complex **4** was recently prepared in our laboratories with a view to the development of electrochemiluminescent Ru(II)-peptide nucleic acid bioconjugates as either DNA/RNA biosensors or cellular uptake enhancers.[45−47] Herein, we also describe the synthesis and characterization of the two Ru(II) complexes **2** and **3** (Figure 1), including the X-ray crystal structure of **2**. This work, to the best of our knowledge, presents one of the most detailed biological evaluations of a polypyridyl Ru(II) complex, **3**, which was found extremely cytotoxic on different cancer cell lines.

RESULTS AND DISCUSSION

Synthesis and Characterization of the Ru(II) Complexes. The two Ru(II) complexes **1** and **4** presented in Figure 1 were prepared as previously reported by our groups.[44,45] Compounds **2** and **3** were synthesized in an analogous manner by reacting $[Ru(Cpp\text{-}NH\text{-}Hex\text{-}COOH)(CO)_2Cl_2]$,[45] and $[Ru(CppH)(CO)_2Cl_2]$,[44] with bipy and dppz, respectively (Scheme 1). All Ru(II) complexes were unambiguously characterized by ^{1}H NMR spectroscopy, ESI mass spectrometry, and elemental analysis (see Experimental Section for further details and Figures S1−S4 in Supporting Information for the ^{1}H NMR spectra of **2** and **3** as well as the absorption and emission spectra of **1**−**4**).

X-ray Crystal Structures. During the preparation of **1**−**4**, single crystals of **1** and **2** were obtained and their structures were elucidated by X-ray crystallography. The asymmetric unit (ASU) of **1** consists of a $[Ru(bipy)_2(CppH)]^{2+}$ cation, hexafluorophosphate anions, and noncoordinated water molecules (Figure S5 in the Supporting Information) {A related structure in which the CppH ligand is deprotonated was published recently by our group}.[44] As for **1**, a $[Ru(bipy)_2(Cpp\text{-}NH\text{-}Hex\text{-}COOH)]^{2+}$ unit, perchlorate counteranions, and noncoordinated water molecules define the ASU for **2** (Figure S6 in the Supporting Information). The X-ray structural analysis showed Ru(II) center to reside in a distorted octahedral geometry in both complexes, with bond distances and angles typical of Ru(II) diimine complexes.[44,48] The *trans*-N−Ru−N angles and N−Ru−N bite angles, formed between the nitrogen atoms of the 2,2′-bipyridine and 2-(2′-pyridyl)-pyrimidine (Cpp) rings and the Ru(II) center, are in the typical range (172.29(14)−175.40(13)° and 78.60(15)−79.03(14)°, respectively), as reported for other tris(diimine)Ru(II) complexes (Table S1 in Supporting Information).[44,48] Coordination of the Cpp unit to the Ru(II) center in **1** and **2** involves the N4 and N3 nitrogen atoms and the carboxylate group points away from the Ru(II) center as previously observed for other Ru(II)-2-(2′-pyridyl)pyrimidine-4-carboxylic acid complexes.[44] The crystal structure for **2** (see Figure S7 in the Supporting Information) also shows hydrogen-bonding of the N−H and O−H (protonated carboxylate) groups with the perchlorate counteranions present in the crystal lattice along with C−H....π interactions between the aromatic protons and π-electron rich bipyridyl ring.

Cytotoxicity Studies. The cytotoxicity of complexes **1**−**4** toward human cervical cancer HeLa, breast carcinoma MCF7, osteosarcoma U2OS, ovarian carcinoma A2780, and cisplatin-resistant ovarian carcinoma A2780-CP70 cell lines was investigated using a fluorometric cell viability assay (Resazurin).[49] As a control, the toxicity of the compounds was also tested toward human lung fibroblasts MRC-5. Furthermore, for the purposes of comparison the toxicities of cisplatin and dequalinium chloride hydrate, a known antiproliferative compound with a mitochondrial implication in cell death,[50,51] were also determined on the same cell lines (see Figures S8−S10 in the Supporting Information for the graphs of the Resazurin assays of compound **3**, cisplatin and dequalinium chloride hydrate). As shown in Table 1, the Ru(II) bipyridyl derivatives **1** and **2** did not present cytotoxcity in any of the cell lines tested. These observations are in contrast to the results obtained for the Ru(II) dppz derivatives **3** and **4**, which were cytotoxic toward all the six cell lines employed in this study. Of particular interest is the observation that the IC_{50} values determined for **3** are close, or even lower, than those for cisplatin and in a similar range to dequalinium chloride hydrate. Notably, **3** was found to be more active on a cisplatin-resistant cell line than cisplatin itself, an observation that points to its therapeutic potential, particularly in light of the worrying emergence of cisplatin resistance in tumors.[52] Moreover, the finding that **3** was found to be less cytotoxic than cisplatin on the healthy cell line studied in this work is suggestive of a better therapeutic profile than cisplatin. Another striking result is that **4**, the structurally similar derivative of **3**, displayed much higher IC_{50} values than **3** (>12-fold on the A2780 cell line). This rather surprising finding clearly indicates that subtle structural changes have an important impact on the toxicity and prompted us to further investigate the origin of this behavior.

Cellular Localization. As a first step toward elucidating the mechanism of action of **3**, the favorable photophysical properties of **1**−**4** have been used to evaluate their localization in HeLa cells. It was anticipated that the cellular localization of the complexes bearing the dppz moieties (**3** and **4**) could be possible if they were directed to a hydrophobic environment as the fluorescence of these compounds is quenched in aqueous media. On the contrary, the fluorescence properties of **1** and **2** should not be so significantly solvent-dependent and it was expected that they could be detected in any cellular

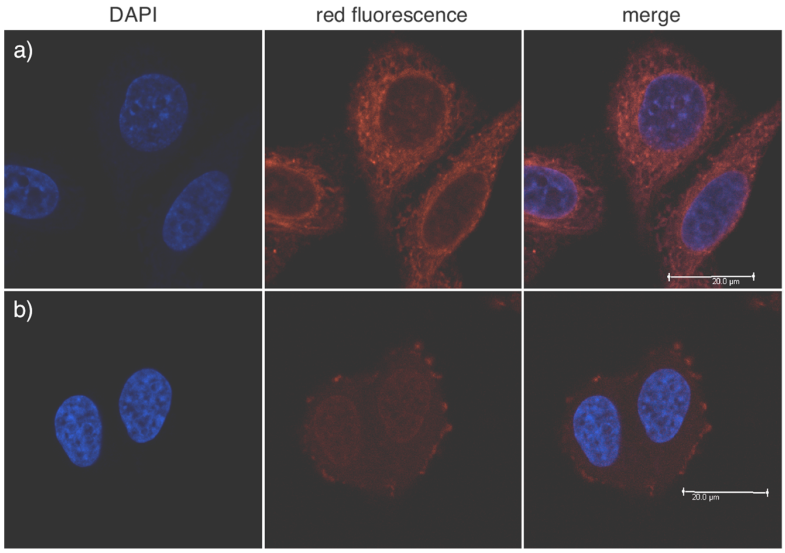

Figure 2. Fluorescence confocal microscopy images of HeLa cells incubated with (a) **3** (20 μM) and (b) **4** (60 μM) for 2 h. Images show DAPI staining, cellular staining of ruthenium compounds, and the overlay.

compartments. The localization of the complexes was then assessed by fluorescence microscopy (see Figure S11 in the Supporting Information). The presence of **1** and **2** in living cells or after fixation in formaldehyde was very difficult to evaluate. Only a weak fluorescence could be detected which we have assumed indicates that these compounds were poorly taken up by the cells. However, very clear confocal microscopy images were obtained for **3** and **4** after cell fixation with formaldehyde (Figure 2). The most important finding to emerge from these studies is that, even though **3** and **4** are structurally quite similar, their cellular localization was extremely different. Compound **4** diffused throughout the cell, including the nucleus. In addition, the outer cellular membrane also seemed to be a primary target of **4**. On the contrary, **3** localized mainly to the cytoplasm with only weak fluorescence detectable in the nucleus. This significant difference in localization is likely to be responsible for the disparity in cytotoxicity observed for these Ru(II) complexes. To obtain further information on the exact localization of **3**, colocalization experiments were performed. Mitotracker green FM was employed for this purpose as it was anticipated that **3** could be localized in the mitochondria. As shown in Figure 3, an excellent superimposition pattern between the commercially available dye and **3** could be observed (see also the online video in Supporting Information). To the best of our knowledge, there are only a handful of reports which so clearly demonstrate by fluorescence microscopy that mitochondria are the target of inert polypyridyl Ru complexes,[40,41,53] although these organelles have only recently been considered as target of such compounds.[32,33,40−42,54] Of particular relevance here is the fact that mitochondria are critical targets of cytotoxic gold compounds.[55−59]

As **3** mainly exhibits fluorescence in a hydrophobic environment, it could also be localized in another cellular organelle hampering visualization by fluorescence microscopy. High-resolution continuum source atomic absorption spectrometry (HR-CS AAS) is an analytical method of choice in this situation, as it allows the detection of trace metal concentrations in biological tissues.[60−62] In previous studies,

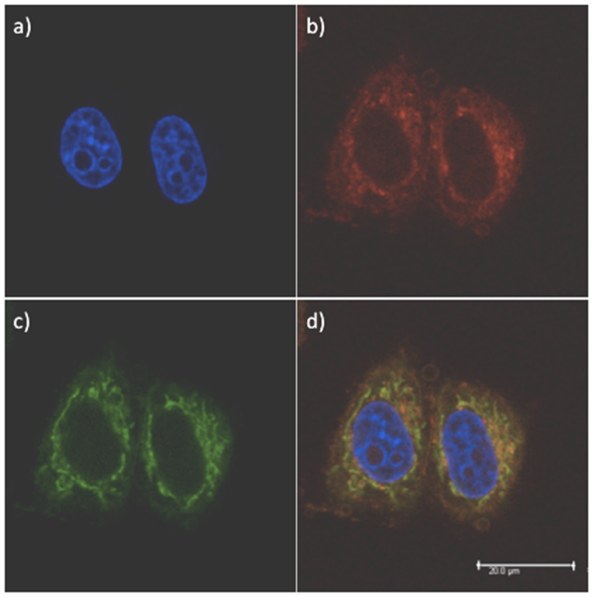

Figure 3. Fluorescence confocal microscopy images of HeLa cells incubated with **3** (20 μM) for 2 h and Mitotracker green FM for 45 min: (a) DAPI staining; (b) cellular staining of **3**; (c) Mitotracker green FM staining; and (d) the overlay image.

it has been reported that the amount of ruthenium taken up by cancer cells can be a deciding factor in obtaining active ruthenium compounds.[33,38,63] In this study, we decided to go one step further by endeavoring to ascertain that **3** mainly targets mitochondria. Therefore, we incubated HeLa cells with 50 μM of **3** for 2 h and isolated the mitochondria from the cells. The uptake of **3** into whole cells and into their mitochondrial fractions was quantified by determination of the ruthenium content by HR-CS AAS (Figure 4). The cellular and mitochondrial protein content of the same samples was determined by the method of Bradford[64] and the measured

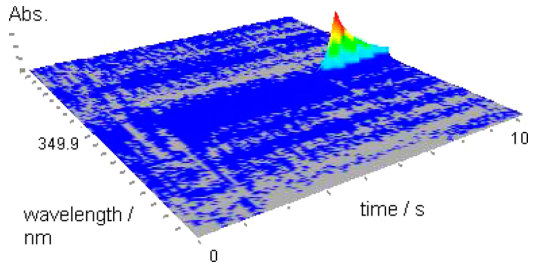

Figure 4. Ruthenium absorption signal of a mitochondrial fraction measured by HR-CS AAS.

ruthenium levels were correlated to the respective protein content. The analysis revealed a high mitochondrial uptake of **3** with a concentration of 29.3 nmol Ru/mg mitochondrial protein. This corresponds to 68% of the total cellular uptake of **3** into HeLa cells.

All in all, fluorescence microscopy and high-resolution continuum source atomic absorption spectrometry indicate that uptake into the mitochondria may be a major pathway for the biodistribution of **3**.

Stability in Human Plasma. To determine whether **3** was stable in biological media, its stability in human plasma was assessed following an experimental protocol that we have recently used in the study of ferrocenyl derivatives.[65] As clearly evident from the LC−MS traces (Figure S12 and Table S2 in the Supporting Information), **3** shows no significant decomposition in human plasma when monitored over a period of three days. This observation is an excellent indication that the intact Ru(II) complex is responsible for the observed cytotoxic activity.

Cellular Uptake Mechanism. To obtain more insight into the mechanism of the cellular entry of compound **3**, we first assessed whether cellular uptake is energy dependent. As nicely explained in a recent review by Pucket and Barton,[66] endocytosis and active transport proteins require energy while passive diffusion through the membrane and diffusion are energy independent. In this respect, **3** was incubated into HeLa cells at 4, 23, and 37 °C for 6 h, and the relative uptake of **3** was assayed by flow cytometry (see Figure S13 in the Supporting Information). As shown in Figure S14a in the Supporting Information, the uptake of **3** increased with temperature, indicating that it was energy-dependent. With no significant perturbation observed in mitochondrial membrane potential of untreated HeLa cells between 4 and 37 °C (Supporting Information, Figure S14b), it implies that the uptake of **3** into HeLa cells is not only due to passive diffusion as it could have been first anticipated.

Distribution Coefficient (logD) and Electrochemical Studies. The lipophilicity of a compound is well-known to have a strong influence on its cellular uptake and localization,[66−68] and it has been shown that lipophilic cations accumulate in mitochondria as a result of the negative potential difference across the mitochondrial membrane.[66,69,70] With this in mind, we have evaluated the lipophilicity of the Ru complexes by determining the distribution coefficients at pH = 7.01, a good approximation of physiological conditions, using the "shake-flask" method. The distribution coefficient (logD) is a measure of partitioning of a compound, in its ionized form, between organic and water phases, and consequently it is pH dependent. As shown in Table 2, compounds **3** and **4** are the most lipophilic compounds of the series due to the presence of

Table 2. Distribution Coefficients between Octanol and Phosphate Buffer 10 mM (pH 7.01) Obtained Using the "Shake-Flask" Method and Midpoint Potentials (E_m)[a] Determined from Cyclic Voltammetry at a Glassy Carbon Electrode Using a Scan Rate of 100 mV s^{-1} in MeCN (0.1 M nBu_4NPF_6) at (20 ± 2) °C

	$logD_{7.01}$[b]	E_m/mV
1	−1.81	980[44]
2	−1.58	970
3	−0.21	1100
4	−0.05	1065

[a]Midpoint potential = $E_m = (E_p^{ox} + E_p^{red})/2$, quoted versus $Fc^{0/+}$ [b]Complex concentrations range between 37 and 50 μM.

the two dppz ligands. Of note, the $logD_{7.01}$ values correlate well with the solubility of **1**−**4** in buffer, namely, **1** and **2** are comparatively more soluble in buffer than **3** and **4** (up to 50 μM). As expected, addition of an alkyl chain in **2** and **4** also increases the lipophilicity of the compounds compared to the parent compounds **1** and **3**, respectively.

To evaluate whether a correlation exists between the electrochemical behavior of the Ru complexes and their cytotoxicities, the midpoint potentials E_m for the Ru(II)/Ru(III) couple of **2**−**4**, namely, the average of the oxidation and reduction peak potentials, were determined from the cyclic voltammograms (see Table S3 and Figures S15−S18 in Supporting Information). The E_m values are equal to the reversible potentials, provided the diffusion coefficient of the oxidized Ru(III) and reduced Ru(II) form are equal. Although the E_m values of the compounds are similar, complex **3**, which is the hardest to oxidize, is the most cytotoxic compound of the series. However, there is no clear trend between the potential and cytotoxicity. As expected, the oxidation process is diffusion controlled (plot of peak current vs scan rate is linear), as is generally the case with tris(diimine) Ru(II) complexes,[45,46,48] and diffusion coefficients of **1**−**4** could be determined (see Table S3 in the Supporting Information) by applying the Randles−Sevcik relationship.[71−73]

DNA and Protein Binding Experiments. The ability of transition metal polypyridyl complexes to reversibly bind DNA through intercalation or groove binding is well documented.[74−76] Depending on the type of metal complexes, this feature was employed to develop imaging agents in living cells.[77] As mentioned in the introduction, however, noncovalent binding to DNA of these coordinatively saturated and substitutionally inert polypyridyl Ru(II) compounds was also assumed to be responsible for the cytotoxic effects observed for some of these complexes. We therefore investigated the binding of complexes **3** and **4** to calf-thymus DNA (CT-DNA).[78,79] The absorption spectra shown in Figures S19 and S20 in the Supporting Information confirm an intercalative mode of DNA binding for **3** and **4** rather than groove binding or electrostatic binding interactions. A significant change in absorbance (hypochromism for **3** and **4** as well as a supplementary red shift for **4**) ascribable to stacking of the aromatic chromophore between the DNA nucleobase pairs is indeed noticed.[76] In comparison, as expected, no change in absorption is observed for complexes **1** and **2** (Figures S21 and S22 in the Supporting Information). The intrinsic binding constants (K_b) for intercalation of **3** and **4** into DNA were obtained by fitting the absorption and emission titrations data to the noncooperative model for DNA binding[80−82] (Figures S23 and

Table 3. DNA Binding Constants Obtained by DNA Titrations of All the Complexes in Phosphate Buffer at pH 7.01[a]

	absorbance data		emission data	
	K_b (M^{-1} per nucleotide)	binding site size(s)	K_b (M^{-1} per nucleotide)	binding site size(s)
3	$(3.95 \pm 0.40) \times 10^6$ (at (at 364 nm)	1.25 ± 0.30	$(2.13 \pm 0.60) \times 10^6$ (at 628 nm)	1.17 ± 0.10
4	$(9.29 \pm 0.60) \times 10^6$ (at 364 nm)	0.65 ± 0.05	$(2.47 \pm 0.40) \times 10^6$ (at 623 nm)	0.89 ± 0.03
$[Ru(L)(dppz)_2]^{4+}$ [85]	$(2.2 \pm 0.5) \times 10^6$ (at 447 nm)	1.2	NA[b]	NA[b]
$[Ru(bipy)_2dppz]^{2+}$ [81]	2.9×10^6 (at 369 nm)	0.84	1×10^7	0.95

[a]Measurement buffer contained 10 mM phosphate buffer and 50 mM NaCl. Abbreviations: L = 5,5′-di(1-(trimethylammonio)methyl)-2,2′-dipyridyl cation; bipy = 2,2′-bipyridine; dppz = dipyrido[3,2-*a*:2′,3′-*c*]phenazine]. [b]Not Available.

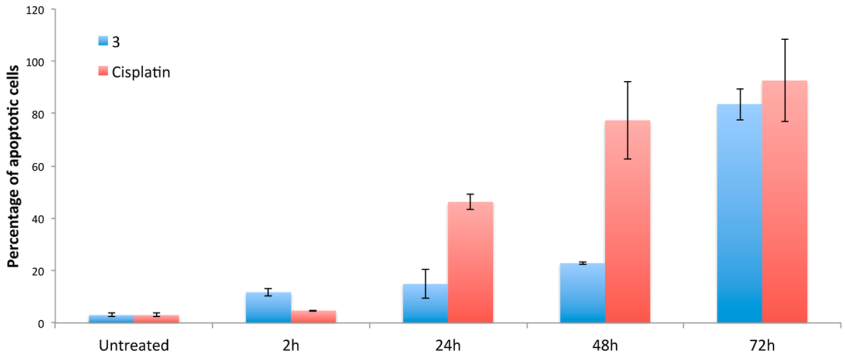

Figure 5. Quantification of apoptotic cells using the YO-PRO assay. HeLa cells were incubated with **3** (20 μM) and cisplatin (20 μM) for 2, 24, 48, or 72 h at 37 °C.

S24 in Supporting Information) and are presented in Table 3. The obtained values (>10^6 M^{-1} range) indicate a high binding affinity for DNA and correlate well with other dppz-containing Ru(II) complexes (Table 3). The less than unity binding site size(s) obtained from the K_b fits for **4** also shows an extent of cooperativity for intermolecular stacking of the dppz ligands on the DNA surface.[83,84] Such π-stacking and aggregation of cationic Ru(II) complex can be further facilitated by polyanionic DNA backbone.[83] The stronger binding of **4**, compared to **3**, was further examined by DNA gel experiments (Figure S25 in the Supporting Information), which revealed a stronger interaction with DNA for **4** than for **3**. Thus, a contribution from such surface aggregation of **4** on DNA surface to its binding affinity cannot be ruled out. Given that the charge of the two complexes at pH = 7.0 is identical (+1), we speculate that the slightly higher binding affinity for **4** could be reflecting the ability of the more "flexible" anionic carboxylate group in **4** to hydrogen-bond with protons present on the DNA, and its slightly greater hydrophobicity. As proteins can be the targets of metallo-drugs,[27] we incubated the ruthenium complexes with proteins of varying molecular weight resolved by SDS-polyacrylamide gel electrophoresis (Figure S26 in the Supporting Information). Similar to DNA, complex **4** was found to bind more strongly to the proteins than **3**. A possible explanation to this observation could be that the carboxylate group in **4** is likely to bind more to protonated amino acids due to its "flexibility". Regardless of the origin of the greater binding affinity of **4**, it is important to highlight the fact that the most cytotoxic compound is not the one binding most strongly to DNA or proteins.

Mechanism of Cytotoxicity. To assess whether **3** causes cell death by apoptosis or necrosis, the YO-PRO and the annexin-V assays were performed. For the former, cytofluorometric analysis of programmed cell death (apoptosis) allows detection of cell membrane permeabilization, an event taking place during apoptosis.[86] Hence, HeLa cells were treated with 20 μM of either **3** or cisplatin for 2, 24, 48, or 72 h before being incubated with the dye YO-PRO (2.5 μM). As shown in Figure 5, **3** does induce apoptosis during the first 48 h but only slightly, with the percentage of apoptotic cells increasing by a factor of ~5 after 72 h. In comparison, cisplatin induced apoptosis in a more gradual manner. The data showed that, after 48 h of treatment with **3** at a dose corresponding to the IC_{50}, only 20% of the cells were apoptotic, indicating that apoptosis is triggered at a later stage. As expected, the annexin-V assay confirmed the results obtained with the YO-PRO assay as it was again found that **3** induced apoptosis (see Figure S27 in the Supporting Information). In the case of the annexin-V assay, apoptosis was found to occur at a slightly faster rate than for the YO-PRO assay.

To clarify the mechanism by which **3** induces apopotosis, the activity of caspases 3/7 was examined using the Caspase-Glo 3/7 assay. These caspases are known to be the apoptosis executers, to which extrinsic and intrinsic pathway converge.[87] The data showed a higher caspase activity upon incubation of cells with **3** (20 μM, 24 h). The low-specificity kinase inhibitor staurosporin (150 nM, 6 h) was used as positive control, confirming that **3** induced cell death by apoptosis (see Figure S28 in the Supporting Information).

Another important factor which could explain the cytotoxicity exerted by **3** is the production of reactive oxidative species

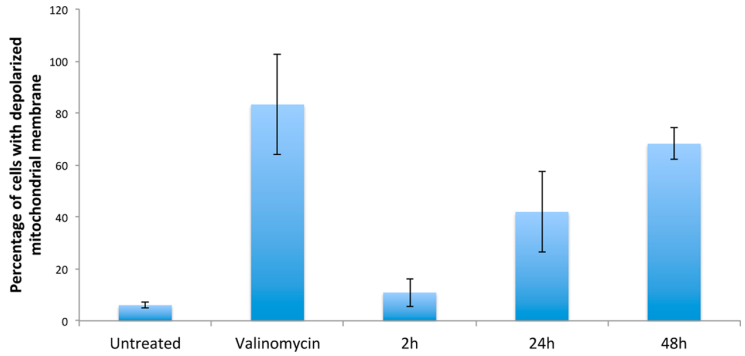

Figure 6. Effect of **3** (20 μM) on the mitochondrial membrane potential in HeLa cells. Cells were treated for 2, 24, or 48 h with **3** at 37 °C and the percentage of cells with depolarized mitochondrial membrane was determined. Valinomycin treatment was taken as positive control.

(ROS). This was recently observed with ruthenium-Norharman and ruthenium β-carboline complexes as well as ruthenium containing bis-benzimidazole derivatives complexes.[32,33,88] In this respect, HeLa cells were treated with **3** in the presence or absence of *N*-acetylcysteine (NAC), which is known to scavenge ROS. As can be seen in Figure S29 in the Supporting Information, ROS were not produced during treatment with **3** at concentrations up to 2-fold the IC_{50}.

Very recently, Meggers, Xu, Wong, Zheng and co-workers reported that Ru(II) complexes could induce cell death by interferring with the membrane potential finally leading to cell apoptosis.[32,33,40,42,43,88] To assess whether **3** displays a similar behavior, the mitochondrial membrane potential ($\Delta\Psi$m) was evaluated in HeLa using JC-1 (5,5′,6,6′-tetrachloro-1,1′,3,3′-tetraethylbenzimidazolylcarbocyanine iodide) and valinomycin as positive control. As shown in Figure 6, the impairment induced by **3** (which is reflected in $\Delta\Psi$m) is clearly time-dependent (see Figure S30 in Supporting Information for the flow cytometry dot blots). On the contrary, within the temperature range investigated and considering that complex **3** affects the mitochondrial membrane potential of HeLa cells only at 37 °C (see Figure S31 in Supporting Information), a similar clear-cut trend in its temperature-dependent behavior cannot be perceived. It can be postulated that the hydrophobic dppz moieties of **3** intercalate into the mitochondria membrane, thus impairing its potential. This, in turn, leads to the release of the mitochondrial cytochrome c, that induces cell permeabilization and apoptosis.

CONCLUSIONS

After platinum complexes, ruthenium compounds are the most advanced metal-based anticancer drug candidates in medicinal inorganic chemistry with two complexes, namely, NAMI-A[24] and KP1019,[21] already in clinical trials. However, for nearly all ruthenium anticancer agents studied, a ligand exchange, often with a biomolecule, is required for the antiproliferative activity. In this study, we demonstrate that coordinatively saturated and substitutionally inert polypyridyl Ru(II) compounds like **3** can be also very effective as anticancer drug candidates by presenting one of the most detailed biological studies of a cytotoxic inert Ru(II) complex. We could show, with **3** and **4** as examples, that subtle structural changes can have a significant impact on both the cytotoxicity and cellular localization. Using two different techniques, namely, confocal microscopy and atomic absorption spectrometry, **3** was shown to accumulate in mitochondria. This correlation provides solid evidence for the mechanism of action proposed in this study. Interestingly, while **3** was found to have IC_{50} values relatively close to those of the well-known cisplatin on three cancer cell lines, and to be more active on a cisplatin-resistant cell line than cisplatin itself, **4** presented significantly higher IC_{50} values. We have also demonstrated that **3** exerted its toxicity through a mitochondria related pathway rather than the nuclear DNA mode of action similar to cisplatin, as would have been presumed due the presence of DNA intercalating ligands.

In summary, these promising findings provide great encouragement to pursue the investigations toward the use of inert Ru complexes in anticancer research.

EXPERIMENTAL SECTION

Materials. Ruthenium trichloride hydrate (Pressure Chemicals) and other chemicals were either of reagent or analytical grade and used as purchased from commercial sources. Analytical grade solvents were degassed by purging with dry, oxygen-free nitrogen for at least 30 min before use if necessary. Acetonitrile was dried by standing over calcium hydride overnight. Deionized water was used for all reactions in aqueous solution. All reagents and solvents were of HPLC grade, purchased from Acros (Geel, Belgium), Aldrich/Sigma/Fluka (Deisenhofen, Germany), Merck (Darmstadt, Germany) and IRIS Biotech (Marktredwitz, Germany) and used without further purification. $[Ru(CppH)(CO)_2Cl_2]$,[44] $[Ru(Cpp\text{-}NH\text{-}Hex\text{-}COOH)(CO)_2Cl_2]$,[45] **1**[44] and **4**[45] were synthesized according to the literature procedures. All the characterization data was in agreement with literature reports.[44,45]

Instrumentation and Methods. A vacuum line and Schlenk glassware were employed when reactions had to be carried out under an atmosphere of dry, oxygen-free nitrogen and assemblies were protected from light if necessary by wrapping them with aluminum foil. *^1H and ^{13}C NMR spectra* were measured on Bruker AC200, AM300 or DRX 400 spectrometers using the signal of the deuterated solvent as an internal standard.[89] The chemical shifts δ are reported in parts per million (ppm) relative to tetramethylsilane (TMS) or signals from the residual protons of deuterated solvents. Coupling constants *J* are given in hertz (Hz). The abbreviations for the peak multiplicities are as follows: s (singlet), d (doublet), t (triplet) and m (multiplet). *ESI mass spectrometry* was performed using a Bruker Esquire 6000 or a Micromass Platform II mass spectrometer fitted with an ESI source (capillary voltage was 3.5 eV and the cone voltage 35 V). In the assignment of the mass spectra, the most intense peak is listed. *High-resolution accurate mass spectra* were recorded with a Bruker BioApex II 47e FT-ICR MS fitted with an Analytica Electrospray Source. Samples were introduced by a syringe pump at a rate of 1 μL min^{-1} and the capillary voltage was at 200 V. Infrared spectra were recorded on a Perkin-Elmer 1600 Series FTIR spectrometer in the range 4000−500 cm^{-1} with a resolution of ±4.0 cm^{-1}. Samples were measured as KBr disks or neat as indicated. *Microanalysis* of inorganic compounds was

carried out at Campbell Microanalytical Laboratory, University of Otago, New Zealand. *UV/vis spectra* were recorded in 1 cm quartz cuvettes using Varian Cary Bio 300 or 5G spectrophotometers. *Emission spectra* were obtained following excitation at 450 nm on a Fluoromax-4 spectrofluorometer (Horiba Jobin Yvon, Inc., France) and were corrected for instrumental response using manufacturer provided correction factors. The excitation and emission slit width were set to 3.0 and 2.5 nm, respectively, for recording the emission spectra of the complexes. *Emission spectra* for the DNA binding evaluations were obtained following excitation at 440 nm on a Perkin-Elmer Luminescence spectrometer LS 50 B and were corrected for instrumental response using manufacturer provided correction factors. The excitation and emission slit width were set to 5.0 and 10.0 nm, respectively. *Thin layer chromatography (TLC)* was performed using silica gel 60 F-254 (Merck) plates with detection of spots being achieved by exposure to iodine or UV light or by using ninhydrin stain. *Column chromatography* was done using Silica gel 60 (0.040−0.063 mm mesh, Merck) or activated neutral alumina (Brockmann I, Sigma-Aldrich). Eluent mixtures are expressed as volume to volume (v/v) ratios.

Electrochemical Measurements. Cyclic voltammetry measurements were performed at (20 ± 2)°C in acetonitrile solutions containing 0.1 M nBu_4NPF_6 as the supporting electrolyte, over the scan rate range of 100−1000 mV s^{-1} using a BAS 100B (Bioanalytical Systems) electrochemical workstation. Solutions used in electrochemical measurements were deoxygenated by purging with high purity nitrogen for at least 10 min before commencing the experiments. A conventional three electrode cell was employed which comprised a glassy carbon working electrode (area = 0.0079 cm^2), a large surface area Pt counter electrode and an Ag/Ag^+ (0.1 M $AgNO_3$ in CH_3CN) reference electrode. The potential of the Ag/Ag^+ reference electrode was frequently calibrated against that of ferrocene/ferrocinium ($Fc^{0/+}$) redox couple under the same conditions used for voltammetric measurements with the Ru(II) complexes. The working electrode was polished with an aqueous slurry of aluminum oxide (0.3 μm), then rinsed with acetone and dried before each voltammetric experiment.

Synthesis and Characterization. *[Ru(bipy)$_2$(Cpp-NH-Hex-COOH)](PF$_6$)$_2$·4H$_2$O (2).* Complex **2** was obtained as an orange solid following the same method as for **4**,[45] using 2,2′-bipyridine (bipy) (0.780 g, 5.00 mmol), trimethylamine-*N*-oxide dihydrate (1.00 g, 9.00 mmol), and [Ru^{II}(Cpp-NH-Hex-COOH)(CO)$_2$Cl$_2$] (1.10 g, 2.00 mmol) in 20 mL of deoxygenated 2-methoxyethanol. Yield: 1.50 g (75%). Crystals of the perchlorate salt of **2**, [Ru(bipy)$_2$(Cpp-NH-Hex-COOH)](ClO$_4$)$_2$·2H$_2$O, suitable for X-ray structure determination were obtained by slow evaporation of a solution prepared by dissolving a sample of the PF_6^- salt in an acetone/water mixture and then adding aqueous $NaClO_4$ solution (1 M). Anal. Calcd for $C_{36}H_{42}F_{12}N_8O_7P_2Ru$ (%): C, 39.68; H, 3.88; N, 10.28. Found: C, 39.81; H, 3.93; N, 10.29. IR (KBr): ν 3103 (C−H_{arom}), 2929 (C−H_{aliph}), 2864 (C−H_{aliph}), 1676 (C═O), 1533, 1438, 1413, 1243, 1162, 1020, 841, 762, 731 cm^{-1}. ^{1}H NMR (400 MHz, DMSO-d_6): δ 9.55−9.52 (m, 1H, aromatic cpp), 9.32 (d, ^3J = 7.5 Hz, 1H, aromatic cpp), 8.82−8.79 (m, 4H, aromatic bpy), 8.28−8.24 (m, 2H, aromatic bpy), 8.20−8.14 (m, 4H, aromatic cpp and bpy), 8.05 (d, ^3J = 5.1 Hz, 1H, −N*H*CO-cpp), 7.95 (d, ^3J = 5.9 Hz, 1H, aromatic cpp), 7.78−7.73 (m, 2H, aromatic bpy), 7.71−7.65 (m, 3H, aromatic bpy), 7.56−7.51 (m, 3H, aromatic bpy), 7.49−7.46 (m, 1H, aromatic cpp), 2.21 (t, ^3J = 7.2 Hz, 2H, −CH_2CH_2COOH), 1.63−1.51 (m, 4H, alkyl CH_2), 1.38−1.30 (m, 2H, −NH$(CH_2)_2CH_2(CH_2)_2$COOH) ppm. Two proton signals are masked by residual water from DMSO-d_6. MS (ESI^+): *m*/*z* 364.1 [M − 2PF_6]$^{2+}$, 873.1 [M − PF_6]$^+$. HR-ESI mass spectrum (CH_3CN/MeOH 1:4): found 364.0902; calcd for [$C_{36}H_{34}N_8O_3Ru$]/*z* 364.0899. ε_{440} = 12 900 M^{-1}·cm^{-1} (H_2O in 0.2% DMSO).

[Ru(dppz)$_2$(CppH)](PF$_6$)$_2$·4H$_2$O (3). Complex **3** was prepared in a similar manner to **2**, using dipyrido[3,2-*a*:2′,3′-*c*]phenazine (dppz) (0.212 g, 0.752 mmol), trimethylamine-*N*-oxide dehydrate (0.150 g, 1.35 mmol), and [Ru^{II}(CppH)(CO)$_2$(Cl)$_2$] (0.129 g, 0.301 mmol) in 12 mL of 2-methoxyethanol. The crude product was purified by column chromatography on neutral alumina, gradually changing the eluent from CH_3CN/H_2O/sat. KNO_3 (16:3:1) to CH_3CN/H_2O/sat. KNO_3 (10:3:1). The dark orange band was collected, and the solvent removed under reduced pressure. The concentrate was passed through a Sephadex LH-20 column with acetonitrile as eluent to remove inorganic salts. The intense orange band was collected, concentrated and the residue suspended in water followed by dropwise addition of HPF_6 (60%) to complete the precipitation of the product as a hexafluorophosphate salt. The precipitate was collected by filtration, washed with hot toluene and dried *in vacuo* to obtain **3** as an orange solid. Yield: 0.228 g (66%). Anal. Calcd for $C_{46}H_{35}F_{12}N_{11}O_6P_2Ru$ (%): C, 44.96; H, 2.87; N, 12.54. Found: C, 45.11; H, 2.98; N, 12.58. IR (KBr): ν 1717 (C═O), 1636, 1420, 1357, 1234, 1079, 844, 763, 729 cm^{-1}. ^{1}H NMR (400 MHz, DMSO-d_6): δ 9.66−9.64 (m, 2H, aromatic dppz), 9.57−9.54 (m, 2H, aromatic dppz), 8.94 (d, ^3J = 7.8 Hz, 1H, aromatic cpp), 8.63−8.61 (m, 1H, aromatic cpp), 8.52−8.46 (m, 4H, aromatic dppz), 8.35−8.33 (m, 1H, aromatic cpp), 8.29−8.25 (m, 2H, aromatic dppz), 8.23−8.16 (m, 5H, aromatic dppz), 8.12−8.06 (m, 3H, aromatic cpp and dppz), 7.91−7.85 (m, 3H, aromatic cpp and dppz), 7.60−7.54 (m, 2H, aromatic dppz) ppm. MS (ESI^+): *m*/*z* 433.3 [M − 2PF_6]$^{2+}$. HR-ESI mass spectrum (CH_3CN/MeOH 1:4): found 433.5704; calcd for [$C_{46}H_{27}N_{11}O_2Ru$]/*z* 433.5696. ε_{440} = 19 650 M^{-1}·cm^{-1} (H_2O in 0.2% DMSO).

Distribution Coefficients. The distribution coefficient of each complex, defined as

$$\log D_{o/w} = \log\left(\frac{[\text{solute}]_{\text{octanol}}}{[\text{solute}]^{\text{ionized}}_{\text{water}} + [\text{solute}]^{\text{neutral}}_{\text{water}}}\right)$$

was experimentally determined by using the "shake-flask" method. Briefly, each complex was dissolved in a 10 mM phosphate buffer (pH 7.01), previously saturated with octanol, to give about 1 mL of a solution with a concentration reported in Table 4 for each complex.

Table 4. Extinction Coefficients (ε) of Ru(II) Complexes 1−4

		ε_{molar} (M^{-1} cm^{-1})	
complex	λ_{max} (nm) [MLCT]	phosphate buffer (10 mM, pH 7.01)[a]	H_2O (0.2% DMSO)[b]
1	444	12500	13400
2	440	12300	12900
3	451	17400	14500
4	451	17600	18200

[a][**1**] = 50 μM, [**2**] = 50 μM, [**3**] = 42 μM and [**4**] = 37 μM. [b][complex] = 10 μM.

The same volume of octanol (previously saturated with 10 mM phosphate buffer) was then added and the solution was shaken 100 times and equilibrated for 4.5 h. The concentration of the complex in the aqueous phase was then evaluated by UV−vis spectroscopy, using extinction coefficients for PBS solutions of the complexes (Table 4). The evaluation on each complex was repeated 3 times.

DNA Binding (UV−visible and Fluorescence Experiments). DNA and Ru complexes concentrations were evaluated by spectroscopy, using the extinction coefficients presented in Table 4.

The absorption titrations were performed at room temperature in 10 mM phosphate buffer with 50 mM NaCl (pH 7.01). For every sample, the Ru complex concentration was constant, between 3 μM and 20 μM, depending on the compound, and a concentrated solution of CT DNA (type I, fibers) was added ($\varepsilon_{260,\ CTDNA}$ = 6600 M^{-1} cm^{-1} per nucleotide). A reference cell loaded with buffer was necessary, in which the DNA was added each time, to minimize the changes due to the DNA in absorption at 260 nm. After every addition, samples were incubated at room temperature for 10 min, and then the UV−visible spectra were recorded. Additions of DNA were carried on until no further changes in spectra were observed.

Fluorescent DNA titrations were performed in the same way, by using Ru complex solution between 3 and 27 μM, depending on the

complex, in the same buffer and by adding DNA until no more changes were observed. In these cases, no reference cell was necessary.

DNA binding constant (K_b) was determined by fitting the titration data to the McGhee-Von Hippel equation, as previously reported.[81,82]

$$(\varepsilon_a - \varepsilon_f)/(\varepsilon_b - \varepsilon_f) = (b - (b^2 - 2K_b{}^2C[\mathrm{DNA}]/s))^{1/2}/2K_bC$$

$$b = 1 + K_bC + K_b[\mathrm{DNA}]/2s$$

where [DNA] is the concentration of CT-DNA in nucleotides, ε_a is the apparent extinction coefficient of Ru complexes at a given DNA concentration, ε_f is the extinction coefficient of Ru complexes in absence of DNA, ε_b is the extinction coefficient of Ru complexes when completely bound to DNA, C is the total Ru complex concentration, and s is the binding site size in base pairs. From plots of $(\varepsilon_a - \varepsilon_f)/(\varepsilon_b - \varepsilon_f)$ versus [DNA], K_b values were calculated by fitting the curves with OriginLab 8.6.

DNA binding constants from emission data were determined by fitting the data with the same equation, but using I_a instead of ε_a, as the luminescence intensity of ruthenium complexes at a given DNA concentration, and I_f and I_b (instead of ε_f and ε_b), as the luminescence intensity of complexes in their free and completely bound forms, respectively.

DNA Binding (Gel Experiments). To test the DNA binding ability of metal complexes, 0.5 μg of 1 kb DNA ladder (New England BioLabs) was resolved on multiple lanes of a 1% agarose gel. Individual lanes were excised and incubated with 2.5 μM ruthenium complex solutions. As positive control, a lane of the agarose gel was stained with ethidium bromide (EtBr). The reconstituted gel was analyzed using an Alpha Innotech Imaging system with the EtBr colorimetric filter (365 nm).

Protein Binding. To test the protein binding ability of metal complexes, 3 μg of Broad Range Molecular Weight Markers (Bio-Rad) were resolved on multiple lanes of an 8% SDS-gel. Individual lanes were excised, fixed with 30% ethanol/10% acetic acid and incubated with 2.5 μM ruthenium complex solutions. Coomassie blue staining was taken as a positive control. The reconstituted gel was analyzed using an Alpha Innotech Imaging system using visible light as illumination source.

Stability of 3 in Human Plasma. These experiments were performed following a procedure recently described by our group.[65] The human plasma was provided by the Blutspendezentrum, Zurich, Switzerland. Diazepam (internal standard) was obtained from Sigma-Aldrich. Stock solutions of **3** (20 mM) and diazepam (800 μM) were prepared in DMSO. For a typical experiment, an aliquot of the respective stock solutions and DMSO were then added to the plasma solution (975 μL) to a total volume of 1000 μL and final concentrations of 20 μM for **3** and 10 μM of diazepam. The resulting plasma solution was incubated for 72 h at 37 °C with continuous and gentle shaking (ca. 300 rpm). The reaction was stopped by addition of 2 mL of methanol, and the mixture was centrifuged for 45 min at 650g at 4 °C. The methanolic solution was evaporated and the residue was suspended in 200 μL of 1:1 (v/v) acetonitrile/H_2O solution. The suspension was filtered and analyzed using LC−MS. A total of 40 μL of the solution was injected into the HPLC (Acquity Ultra Performance LC, Waters) that was connected to a mass spectrometer (Bruker Esquire 6000) operated in ESI mode. The Nucleosil 100-5 C18 (250 × 3 mm) reverse phase column was used with a flow rate of 0.5 mL min^{-1} and UV-absorption was measured at 300 nm. The runs were performed with a linear gradient of A (acetonitrile (Sigma-Aldrich HPLC-grade) and B (distilled water containing 0.02% TFA and 0.05% HCOOH): t = 0−3 min, 20% A; t = 7 min, 50% A; t = 20 min, 90% A; t = 23 min, 100% A; t = 25 min, 100% A; t = 28 min, 20% A.

Cell Culture. Human cervical carcinoma (HeLa) cells were cultured in DMEM (Gibco) supplemented with 5% fetal calf serum (FCS, Gibco), 100 U/mL penicillin, 100 μg/mL streptomycin at 37 °C and 5% CO_2. The human osteosarcoma cell line U2OS was maintained in DMEM (Gibco) supplemented with 10% FCS (Gibco), penicillin (100 U/mL), and streptomycin (100 μg/mL). The human breast carcinoma MCF7 cell line was cultured in MEM medium (Gibco) supplemented with 10% FCS (Gibco), 200 mM L-glutamine, penicillin (100 U/mL), and streptomycin (100 μg/mL). The human ovarian carcinoma A2780 cell line and a cisplatin-resistant subline CP70 were cultured in RPMI-1640 medium (Gibco) supplemented with 10% FCS (Gibco), penicillin (100 U/mL), and streptomycin (100 μg/mL). The normal human fetal lung fibroblast MRC-5 cell line was maintained in F-10 medium (Gibco) supplemented with 10% FCS (Gibco, penicillin (100 U/mL), and streptomycin (100 μg/mL).

***In Vitro* Fluorescence Evaluation.** Cellular localization of fluorescent ruthenium complexes was assessed by fluorescence microscopy. HeLa cells were grown on 35 mm Cellview glass bottom dishes (Greiner) or on 18 mm Menzel-gläser coverslips at a density of 1 × 10^5 cells/mL and incubated for 2 h with ruthenium complexes at their IC_{50} or at 100 μM for nontoxic complexes. Cells were fixed in 4% formaldehyde solution (10% formaldehyde in 90% PBS) and either mounted on slides for viewing by confocal microscopy or kept in water for imaging on an Olympus IX 81 motorized inverted microscope (Olympus, Hamburg, Germany), using 10× dry and 60× oil-immersion lenses and digital camera. Alternatively, fixed cells were viewed on a CLSM Leica SP5 microscope. The ruthenium complexes were visualized using the Cy3 filter set of the Olympus microscope (ex., 550 nm; em., 570 nm) or using the red wavelength selection (ex, 458 nm; em, 600−650 nm) on the CLSM Leica SP5 microscope.

Mitochondrial Staining. Colocalization of ruthenium complex **3** with mitochondria was examined by means of Mitotracker green FM (Molecular Probes), a mitochondria-specific dye.[41] Briefly, a 1 mM Mitotracker Green FM stock solution made in DMSO was diluted to 10 μM working concentration in cell medium (DMEM, 5% FCS). Staining of mitochondria was accomplished by adding a 50 nM final concentration of Mitotracker Green FM to the culture medium for the last 45 min of ruthenium complex incubation. The medium was removed and cells were fixed in 4% formaldehyde solution before being mounted on slides for viewing by confocal microscope.

Cytotoxicity Studies. Cytotoxicity studies were performed on six different cell lines, namely, HeLa, MCF7, U2OS, A2780, CP-70 and MRC-5, by a fluorometric cell viability assay using Resazurin (Promocell GmbH). Briefly, one day before treatment, cells were plated in triplicates in 96-well plates at a density of 4 × 10^3 cells/well in 100 μL. Upon treating cells with increasing concentrations of the ruthenium complexes for 48 h, the medium was removed, and 100 μL of complete medium containing resazurin (0.2 mg/mL final concentration) was added. After 4 h of incubation at 37 °C, the fluorescence of the highly red fluorescent resorufin product was quantified at 590 nm emission with 540 nm excitation wavelength in a SpectraMax M5 microplate Reader.

Flow Cytometry. HeLa cells suspensions were washed twice in 1× PBS and centrifuged at 130g for 6 min to remove the medium and the metal complex. The cellular uptake of ruthenium complex was detected in the PE-Texas Red channel (excitation at 488 nm; emission at 575/25 nm). JC-1 monomers used in determination of the mitochondrial membrane potential health condition as well as annexin V-FITC conjugate used in the detection of apoptotic cells were detected in the FITC channel, whereas JC-1 aggregates were detected in the APC channel. A total of 15 000 cells were collected for each sample by the flow cytometer CyAn ADP 9 and analyzed with Summit 4.3 software. Nonviable cells were excluded from the analysis. Data are represented as mean ± SEM.

Uptake Studies. To determine the cellular uptake efficiency of ruthenium complex **3**, flow cytometric analysis was performed. To this end, 3 × 10^5 HeLa cells were seeded in 6 cm dishes one day before treatment and incubated at 4, 23, and 37 °C and 5% CO_2 for 6 h with 20 μM of **3**. The cells were treated with trypsin, centrifuged, washed twice in 1× PBS and finally resuspended in 1 tmePBS prior to flow cytometric analysis.

Evaluation of Mitochondrial Membrane Potential ($\Delta\Psi$m). The mitochondrial membrane potential was measured by the JC-1 (5,5′,6,6′-tetrachloro-1,1′,3,3′-tetraethylbenzimidazolylcarbocyanine iodide) (Sigma-Aldrich). HeLa cells were seeded in 6-well plates at a density of 4 × 10^5 cells one day before treatment and incubated for 2, 24, and 48 h with 20 μM **3** at either 4, 23, or 37 °C. Following this,

cells were then treated with trypsin and resuspended in 5 mL of complete medium. The cell suspension was then stained according to the manufacturer's instructions.

Intracellular ROS Measurement. The production of intracellular ROS was detected by 2′,7′-dichlorofluorescin diacetate (H_2DCF-DA, Sigma-Aldrich), a cell-permeable nonfluorescent probe which is de-esterified in cell and upon oxidation turns to highly fluorescent 2′,7′ dichlorofluorescein. HeLa cells were seeded in white 96-well plates at a density of 8×10^3 cells one day before treatment. The medium was removed and H_2DCF-DA (10 μM) was added to cells for 30 min at 37 °C in the dark. The cells were subsequently washed in serum-free medium and treated for 30 min, 1 h, 2 h, or 6 h with **3**, in presence or absence of 10 mM NAC, an antioxidant. Fluorescence was quantified at 530 nm emission with 488 nm excitation wavelength in a SpectraMax M5 microplate Reader.

Apoptosis Detection. Apoptosis was detected by means of YO-PRO (Molecular Probes) staining, a nucleic acid dye permeating exclusively apoptotic cells. HeLa cells were seeded in 96-well plates at a density of 5×10^3 cells one day before treatment. The medium was replaced and cells were treated for 2, 24, 48, or 72 h with **3** (20 μM). YO-PRO (2.5 μM final concentration in 20 mM Na-citrate pH 4.0, 26.8 mM NaCl) was added to the culture medium for 10 min at 25 °C in the dark. Fluorescence was quantified at 530 nm emission with 485 nm excitation wavelength in a SpectraMax M5 microplate Reader. Finally, cells were lysed in 25 μL of lysis buffer (0.1% NP40, 5 mM EDTA, 5 mM EGTA) for 30 min at 25 °C in the dark and fluorescence was quantified again. The ratio between the fluorescence measured before and after lysis equals the percentage of apoptotic cells in the population examined.

Apoptosis was also detected by means of annexin V-FITC conjugate purchased from BD Pharmingen (BD Bioscience), which has a high affinity binding for the membrane phospholipid phosphatidylserine, translocated from the inner to the outer leaflet of the plasma membrane during apoptosis. HeLa cells were seeded in 6 cm dishes at a density of 4×10^5 cells one day before treatment. The medium was replaced and cells were treated for 2, 24, 48, or 72 h with **3** (20 μM). Cells were then stained with annexin V-FITC according to the manufacturer's instructions.

Caspase 3/7 Assay. Caspases 3/7 activity was assessed using the Caspase-Glo 3/7 assay kit (Promega). HeLa cells were seeded in white 96-well plates at a density of 8×10^3 cells one day before treatment. Cells were treated with **3** (20 μM) for 24 h or with 150 nM staurosporin for 6 h at 37 °C. Caspase 3/7 activity was detected according to the manufacturer's instructions. Luminescence in RLUs was quantified in a SpectraMax M5 microplate Reader.

Mitochondria Isolation from HeLa Cells. Mitochondria were isolated by means of the Mitochondria isolation kit (Sigma Aldrich). HeLa cells were cultured in 175 cm^2 flask at a density of 13×10^6 cells and treated with 50 μM of **3**. Mitochondria were then isolated from whole cell extract according to the manufacturer's instructions. Before the isolation procedure, an aliquot was removed to determine the total cellular ruthenium concentration. Mitochondria, as well as cell pellets, were then lyophilized prior Atomic Absorption measurements.

HR-CS AAS Measurements. For metal quantification, the lyophilized samples were resuspended in 100 μL of deionized water and 100 μL of storage buffer (1:5) for mitochondria pellets. An aliquot of 10 μL was then removed to quantify the protein concentration of the samples by Bradford method.[64] A contrAA 700 high-resolution continuum source atomic absorption spectrometer (AnalytikJena AG) was used for the ruthenium quantification at a wavelength of 349.900 nm. Aqueous standard samples of **3** were used for calibration purposes. To 90 μL of all probes and standards each 9 μL Triton X-100 (1%) and 9 μL hydrochloric acid (18%) were added. Samples were injected at a volume of 25 μL into coated standard graphite tubes ("AAS IC-Standardrohr, beschichtet", AnalytikJena AG). A furnace program as described in the literature was used.[30] During the temperature program, the graphite tube was purged with a constant argon gas flow, which was only halted during the zeroing and atomization steps. The mean integrated absorbances of double injections were used throughout the study. The results are expressed as nmol ruthenium per milligram of protein. A percentage value of **3** accumulated in mitochondria compared to the total cellular ruthenium concentration was also calculated.

X-ray Crystallography. Intensity data for red crystals of **1** (0.20 × 0.20 × 0.05 mm) and **2** (0.38 × 0.10 × 0.05 mm) were measured at 173 K on a Bruker Apex II CCD fitted with graphite monochromated Mo Kα radiation (0.71073 Å). The data were collected to a maximum 2θ value of 50° and processed using the Bruker Apex II software package. Crystal parameters and details of the data collection are summarized in Table S4 in the Supporting Information. Each structure was solved by direct methods and expanded using standard Fourier routines in the SHELX-97.[90,91] All hydrogen atoms were placed in idealized positions, except for the hydrogen on the oxygen atom of the carboxylic group and the nitrogen atom (in **2**) which were located on the Fourier difference map and refined with restrained O−H and N−H distances. The isotropic thermal parameters for O−H and N−H hydrogen atoms were fixed at 1.2 times that of the respective oxygen or nitrogen atom. A PF_6^- counteranion in **1** and ClO_4^- counteranion in **2** were found disordered and refined anisotropically using part command. The hydrogen atoms associated with the water molecules of crystallization could not be located on the Fourier Difference map. All non-hydrogen atoms were refined anisotropically.

Abbreviations. AAS, atomic absorption spectrometry; bipy, 2,2′-bipyridine; Boc, *tert*-butoxycarbonyl; CppH, 2-(2′-pyridyl)pyrimidine-4-carboxylic acid; Cpp-NH-Hex-COOH, 6-(2-(pyridin-2-yl)-pyrimidine-4-carboxamido)hexanoic acid; CT-DNA, calf-thymus DNA; dppz, dipyrido[3,2-*a*:2',3'-*c*]phenazine; DIPEA, diisopropylethylamine; ESI-MS, electrospray ionisation mass spectrometry; Fmoc, fluorenylmethoxycarbonyl; Gly, glycine; HR-CS AAS, high-resolution continuum source atomic absorption spectrometry; KP1019, *trans*-[tetrachlorobis(1*H*-indazole)ruthenate(III)]; MALDI-TOF, matrix assisted laser/desorption ionization−time of flight; NAC, *N*-acetylcysteine; NAMI-A, *trans*-[tetrachloro(dimethylsulfoxide)-(1*H*-imidazole)ruthenate(III).

■ ASSOCIATED CONTENT

Supporting Information

^{1}H NMR spectra of **2** and **3** (Figures S1−S2), absorption and emission spectra of **1**−**4** (Figures S3−S4), thermal ellipsoid plots of **1** and **2** (Figures S5−S6), molecular packing of **2** (Figure S7), selected bond lengths and angles for **1** and **2** (Table S1), plots of the Resazurin assays of **3**, cisplatin and dequalinium chloride hydrate (Figures S8−S10), fluorescence confocal microscopy images of **1**−**4** in HeLa cells (Figure S11), UV traces (300 nm) of the LC−MS analysis of 3 in human plasma at t = 0 and 72 h (Figure S12), ratios of peak areas of **3**/Diazepam in human plasma at t = 0 and 72 h (Table S2), flow cytometry dot plots of the uptake of **3** (Figure S13), effect of temperature on the uptake of **3** (Figure S14), cyclic voltammetric data of **2**−**4** (Table S3), cyclic voltammograms of **2**−**4** (Figures S15−S18), CT-DNA titration of **1**−**4** (Figures S19−S24), gels for DNA and protein binding of **1**−**4** (Figures S25−S26), annexin-V activity measurements of **3**(Figure S27), caspase 3/7 activity measurements of **3** (Figure S28), ROS production measurements of **3** (Figure S29), flow cytometry dot plots of MMP of **3** in HeLa cells (Figure S30), effect of **3** with temperature on mitochondrial potential of Hela cells (Figure S31), crystallography collection and refinement data of **1** and **2** (Table S4). X-ray crystallographic files for **1** and **2** in CIF format. Video of the colocalization studies of **3** in avi format. This material is available free of charge via the Internet at http://pubs.acs.org.

AUTHOR INFORMATION

Corresponding Author

leone.spiccia@monash.edu; sferrari@imcr.uzh.ch; gilles.gasser@aci.uzh.ch

Notes

The authors declare no competing financial interest.

ACKNOWLEDGMENTS

This work was financially supported by the Swiss National Science Foundation (SNSF Professorship to G.G. and Research Grants to G.G. and S.F.), the University of Zurich (G.G. and S.F.), the Stiftung für Wissenschatliche Forschung of the University of Zurich (S.F.), the Stiftung zur Krebsbekämpfung (S.F), the Huggenberger-Bischoff Stiftung (S.F), the University of Zurich Priority Program (S.F.), the Fonds der Chemischen Industrie (I.O.), and the Australian Research Council through the Australian Centre of Excellence for Electromaterials Science (L.S.). T.J. is a recipient of Monash Graduate Scholarship, Monash International Postgraduate Research Scholarship and Postgraduate Publication Award. The authors thank Prof. Alan M. Bond and Dr. Malay Patra for helpful discussions and Dr. Urs Ziegler (University of Zurich, Center for Microscopy and Image Analysis) for guidance in the optimization of cell imaging.

REFERENCES

(1) Rosenberg, B.; VanCamp, L.; Krigas, T. *Nature* **1965**, *222*, 385−386.

(2) Fricker, S. P. *Dalton Trans.* **2007**, 4903−4917 and references therein.

(3) Lippert, B. *Cisplatin, Chemistry and Biochemistry of a Leading Anticancer Drug*; Verlag Helvetica Chimica Acta: Zürich, 1999.

(4) Dhar, S.; Lippard, S. J. In *Bioinorganic Medicinal Chemistry*; Alessio, E., Ed.; Wiley-VCH: Weinheim, 2011; pp 351−382.

(5) Dabrowiak, J. C. *Metals in Medicine*; John Wiley & Sons Ltd: Chichester, 2009.

(6) *Bioinorganic Medicinal Chemistry*; Alessio, E., Ed.; Wiley-VCH Verlag: Weinheim, 2011.

(7) Sessler, J. L.; Doctrow, S. R.; McMurry, T. J.; Lippard, S. J. *Medicinal Inorganic Chemistry*; American Chemical Society: Washington, D.C, 2005; Vol. *903*.

(8) Bratsos, I.; Gianferrara, T.; Alessio, E.; Hartinger, C. G.; Jakupec, M. A.; Keppler, B. K. In *Bioinorganic Medicinal Chemistry*; Alessio, E., Ed.; Wiley-VCH: Weinheim, 2011; pp 151−174.

(9) Süss-Fink, G. *Dalton Trans.* **2010**, *39*, 1673−1688 and references therein.

(10) Dyson, P. J.; Sava, G. *Dalton Trans.* **2006**, 1929−1933 and references therein.

(11) Dougan, S. J.; Sadler, P. J. *Chimia* **2007**, *61*, 704−715.

(12) Melchart, M.; Sadler, P. J. In *Bioorganometallics*; Jaouen, G., Ed.; Wiley-VCH: Weinheim, 2006; pp 39−64.

(13) Peacock, A. F. A.; Sadler, P. J. *Chem. Asian J.* **2008**, *3*, 1890−1899.

(14) Gasser, G.; Ott, I.; Metzler-Nolte, N. *J. Med. Chem.* **2011**, *54*, 3−25.

(15) Sava, G.; Bergamo, A.; Dyson, P. J. *Dalton Trans.* **2011**, *40*, 9069−9075.

(16) Smith, G. S.; Therrien, B. *Dalton Trans.* **2011**, *40*, 10793−10800.

(17) Gianferrara, T.; Bratsos, I.; Alessio, E. *Dalton Trans.* **2009**, 7588−7598.

(18) Gasser, G.; Metzler-Nolte, N. *Curr. Opin. Chem. Biol.* **2012**, *16*, 84−91.

(19) Sava, G.; Zorzet, S.; Turrin, C.; Vita, F.; Soranzo, M. R.; Zabucchi, G.; Cocchietto, M.; Bergamo, A.; Di Giovine, S.; Pezzoni, G.; Sartor, L.; Garbisa, S. *Clin. Cancer Res.* **2003**, *9*, 1898−1905.

(20) Bergamo, A.; Sava, G. *Dalton Trans.* **2011**, *40*, 7817−7823.

(21) Hartinger, C. G.; Jakupec, M. A.; Zorbas-Seifried, S.; Groessl, M.; Egger, A.; Berger, W.; Zorbas, H.; Dyson, P. J.; Keppler, B. K. *Chem. Biodiversity* **2005**, *5*, 2140−2154 and references therein.

(22) Bratsos, I.; Jedner, S.; Gianferrara, T.; Alessio, E. *Chimia* **2007**, *61*, 692−697.

(23) Hartinger, C. G.; Jakupec, M. A.; Zorbas-Seifried, S.; Groessl, M.; Egger, A.; Berger, W.; Zorbas, H.; Dyson, P. J.; Keppler, B. K. *Chem. Biodiversity* **2008**, *5*, 2140−2154 and references therein.

(24) Sava, G.; Alessio, E.; Bergamo, A.; Mestroni, G. In *Metallopharmaceuticals*; Clarke, M. J., Sadler, P. J., Eds.; Springer: Berlin, 1999; Vol. *1*, pp 143−169.

(25) Mulcahy, S. P.; Meggers, E. In *Medicinal Organometallic Chemistry*; Jaouen, G., Metzler-Nolte, N., Eds.; Springer-Verlag: Heidelberg, 2010; Vol. *32*, pp 141−153.

(26) Meggers, E. *Chem. Commun.* **2009**, 1001−1010 and references therein.

(27) Gasser, G.; Metzler-Nolte, N. In *Bioinorganic Medicinal Chemistry*; Alessio, E., Ed.; Wiley-VCH Verlag: Weinheim, 2011; pp 351−382.

(28) Gill, M. R.; Thomas, J. A. *Chem. Soc. Rev.* **2012**, *41*, 3179−3192.

(29) Kilah, N. L.; Meggers, E. *Aust. J. Chem.* **2012**, *65*, 1325−1332 and references therein.

(30) Schaefer, S.; Ott, I.; Gust, R.; Sheldrick, W. S. *Eur. J. Inorg. Chem.* **2007**, 3034−3046.

(31) Gill, M. R.; Derrat, H.; Smythe, C. G. W.; Battaglia, G.; Thomas, J. A. *ChemBioChem* **2011**, *12*, 877−880.

(32) Tan, C.; Wu, S.; Lai, S.; Wang, M.; Chen, Y.; Zhou, L.; Zhu, Y.; Lian, W.; Peng, W.; Ji, L.; Xu, A. *Dalton Trans.* **2011**, *40*, 8611−8621.

(33) Tan, C.; Lai, S.; Wu, S.; Hu, S.; Zhou, L.; Chen, Y.; Wang, M.; Zhu, Y.; Lian, W.; Peng, W.; Ji, L.; Xu, A. *J. Med. Chem.* **2010**, *53*, 7613−7624.

(34) Liu, J.; Zheng, W.; Shi, S.; Tan, C.; Chen, J.; K., Z.; Ji, L. *J. Inorg. Biochem.* **2008**, *102*, 193−202.

(35) Salassa, L. *Eur. J. Inorg. Chem.* **2011**, *32*, 4931−4947 and references therein.

(36) Corral, E.; Hotze, A. C. G.; den Dulk, H.; Leczkowska, A.; Rodger, A.; Hannon, M. J.; Reedijk, J. *J. Biol. Inorg. Chem.* **2009**, *14*, 439−448.

(37) Huang, H.-L.; Zheng-Zheng, Li, Z.-Z.; Liang, Z.-H.; Liu, Y.-J. *Eur. J. Inorg. Chem.* **2011**, 5538−5547.

(38) Schatzschneider, U.; Niesel, J.; Ott, I.; Gust, R.; Alborzinia, H.; Wölfl, S. *ChemMedChem* **2009**, *3*, 1104−1109.

(39) Kou, J.-F.; Qian, C.; Wang, J.-Q.; Chen, X.; Wang, L.-L.; Chao, H.; Ji, L.-N. *J. Biol. Inorg. Chem.* **2012**, *17*, 81−96.

(40) Chen, T.; Liu, Y.; Zheng, W.-J.; Liu, J.; Wong, Y.-S. *Inorg. Chem.* **2010**, *49*, 6366−6388.

(41) Pisani, M. J.; Fromm, P. D.; Mulyana, Y.; Clarke, R. J.; Körner, H.; Heimann, K.; Collins, J. G.; Keene, F. R. *ChemMedChem* **2011**, *6*, 848−858.

(42) Mulcahy, S. P.; Gründler, K.; Frias, C.; Wagner, L.; Prokop, A.; Meggers, E. *Dalton Trans.* **2010**, *39*, 8177−8182.

(43) Chen, T.; Mei, W.-J.; Wong, Y.-S.; Liu, J.; Liu, Y.; Xie, H.-S.; Zheng, W.-J. *MedChemComm* **2012**, *1*, 73−75.

(44) Nickita, N.; Gasser, G.; Pearson, P.; Goh, L. Y.; Bond, A. M.; Deacon, G. B.; Spiccia, L. *Inorg. Chem.* **2009**, *48*, 68−81.

(45) Joshi, T.; Barbante, G. J.; Francis, P. S.; Hogan, C. F.; Bond, A. M.; Gasser, G.; Spiccia, L. *Inorg. Chem.* **2012**, *51*, 3302−3315.

(46) Joshi, T.; Barbante, G. J.; Francis, P. S.; Hogan, C. F.; Bond, A. M.; Spiccia, L. *Inorg. Chem.* **2011**, *50*, 12172−12183.

(47) Joshi, T.; Gasser, G.; Martin, L. L.; Spiccia, L. *RSC Adv.* **2012**, *2*, 4703−4712.

(48) Nickita, N.; Belousoff; Bhatt, A. I.; Bond, A. M.; Deacon, G. B.; Gasser, G.; Spiccia, L. *Inorg. Chem.* **2007**, *46*, 8638−8651.

(49) Ahmed, S. A.; Gogal, R. M. J.; Walsh, J. E. *J. Immunol. Methods* **1994**, *170*, 211−224.

(50) Weiss, M. J.; Wong, J. R.; Ha, C. S.; Bleday, R.; Salem, R. R.; Steele, G. D. J., Jr.; Chen, L. B. *Proc. Natl. Acad. Sci. U.S.A.* **1987**, *84*, 5444−5448.

(51) Galeano, E.; Nieto, E.; García-Pérez, A. I.; Delgado, M. D.; Pinilla, M.; Sancho, P. *Leuk. Res.* **2005**, *29*, 1201−1211.
(52) Siddik, Z. H. *Oncogene* **2003**, *22*, 7265−7279 and references therein.
(53) Ke, H.; Wang, H.; Wong, W. K.; Mak, N. K.; Kwong, D. W.; Wong, K. L.; Tam, H. L. *Chem. Commun.* **2010**, *46*, 6678−6680.
(54) Kasper, C.; Alborzinia, H.; Can, S.; Kitanovic, I.; Meyer, A.; Geldmacher, Y.; Oleszak, M.; Ott, I.; Wölfl, S.; Sheldrick, W. S. *J. Inorg. Biochem.* **2012**, *106*, 126−133.
(55) Barnard, P. J.; Wedlock, L. E.; Baker, M. V.; Berners-Price, S. J.; Joyce, D. A.; Skeleton, B. W.; Steer, J. H. *Angew. Chem., Int. Ed.* **2006**, *45*, 5966−5970.
(56) Berners-Price, S. J. In *Bioinorganic Medicinal Chemistry*; Alessio, E., Ed.; Wiley-VCH: Weinheim, 2011; pp 197−222.
(57) Rackham, O.; Nichols, S. J.; Leedman, P. J.; Berners-Price, S. J.; Filipovska, A. *Biochem. Pharmacol.* **2007**, *74*, 992−1002.
(58) Barnard, P. J.; Berners-Price, S. J. *Coord. Chem. Rev.* **2007**, *251*, 1889−1902.
(59) Rubbiani, R.; Can, S.; Kitanovic, I.; Alborzinia, H.; Stefanopoulou, M.; Kokoschka, M.; Mönchgesang, S.; Sheldrick, W. S.; Wölfl, S.; Ott, I. *J. Med. Chem.* **2011**, *54*, 8646−8657.
(60) Kirin, S. I.; Ott, I.; Gust, R.; Mier, W.; Weyhermueller, T.; Metzler-Nolte, N. *Angew. Chem., Int. Ed.* **2008**, *47*, 955−959.
(61) Patra, M.; Gasser, G.; Pinto, A.; Merz, K.; Ott, I.; Bandow, J. E.; Metzler-Nolte, N. *ChemMedChem* **2009**, *4*, 1930−1938.
(62) Ott, I.; Scharwitz, M.; Scheffler, H.; Sheldrick, W. S.; Gust, R. *J. Pharm. Biomed. Anal.* **2008**, *47*, 938−942.
(63) Oehninger, L.; Stefanopoulou, M.; Alborzinia, H.; Schur, J.; Ludewig, S.; Namikawa, K.; Muñoz-Castro, A.; Köster, R. W.; Baumann, K.; Wölfl, S.; Sheldrick, W. S.; Ott, I. *Dalton Trans.* **2013**, DOI: 10.1039/c2dt32319b.
(64) Bradford, M. M. *Anal. Biochem.* **1976**, *72*, 248−254.
(65) Patra, M.; Ingram, K.; Pierroz, V.; Ferrari, S.; Spingler, B.; Keiser, J.; Gasser, G. *J. Med. Chem.* **2012**, *55*, 8790−8798.
(66) Puckett, C. A.; Ernst, R. J.; Barton, J. K. *Dalton Trans.* **2010**, *39*, 1159−1170.
(67) Puckett, C. A.; Barton, J. K. *J. Am. Chem. Soc.* **2007**, *129*, 46−47.
(68) Puckett, C. A.; Barton, J. K. *Biochemistry* **2008**, *47*, 11711−11716.
(69) Liberman, E. A.; Topali, V. P.; Tsofina, L. M.; Jasaitis, A. A.; Skulachev, V. P. *Nature* **1969**, *222*, 1076−1078.
(70) Johnson, L. V.; Walsh, M. L.; Chen, L. B. *Proc. Natl. Acad. Sci. U.S.A.* **1980**, *77*, 990−994.
(71) Bard, A. J.; Faulkner, L. R. *Electrochemical Methods, Fundamentals and Application*; 2nd ed.; Brisbane: Australia, 2001.
(72) Sevcik, A. *Collect. Czech. Chem. Commun.* **1948**, *13*, 349−377.
(73) Randles, J. E. B. *Trans. Faraday Soc.* **1948**, *44*, 322−327.
(74) Friedman, A. E.; Chambron, J.-C.; Sauvage, J.-P.; Turro, N. J.; Barton, J. K. *J. Am. Chem. Soc.* **1990**, *112*, 4960−4962.
(75) Jenkins, Y.; Friedman, A. E.; Turro, N. J.; Barton, J. K. *Biochemistry* **1992**, *31*, 10809−10816.
(76) Pyle, A. M.; Rehmann, J. P.; Meshoyrer, R.; Kumar, C. V.; Turro, N. J.; Barton, J. K. *J. Am. Chem. Soc.* **1989**, *111*, 3051−3058.
(77) Fernandez-Moreira, V.; Thorp-Greenwood, F. L.; Coogan, M. P. *Chem. Commun.* **2010**, *46*, 186−202 and references therein..
(78) Thorp-Greenwood, F. L.; Coogan, M. P.; Mishra, L.; Kumari, N.; Rai, G.; Saripella, S. *New. J. Chem.* **2012**, *36*, 64−72.
(79) Zhang, A.-G.; Zhang, Y.-Z.; Duan, Z.-M.; Wang, K.-T.; Wei, H.-B.; Bian, Z.-Q.; Huang, C.-H. *Inorg. Chem.* **2011**, *50*, 6425−6436.
(80) Carter, M. T.; Rodriguez, M.; Bard, A. J. *J. Am. Chem. Soc.* **1989**, *111*, 8901−8911.
(81) Dalton, S. R.; Glazier, S.; Leung, B.; Sanda Win, S.; Megatulski, C.; Nieter Burgmayer, S. J. *J. Biol. Inorg. Chem.* **2008**, *13*, 1133−1148.
(82) Kalsbeck, W. A.; Thorp, H. H. *J. Am. Chem. Soc.* **1993**, *115*, 7146−7151.
(83) Angeles-Boza, A. M.; Bradley, P. M.; Fu, P. K.-L.; Wicke, S. E.; Bacsa, J.; Dunbar, K. R.; Turro, C. *Inorg. Chem.* **2004**, *43*, 8510−8519.
(84) Nair, R. B.; Teng, E. S.; Kirkland, S. L.; Murphy, C. J. *Inorg. Chem.* **1998**, *37*, 139−141.
(85) Sun, J.; Wu, S.; Han, Y.; Liu, J.; Ji, L.-N.; Mao, Z.-W. *Inorg. Chem. Commun.* **2008**, *11*, 1382−1384.
(86) Idziorek, T.; Estaquier, J.; De Bels, F.; Ameisen, J.-C. *J. Immunol. Methods* **1995**, *185*, 249−258.
(87) Adams, J. M. *Genes Dev.* **2003**, *17*, 2481−2495.
(88) Li, L.; Wong, Y.-S.; Chen, T.; Fan, C.; Zheng, W. *Dalton Trans.* **2012**, *41*, 1138−1141.
(89) Gottlieb, H. E.; Kotlyar, V.; Nudelman, A. *J. Org. Chem.* **1997**, *62*, 7512−7515.
(90) *SHELXS97: Program for Crystal Structure solution*; Sheldrick, G. M., Ed.; University of Göttingen: Göttingen, Germany, 1997.
(91) *SHELXL97: Program for Crystal Structure Refinement*; Sheldrick, G. M., Ed.l University of Göttingen: Göttingen, Germany, 1997.

2.1.3. BIS(DIPYRIDOPHENAZINE)(2-(2'-PYRIDYL)PYRIMIDINE-4-CARBOXILIC ACID) RUTHENIUM(II) HEXAFLUOROPHOSPHATE: A LESSON IN STUBBORNNESS

In order to examine the influence of lipophilicity, charge, and size on the anticancer activity of the Ru(II) complex, a broad range of Ru(II) derivatives were synthetized and their toxicity and localization analysed. These modifications revealed the presence of carboxylic acid functionality as necessary to confer cytotoxicity to the Ru(II) complex.

DOI: 10.1002/cmdc.201400029

Bis(dipyridophenazine)(2-(2′-pyridyl)pyrimidine-4-carboxylic acid)ruthenium(II) Hexafluorophosphate: A Lesson in Stubbornness

Tanmaya Joshi,*[a] Vanessa Pierroz,[a, b] Stefano Ferrari,[b] and Gilles Gasser*[a]

Ruthenium complexes are currently considered to be among the most promising alternatives to platinum anticancer drugs. In this work, thirteen structural analogues and organelle/receptor-targeting peptide bioconjugates of a cytotoxic bis(dppz)-Ru^{II} complex $[Ru(dppz)_2(CppH)](PF_6)_2$ (**1**) were prepared, characterized, and assessed for their cytotoxicity and cellular localization (CppH = 2-(2′-pyridyl)pyrimidine-4-carboxylic acid; dppz = dipyrido[3,2-*a*:2′,3′-*c*]phenazine). It was observed that structural modifications (lipophilicity, charge, and size-based) result in the cytotoxic potency of **1** being compromised. Confocal microscopy studies revealed that unlike **1**, the screened complexes/bioconjugates do not have a preferential accumulation in mitochondria. The results of this important structure–activity relationship strongly support our initial hypothesis that accumulation in mitochondria is crucial for **1** to exert its cytotoxic action.

Introduction

From the biological application point of view, research interest in coordinatively saturated and substitutionally inert ruthenium(II) polypyridyl complexes have seen considerable advancement beyond their "popular" role as targeted biomolecular probes. For example, the strong DNA interaction of Ru^{II} polypyridyl scaffolds bearing ligands with extended planarity have not only been exploited for imaging and sensing applications, but have also been revisited as therapeutics.[1–11] With DNA playing a central role in many cellular processes, assessing the Ru^{II} polypyridyl complexes in a therapeutic role is certainly a judicious expansion of an already wide application window. Research on Ru^{II} polypyridyl systems with a view to their application as anticancer agents has, however, revealed that the DNA binding interaction is not always essential for such complexes to show promising cytotoxicity. For example, the activity could also arise from such complexes accumulating in, or interfering with, membrane function or otherwise inducing mitochondria-mediated apoptosis.[12–19] This "nonconventional" mode of action for some of the recently emerged cytotoxic mononuclear and dinuclear polypyridyl Ru^{II} complexes has guided a new paradigm for anticancer research focused on Ru^{II} polypyridyl chemistry.[1,2,5]

Despite a similar octahedral coordination geometry, the cytotoxicity of Ru^{II} polypyridyl complexes can vary significantly depending on several characteristic properties. An insight into the molecular mechanism of their activity is crucial to the future development of therapeutics.[20] A pool of studies have been dedicated to understand the interplay between cellular uptake mechanism, cellular localization, and lipophilicity in the antiproliferative and apoptotic effects of polypyridyl Ru^{II} systems against various cancer cell types.[1,5,13–18] However, the complexity of the interactions that can occur in the cellular microenvironment makes it challenging to outline a general trend for the cytotoxic behavior of Ru^{II} polypyridyl complexes. In our efforts to contribute to research in this direction, we recently reported the cytotoxic behavior of $[Ru(dppz)_2(CppH)]^{2+}$ (CppH = 2-(2′-pyridyl)pyrimidine-4-carboxylic acid; dppz = dipyrido[3,2-*a*:2′,3′-*c*]phenazine), a bis(dppz)-Ru^{II} polypyridyl complex (**1**, Figure 1).[18] This particular complex showed a cytotoxicity profile (against both specific cancer and noncancer cells) similar to that of cisplatin, the most well-known platinum-containing anticancer drug. The cytotoxic effect of **1** was linked to its accumulation in mitochondria, causing mitochondria-mediated apoptosis.[18] Mitochondria are believed to play a critical role in cell death by both apoptosis and necrosis.[21,22] If this is indeed the case, drugs that target mitochondria can be used for inducing apoptosis in cancerous cells or for manipulating mitochondrial function upon demand, in general. However, this organelle is also a principal site of energy metabolism and a primary source of ATP in cells, central to their functioning and survival; this is apart from several other primary roles associated with mitochondria.[21,22] Thus, for Ru^{II} complexes such as **1** to be effective as anticancer drugs in the near future, it is essential for mitochondria-mediated apoptosis to be controlled and rather selective. Restricting the intentionally induced toxicity exclusively to cancer cells, and minimizing the

[a] *Dr. T. Joshi,[+] V. Pierroz,[+] Prof. Dr. G. Gasser*
Department of Chemistry, University of Zurich
Winterthurerstrasse 190, 8057 Zurich (Switzerland)
E-mail: tanmaya.joshi3@uzh.ch
gilles.gasser@chem.uzh.ch
Homepage: http://www.gassergroup.com

[b] *V. Pierroz,[+] Priv.-Doz. Dr. S. Ferrari*
Institute of Molecular Cancer Research, University of Zurich
Winterthurerstrasse 190, 8057 Zurich (Switzerland)

[+] *These authors contributed equally to this work.*

Supporting information for this article is available on the WWW under http://dx.doi.org/10.1002/cmdc.201400029.

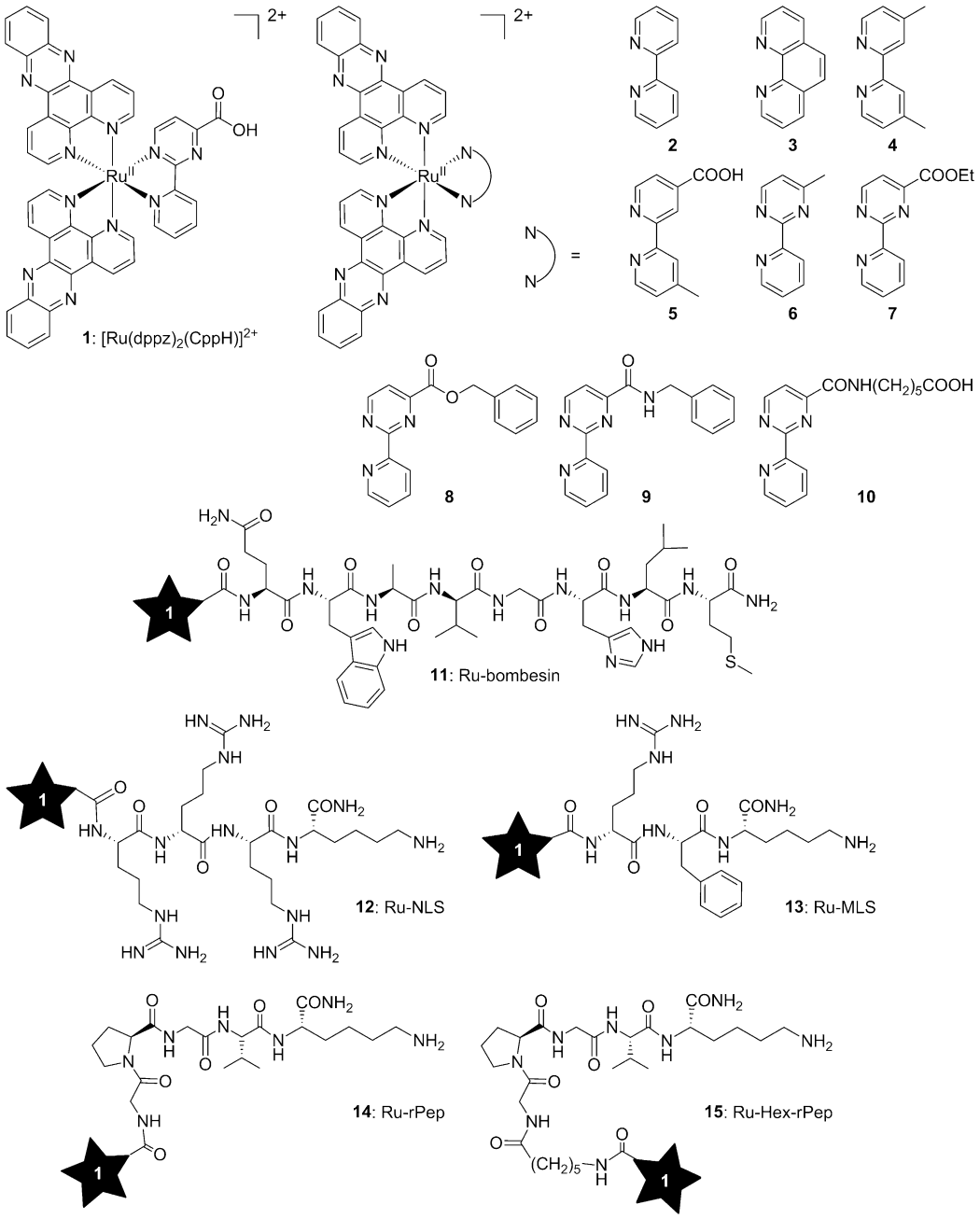

Figure 1. Structures of bis(dppz)-Ru^{II} derivatives (racemic mixtures) investigated in this work (isolated as hexafluorophosphate salts).

inevitable collateral damage are indeed the highly desirable objectives in anticancer drug discovery.[20,23]

As for the other substitutionally inert Ru^{II} polypyridyl complexes, precise understanding of the exact mechanism behind the anticancer efficacy of this complex is still developing. The structure–activity correlations aimed to obtain additional insight into the specificity displayed by **1** may serve as the basis for development of bis(dppz)-Ru^{II} complexes with improved efficacy.[23] With this in mind, in this work, we evaluated the influence of the CppH ligand on the cytotoxicity of **1**. The Ru^{II} polypyridyl complexes of the CppH ligand have previously been used by us for metalation of artificial nucleic acids.[6,24] A series of bis(dppz)-Ru^{II} analogues of the lead complex **1** were synthesized and screened for their cytotoxic properties (**2**–**9**, Figure 1). In these complexes, either the pyrimidine carboxylic acid framework of the original CppH ligand was replaced with a substituted pyridine, or the carboxylic acid functionality was derivatized to incorporate an ester/amide linkage or an alkyl group. The observed cytotoxic effects were also compared with those of **10** (Figure 1), a structurally related bis(dppz)-Ru^{II} complex containing a hexyl spacer between the metal coordinating Cpp unit and the carboxylic acid moiety, reported re-

cently by us.[18] Furthermore, specific organelle/receptor-targeting peptide bioconjugates of **1** (**11**–**15**, Figure 1) were prepared, and their cytotoxic potency was evaluated. These Ru^{II}-peptide bioconjugates were investigated as part of an attempt to further improve the selectivity and efficacy of **1** through its short construct-promoted delivery to specific cell organelles. This strategy was successfully adopted for the targeted delivery of Ru^{II} (and other metal) complexes to cellular compartments.[4,25–29] However, despite all hypothesized advantages, pursuing this approach in our case did not lead to any improvement in the cytotoxic potency of the parent Ru^{II} complex, **1** (see below).

Results and Discussion

Synthesis and characterization

The bis(dppz)-Ru^{II} derivatives **2**–**9** were prepared from their respective ruthenium(II) *cis*-dicarbonyl precursors following chemical decarbonylation methodology, as described in Scheme 1. The coordination mode of the asymmetric 2-(pyridin-2-yl)pyrimidine unit in compounds **6**–**9** was established on the basis of X-ray crystal structures of other bis(diimine)-Ru^{II}-2-(2′-pyridyl)pyrimidine complexes previously prepared through this decarbonylation route, showing the carboxylate group to point away from the Ru^{II} center.[18,30] The desired complexes were isolated as racemic mixtures and characterized by ^{1}H NMR spectroscopy, mass spectrometry, and elemental analysis. Furthermore, taking advantage of the carboxylic acid functionality present in **1**, the Ru^{II}-NLS (nuclear localization signal) and Ru^{II}-MLS (mitochondrial localization signal) peptide bioconjugates **12** and **13** (Figure 1) were prepared, intending specific delivery of the active molecule to the nuclei and mitochondria, respectively.[31,32] In addition, a Ru^{II}-bombesin bioconjugate **11** (Figure 1) was also synthesized to evaluate its toxicity toward HeLa cells. The truncated bombesin[33] sequence (QWAVGHLM) was chosen for improved cellular internalization of the Ru^{II} complex, as the peptide is known to have high recognition affinity for gastrin-releasing peptide receptors (GRPrs), found to be overexpressed in HeLa cells.[33,34] As controls, **14** and **15**, the random five-residue sequence (GPGVK) bioconjugates of complexes **1** and **10**, were also prepared. The identity and purity of the HPLC-purified Ru^{II}-peptide bioconjugates were assessed by LC–MS (see Supporting Information).

Cytotoxicity studies

The cytotoxic action of the complexes **2**–**15** was evaluated on human cervical cancer (HeLa) and noncancerous lung fibroblast (MRC-5) cell lines. Cell viability was quantified by resazurin-based fluorimetric assays. The IC_{50} values obtained were compared with those of the lead Ru^{II} complex **1** and of cisplatin (Table 1). Overall, the tested complexes were found to be less active toward the cancerous (HeLa) and noncancerous (MRC-5) cells than the parent prototype complex or cisplatin. Inclusion of a 2,2′-bipyridyl or a 1,10-phenanthroline ligand in **2** and **3**, respectively, was found to severely affect the cytotoxic potency of the corresponding bis(dppz) complexes (IC_{50} ~ 70 μM). A similar cytotoxic response toward both cell lines was observed for **4**, which incorporated a (bis)methyl substituted 2,2′-bipyridyl ligand, Me_2bpy, in the metal coordination sphere. Interestingly, complex **5**, in which one of the methyl groups is replaced with a carboxylic acid functionality, showed a twofold improvement in cytotoxicity toward HeLa cells (IC_{50} = 33.3 μM). This particular complex was also found to be selective in its cytotoxic action; no IC_{50} values were reached up to the

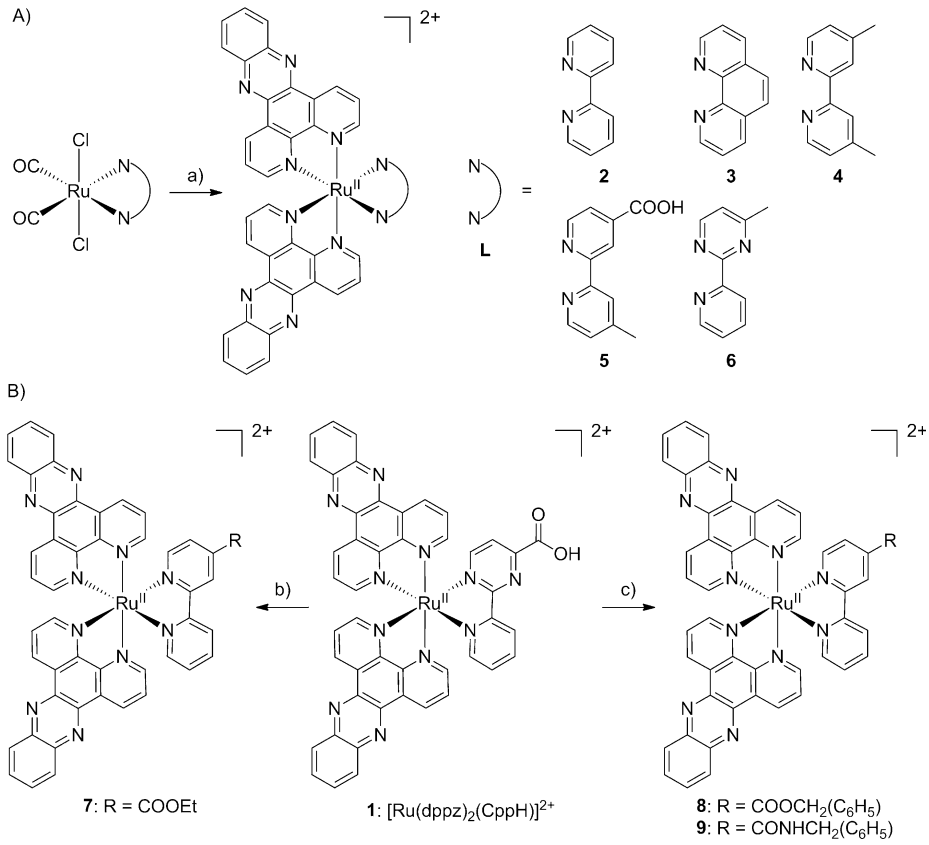

Scheme 1. Chemical decarbonylation route for the preparation of **2**–**9** (racemic mixtures). *Reagents and conditions*: a) dppz, Me_3NO, 2-methoxyethanol, Δ, 4 h; 45–68%; b) $SOCl_2$, EtOH, Δ, 24 h, 76%; c) benzyl alcohol **7**/benzylamine **8**, HATU, DMAP, Et_3N, DMF, Δ, 24 h, ~50%.

Table 1. Cytotoxic activity data for Ru^{II} complexes **1**–**15** against human cervical cancer (HeLa) and noncancerous fibroblast (MRC-5) cell lines.

Complex	IC_{50} [μM][b]		Formal charge	log *D*[a]	N^N = L
	HeLa	MRC-5	(pH 7.0)		
1[18]	10.0 ± 1.3	15.1 ± 2.2	1+	−1.74	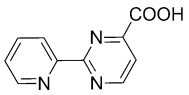
2	63.5 ± 8.7	72.0 ± 0.1	2+	1.96	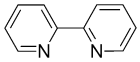
3	69.0 ± 5.6	68.5 ± 0.3	2+	2.29	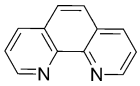
4	70.2 ± 1.2	65.4 ± 0.9	2+	2.98	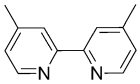
5	33.3 ± 3.9	> 100	1+	−1.03	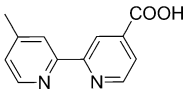
6	> 100	> 100	2+	1.75	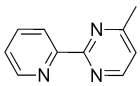
7	34.2 ± 0.2	36.5 ± 1.9	2+	1.94	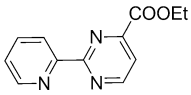
8	38.5 ± 3.1	90.5 ± 10.1	2+	3.32	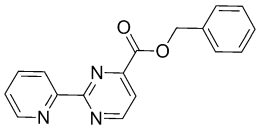
9	69.4 ± 3.8	81.1 ± 0.2	2+	2.68	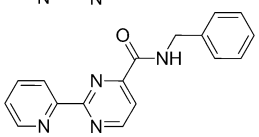
10[18]	57.5 ± 4.8	66.3 ± 8.1	1+	−1.22	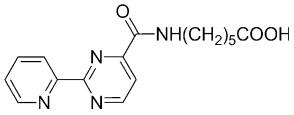
11	71.8 ± 4.2	> 100	2+		
12	43.1 ± 0.1	ND	3+		
13	> 100	ND	3+		
14	> 100	ND	3+		
15	> 100	ND	3+		
cisplatin	9.9 ± 0.9	8.5 ± 0.9			

[a] Octanol–water distribution coefficient at pH 7.0 for the ligands was calculated using Calculator Plugins for structure property prediction and calculation; Marvin 6.1.0, 2013, ChemAxon (http://www.chemaxon.com). [b] Data are the average ± SD of at least two independent experiments, each performed in triplicate per concentration level; ND: not determined.

maximum tested concentrations of 100 μM toward the MRC-5 cell line.

When functional modifications were performed on the pyrimidine ring of the CppH ligand, the resulting complexes **6**–**9** exhibited a broader cytotoxic response window. The IC_{50} values on HeLa cells of the tested complexes varied from ~34 μM (complex **7**) to showing no inhibitory effect up to the highest complex concentration (100 μM) used in the case of methyl-substituted complex **6**. Notably, none of the tested analogues showed an improvement in cytotoxicity against cancer cells relative to the lead compound **1**, the most potent complex **7** being almost threefold less active. This observation is in good agreement with our earlier reports in which a similar decrease in activity was observed with subtle changes in the structure for **1**.[18] Also, much to our surprise, relative to **1**, peptide conjugation lowered the cytotoxicity by at least fourfold in the case of **12**, the most active Ru^{II}-peptide conjugate screened. No IC_{50} values were obtained from the highest concentration (100 μM) of **14** and **15**, the random five-residue sequence based **1** conjugates used as controls, to which the cells were exposed.

Cellular localization

Aiming to obtain a qualitative correlation between the cytotoxicity and intercellular localization of the tested Ru^{II} complexes, the *in cellulo* luminescence response for the complexes was probed with confocal laser scanning microscopy (CLSM; Figure 2). The intrinsic capacity of the Ru^{II}-polypyridyl complexes to produce luminescence in the cellular microenvironment was previously shown to be highly relevant to their application in cellular imaging.[1,35–38] Furthermore, this characteristic property has been exploited as an indirect measure of their cellular uptake, which in general finds good agreement with the alternative techniques explored for quantification, alongside CLSM.[1,35] Specific to our lead complex **1**, we could previously show an extremely good correlation between the mitochondrial uptake visually observed from the confocal microscopy studies and its quantification thereafter using high-resolution continuum source atomic absorption spectrometry (HR-CS AAS).[18]

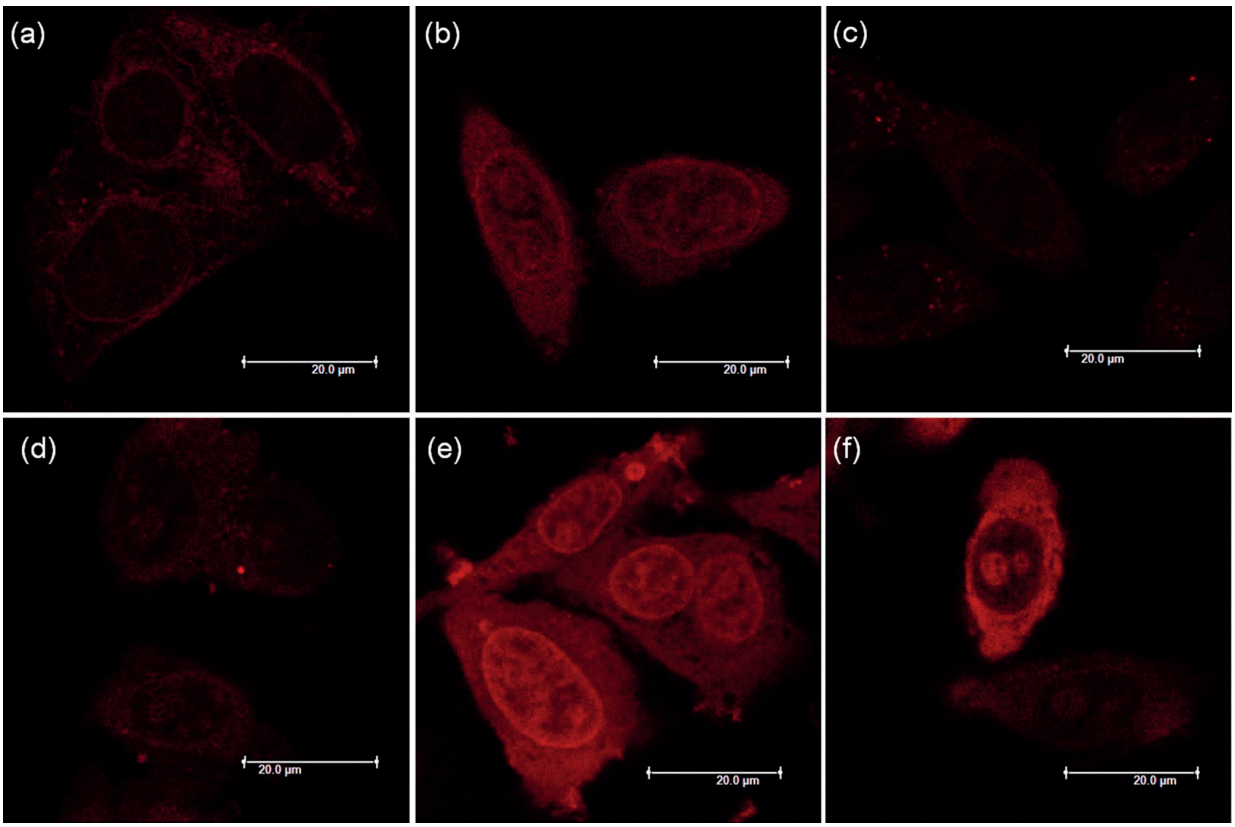

Figure 2. Fluorescence confocal microscopy images showing cellular staining patterns for HeLa cells incubated with Ru^{II} complexes a) **5** (40 μM), b) **6** (100 μM), c) **7** (30 μM), d) **8** (30 μM), e) **11** (70 μM), and f) **12** (40 μM) for 2 h.

Prior to visualization by confocal microscopy, HeLa cells were exposed to the test complex (at their respective IC_{50} values, or at 100 μM if no IC_{50} could be reached) for 2 h. In all cases, the co-staining of DNA with 4′,6-diamidino-2-phenylindole (DAPI), a commonly used fluorescent nuclear counterstain, was also performed for definitive evidence of nuclear internalization of the Ru^{II} complexes investigated as part of this work. Although displaying varying emission intensities in cells relative to the lead prototype **1**, the tested complexes appeared to be internalized in cells in a rather nonspecific manner (Figure 2 and Figures S13–S23, Supporting Information).

Imaging analysis of the fixed HeLa cells points toward the presence of the complexes **2**, **3**, and **6** in the cytoplasm, along with an intense luminescence signal in the nucleoli. Complexes **4**, **5**, and the ester derivatives **7** and **8** seemed to accumulate mainly in the cytoplasm, showing a relatively weak luminescence signal from the nucleoli, whereas the amide derivative **9** displayed a qualitatively homogenous spread in the cytoplasm and nucleus. Distinct targeting of the nuclear membrane was observed in the case of complex **4** (Figure S15, Supporting Information), albeit at a relatively high concentration of 100 μM. A rather interesting cellular accumulation pattern was observed for the Ru^{II}-peptide conjugates **11**–**15**. The bombesin conjugation foreseen to increase the cellular uptake of **1** led to an intense staining of the cytoplasmic region alongside the relatively stronger nucleus-associated emission for **11** (Figure 2e). Covalent linkage of the NLS peptide resulted in the cytoplasm and nucleoli becoming the regions of accumulation for **12** (Figure 2f). The MLS-conjugated Ru^{II} complex **13** also followed a similar staining pattern, although with a much lower luminescence intensity (Figure S22, Supporting Information). Interestingly, whilst incorporation of a hexyl spacer between the randomly selected peptide and **1** in Ru^{II}-bioconjugate **15** delivered it exclusively to the cell nucleus, its direct attachment to the CppH ligand in **14** showed almost no visible cellular uptake up to the highest tested concentration (100 μM; Figure S23, Supporting Information).

The relative hydrophobicity of ligands can play a crucial role in the cellular uptake and localization of the Ru^{II} polypyridyl complexes. Depending on whether the mechanism of cellular uptake is exclusively energy dependent or independent, or a combination of both, the localization in one cellular compartment could be preferred over others.[1,35,39–41] With only the CppH ligand being a variable in the derivatives investigated in this work, it can be rationally argued that the overall differences in the lipophilicity of the complexes should follow the trend in lipophilicity of the individual 2,2′-bipyridyl- or pyrimidine-ring-modified ligands. The theoretically calculated log $D_{octanol/water}$ values indicate that the ligands have increased lipophilic character over the CppH ligand (Table 1). It should be noted that this theoretically predicted trend, which is based on

the lipophilic character of the individual 2,2′-bipyridyl- or pyrimidine-ring-modified ligands, fits with the experimental log $D_{octanol/water}$ values for the dicationic Ru^{II} complexes **1** and **10** previously determined by shake-flask method (−0.21 vs. −0.05).[18] As discussed earlier, in our case, in general the investigated derivatives mainly showed cytoplasmic staining, and decreased nuclear targeting. Taking together these two observations, cellular uptake appears to occur by passive diffusion. Notably, the CLSM studies were performed at different complex concentrations. In addition, the polarity and water accessibility of bis(dppz)-Ru^{II} complexes in the cellular microenvironment could affect the intensity of the emission signals.[1,37,38] Interestingly, however, the cytotoxic potency of the complexes investigated in this work cannot be explained only in terms of their lipophilicity. The overall cationic charge of complex **5** (+1) at pH 7.0, and the hydrolytic susceptibility of the ester functionalities in **7** and **8** could contribute to their observed modest cytotoxic activity relative to **1**. The precise reasons cannot be explained with certainty at this stage, however, and are a subject of our further investigations.

Conclusions

In summary, the studies conducted herein highlight the sensitivity in cytotoxic action of a substitutionally inert bis(dppz) Ru^{II} complex, **1**. Subtle structural alterations in this lead prototype were found to have a detrimental effect on its cytotoxic potency; at least a fourfold decrease in activity was observed for the investigated analogues. Furthermore, CLSM studies revealed that with lipophilicity, charge, and size-based modifications, the bis(dppz)-Ru^{II} complexes lose out on the preference for mitochondrial accumulation previously observed for **1**. In conjunction, these results support our original hypothesis that mitochondrial accumulation is crucial for the high cytotoxicity of **1**. More importantly, these findings establish **1** as a promising candidate for the future design of Ru^{II}-polypyridyl anticancer prodrugs.[42] Overall, our results also underscore the difficulty in finding a rationale between chemical structures and antiproliferative effect for substitutionally inert metal complexes.

Experimental Section

Materials: All chemicals were of reagent-grade quality or better, obtained from commercial suppliers and used without further purification. Solvents were used as received or distilled using standard procedures. Deionized water was used for all reactions in aqueous solution. Reagents and solvents for solid-phase peptide synthesis were of HPLC grade and purchased from Acros (Geel, Belgium), Aldrich/Sigma/Fluka (Deisenhofen, Germany), Merck (Darmstadt, Germany), and IRIS Biotech (Marktredwitz, Germany), and were used without further purification. The preloaded polystyrene resins were purchased from Rapp Polymers (Tübingen, Germany). Unless otherwise mentioned, only L-amino acids were used throughout. Thin-layer chromatography (TLC) was performed using silica gel 60 F_{254} (Merck) plates with detection of spots by exposure to iodine or UV light. Column chromatography was done using silica gel 60 (0.040–0.063 mm mesh, Merck) or activated neutral alumina (Brockmann I, Sigma–Aldrich). Eluent mixtures are expressed as volume to volume (*v/v*) ratios.

Instrumentation and methods: A vacuum line and Schlenk glassware were employed when reactions had to be carried out under an atmosphere of dry, oxygen-free nitrogen, and assemblies were protected from light if necessary by wrapping them in aluminum foil. ^1H and $^{13}C\{^1H\}$ NMR spectra were measured on Bruker DRX 400 and 500 spectrometers at room temperature. Chemical shift values (δ) are reported in parts per million (ppm), using the signal of the deuterated solvent as an internal standard.[43] The abbreviations for the peak multiplicities are as follows: s (singlet), d (doublet), dd (doublet of doublets), t (triplet), q (quartet), m (multiplet), and br (broad). ESI mass spectrometry was performed using a Bruker Esquire 6000 spectrometer. In the assignment of the mass spectra, the most intense peak is listed. Infrared spectra were recorded on PerkinElmer FTIR spectrometer fitted with an ATR platform. Peak intensities are given as broad (br), very strong (vs), strong (s), medium (m) and weak (w). Microanalysis was performed on a LecoCHNS-932 elemental analyzer. HPLC purification of Ru^{II}-peptides was performed on a Varian ProStar system equipped with a diode array UV/Vis spectrometer equipped with Agilent Zorbax 300SB-C_{18} semi-prep (5 μm particle size, 300 Å pore size, 250×9.4 mm; flow rate: 4 mL min^{-1}) or Agilent Zorbax 300SB-C_{18} prep (5 μm particle size, 300 Å pore size, 150×21.2 mm; flow rate: 20 mL min^{-1}) column. Chromatographic separations were performed with a linear gradient of A (distilled H_2O containing 0.1% *v/v* TFA) and B (CH_3CN (Sigma–Aldrich HPLC grade), containing 0.1% *v/v* TFA). Preparative runs: $t=0$ min, 5% B; $t=6$ min, 30% B; $t=15$ min, 55% B; $t=21$ min, 81% B; $t=25.5$ min, 100% B; $t=31$ min, 100% B; $t=33$ min, 5% B. The LC–MS spectra of metallopeptides were measured on an Acquity Waters system equipped with a PDA detector and an autosampler using an Agilent Zorbax 300SB-C_{18} analytical column (3.5 mm particle size, 300 Å pore size, 150×4.6 mm). The LC was coupled to an Esquire HCT from Bruker (Bremen, Germany) for the MS measurements. The LC run (flow rate: 0.3 mL min^{-1}) was performed with a linear gradient of A (distilled H_2O containing 0.1% *v/v* formic acid) and B (CH_3CN (Sigma–Aldrich HPLC-grade), containing 0.1% *v/v* formic acid); $t=0$ min, 5% B; $t=3$ min, 5% B; $t=17$ min, 100% B; $t=20$ min, 100% B; $t=25$ min, 5% B. The purity of all the Ru^{II} complexes and the Ru-peptide conjugates, as analyzed from microanalysis or the corresponding LC traces, was found to be >95%.

Synthesis: Compounds 4-methyl-2-(pyridin-2-yl)pyrimidine (Mpp),[30] dipyrido[3,2-*a*:2′,3′-*c*]phenazine (dppz),[44] $[Ru(CO)_2Cl_2]_n$,[45] $[Ru^{II}(bpy)(CO)_2Cl_2]$,[45] $[Ru^{II}(phen)(CO)_2Cl_2]$,[45] $[Ru^{II}(Me_2bpy)(CO)_2Cl_2]$,[45] $[Ru(dppz)_2(CppH)](PF_6)_2$ (**1**),[18] and $[Ru(dppz)_2(MebpyCOOH)](PF_6)_2$ (**5**)[46] were synthesized according to published procedures. The characterization data were in agreement with the published data.

$[Ru^{II}(Mpp)(CO)_2Cl_2]$: 4-methyl-2-(pyridin-2-yl)pyrimidine (Mpp) (0.140 g, 0.82 mmol) was added to deoxygenated CH_3OH (12 mL) and heated at 60 °C until its complete dissolution was achieved. $[Ru(CO)_2Cl_2]_n$ (0.230 g, 1.01 mmol) was added, and the reaction mixture was held at reflux under nitrogen for 2 h. The solution was cooled to 2 °C overnight to afford a yellow precipitate, which was collected by filtration. The collected filtrate was restored at −4 °C overnight for complete precipitation of the product, which was collected by filtration, and washed with ice-cold CH_3OH to obtain the second crop as a yellow solid. Yield: 0.123 g (39%); ^1H NMR (500 MHz, [D$_6$]DMSO): $\delta=9.39$ (d, $^3J=5.5$ Hz, 1H), 9.26–9.24 (m, 1H), 8.77–8.75 (m, 1H), 8.44–8.40 (m, 1H), 7.99–7.96 (m, 1H), 7.83 (d, $^3J=6.0$ Hz, 1H), 2.78 ppm (s, 3H); ^{13}C NMR (125 MHz,

[D_6]DMSO): $\delta = 197.0$, 196.8, 172.5, 162.8, 160.4, 154.6, 153.5, 142.1, 130.9, 127.1, 124.5, 25.2 ppm; IR (ATR): $\tilde{\nu} = 3096$ (C-H_{arom}), 2059 (C≡O), 1987 (C≡O), 1590 1578, 1412, 1322, 1031, 824, 773 cm^{-1}; MS (ESI^+): *m/z* 542.9 $[M+H]^+$; Anal. calcd for $C_{12}H_9Cl_2N_3O_2Ru$ (%): C 36.11, H 2.27, N 10.53, found: C 36.39, H 2.31, N 10.76.

[Ru(dppz)$_2$(bpy)](PF$_6$)$_2$ (2): Complex **2** was obtained as a red solid following the procedure described for [Ru(dppz)$_2$(CppH)](PF$_6$)$_2$,[18] using dipyrido[3,2-*a*:2′,3′-*c*]phenazine (dppz) (0.170 g, 0.603 mmol), trimethylamine-*N*-oxide dihydrate (0.130 g, 1.17 mmol), and [Ru^{II}(bpy)(CO)$_2$(Cl)$_2$] (0.100 g, 0.260 mmol) in 5 mL 2-methoxyethanol. Yield: 0.189 g (65%); ^{1}H NMR (400 MHz, CD_3CN): $\delta = 9.75$–9.72 (m, 2H), 9.65–9.62 (m, 2H), 8.59–8.57 (m, 2H), 8.51–8.46 (m, 4H), 8.31–8.29 (m, 2H), 8.18–8.14 (m, 6H), 8.11–8.07 (m, 2H), 7.99–7.95 (m, 2H), 7.89–7.88 (m, 2H), 7.78–7.75 (m, 2H), 7.36–7.33 ppm (m, 2H); MS (ESI^+): *m/z* 411.0 $[M-2PF_6]^{2+}$; Anal. calcd for $C_{46}H_{28}F_{12}N_{10}P_2Ru$ (%): C 49.69, H 2.54, N 12.60, found: C 49.87, H 2.54, N 12.28.

[Ru(dppz)$_2$(phen)](PF$_6$)$_2$·1.5 H$_2$O (3): Complex **3** was isolated as a red solid from dipyrido[3,2-*a*:2′,3′-*c*]phenazine (dppz) (0.242 g, 0.851 mmol), trimethylamine-*N*-oxide dihydrate (0.183 g, 1.65 mmol), and [Ru^{II}(phen)(CO)$_2$(Cl)$_2$] (0.150 g, 0.367 mmol) in 5 mL 2-methoxyethanol, using the same method as for **2**. Yield: 0.251 g (60%); ^{1}H NMR (400 MHz, CD_3CN): $\delta = 9.67$–9.65 (m, 4H), 8.66–8.64 (m, 2H), 8.50–8.48 (m, 4H), 8.31–8.30 (m, 4H), 8.24–8.22 (m, 2H), 8.17–8.11 (m, 6H), 7.84–7.78 (m, 4H), 7.71–7.67 ppm (m, 2H); MS (ESI^+): *m/z* 423.0 $[M-2PF_6]^{2+}$, 990.8 $[M-PF_6]^+$; Anal. calcd for $C_{48}H_{28}F_{12}N_{10}P_2Ru·1.5H_2O$ (%): C 49.58, H 2.69, N 12.05, found: C 49.63, H 2.45, N 11.76.

[Ru(dppz)$_2$(Me$_2$bpy)](PF$_6$)$_2$·3 H$_2$O (4): The synthesis was as described for complex **2**, but using dipyrido[3,2-*a*:2′,3′-*c*]phenazine (dppz) (0.103 g, 0.528 mmol), trimethylamine-*N*-oxide dihydrate (0.139 g, 1.25 mmol) and [Ru^{II}(Me$_2$bpy)(CO)$_2$(Cl)$_2$] (0.103 g, 0.250 mmol) in 15 mL 2-methoxyethanol, affording the **4** as a red solid. Yield: 0.193 g (68%); ^{1}H NMR (400 MHz, CD_3CN): $\delta = 9.73$–9.71 (m, 2H), 9.63–9.61 (m, 2H), 8.51–8.44 (m, 6H), 8.31–8.29 (m, 2H), 8.17–8.14 (m, 6H), 7.99–7.95 (m, 2H), 7.76–7.73 (m, 2H), 7.69–7.67 (m, 2H), 7.19–7.17 (m, 2H), 2.54 ppm (s, 6H); MS (ESI^+): *m/z* 425.2 $[M-2PF_6]^{2+}$, 995.0 $[M-PF_6]^+$; Anal. calcd for $C_{48}H_{32}F_{12}N_{10}P_2Ru·3H_2O$ (%): C 48.29, H 3.21, N 11.73, found: C 48.38, H 2.90, N 12.38.

[Ru(dppz)$_2$(Mpp)](PF$_6$)$_2$ (6): Complex **6** was prepared using dipyrido[3,2-*a*:2′,3′-*c*]phenazine (dppz) (0.072 g, 0.255 mmol), trimethylamine-*N*-oxide dihydrate (0.062 g, 0.558 mmol), and [Ru^{II}(Mpp)(CO)$_2$(Cl)$_2$] (0.050 g, 0.125 mmol) in 6.5 mL 2-methoxyethanol. The synthesis was as for **2**, with purification by silica gel column chromatography (eluent polarity gradually changed from 100% EtOAc to CH_3CN/H_2O/satd KNO_3 (16:3:1)). The fractions containing an intense orange band were combined, solvent was removed under reduced pressure, and the residue was resuspended in CH_3CN and filtered. The filtrate was evaporated to dryness, and residue was suspended in H_2O (5 mL). The hexafluorophosphate salt of the desired complex was precipitated by dropwise addition of saturated aqueous solution of NH_4PF_6 to the aqueous suspension. The precipitate was collected by filtration, washed with H_2O and Et_2O, and dried under vacuum to obtain **6** as a red solid. Yield: 0.064 g (45%); ^{1}H NMR (400 MHz, CD_3CN): $\delta = 9.76$–9.74 (m, 2H), 9.66–9.62 (m, 2H), 8.84–8.82 (m, 1H), 8.52–8.46 (m, 5H), 8.34–8.32 (m, 1H), 8.19–8.12 (m, 7H), 8.00–7.97 (m, 2H), 7.90–7.86 (m, 2H), 7.79–7.74 (m, 2H), 7.48–7.43 (m, 1H), 7.26–7.24 (m, 1H), 2.71 ppm (s, 3H); MS (ESI^+): *m/z* 418.5 $[M-2PF_6]^{2+}$, 982.1 $[M-PF_6]^+$; Anal. calcd for $C_{46}H_{29}F_{12}N_{11}P_2Ru$ (%): C 49.03, H 2.59, N 13.67, found: C 48.91, H 2.70, N 13.49.

[Ru(dppz)$_2$(Cpp-OEt)](PF$_6$)$_2$·2 H$_2$O (7): [Ru(dppz)$_2$(CppH)] (PF$_6$)$_2$ (0.020 g, 0.017 mmol) was added to anhydrous EtOH (8 mL, pre-acidified by dropwise addition of $SOCl_2$ (1.5 mL) at 0 °C), and the reaction mixture was held at reflux under nitrogen for 24 h. The solvent was evaporated in vacuo, and the residue was suspended in H_2O (3 mL). Saturated aqueous solution of NH_4PF_6 was added dropwise until no further precipitation was observed. The orange precipitate was collected by filtration, air-dried, and extracted with 10 mL $CHCl_3/CH_2Cl_2$ (7:3 *v/v*) to remove unreacted [Ru(dppz)$_2$(CppH)](PF$_6$)$_2$. The filtrate was evaporated to dryness, the residue was dissolved in minimal volume of CH_2Cl_2 and layered with Et_2O. The precipitate so formed on standing at room temperature was collected by filtration, washed thoroughly with $CHCl_3/Et_2O$ (2:8 *v/v*) and dried in vacuo to afford **7** as an orange solid. Yield: 0.015 g (76%); ^{1}H NMR (400 MHz, CD_3CN): $\delta = 9.77$–9.75 (m, 2H), 9.68–9.65 (m, 2H), 8.89 (d, $^3J = 7.8$ Hz, 1H), 8.52–8.46 (m, 5H), 8.38–8.31 (m, 2H), 8.20–8.13 (m, 7H), 8.02–7.77 (m, 6H), 7.54–7.48 (m, 1H), 4.48 (q, $^3J = 7.1$ Hz, 2H), 1.40 ppm (t, $^3J = 7.1$ Hz, 3H); MS (ESI^+): *m/z* 447.6 $[M-2PF_6]^{2+}$; Anal. calcd for $C_{48}H_{31}F_{12}N_{11}O_2P_2Ru·2H_2O$ (%): C 47.22, H 2.89, N 12.62, found: C 47.58, H 2.51, N 12.39.

[Ru(dppz)$_2$(Cpp-OC$_6$H$_5$)](PF$_6$)$_2$·2 H$_2$O (8): A solution of [Ru(dppz)$_2$(CppH)](PF$_6$)$_2$ (0.025 g, 0.022 mmol), benzyl alcohol (0.012 mL, 0.110 mmol), HATU (0.017 g, 0.044 mmol), DMAP (0.014 g, 0.110 mmol), and Et_3N (0.006 mL, 0.044 mmol) in dry DMF (8 mL) was heated at 80 °C under nitrogen atmosphere for 24 h. The solvent was removed under reduced pressure, the residue was diluted with H_2O (3 mL), and an aqueous solution (satd) of NH_4PF_6 (1 mL) was added to it, resulting in the formation of an orange precipitate. The precipitate was collected by filtration on a sintered glass frit, washed thoroughly with H_2O and Et_2O, and the washings were discarded. The solid was extracted with 10 mL $CHCl_3/CH_2Cl_2$ (7:3 *v/v*) to remove unreacted [Ru(dppz)$_2$(CppH)](PF$_6$)$_2$, the filtrate was collected, and concentrated under reduced pressure. The residue obtained was dissolved in minimal amount of CH_2Cl_2, layered with Et_2O and left standing at room temperature overnight. This resulted in the formation of a precipitate which was collected by suction filtration, washed with $Et_2O/CHCl_3$ (8:2 *v/v*) and ether, and dried under high vacuum to obtain **8** as an orange solid. (Note: alternatively, silica gel column chromatography using CH_3CN/H_2O/satd KNO_3 (16:3:1) as eluent could be performed for a scale-up reaction). Yield: 0.014 g (51%); ^{1}H NMR (400 MHz, CD_3CN): $\delta = 9.76$–9.74 (m, 2H), 9.67–9.63 (m, 2H), 8.86 (d, $^3J = 7.8$ Hz, 1H), 8.51–8.45 (m, 5H), 8.38–8.30 (m, 2H), 8.19–8.13 (m, 7H), 8.00–7.94 (m, 2H), 7.91–7.89 (m, 1H), 7.84–7.75 (m, 3H), 7.51–7.49 (m, 3H), 7.44–7.38 (m, 3H), 5.48 ppm (s, 2H); MS (ESI^+): *m/z* 478.6 $[M-2PF_6]^{2+}$; Anal. calcd for $C_{53}H_{33}F_{12}N_{11}O_2P_2Ru·2H_2O$ (%): C 49.62, H 2.91, N 12.01, found: C 49.38, H 2.52, N 11.93.

[Ru(dppz)$_2$(Cpp-NHC$_6$H$_5$)](PF$_6$)$_2$·2 H$_2$O (9): The synthesis was carried out as for **8**, but using benzylamine (0.012 mL, 0.110 mmol) in 8 mL dry DMF (8 mL). The product was isolated as an orange solid. Yield: 0.012 g (45%); ^{1}H NMR (400 MHz, CD_3CN): $\delta = 9.76$–9.74 (m, 2H), 9.67–9.63 (m, 2H), 9.14–9.12 (m, 1H), 9.06–9.00 (m, 1H), 8.51–8.43 (m, 5H), 8.35–8.28 (m, 2H), 8.20–8.11 (m, 7H), 8.00–7.90 (m, 4H), 7.81–7.76 (m, 2H), 7.52–7.48 (m, 1H), 7.43–7.35 (m, 4H), 7.32–7.28 (m, 1H), 4.69 ppm (m, 2H); MS (ESI^+): *m/z* 478.1 $[M-2PF_6]^{2+}$; Anal. calcd for $C_{53}H_{34}F_{12}N_{12}OP_2Ru·2H_2O$ (%): C 49.66, H 2.99, N 13.11, found: C 49.59, H 3.07, N 13.08.

Synthesis of Ru^{II}-peptide conjugates 11–15: The Ru-peptide conjugates were prepared by manual Fmoc SPPS, following protocols established for synthesis of other metal–peptide bioconjugates.[29] The peptide sequences used were QWAVGHLM (**11**), RR_DRK (**12**), R_DFK (**13**), and GPGVK for **14** and **15** (written from N to C termi-

nus). Following the Fmoc deprotection of the last amino acid of the desired peptide sequence, solid-phase insertion of **1** (or complex **10** in the case of Ru^{II}-peptide bioconjugate **15**) at the N-terminus of the peptide sequence was achieved by reacting a solution of the complex (5 equiv), pre-activated in an Eppendorf tube for 2 min with HATU (4.5 equiv), DIPEA and 2,6-lutidine (10 equiv each), with the peptide preloaded polystyrene resin for 10 h at 400 rpm on a mechanical shaker. The Ru^{II}-peptide bioconjugates were cleaved using a mixture of TFA/triisopropylsilane/phenol 85:5:10 (*v*/*v*/*v*) [3×400 μL (1.5 h each)]. Before cleavage, the resin was contracted with CH_3OH and dried. TFA was removed from the resulting solutions under high vacuum before the crude oligomers being precipitated with ice-cold ether. The solids were centrifuged (10 min, 10000 *g*), washed with ice-cold ether and finally air dried. The obtained crude products were purified with RP-HPLC and finally characterized by ESIMS. The purity was assessed by LC–MS. Characterization of **11**: LC–MS: $t_R = 12.5$ min; ESIMS: *m/z* 894.3 $[M]^{2+}$, 596.7 $[M+H]^{3+}$. Characterization of **12**: LC–MS: $t_R = 11.7$ min; ESIMS: *m/z* 731.2 $[M]^{2+}$, 487.8 $[M+H]^{3+}$, 366.1 $[M+2H]^{4+}$. Characterization of **13**: LC–MS: $t_R = 13.3$ min; ESIMS: *m/z* 648.7 $[M]^{2+}$, 432.8 $[M+H]^{3+}$. Characterization of **14**: LC–MS: $t_R = 13.5$ min; ESIMS: *m/z* 652.1 $[M]^{2+}$, 435.1 $[M+H]^{3+}$. Characterization of **15**: LC–MS: $t_R = 14.3$ min; ESIMS: *m/z* 708.7 $[M]^{2+}$, 472.9 $[M+H]^{3+}$.

Determination of Ru-peptide concentrations: Stock solutions of the Ru-peptides **11**–**15** were prepared in nanopure water, and molar concentrations were determined from the slope of the absorption (A_{450}) versus concentration curve, using the ε_{450} values calculated for $[Ru(dppz)_2(CppH)](PF_6)_2$.[18]

Cell culture: Human cervical carcinoma cells (HeLa) were cultured in DMEM (Gibco) supplemented with 5% fetal calf serum (FCS, Gibco), 100 U mL^{-1} penicillin, 100 μg mL^{-1} streptomycin. The normal human fetal lung fibroblast cell line (MRC-5) was grown in F-10 medium (Gibco) supplemented with 10% FCS (Gibco), penicillin (100 U mL^{-1}), and streptomycin (100 μg mL^{-1}). The cells were cultured at 37 °C and in 5% CO_2 humidified atmosphere.

Cytotoxicity determination: The toxicity of the Ru^{II} complexes and the Ru^{II}-peptides toward HeLa and MRC-5 cells was evaluated using a resazurin-based fluorimetric cell viability assay. Stock solutions of the Ru^{II} complexes (20 mM) were either prepared in DMSO or milli-Q H_2O (for the Ru^{II}-peptides). The respective stock solutions were further diluted with complete medium to the desired working concentrations. For a typical experiment, 100 μL aliquots of cells in growth medium were seeded in 96-well plates (density of 4×10^3 and 7.5×10^3 cells per well for HeLa and MRC-5, respectively) and incubated at 37 °C and 5% CO_2. After 24 h incubation, cells were treated with various concentrations (0.8–100 μM, 200 μL final well volume) of the test compound and incubated for 48 h. Thereafter, the medium was removed, 100 μL of freshly prepared resazurin-containing complete medium (0.2 mg mL^{-1} final concentration) was added, and the cells were incubated at 37 °C for another 4 h. At the end of the incubation period, fluorescence of the highly red fluorescent resorufin product ($\lambda_{ex} = 540$ nm, $\lambda_{em} = 590$ nm) was quantified using a SpectraMax M5 microplate Reader. The reported cytotoxicity data are the average of at least two independent experiments, each performed in triplicate per concentration level. Final DMSO concentration in the wells was $<0.5\%$ (*v*/*v*). Control experiments on cells treated with same amounts of DMSO in culture medium showed no cytotoxic effect (results not shown).

In vitro fluorescence evaluation: Cellular localization of luminescent Ru^{II} complexes was assessed by confocal microscopy. As for the cytotoxicity assays, stock solutions of the Ru^{II} complexes (20 mM) were prepared in DMSO (for the Ru^{II}-peptides in milli-Q H_2O) and diluted to the desired concentrations with culture medium. HeLa cells were grown on 18 mm Menzel–Gläser coverslips at a density of 1×10^5 cells mL^{-1} in cell culture medium. Cells were incubated with Ru^{II} complexes at their desired incubation concentration (either IC_{50} values or at 100 μM for the nontoxic complexes) for 2 h, at 37 °C under 5% CO_2. The medium was discarded, cells were fixed with a 4% formaldehyde solution in PBS and mounted on slides for viewing by confocal microscopy. If required, co-staining of cell nuclei with DAPI was performed by using a mounting solution containing DAPI ($\lambda_{ex} = 402$ nm, $\lambda_{em} > 420$ nm). Fixed cells were imaged on a Leica SP5 confocal laser scanning microscope, using the red wavelength selection ($\lambda_{ex} = 458$ nm, $\lambda_{em} = 600$–650 nm).

Abbreviations

CLSM: confocal laser scanning microscopy; DAPI: (4′,6-diamidino-2-phenylindole); DMAP: 4-(dimethylamino)pyridine; DMF: *N*,*N*′-dimethylformamide; HATU: *O*-(7-azabenzotriazol-1-yl)-*N*,*N*,*N*′,*N*′-tetramethyluronium hexafluorophosphate; HR-CS AAS: high-resolution continuum source atomic absorption spectrometry; MLS: mitochondrial localization signal; NLS: nuclear localization signal; rPep: random peptide sequence (GPGVK, written from N to C terminus); TFA: trifluoroacetic acid.

Acknowledgements

This work was supported by the Swiss National Science Foundation (Professorship No. PP00P2_133568 to G.G.), the University of Zurich (G.G. and S.F.), the Stiftung für Wissenschaftliche Forschung of the University of Zurich (G.G. and S.F.), the Stiftung zur Krebsbekämpfung (S.F.), the Huggenberger-Bischoff Stiftung (S.F.), and the University of Zurich Priority Program (S.F.). The authors gratefully acknowledge the assistance and support of the Center for Microscopy and Image Analysis of the University of Zurich.

Keywords: anticancer agents · bioinorganic chemistry · cytotoxicity · ruthenium polypyridyl complexes · structure–activity relationships

[1] M. R. Gill, J. A. Thomas, *Chem. Soc. Rev.* **2012**, *41*, 3179–3192.
[2] N. L. Kilah, E. Meggers, *Aust. J. Chem.* **2012**, *65*, 1325–1332.
[3] J. G. Vos, J. M. Kelly, *Dalton Trans.* **2006**, 4869–4883.
[4] Q. Zhao, C. Huang, F. Li, *Chem. Soc. Rev.* **2011**, *40*, 2508–2524.
[5] L. Salassa, *Eur. J. Inorg. Chem.* **2011**, 4931–4947.
[6] T. Joshi, G. J. Barbante, P. S. Francis, C. F. Hogan, A. M. Bond, G. Gasser, L. Spiccia, *Inorg. Chem.* **2012**, *51*, 3302–3315.
[7] T. Joshi, G. J. Barbante, P. S. Francis, C. F. Hogan, A. M. Bond, L. Spiccia, *Inorg. Chem.* **2011**, *50*, 12172–12183.
[8] C. Bischof, T. Joshi, A. Dimri, L. Spiccia, U. Schatzschneider, *Inorg. Chem.* **2013**, *52*, 9297–9308.
[9] V. Fernández-Moreira, F. L. Thorp-Greenwood, M. P. Coogan, *Chem. Commun.* **2010**, *46*, 186–202, and references therein.
[10] K. K.-W. Lo, A. W.-T. Choi, W. H.-T. Law, *Dalton Trans.* **2012**, *41*, 6021–6047.
[11] A. Yadav, T. Janaratne, A. Krishnan, S. S. Singhal, S. Yadav, A. S. Dayoub, D. L. Hawkins, S. Awasthi, F. M. MacDonnell, *Mol. Cancer Ther.* **2013**, *12*, 643–653.
[12] C. Qian, J.-Q. Wang, C.-L. Song, L.-L. Wang, L.-N. Ji, H. Chao, *Metallomics* **2013**, *5*, 844–854.
[13] T. Chen, Y. Liu, W.-J. Zheng, J. Liu, Y.-S. Wong, *Inorg. Chem.* **2010**, *49*, 6366–6368.

[14] T. Chen, W.-J. Mei, Y.-S. Wong, J. Liu, Y. Liu, H.-S. Xie, W.-J. Zheng, *MedChemComm* **2010**, *1*, 73 – 75.
[15] M. J. Pisani, P. D. Fromm, Y. Mulyana, R. J. Clarke, H. Körner, K. Heimann, J. G. Collins, F. R. Keene, *ChemMedChem* **2011**, *6*, 848 – 858.
[16] U. Schatzschneider, J. Niesel, I. Ott, R. Gust, H. Alborzinia, S. Wölfl, *ChemMedChem* **2008**, *3*, 1104 – 1109.
[17] O. Zava, S. M. Zakeeruddin, C. Danelon, H. Vogel, M. Grätzel, P. J. Dyson, *ChemBioChem* **2009**, *10*, 1796 – 1800.
[18] V. Pierroz, T. Joshi, A. Leonidova, C. Mari, J. Schur, I. Ott, L. Spiccia, S. Ferrari, G. Gasser, *J. Am. Chem. Soc.* **2012**, *134*, 20376 – 20387.
[19] X. Tian, M. R. Gill, I. Cantón, J. A. Thomas, G. Battaglia, *ChemBioChem* **2011**, *12*, 548 – 551.
[20] A. Kamb, S. Wee, C. Lengauer, *Nat. Rev. Drug Discovery* **2007**, *6*, 115 – 120.
[21] M. P. Murphy, R. A. J. Smith, *Adv. Drug Delivery Rev.* **2000**, *41*, 235 – 250.
[22] M. P. Murphy, R. A. J. Smith, *Annu. Rev. Pharmacol. Toxicol.* **2007**, *47*, 629 – 656.
[23] M. Schenone, V. Dancik, B. K. Wagner, P. A. Clemons, *Nat. Chem. Biol.* **2013**, *9*, 232 – 240.
[24] T. Joshi, M. Patra, L. Spiccia, G. Gasser, *Artif. DNA PNA XNA* **2013**, *4*, 11 – 18.
[25] C. A. Puckett, J. K. Barton, *J. Am. Chem. Soc.* **2009**, *131*, 8738 – 8739.
[26] C. A. Puckett, J. K. Barton, *Bioorg. Med. Chem.* **2010**, *18*, 3564 – 3569.
[27] U. Neugebauer, Y. Pellegrin, M. Devocelle, R. J. Forster, W. Signac, N. Moran, T. E. Keyes, *Chem. Commun.* **2008**, 5307 – 5309.
[28] L. Cosgrave, M. Devocelle, R. J. Forster, T. E. Keyes, *Chem. Commun.* **2010**, *46*, 103 – 105.
[29] A. Leonidova, V. Pierroz, R. Rubbiani, J. Heier, S. Ferrari, G. Gasser, *Dalton Trans.* **2014**, *43*, 4287 – 4294.
[30] N. Nickita, G. Gasser, P. Pearson, M. J. Belousoff, L. Y. Goh, A. M. Bond, G. B. Deacon, L. Spiccia, *Inorg. Chem.* **2009**, *48*, 68 – 81.
[31] D. Kalderon, B. L. Roberts, W. D. Richardson, A. E. Smith, *Cell* **1984**, *39*, 499 – 509.
[32] H. Szeto, *AAPS J.* **2006**, *8*, E277 – E283.
[33] L. Hosta-Rigau, I. Olmedo, J. Arbiol, L. J. Cruz, M. J. Kogan, F. Albericio, *Bioconjugate Chem.* **2010**, *21*, 1070 – 1078.
[34] D. B. Cornelio, L. Meurer, R. Roesler, G. Schwartsmann, *Oncology* **2007**, *73*, 340 – 345.
[35] C. A. Puckett, R. J. Ernst, J. K. Barton, *Dalton Trans.* **2010**, *39*, 1159 – 1170.
[36] R. J. E. Harrison, *Aust. J. Chem.* **2009**, *62*, 90 – 90.
[37] M. Matson, F. R. Svensson, B. Nordén, P. Lincoln, *J. Phys. Chem. B* **2011**, *115*, 1706 – 1711.
[38] F. R. Svensson, M. Abrahamsson, N. Strömberg, A. G. Ewing, P. Lincoln, *J. Phys. Chem. Lett.* **2011**, *2*, 397 – 401.
[39] A. C. Komor, C. J. Schneider, A. G. Weidmann, J. K. Barton, *J. Am. Chem. Soc.* **2012**, *134*, 19223 – 19233.
[40] A. J. McConnell, H. Song, J. K. Barton, *Inorg. Chem.* **2013**, *52*, 10131 – 10136.
[41] C. A. Puckett, J. K. Barton, *Biochemistry* **2008**, *47*, 11711 – 11716.
[42] T. Joshi, V. Pierroz, C. Mari, L. Gemperle, S. Ferrari, G. Gasser, *Angew. Chem. Int. Ed.* **2014**, DOI: 10.1002/anie.201309576; *Angew. Chem.* **2014**, DOI: 10.1002/ange.201309576.
[43] G. R. Fulmer, A. J. M. Miller, N. H. Sherden, H. E. Gottlieb, A. Nudelman, B. M. Stoltz, J. E. Bercaw, K. I. Goldberg, *Organometallics* **2010**, *29*, 2176 – 2179.
[44] A. Greguric, I. D. Greguric, T. W. Hambley, J. R. Aldrich-Wright, J. G. Collins, *J. Chem. Soc. Dalton Trans.* **2002**, 849 – 855.
[45] P. A. Anderson, G. B. Deacon, K. H. Haarmann, F. R. Keene, T. J. Meyer, D. A. Reitsma, B. W. Skelton, G. F. Strouse, N. C. Thomas, *Inorg. Chem.* **1995**, *34*, 6145 – 6157.
[46] N. Nickita, M. J. Belousoff, A. I. Bhatt, A. M. Bond, G. B. Deacon, G. Gasser, L. Spiccia, *Inorg. Chem.* **2007**, *46*, 8638 – 8651.

Received: January 11, 2014
Published online on March 3, 2014

2.1.4. A BIS(DIPYRIDOPHENAZINE)(2-(2-PYRIDYL)PYRIMIDINE-4-CARBOXYLIC ACID) RUTHENIUM(II) COMPLEX WITH ANTICANCER ACTION UPON PHOTODEPROTECTION

In a final step, this complex could be rendered inactive by masking the carboxylate functionality with a photolabile protecting group, allowing anticancer activity to be retrieved upon UV-A irradiation (2.58 J/cm^2).

This chapter has been published in *Angew. Chem. Int. Ed. Engl.* in 2014.[45]

Prodrugs

DOI: 10.1002/anie.201309576

A Bis(dipyridophenazine)(2-(2-pyridyl)pyrimidine-4-carboxylic acid)ruthenium(II) Complex with Anticancer Action upon Photodeprotection**

Tanmaya Joshi, Vanessa Pierroz, Cristina Mari, Lea Gemperle, Stefano Ferrari, and Gilles Gasser**

Abstract: *Improving the selectivity of anticancer drugs towards cancer cells is one of the main goals of drug optimization; the prodrug strategy has been one of the most promising. A light-triggered prodrug strategy is presented as an efficient approach for controlling cytotoxicity of the substitutionally inert cytotoxic complex [Ru(dppz)$_2$(CppH)](PF$_6$)$_2$ (**C1**; CppH = 2-(2-pyridyl)pyrimidine-4-carboxylic acid; dppz = dipyrido[3,2-a:2′,3′-c]phenazine). Attachment of a photolabile 3-(4,5-dimethoxy-2-nitrophenyl)-2-butyl (DMNPB) ester ("photocaging") makes the otherwise active complex **C1** innocuous to both cancerous (HeLa and U2OS) and non-cancerous (MRC-5) cells. The cytotoxic action can be successfully unleashed in living cells upon light illumination (350 nm), reaching similar level of activity as the parent cytotoxic compound **C1**. This is the first substitutionally inert cytotoxic metal complex to be used as a light-triggered prodrug candidate.*

Platinum- and ruthenium-based cytotoxic compounds are by far the most explored metal-based anticancer agents.[1] For the majority of such metal complexes, their anticancer activity originates from the presence of a labile ligand and/or a redox-active metal center.[2] (Organo)metallic complexes can, however, also exert anticancer activity in their inert intact form.[3] The best examples are the substitutionally inert Ru^{II} scaffolds, which have been found to not only act as potent kinase inhibitors, but also as effective cytotoxic compounds.[2c,e,4] The mechanism of action for cytotoxic Ru^{II} polypyridyl compounds is believed to be a complex function of inherent physicochemical and pharmacological properties. As interest in substitutionally inert metal complexes as anti-cancer drug candidates has only recently regained momentum,[3a,4a,b,d,5] in most cases only limited information is available on their precise mode of action and metabolic activity. Moreover, a scarcity of structure–activity relationship (SAR) studies focusing on these aspects also implies that biochemical understanding on most of these systems is still premature.[4a–c,6]

Nonetheless, targeting the cytotoxic aspects of one such coordinatively saturated and substitutionally inert Ru^{II} complex, [Ru(dppz)$_2$(CppH)]$^{2+}$ (**C1**; Scheme 1), we have demonstrated that this particular bis(dppz) complex exerts its cytotoxic action by disrupting the mitochondrial function.[7] Through correlations from the detailed SAR studies, we could deduce that structural alterations in this lead prototype can significantly diminish its cytotoxic potency.[8] Furthermore, with no decomposition of the complex in human plasma, it was concluded that the intact Ru^{II} complex is responsible for the cytotoxic activity.[7]

Taking the above findings into consideration, we explored the potential of light-triggered prodrug strategy for tuning the intracellular cytotoxic activity of the complex, while retaining the structural integrity of the active parent complex. Such molecules, which are rendered inactive through covalent modification with a photocleavable moiety but can regain biological activity upon light exposure, are commonly referred to as "photocaged" compounds.[9] Light-activatable pro-moieties allow the modulation of the release and activity of a "photocaged" drug as a function of the wavelength, duration, intensity, or location of illumination.[10] Whilst photochemical control of activity (also referred to as "photocaging/uncaging") has been widely explored with organic drugs, application of this concept to metal coordination complexes has been surprisingly limited.[9,11] Of note, metal complexes were previously used in combination with light to trigger biological activity.[3a,11,12] Specific to substitutionally inert Ru^{II} complexes, photoactivation to date has primarily revolved around the studies exploring their capacity to undergo photoinduced ligand exchange/expulsion, DNA binding, DNA cleavage, and cytotoxic effects.[3a,4a–c,13] To the best of our knowledge, this work is the first example of a light-triggered structurally inert metallo-prodrug candidate, with

[*] Dr. T. Joshi,[+] V. Pierroz,[+] C. Mari, L. Gemperle, Prof. Dr. G. Gasser
Department of Chemistry, University of Zurich
Winterthurerstrasse 190, 8057 Zurich (Switzerland)
E-mail: tanmaya.joshi3@uzh.ch
gilles.gasser@aci.uzh.ch
Homepage: http://www.gassergroup.com
V. Pierroz,[+] Priv.-Doz. Dr. S. Ferrari
Institute of Molecular Cancer Research, University of Zurich (Switzerland)
[+] These authors contributed equally to this work.

[**] This work was supported by the Swiss National Science Foundation (Professorship No. PP00P2_133568 to G.G.), the University of Zurich (G.G. and S.F.), the Stiftung für Wissenschaftliche Forschung of the University of Zurich (G.G. and S.F.), the Stiftung zur Krebsbekämpfung (S.F.), the Huggenberger–Bischoff Stiftung (S.F.), and the University of Zurich Priority Program (S.F.). The authors gratefully acknowledge the assistance and support of the Center for Microscopy and Image Analysis of the University of Zurich, and Dr. Jakob Heier from the Laboratory for Functional Polymers, Empa, Swiss Federal Laboratories for Material Science and Technology, for generous access to a near-IR fluorimeter.

Supporting information for this article is available on the WWW under http://dx.doi.org/10.1002/anie.201309576.

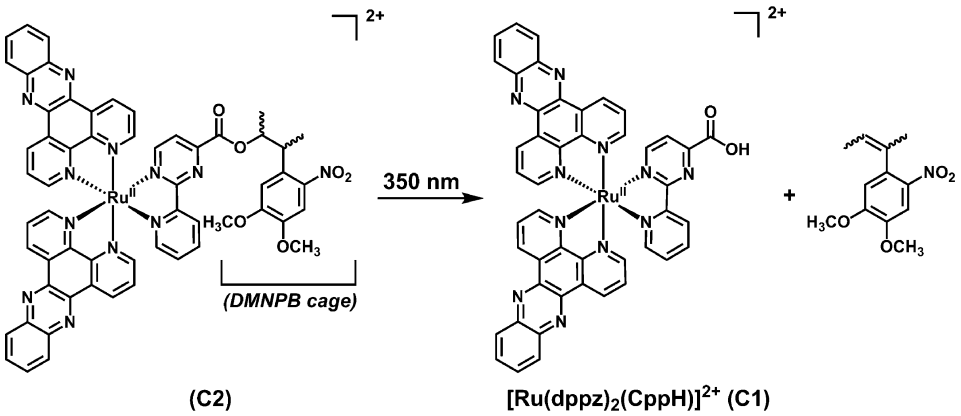

Scheme 1. Chemical structures of the active bis(dppz)Ru^{II} complex **C1** and its photolabile protected version **C2** (isolated as racemic mixtures of hexafluorophosphate salts). The DMNPB group is released upon irradiation at 350 nm.[14] CppH = 2-(2-pyridyl)pyrimidine-4-carboxylic acid; dppz = dipyrido[3,2-*a*:2′,3′-c]phenazine.

no "caged" variants of any substitutionally inert cytotoxic metal complex been previously constructed.

For the proof-of-principle design of a light-activatable Ru^{II} prodrug candidate, inspiration was drawn from the recent structure–activity analysis on the lead prototype. The results pointed towards the presence of the carboxylate functionality on the pyrimidine ring as being essential for cytotoxic activity of the complex, making it an ideal site for attachment of a photocleavable moiety. 3-(4,5-Dimethoxy-2-nitrophenyl)-2-butyl (DMNPB) ester was used as the photocleavable moiety for derivatization of the carboxylic handle (Scheme 1).[14] This *ortho*-nitrophenyl chromophore has previously been used for efficient photocontrolled release of L-glutamate, a neurotransmitter, and for phototriggered cell adhesion of "caged" RGD peptides, at near-UV wavelengths (ca. 360 nm).[15] The synthesis of the aryl butyl esterified Ru^{II} pro-moiety (**C2**) followed the route shown in the Supporting Information, Scheme S1. The identity of **C2** was confirmed by ^{1}H NMR spectroscopy and mass spectrometry, and its purity was determined by elemental analysis (see the Supporting Information for more details).

The hydrolytic stability of **C2** was evaluated by monitoring a sample of this compound in phosphate-buffered saline (PBS) at 25 °C in the dark. Over a time period of 24 h, aliquots were examined by HPLC for the release of **C1**; formation of about 7% **C1** was observed over the time of experiment. Photolytic stability of **C2** was also assessed prior to performing the cytotoxicity experiments. The complex solution in PBS (pH 7.2) was irradiated with 350 nm UV-A radiation, and changes in the UV/Vis absorption spectra were monitored over time (Figure 1). Upon light irradiation, the metal-to-ligand charge transfer (MLCT) band centered at 478 nm is hypsochromically shifted to a broad MLCT band centered at 451 nm. With time, a clear isosbestic point at 467 nm is observed along with increasing absorption intensity in the 250–400 nm region. As the photolytic reaction proceeds, a shoulder at about 318 nm that is characteristic of the free complex **C1** also appears, reflecting its photorelease from **C2**. Furthermore, removal of DMNPB from the prodrug candidate **C2** to release **C1** could also be easily confirmed by UPLC-MS (Supporting Information, Figure S2). With time, gradual disappearance, upon light irradiation, of the peak corresponding to **C2** (t_R = 2.6 min) was seen along with appearance of the peak for free **C1** (t_R = 2.3 min); the observed spectral changes are in agreement with the expected photolytic reaction. After 20 min of light irradiation (5.16 J cm^{-2}), an almost quantitative amount of **C1** (≥ 92%) was photoreleased (Supporting Information, Figure S3), as estimated from UPLC analysis (see the Supporting Information for more details). The calculated quantum yield for the photorelease of **C1**, as determined by comparison with 1-(2-nitrophenyl)ethyl phosphate (Φ = 54%),[16] was found to be 3.8%, indicating a modest photolytic efficiency (Supporting Information, Figure S4).

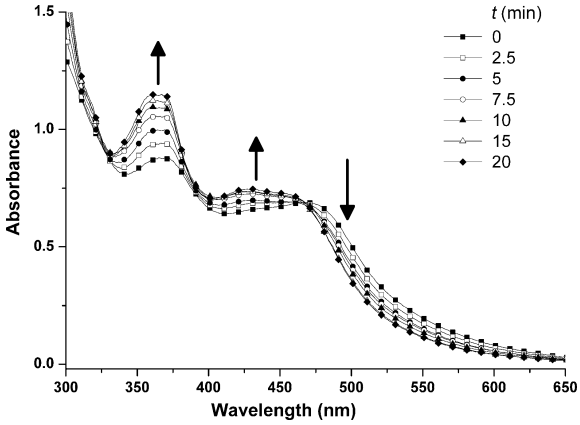

Figure 1. Changes in absorption spectra of **C2** (50 μM in PBS, pH 7.2) as observed upon irradiation at 350 nm. Arrows indicate the direction of change in absorbance with increasing periods of irradiation.

Having confirmed the light-triggered removal of DMNPB from the prodrug candidate **C2** to release **C1**, the cytotoxic evaluations were performed on cervical cancer (HeLa), bone cancer (U2OS), and non-cancerous lung fibroblast (MRC-5) cell lines. Resazurin based fluorometric assay was employed for the cytotoxicity assessment of the prodrug candidate in the dark and upon 350 nm light irradiation (Table 1). Different concentrations of prodrug candidate **C2** administered for 4 h in the dark to both HeLa and U2OS cells, followed by incubation at 37 °C in fresh cell culture media for additional 48 h, were found to be non-toxic up to the highest complex concentration (100 μM) examined in this study. Similar cytotoxic response was also observed on MRC-5 cells upon

Table 1: Cytotoxic activity data (IC_{50}) for **C1**, **C2**, DMPNB (**4**), and cisplatin against human cervical carcinoma (HeLa), human osteosarcoma (U2OS), and non-cancerous lung fibroblast (MRC-5) cell lines.

	IC_{50} [μM]						
	HeLa			U2OS			MRC-5
	4 h (dark)	4 h (+ UV-A)[a]	48 h (dark)	4 h (dark)	4 h (+ UV-A)[a]	48 h (dark)	48 h (dark)
C2	>100	17.0 ± 0.8	85.8 ± 5.8	>100	17.2 ± 3.8	>100	85.3 ± 0.2
C1	16.0 ± 0.1	5.9 ± 1.7	10.0 ± 1.3[7]	30.5 ± 1.1	13.5 ± 2.1	13.5 ± 2.5[7]	15.1 ± 2.2[7]
DMPNB (**4**)	>100	>100	>100	>100	>100	>100	>100
cisplatin	9.8 ± 4.5	12.7 ± 3.6	9.9 ± 0.9	26.8 ± 1.9	32.6 ± 5.1	11.8 ± 1.7[7]	8.5 ± 0.9

[a] 10 min UV-A irradiation (350 nm, 2.58 J cm^{-2}).

incubation with **C2**. Interestingly, even extending the treatment up to 48 h for prodrug candidate **C2** did not induce any cytotoxicity towards U2OS cells up to the highest dosed complex concentration (100 μM), also causing no significant change in its cytotoxic action towards HeLa and MRC-5 cells ($IC_{50} \approx 85$ μM). That prodrug candidate **C2** shows a promising lack of cytotoxicity toward both cells lines, in the dark, is in stark contrast with the cytotoxic activity data obtained for the active Ru^{II} complex, **C1**, for which the IC_{50} values against HeLa, U2OS, and MRC-5 cell lines were determined to be 10.0 μM, 13.5 μM, and 15.1 μM, respectively. The parent cytotoxic complex **C1** losing its activity upon covalent modification reflects similar findings previously reported by us.[7,8] For example, the benzylic and ethyl ester derivatives of **C1** showed 3–4 times less activity on HeLa cells than the parent complex.[8]

The effect of light irradiation on the cytotoxic action of the prodrug candidate **C2** was examined on HeLa and U2OS cells. The cells were first incubated with **C2** in the dark for 4 h, before suspension in fresh cell culture media followed by irradiation at 350 nm for 10 min (2.58 J cm^{-2}) and incubation for additional 48 h. As anticipated, light irradiation of HeLa and U2OS cells exposed to prodrug **C2** restored the cytotoxic effect (Table 1). An IC_{50} value of ca. 17.0 μM was obtained when cells were subjected to light exposure. Notably, the cytotoxicity level re-attained by the pro-moiety **C2** upon light irradiation is in excellent agreement with the cytotoxic response observed for **C1**, in the dark, toward HeLa cells ($IC_{50} = 16.0$ μM) under similar conditions, with an almost twofold increase in cytotoxicity against U2OS cells (Table 1). Control light irradiation experiments performed on HeLa and U2OS cells either in the absence of the complex or after incubation with the photolabile group DMNPB showed no toxic effect on the cells, ruling out their possible contributions to the elevated cytotoxic effects observed upon light activation.

Tris(diimine)–Ru^{II} complexes can produce $^1O_2$ upon light irradiation and therefore induce $^1O_2$-mediated DNA photocleavage, and can also exert phototoxicity.[4b,c,13a,17] In our case, the separately conducted measurements indeed confirmed the ability of **C1** to produce singlet oxygen (see Supporting Information) upon irradiation at 350 nm with the determined quantum yield (Φ) of 0.81 and 0.06 in acetonitrile and PBS (pH 7.2), respectively; the values indicating an extremely efficient singlet oxygen production in lipophilic environments. Given that the prodrug candidate **C2** only regains cytotoxic activity after light activation, it thus follows that any cytotoxic effect introduced on light irradiation of **C1** may have a role to play in the elevated cytotoxic potency of the prodrug candidate **C2**. That the photoinduced toxicity of **C1** contributes to the observed light-triggered increase in activity of **C2** is supported by the fact that light irradiation at 350 nm of HeLa and U2OS cells dosed with **C1** (4 h) further led to up to about threefold increase in cytotoxicity compared to those kept in the dark. Nevertheless, photolytic removal of DMNPB from **C1** still remains the critical first step in the case of **C2** regaining cytotoxicity upon photolysis. Thus, it is conceivable that as the complex **C1** is photoreleased from the prodrug candidate **C2**, the overall enhancement in exerted cytotoxicity in HeLa cells is a cumulative effect of the direct cytotoxic activity of **C1** and the activity, in part, potentially originating as a result of a cascade of photolytic reactions involving the RuN_6 coordination sphere of complexes **C1** and **C2**.

Furthermore, the effect of light irradiation on the cellular localization of the prodrug candidate **C2** was also probed qualitatively using confocal laser scanning microscopy (CLSM; Supporting Information, Figure S7). CLSM studies on HeLa cells treated with **C2** in the dark revealed a non-specific manner of localization (Supporting Information, Figure S7a). Intense luminescence signals were observed from the cytoplasmic regions as well as the cell nucleoli. Furthermore, a distinct sharp signal marking the periphery of the nuclear membrane was also observed, which persisted even after co-staining of cellular DNA with DAPI (4′,6-diamidino-2-phenylindole; Supporting Information, Figure S7c). For the cells exposed to light irradiation (350 nm), a relatively less-intense luminescence was observed in cells (Supporting Information, Figure S7b). Nevertheless, from the respective overlay image with DAPI staining (Supporting Information, Figure S7d), accumulation appeared to mainly occur in cytoplasmic organelles, with weak visual signs of red emission from the nucleus under the conditions used for the confocal microscopy experiments. However, a possibility that the polarity and water accessibility of bis(dppz)–Ru^{II} complexes in the cellular microenvironment is reflected in the decreased intensity of the emission signals, cannot be ruled out. This highlights the uncertainty on precise cellular accumulation of metal complexes as assessed by confocal microscopy. However, in case of **C1**, we could previously show that visually observed mitochondrial accumulation is highly

correlated to that determined using high-resolution continuum source atomic absorption spectrometry (HR-CS AAS).[7]

In conclusion, we report on an efficient approach for controlling cytotoxicity of a substitutionally inert cytotoxic Ru^{II} complex. Attaching an appropriate photolabile moiety to **C1** makes the otherwise active complex innocuous to both cancerous (HeLa and U2OS) and non-cancerous (MRC-5) cells. Furthermore, the cytotoxic action of the pro-moiety **C2** is controlled by light and can be regained upon illumination. With light-induced (350 nm) liberation of **C1** from the pro-moiety, cytotoxic action of the prodrug on the cancer cells is unleashed, reaching similar levels of cytotoxicity as for the original complex in absence of light. Though still at the prototype stage, this light-triggered prodrug strategy holds tremendous potential for designing more sophisticated prodrug systems, where properties are tailored to produce a controllable cytotoxic action in physiologically relevant optical window. Efforts towards this end are currently under investigation. It should be noted, however, that the UV-A light dosage (2.58 $J\,cm^{-2}$) used to induce cytotoxicity in **C2** is comparable to that frequently employed for other UV-A activated metal complexes.[11,12d,18]

Received: November 4, 2013
Revised: December 17, 2013
Published online: February 5, 2014

Keywords: medicinal inorganic chemistry · photolysis · prodrugs · ruthenium · substitutionally inert complexes

[1] E. Alessio, *Bioinorganic Medicinal Chemistry*, Wiley-VCH, Weinheim, **2011**, and references therein.

[2] a) N. P. E. Barry, P. J. Sadler, *Chem. Commun.* **2013**, *49*, 5106 – 5131; b) I. Romero-Canelón, P. J. Sadler, *Inorg. Chem.* **2013**, *52*, 12276 – 12291; c) G. Gasser, I. Ott, N. Metzler-Nolte, *J. Med. Chem.* **2010**, *53*, 3 – 25, and references therein; d) N. Graf, S. J. Lippard, *Adv. Drug Delivery Rev.* **2012**, *64*, 993 – 1004; e) T. W. Hambley, *Science* **2007**, *318*, 1392 – 1393.

[3] a) D.-L. Ma, H.-Z. He, K.-H. Leung, D. S.-H. Chan, C.-H. Leung, *Angew. Chem.* **2013**, *125*, 7820 – 7837; *Angew. Chem. Int. Ed.* **2013**, *52*, 7666 – 7682; b) D. Can, B. Spingler, P. Schmutz, F. Mendes, P. Raposinho, C. Fernandes, F. Carta, A. Innocenti, I. Santos, C. T. Supuran, R. Alberto, *Angew. Chem.* **2012**, *124*, 3410 – 3413; *Angew. Chem. Int. Ed.* **2012**, *51*, 3354 – 3357; c) I. Neundorf, J. Hoyer, K. Splith, R. Rennert, H. W. Peindy N'-Dongo, U. Schatzschneider, *Chem. Commun.* **2008**, 5604 – 5606; d) E. A. Hillard, A. Vessières, G. Jaouen in *Medicinal Organometallic Chemistry*, *Vol. 32* (Eds.: G. Jaouen, N. Metzler-Nolte), Springer, Heidelberg, **2010**, pp. 81 – 117; e) A. M. Pizarro, A. Habtermariam, P. J. Sadler, in *Medicinal Organometallic Chemistry*, *Vol. 32* (Eds.: G. Jaouen, N. Metzler-Nolte), Springer, Heidelberg, **2010**, pp. 21 – 56, and references therein; f) F. Giannini, J. Furrer, A.-F. Ibao, G. Süss-Fink, B. Therrien, O. Zava, M. Baquie, P. Dyson, P. Štěpnička, *J. Biol. Inorg. Chem.* **2012**, *17*, 951 – 960.

[4] a) M. R. Gill, J. A. Thomas, *Chem. Soc. Rev.* **2012**, *41*, 3179 – 3192; b) N. L. Kilah, E. Meggers, *Aust. J. Chem.* **2012**, *65*, 1325 – 1332; c) L. Salassa, *Eur. J. Inorg. Chem.* **2011**, 4931 – 4947; d) A. Bergamo, G. Sava, *Dalton Trans.* **2011**, *40*, 7817 – 7823; e) E. Meggers, *Chem. Commun.* **2009**, 1001 – 1010.

[5] J. G. Vos, J. M. Kelly, *Dalton Trans.* **2006**, 4869 – 4883.

[6] a) M. J. Pisani, P. D. Fromm, Y. Mulyana, R. J. Clarke, H. Körner, K. Heimann, J. G. Collins, F. R. Keene, *ChemMedChem* **2011**, *6*, 848 – 858; b) U. Schatzschneider, J. Niesel, I. Ott, R. Gust, H. Alborzinia, S. Wölfl, *ChemMedChem* **2008**, *3*, 1104 – 1109; c) T. Chen, Y. Liu, W.-J. Zheng, J. Liu, Y.-S. Wong, *Inorg. Chem.* **2010**, *49*, 6366 – 6368; d) C. Qian, J.-Q. Wang, C.-L. Song, L.-L. Wang, L.-N. Ji, H. Chao, *Metallomics* **2013**, *5*, 844 – 854.

[7] V. Pierroz, T. Joshi, A. Leonidova, C. Mari, J. Schur, I. Ott, L. Spiccia, S. Ferrari, G. Gasser, *J. Am. Chem. Soc.* **2012**, *134*, 20376 – 20387.

[8] T. Joshi, V. Pierroz, S. Ferrari, G. Gasser, **2014**, DOI: 10.1002/cmdc.201400029.

[9] a) C. Brieke, F. Rohrbach, A. Gottschalk, G. Mayer, A. Heckel, *Angew. Chem.* **2012**, *124*, 8572 – 8604; *Angew. Chem. Int. Ed.* **2012**, *51*, 8446 – 8476; b) G. Mayer, A. Heckel, *Angew. Chem.* **2006**, *118*, 5020 – 5042; *Angew. Chem. Int. Ed.* **2006**, *45*, 4900 – 4921.

[10] a) H.-M. Lee, D. R. Larson, D. S. Lawrence, *ACS Chem. Biol.* **2009**, *4*, 409 – 427; b) G. C. R. Ellis-Davies, *Nat. Methods* **2007**, *4*, 619 – 628.

[11] K. L. Ciesienski, K. J. Franz, *Angew. Chem.* **2011**, *123*, 840 – 850; *Angew. Chem. Int. Ed.* **2011**, *50*, 814 – 824, and references therein.

[12] a) D. P. Kennedy, C. Gwizdala, S. C. Burdette, *Org. Lett.* **2009**, *11*, 2587 – 2590; b) H. W. Mbatia, S. C. Burdette, *Biochemistry* **2012**, *51*, 7212 – 7224; c) A. A. Kumbhar, A. T. Franks, R. J. Butcher, K. J. Franz, *Chem. Commun.* **2013**, *49*, 2460 – 2462; d) F. S. Mackay, J. A. Woods, P. Heringová, J. Kašpárková, A. M. Pizarro, S. A. Moggach, S. Parsons, V. Brabec, P. J. Sadler, *Proc. Natl. Acad. Sci. USA* **2007**, *104*, 20743 – 20748; e) B. J. Heilman, J. St. John, S. R. J. Oliver, P. K. Mascharak, *J. Am. Chem. Soc.* **2012**, *134*, 11573 – 11582; f) A. E. Pierri, A. Pallaoro, G. Wu, P. C. Ford, *J. Am. Chem. Soc.* **2012**, *134*, 18197 – 18200; g) C. Spagnul, R. Alberto, G. Gasser, S. Ferrari, V. Pierroz, A. Bergamo, T. Gianferrara, E. Alessio, *J. Inorg. Biochem.* **2013**, *122*, 57 – 65.

[13] a) U. Schatzschneider, *Eur. J. Inorg. Chem.* **2010**, 1451 – 1467; b) X. Chen, F. Gao, W.-Y. Yang, Z.-X. Zhou, J.-Q. Lin, L.-N. Ji, *Chem. Biodiversity* **2013**, *10*, 367 – 384; c) M. Frasconi, Z. Liu, J. Lei, Y. Wu, E. Strekalova, D. Malin, M. W. Ambrogio, X. Chen, Y. Y. Botros, V. L. Cryns, J.-P. Sauvage, J. F. Stoddart, *J. Am. Chem. Soc.* **2013**, *135*, 11603 – 11613; d) E. Wachter, D. K. Heidary, B. S. Howerton, S. Parkin, E. C. Glazer, *Chem. Commun.* **2012**, *48*, 9649 – 9651.

[14] A. Specht, J.-S. Thomann, K. Alarcon, W. Wittayanan, D. Ogden, T. Furuta, Y. Kurakawa, M. Goeldner, *ChemBioChem* **2006**, *7*, 1690 – 1695.

[15] a) S. Petersen, J. M. Alonso, A. Specht, P. Duodu, M. Goeldner, A. del Campo, *Angew. Chem.* **2008**, *120*, 3236 – 3239; *Angew. Chem. Int. Ed.* **2008**, *47*, 3192 – 3195; b) M. Wirkner, S. Weis, V. San Miguel, M. Álvarez, R. A. Gropeanu, M. Salierno, A. Sartoris, R. E. Unger, C. J. Kirkpatrick, A. del Campo, *ChemBioChem* **2011**, *12*, 2623 – 2629.

[16] J. W. Walker, G. P. Reid, J. A. McCray, D. R. Trentham, *J. Am. Chem. Soc.* **1988**, *110*, 7170 – 7177.

[17] a) O. J. Stacey, S. J. A. Pope, *RSC Adv.* **2013**, *3*, 25550 – 25564; b) S. Swavey in *Ruthenium: Properties, Production and Applications* (Ed.: D. B. Watson), Nova Science, New York, **2011**, pp. 249 – 268.

[18] a) Y. Zhao, J. A. Woods, N. J. Farrer, K. S. Robinson, J. Pracharova, J. Kasparkova, O. Novakova, H. Li, L. Salassa, A. M. Pizarro, G. J. Clarkson, L. Song, V. Brabec, P. J. Sadler, *Chem. Eur. J.* **2013**, *19*, 9578 – 9591; b) A. Leonidova, V. Pierroz, R. Rubbiani, J. Heier, S. Ferrari, G. Gasser, *Dalton Trans.* **2014**, DOI: 10.1039/C3DT51817E.

2.2. RU(II) COMPLEXES AS PROMISING PHOTOSENSITIZERS IN PDT

2.2.1. CONTRIBUTION TO THE WORK

V.P.: conducted all the experiments, except the Agarose gel in Figure 10.A performed by Dr. Riccardo Rubbiani. She also wrote the first draft of the manuscript.

2.2.2. MECHANISM OF ACTION OF A DNA INTERCALATING RU(II) POLYPYRIDYL COMPLEX UPON UV-A IRRADIATION: FROM DNA CLEAVAGE TO APOPTOSIS

2.2.2.1. ABSTRACT

We have previously reported the property of $[Ru^{II}(bipy)_2dppz]^{2+}$ derivatives to accumulate in the nucleus of HeLa cells, impairing cell viability upon UV-A irradiation. Here we confirm the ability of one derivative, namely $[Ru(bipy)_2$-dppz-7-methoxy$][PF_6]_2$ (**Ru65** hereafter), to localize to the nucleus of cancer and normal cells and to selectively display cytotoxicity in response to UV-A irradiation. With regard to its molecular mechanism of action, we demonstrate that **Ru65** intercalates in DNA and, in response to UV-A irradiation, generates singlet oxygen ($^1O_2$). The latter promotes oxidation of guanine in solution and in plasmid DNA, resulting in nicks in the double helix. With dedicated assays we confirm this mechanism of action in living cells and show that UV-A irradiation of **Ru65** results in DNA double-strand breaks. At the molecular level, we observe an early and transient DNA damage response in cells treated with **Ru65**, which is followed by a more pronounced, delayed response, leading to accumulation in the S- and G2-phases of the cell cycle and followed by loss of viability and death by apoptosis.

2.2.2.2. INTRODUCTION

Cancer therapy is still largely based on the use of DNA damaging agents, despite evident drawbacks such as their intrinsic genotoxic potential.[31, 46] In recent years, the rational design of molecules targeting oncogenic pathways that are hyper-functional in cancer cells or to which cancer cells become addicted,[46, 47] has provided an alternative approach to the use of "dirty" drugs. Although the introduction of "magic bullets" represented a great leap forward with respect to the use of chemotherapeutics, the well-documented adaptability of cancer cells to external insults, exemplified by

the induction of point mutations rendering the target protein resistant to first generation compounds,[48] along with more general responses such as increased metabolization and extrusion of the drug from cells, continuously demands the implementation of novel strategies. The use of light to activate drugs has gained increasing attention as promising alternative to the treatment of a number of pathologies. Among the different medical techniques relying on light activation (e.g. photothermal therapy, photoactivated chemotherapy, etc.), photodynamic therapy (PDT) has been undoubtedly the most successful method reported so far. Initially used in the therapy of macular degeneration or bacterial infections, PTD has been increasingly successful in the treatment of a variety of cancers, including those of skin and prostate or, supported by the use of optic fibers to reach cavities, in targeting cancers of the lung and the esophagus.[49, 50] More specifically, PTD relies on the activation of a photosensitizer (PS) by light at a defined wavelength, resulting in the production of reactive oxygen species (ROS), mainly consisting of singlet oxygen ($^1O_2$) that has an estimated half-life of 40 ns in a biological environment.[51, 52] ROS will then rapidly react with biomolecules in close proximity of the PS, impairing metabolic functions and ultimately leading to cell death. The advantage of PDT over conventional chemotherapeutic treatments of solid tumors is its decreased toxicity, since generation of ROS is guided by light at defined locations as opposed to the mere uptake of an active drug in the cells. PTD appears also to be a better alternative to chemotherapy when used in combination with surgery.[53] Indeed, local application of PDT upon surgical removal of portions of tissues or organs allows targeting the tumor while preserving healthy tissue, not last to the benefit of the aesthetic. Nonetheless, currently approved PSs (porphyrin, phtalocyanine) suffer from drawbacks inherent to their molecular structure, such as low solubility in water and a prolonged photosensitivity for patients treated with PSs.[54] Good PSs should ideally display high solubility in water, good phototoxic dark/light index (PI), good singlet oxygen quantum yield upon activation with non-harmful light and little or no photosensitivity for the patient. In this respect, we recently described an excellent photosensitizer candidate, namely a substitutionally inert Ru(II) polypyridyl complex [Ru(bipy)$_2$-dppz-7-methoxy][PF$_6$]$_2$ (**Ru65**) (Figure 9).[55] **Ru65**, whose phosphorescence can be turned on upon intercalation in a hydrophobic environment, showed nuclear localization *in vivo* and the ability to nick plasmid DNA *in vitro*, suggesting that it

intercalates between bases and damages DNA upon irradiation-induced $^1O_2$ production.[55]

In the present study we set out to characterize in detail the mechanism of action of the **Ru65** complex using a low-dose of UV-A irradiation as trigger. We observed that the normally innocuous complex efficiently localized to the nucleus and, upon UV-A irradiation, caused damage to DNA by oxidation of guanines and the generation of nicks in the double helix, triggering a DNA damage response. We observed that an initially weak but rapid response to **Ru65**-induced ssDNA breaks turned into a potent response characterized by the formation of dsDNA breaks and resulting in cell death.

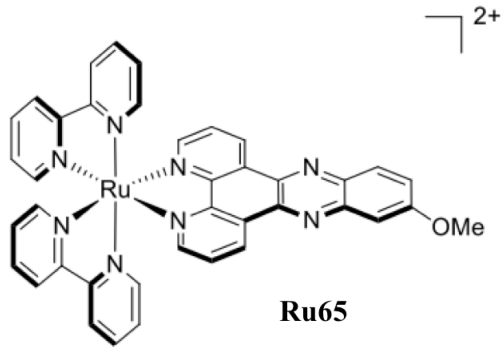

Ru65

Figure 9. Structure of Ru65.

2.2.2.3. RESULTS

Ru65 intercalates in DNA and photo-activation causes oxidative DNA damage

We have previously reported that **Ru65** generates $^1O_2$ upon UV-A irradiation (350 nm, 2.58 J/cm^2) and that this results in relaxation of supercoiled plasmid DNA.[55] To corroborate these findings and clarify the molecular mechanism of DNA damage, we examined binding of **Ru65** to the plasmid pUC18. Treatment with **Ru65** in the absence of UV-A irradiation caused retardation in the mobility of both supercoiled and nicked forms of the plasmid (Fig. 10A and 10B), an indication of the intercalating properties of Ru^{II} metal complexes in DNA. Incubation of pUC18 with **Ru65** followed by UV-A irradiation (350 nm, 0-65-2.58 J/cm^2) confirmed a dose-dependent ability of the metal complex to nick plasmid DNA (Fig. 10A).

We reasoned that generation of ROS such as $^1O_2$ in close proximity to DNA may cause damage to bases, with 8-oxo-guanine being a highly mutagenic lesion.[56] Incubation of pUC18 with **Ru65** followed by UV-A irradiation and treatment with Formamido-pyrimidine DNA Glycosylase (Fpg or 8-oxoguanine DNA Glycosylase), an enzyme that releases damaged purines from dsDNA leaving a one-base gap, showed that supercoiled pUC18 was almost fully converted in the open circular form under these conditions (Fig. 10C). This indicates that activation of **Ru65** intercalated in DNA led to oxidative damage of purines.

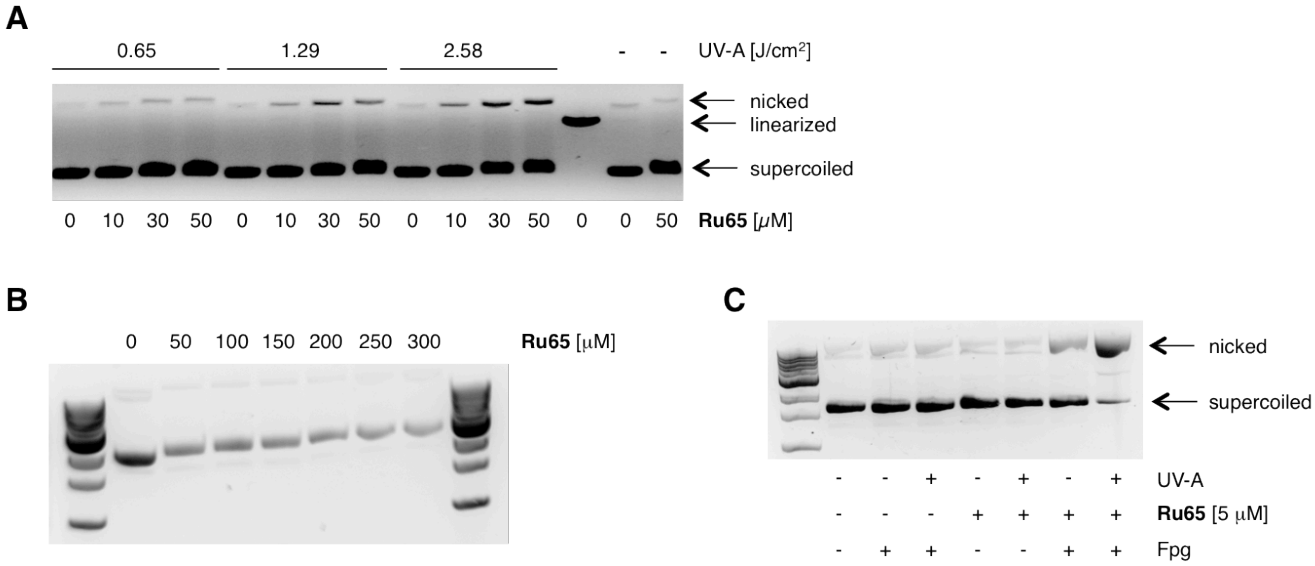

Figure 10. Photo-activation of Ru65 causes DNA damage. A. The plasmid pUC18 (150 ng) was incubated with the indicated concentration of **Ru65** for 30min, UV-A irradiated or kept in the dark, prior to run on a 1% agarose gel in the presence of EtBr. A linearized form of the plasmid was obtained by *EcoRI* digestion. The positions of supercoiled and nicked plasmid are indicated. **B.** DNA intercalation of **Ru65**. The plasmid pUC18 (150 ng) was incubated with the indicated concentration of **Ru65** for 30min prior to run on a 1% agarose gel in the presence of EtBr. **C.** Purine oxidation was assessed by treating pUC18 (150 ng) with **Ru65** and UV-A as indicated, followed by incubation with 0.2 U of Fpg for 1h at 37°C. The products were loaded on a 1% agarose gel in the presence of GelRed.

UV-A-mediated activation of Ru65 causes a DNA damage response

We have previously observed by confocal microscopy that **Ru65** preferentially accumulates into the nucleus of HeLa cells.[55] To corroborate this finding, we examined the subcellular localization of **Ru65** in additional cell lines using the same technique. Analysis of U2OS, MCF7, CAL33 cancer cells and the normal epithelial cell line RPE-1 incubated with **Ru65** (100 μM) for 4h showed nuclear localization of

the metal complex (Fig. 11A). Time-course experiments showed increasing accumulation of the metal complex into the nucleus of U2OS cells over a 24h period, with detectable signal 30 min post-administration and substantial amounts of **Ru65** being internalized at 4h (Fig. 11B).

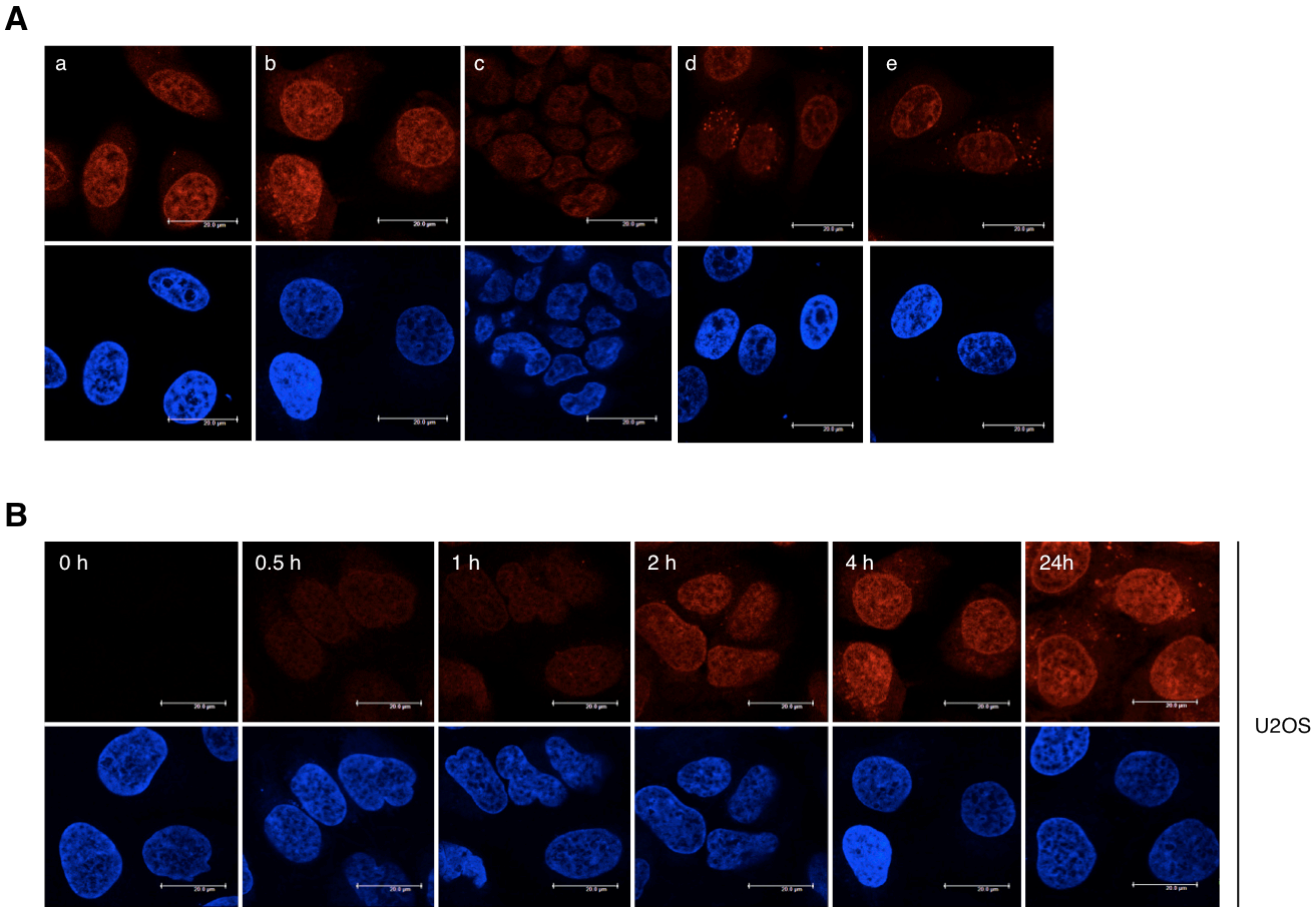

Figure 11. Ru65 localizes in the cell nucleus. A. HeLa (a), U2OS (b), MCF7 (c), CAL33 (d) and normal RPE-1 cells (e) were treated with **Ru65** (100μM) for 2h. After treatment, **Ru65** was removed from the medium, cells were fixed and visualized by confocal microscopy. Scale bar = 20μm. **B.** Time course uptake of **Ru65** (100μM) in U2OS. Cells were fixed and visualized as described in A.

We have also previously shown that UV-A irradiation of HeLa or MRC5 cells treated with **Ru65** led to a remarkable loss of viability if compared to non-irradiated cells.[55] The UV-A dose used in our previous study (350 nm, 2.58 J/cm^2) did not impact cell viability and was significantly below the dose administered by others working with similar metal complexes.[57] Nonetheless, to directly assess the impact on DNA of distinct doses of the UV-A light used to trigger **Ru65**, we performed PFGE analysis of genomic DNA. The data showed that irradiation at 350 nm with a light

dose of 2.58 J/cm^2 in the absence of **Ru65** caused *per se* the formation of significant amounts of double-strand breaks (DSBs) (Fig. 12A). Optimization studies on U2OS cells led us to conclude that at a lower dose of UV-A irradiation (1.29 J/cm^2) caused minimal damage (Fig. 12A), compatible with the studies that we decided to undertake.

To gain mechanistic insights into the cellular effect of activated **Ru65**, we examined the presence of γH2AX, an established marker of the DNA damage response (DDR). To this end, we used a flow cytometry-based method that couples quantification of DNA damage (γH2AX) with analysis of DNA content (DAPI), according to an established protocol.[58] Control experiments, where U2OS cells were treated with 1.29 J/cm^2 UV-A irradiation, showed only a transient phosphorylation of H2AX (Fig. 12B).

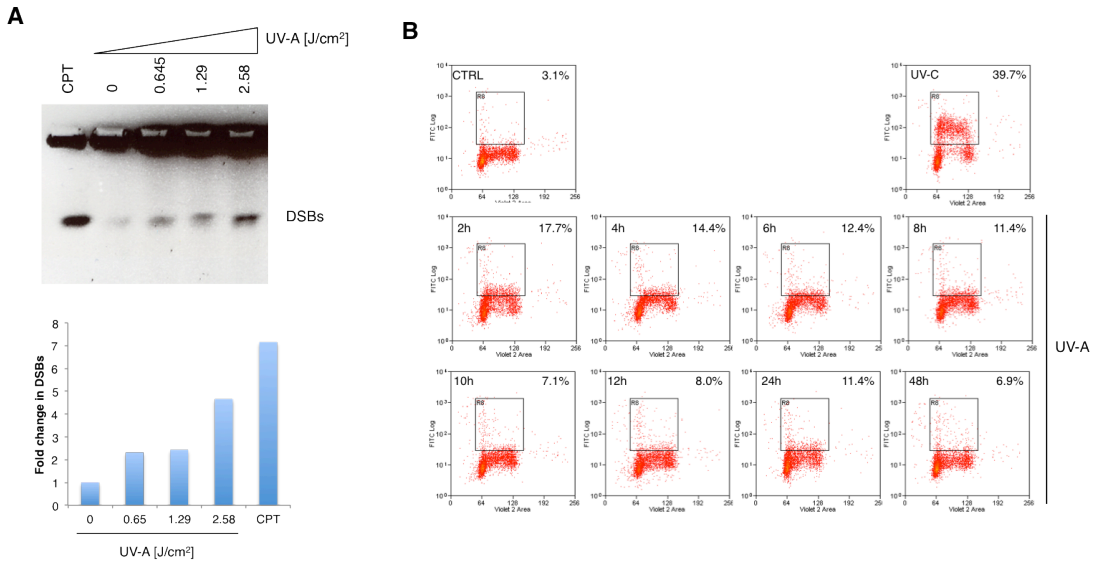

Figure 12. The photosensitizer UV-A does not cause DNA damage. A. PFGE analysis of U2OS cells treated with the indicated amounts of UV-A (upper panel). Quantification of the signal corresponding to DSBs (lower panel) was obtained using ImageJ and normalized to the unsaturated signals of DNA retained in the wells. The fold change in DSBs was obtained by normalizing each treatment to the untreated control. Camptothecin (CPT 1μM, 4h) was used as positive control. **B.** Time-course response of U2OS cells treated with UV-A (1.29 J/cm^2). The phosphorylation of H2AX was determined by flow cytometry as described in Materials and Methods. Irradiation with UV-C (20 J/m^2) was used as positive control.

On the other hand, UV-A irradiation of U2OS cells pre-treated with **Ru65** caused a ~16-fold increase in γH2AX foci 16 h post-irradiation in comparison to cells treated with either **Ru65** or UV-A alone (Fig. 13A). Immunofluorescence (Fig. 13B and 13C)

confirmed the generation of DNA damage upon activation of **Ru65**. Similar results were obtained using CAL33 cells (Fig. 13E).

Damage to DNA triggers a checkpoint response that arrests cell cycle progression and orchestrates repair at the site of damage.[59] To assess effects on the cell cycle, we performed studies using flow cytometry. The cell cycle profile of U2OS cells treated with **Ru65** in the absence of UV-A irradiation showed no difference with respect to that of untreated cells, indicating that the presence of **Ru65** did not disturb cell cycle progression (Fig. 13D). On the other hand, UV-A irradiation of **Ru65** showed a marked accumulation of cells in the S- and G2-phases of the cell cycle at 16 h post-irradiation (Fig. 13D), a time when γH2AX foci were clearly detectable in cells (Fig. 13A).

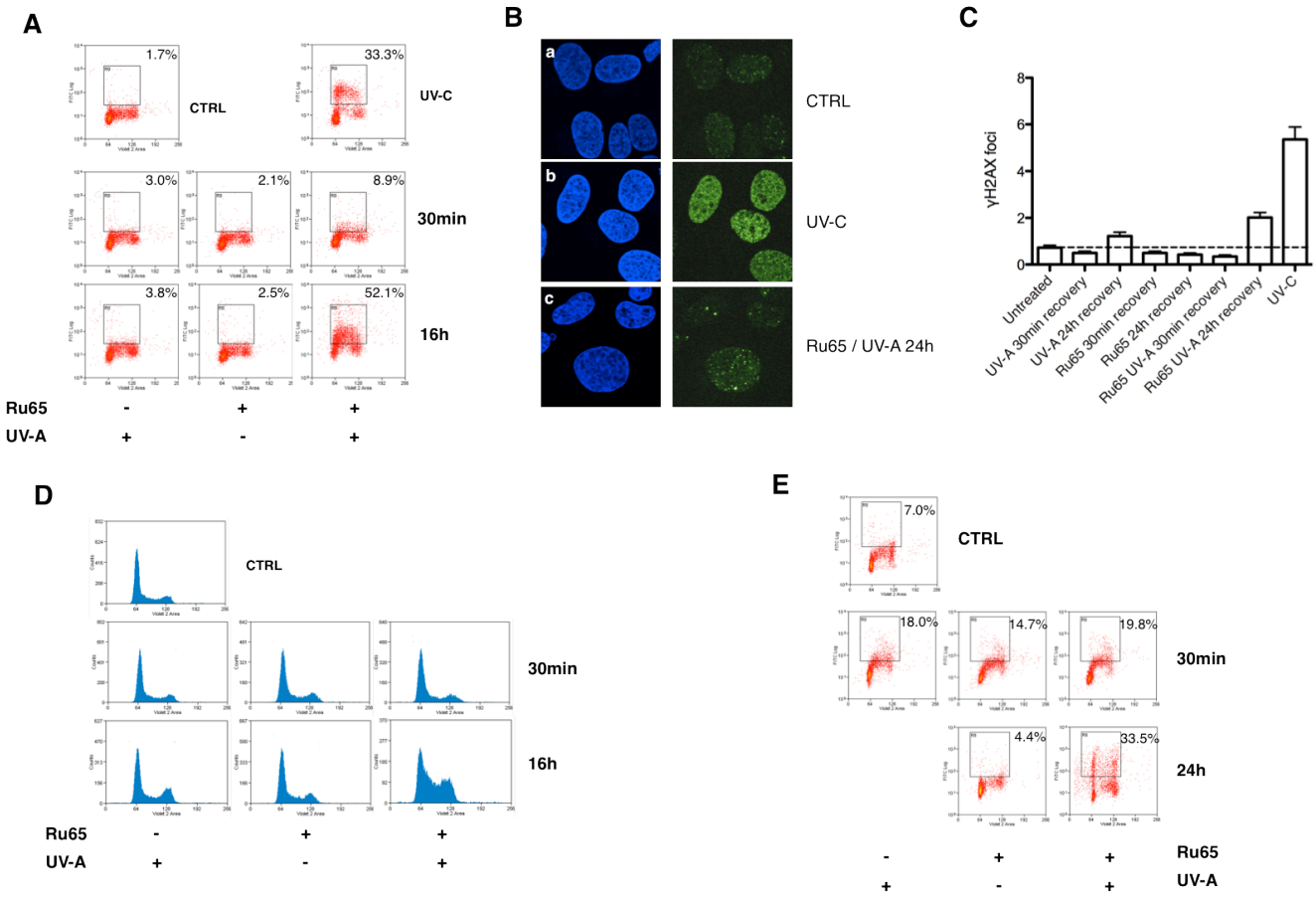

Figure 13. UV-A activated Ru65 triggers a DNA damage response. A. U2OS cells were treated with **Ru65** (50μM) and UV-A (1.29 J/cm^2) as indicated. Upon fixation, cells were probed with anti-γH2AX antibody and examined by flow cytometry. **B.** Representative images of U2OS cells left untreated (a), UV-C irradiated (b) or treated with **Ru65** and UV-A (c). Cells were immuno-stained with γH2AX antibody and visualized by confocal microscopy. **C.** Quantification of foci detected in the cells described in B. n = 200 cells, error bars = SEM. **D.** U2OS cells treated as in A were fixed and stained with DAPI. DNA was examined by flow cytometry. **E.** Dot plots of **Ru65** (50μM) treated CAL33 cells

irradiated with UV-A (1.29 J/cm^2) and allowed to recover for the time indicated. Cells were probed with anti-γH2AX antibody and examined by flow cytometry.

Photo-activation of Ru65 leads to the formation of DSBs in DNA

To elucidate the molecular mechanism of action of **Ru65** and assess the impact of the damage caused to DNA, we performed a set of analyses on living cells The exact nature of the DNA damage caused by **Ru65** was assessed by alkaline Single Cell Gel Electrophoresis (SCGE) or comet assay, which allows detecting DSBs, single-strand breaks (SSBs), abasic sites and DNA adducts.[60, 61] By measuring the % DNA in the tail, we first quantified the increase of DNA damage resulting from UV-A activation of **Ru65** over control treatments. An initial response occurring 30 min upon light irradiation was enhanced at the 16 h time point (Fig. 14A and 14B, see also Fig. 13A). To assess whether **Ru65** would cause base oxidation in living cells similarly to what observed on isolated plasmid DNA, cells treated with **Ru65** were agarose-embedded, incubated with Fpg and examined in alkaline comet assays. The increased pattern of DNA damage observed upon Fpg treatment (Fig. 14C) confirmed that **Ru65** operates in living cells with the same mechanism of action described above for plasmid DNA.

Finally, to assess whether staggered base damage occurring on the two DNA strands would result in the formation of DSBs, we examined the status of DNA in control or **Ru65**-treated cells by pulsed-field gel electrophoresis. The data confirmed that UV-A mediated activation of **Ru65** resulted in the formation of DSBs after 24h (Fig. 14D). To substantiate this observation, we treated U2OS cells with higher doses of **Ru65** and activating UV-A radiation. The data showed that, under these conditions, the extent of DSBs was proportionally increased and, particularly, that in respect to camptothecin, activated **Ru65** caused an evident fragmentation of DNA upon UV-A irradiation and 24h recovery (Fig. 14E).

Taken together, these data indicate that UV-A triggered formation of ROS by **Ru65** results in DNA base damage that is further processed to single- and double-strand breaks

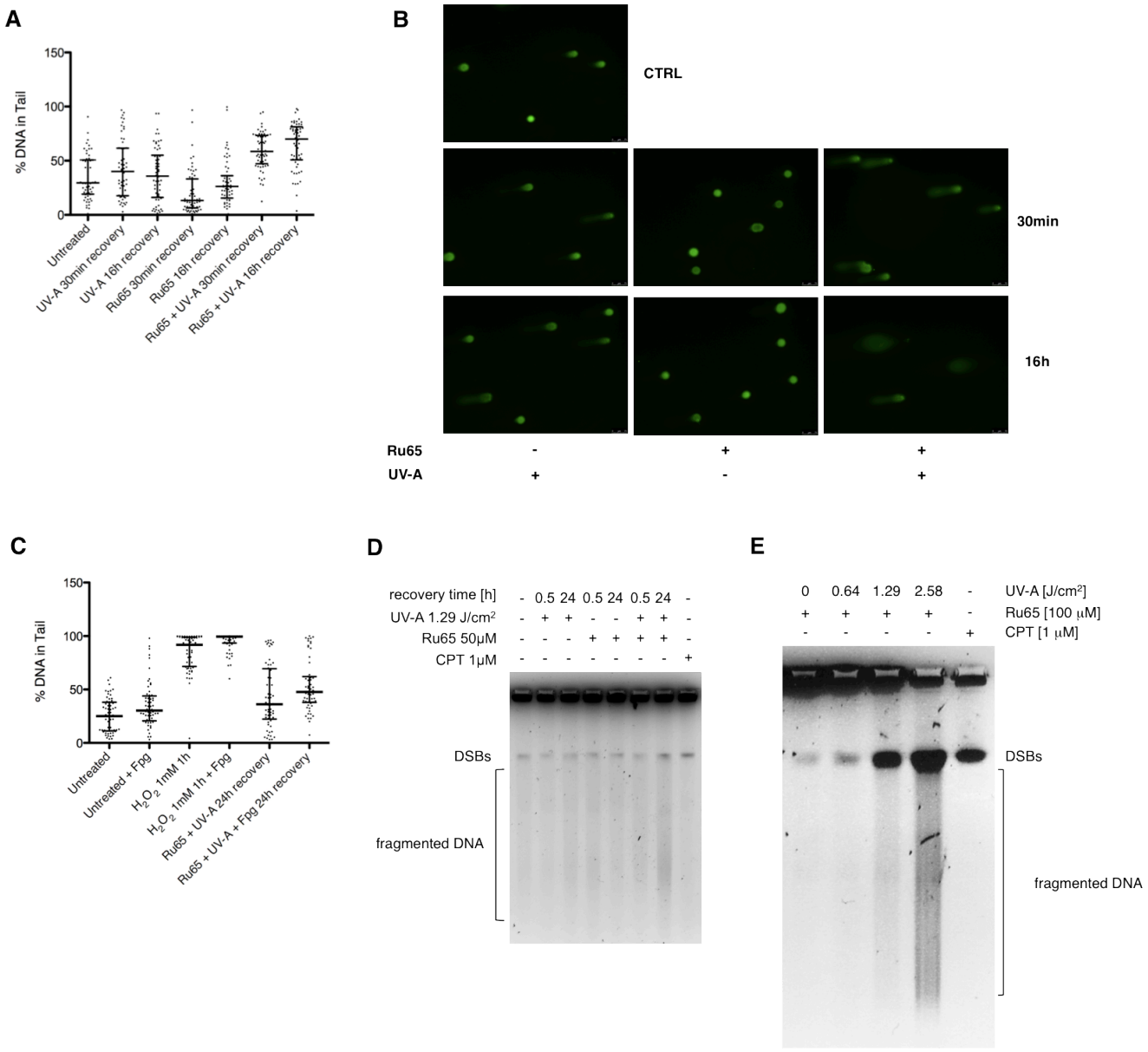

Figure 14. UV-A-activated Ru65 causes base oxidation and double-strand breaks. DNA damage in U2OS cells treated with **Ru65** and UV-A irradiation as indicated, was assessed by alkaline comet assay. **A.** The % of DNA in tail was quantified for each cell using the software Comet Assay IV (Perceptive Instruments). Each spot represents a single cell; 60 comet images were taken for each treatment. **B.** Representative micrographs of fluorescent DNA stain. **C.** The extent of oxidative damage in DNA upon treatment of U2OS cells with **Ru65** and UV-A irradiation was visualized by incubating cells embedded in agarose plugs with 0.2 U of Fpg for 1h at 37°C and resolving cells by alkaline comet assay. H_2O_2 was used as positive control. The % of DNA in tail was quantified as described in A. PFGE of U2OS cells treated as indicated and allowed to recover for 0.5 or 24h (**D**) and for 24h (**E**). Camptothecin (CPT 1μM, 4h) was used as positive control.

Photo-activation of Ru65 causes loss of viability and death by apoptosis

To evaluate the effect the mid-term cellular response to photo-induced activation of **Ru65** we performed MTT assays on a set of cell lines. The data showed that **Ru65** caused loss of viability in all cell lines tested (Table 1). To extend these observations, we decided to assess the long-term cellular response to **Ru65** by clonogenic survival assays.[62] Consistent with the data above, cytotoxicity was observed only upon UV-A irradiation of **Ru65** (Fig. 15A). Dose-response studies confirmed a decrease of survival at increasing **Ru65** doses (Fig. 15B).

Table 1. IC_{50} values determined upon incubation of a set of cell lines with **Ru65** in the dark for 4h and upon 4h incubation followed by UV-A irradiation. Cisplatin was used as comparison.

	IC_{50} (μM)							
	HeLa		U2OS		CAL33		RPE-1 hTERT	
	4 h (dark)	4 h (UV-A)[a]	4 h (dark)	4 h (UV-A)[a]	4 h (dark)	4 h (UV-A)[a]	4 h (dark)	4 h (UV-A)[a]
Ru65	> 100	20.0 ± 6.1	> 100	30.5 ± 2.9	> 100	17.4 ± 5.3	> 100	35.4 ± 3.3
Cisplatin	30.9 ± 3.6	27.4 ± 2.3	26.8 ± 1.9	21.6 ± 0.3	30.2 ± 7.2	25.0 ± 4.2	62.3 ± 9.7	64.1 ± 3.8

[a] 5 min UV-A irradiation (350 nm, 1.29 J cm^{-2}).

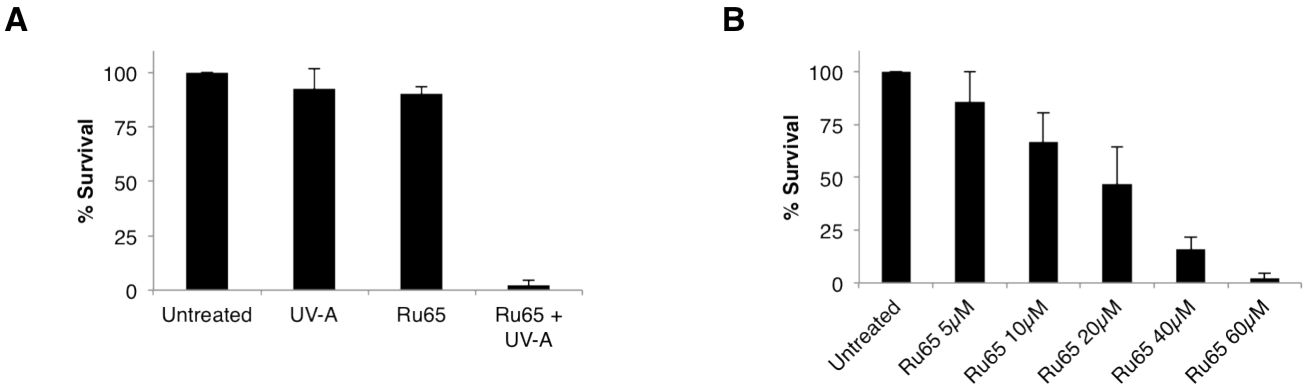

Figure 15. Activated Ru65 causes apoptosis. A. U2OS cells were treated with **Ru65** (50 μM) for 4h and UV-A (1.29 J/cm^2) as indicated prior to trypsinization and re-seeding at low density. Single colonies were stained after 12-14 days and the survival fraction determined by the ratio of plating efficiency for treated and untreated cells. Plotted values are the average of triplicates from 3 independent experiments with indication of standard error of the mean (SEM). **B.** U2OS cells were treated with increasing amounts of **Ru65** as indicated and examined as described in A.

2.2.2.4. DISCUSSION

The application of Ru^{II} complexes in cell imaging as well as their potential in therapy is well documented.[30, 63] With regard to their molecular mode of action, the ability of Ru complexes to bind canonical and non-canonical DNA structures has been reviewed at length.[63] We have recently reported the synthesis, characterization, photophysical properties and biological evaluation of a set of substitutionally inert polypyridyl Ru^{II} complexes. Notably, we have demonstrated the ability of such complexes to produce singlet oxygen ($^1O_2$) in response to irradiation at a defined wavelength and proposed their application as photosensitizers in PDT.[55] In the study reported here, we examined in detail the molecular mechanism of action of one such complexes (**Ru65**) upon intercalation in DNA. We observed that **Ru65** is efficiently internalized in a number of cell lines, that it mainly localizes to the nucleus and exerts specific cytotoxicity upon irradiation with UV-A. The dose of UV-A irradiation used in our experiments is ~4-fold lower than what reported by Gicquel *et al*. and it is comparable to what is locally employed in combination with psoralen for the treatment of psoriasis, which is generally innocuous for skin types >II.[57, 64]

Mechanistically, using a set of biochemical and biological assays we demonstrate that activated **Ru65** causes the oxidation of purines on isolated plasmid DNA as well as in living cells. Among purines, guanine is characterized by a low redox potential and can be easily oxidized.[65] 8-oxo-7,8-dihydroguanine (8-oxo-G) is one of the most stable and miscoding lesions caused by ROS that originate from endogenous cellular processes or are produced by external sources like ionizing or UV radiation.[56] Such lesion is normally rapidly removed by the pathway of Base Excision-Repair (BER), with DNA glycosylase OGG1 being the enzyme responsible for recognition and excision of 8-oxo-G when it is regularly paired to cytosine.[66]

Using structurally similar DNA intercalating Ru^{II} polypyridyl complexes, Gicquel and colleagues have argued that their complexes must cause single- and double-strand breaks, based on the ability of specific DNA repair proteins to bind the DNA structures that were generated.[57] In our study, using comet assays as well as pulse-field gel electrophoresis and a by far lower amount of activating UV-A radiation, we provide formal and direct demonstration for the ability of activated **Ru65** to generate DNA double-strand breaks.

In analogy to the response to DNA mismatches generated by S(N)1-type alkylating agents that were previously described in studies conducted at IMCR, we speculate that cells treated with **Ru65** may cope with the presence of residual base damage during the first cycle of cell division and that unaddressed damage becomes critical during the S-phase of the second cell cycle when it is converted in double strand breaks.[67] We speculate that the latter may originate either from staggered base oxidations on opposite DNA strands that are not fully addressed in the first wave of repair or from replication-dependent conversion of nicks, that result from the effective removal of oxidized bases, into double-strand breaks. These hypotheses explain the cell cycle profile data and the late pattern of γH2AX foci formation in response to UV-A activated **Ru65**.

In conclusion, our study highlights the mechanism of action of Ru^{II}-based metal complexes as DNA targeting molecules that can be activated at will with innocuous UV-A irradiation and formally demonstrates that activated **Ru65** causes DNA double-strand breaks ultimately resulting in cell death. Taken together, our observations open the perspective of using Ru^{II}-based metal complexes in the photodynamic therapy of cancer.[55, 57]

2.2.2.5. FUTURE WORK BASED ON PRELIMINARY RESULTS

Understanding the mechanism involved in the repair of the DNA damage triggered by UV-A activation of **Ru65** is crucial to define the most likely application for this drug candidate. Indeed, a tumor lacking the specific machinery that addresses repair of the damage caused by **Ru65** would be more vulnerable to the treatment, as opposed to a tumor proficient in such pathway, which would rather survive and acquire further mutations, resulting in resistance to therapy and more pronounced malignancy. To this end, the repair machinery involved, the mechanism of cell death and possible genome threats could be investigated.

A. To dissect the contribution of established signaling pathways to the observed pattern of γH2AX foci, we can envisage to examine by immunoblotting markers for the ATM or ATR pathways, namely the phosphorylation status of ATM, KAP1 for the former and ATR, CHK1 for the latter. Additionally, we could employ specific

inhibitors of the three apical PI-3K-like kinases and check the pattern of γH2AX foci by flow cytometry.

Considering ATR, preliminary data obtained by Western blot analysis where we looked at its direct downstream target (CHK1), indicate that the ATR pathway is activated already 30 min after **Ru65**-UV-A treatment and remains activated up to 8 h. The involvement of ATR could be explained with the fact that unrepaired DNA single strand breaks at early stage of the response to **Ru65** result in higher amount of γH2AX foci, marker of double strand break at later stage. This could support the hypothesis that primary SSBs left unrepaired, lead to DSBs at later times. On the contrary, the data indicated that the ATM pathway is not induced in **Ru65** treated U2OS cells after irradiation, since no phosphorylation of its downstream target KAP1 could be detected by Western blot, even at late time points (16-24 h) when most γH2AX appears. Similarly, inhibition of ATM with a specific compound showed no differences in γH2AX foci in comparison to non-inhibited conditions. Hence, the appearance of γH2AX foci mainly at 16-24 h in the absence of a detectable ATM activation remains puzzling.

B. A possible explanation of the death consequent to **Ru65** activation is the occurrence of futile cycles of repair. These result from the inability of the base excision repair (BER) pathway to process oxidized bases, thus leading to the formation and persistence of base mismatches. To test this hypothesis we can consider to down-regulate OGG1, which would lead to an increase of unrepaired 8-oxoG lesions in DNA, possibly causing cell death at earlier time points.

C. To explore the mechanism triggering cell death upon photo-activation of **Ru65**, we would like to complement our cell cycle studies (Fig. 13D) with the analysis of apoptotic, necrotic and autophagic markers.

Apoptosis could be investigated *via* caspase 3/7 activation and Annexin-V expression at the cell surface, two specific assays detecting apoptosis in biological samples. Simultaneously, necrotic pattern would also be studied, together with Annexin-V exposure, using Propidium Iodide (PI) staining. Preliminary Annexin-V/PI staining results showed only a slight increase in the amount of early-stage

apoptotic cells at 30 min and at 24 h after combined treatment compared to **Ru65** only treated cells. Moreover, no PI positive cells were detected, a pattern that possibly excludes death by necrosis.

These negative results and the highly vacuolated status of the cytoplasm of the treated and irradiated cells starting already 1 h after **Ru65** activation lead us to consider other forms of programmed cell death. Indeed, **Ru65** treated and irradiated cells show massive vacuolization in the cytoplasm that leads to cell detachment and blebbing prior to cell death. Early experiments investigating autophagy are undertaken. Known inhibitors (Wortmannin, SB202190) would be used, and vacuole formation, as well as presence of LC3B-II protein, would be monitored. At this stage, we cannot exclude a simultaneous or sequential death process and we even consider that **Ru65** could trigger its own paraptotic-like cell death. To exhaustively describe the death pathway, we can imagine to check for different additional known pattern occurring during cell death in a time-lapse approach, such as nuclear fragmentation, chromatin condensation, mitochondria swelling, DNA fragmentation, PARP cleavage, presence of LC3B-II in vacuole membranes or if vacuoles are made of endoplasmic reticulum membranes.

Should **Ru65** trigger its own paraptotic-like cell death, this would be of great interest for the treatment of apoptotic resistant cancer cells, for instance.

D. Finally, since the **Ru65** complex damages DNA, investigation of possible chromosomal aberrations (breaks, fusion) could be undertaken, in order to assess if the compound represents a threat to genome stability.

2.2.2.6. MATERIALS AND METHODS

Antibodies, chemicals and enzymes – Rabbit polyclonal antibodies to phosphorylated histone H2AX (S_{139}), was purchased from Cell Signaling Technology (Beverly, MA, USA). HRP-conjugated anti-mouse and anti-rabbit secondary antibodies were obtained from Amersham-Biosciences/GE-Healthcare (Otelfingen, Switzerland). The Alexa Fluor® 488 anti-rabbit secondary antibody was from Cell Signaling Technology. Formamido-pyrimidine DNA Glycosylase (Fpg) was purchased at New England Biolabs. The CometAssay® kit was from Trevigen (USA). Crystal violet was obtained from Sigma-Aldrich (Switzerland).

Cell culture - U2OS osteosarcoma cells and hTERT-immortalized retinal pigment epithelial cells RPE-1 hTERT were cultured in DMEM (Gibco, Life Technologies, USA) supplemented with 10% fetal calf serum (FCS) (Gibco). HeLa cervical carcinoma cells were maintained in DMEM containing 5% FCS. MCF-7 breast carcinoma cells were grown in MEM (Gibco, Life Technologies, USA) supplemented with 10% FCS and 200 mM L-Glutamine. CAL-33 squamous cell carcinoma were cultured in RPMI (Gibco, Life Technologies, USA) without phenol red supplemented with 10% FCS and 1% Glutamax (Gibco, Life Technologies, USA). All cell lines were complemented with penicillin (100 U/mL), and streptomycin (100 µg/mL) and stored in a humidified incubator containing 5% CO_2 at 37 °C.

Photo-irradiation settings - UV-A treatment was performed in a Rayonet RPR-200 photochemical reactor (Rayonet Corp., USA) containing 6 bulbs (14 W each) emitting in the 300-400 nm range (350 nm maximum intensity). Light intensity (55 W/m^2) was determined using a X11 optometer (Gigahertz-Optik, Germany).

Cell viability and colony formation assays - Cytotoxicity of the Ru(II) complex was assessed by a fluorometric cell viability assay using resazurin (Promocell, Germany). Briefly, one day before treatment, cells were seeded at a density of 4x10^3 cells/well in 100 μl in 96-well plates and the next day incubated for 4 h with either **Ru65** complex or cisplatin. Upon replacement of the medium and UV-A irradiation (1.29 J/cm^2), cells were returned to incubator for 48 h and viability assessed as previously described [68].

For colony formation assays cells were seeded at 3 x 10^5 cells/ml in a 6 cm dish and the next day treated and irradiated as above. Cells were trypsinized and re-seeded in triplicate in 6 well dishes. Colonies were stained with a crystal violet/ethanol solution (0.5%/20%) after 12-14 days of culturing and counted.

Immunofluorescence staining and analysis - Cellular localization of fluorescent ruthenium complex was assessed by fluorescence microscopy. Cells were grown on 18 mm Menzel-Gläser cover slips (Menzel-Gläser, Germany) at a density of 2.5 × 10^5 cells/ml and incubated for 2h with 100 µM **Ru65** at 37 °C. Cells were fixed in 4%

formaldehyde and mounted on slides for viewing by confocal microscopy on a CLSM Leica SP5 microscope (Leica Germany). **Ru65** was visualized using the red wavelength selection (ex, 458 nm; em, 600–650 nm) on the CLSM Leica SP5 microscope.

U2OS cells were seeded at a density of 3 x 10^5 cells/ml in a 6 cm dish containing cover slips. The next day, cells were treated for 4h with **Ru65** (50 μM), the medium was replaced and cells were UV-A irradiated (1.29 J/cm^2). For control UV-C treatment, cells were set in a Stratalinker 1800 (Stratagene, Agilent Technologies, USA) and irradiated with 20 J/m^2. After treatment, cells were placed back to the incubator for 30min or 24h. Cells were fixed for 15min at RT °C in 4% formaldehyde, permeabilized in 0.1 % Triton X-100 for 5min at 4°C, blocked in 3% milk/PBS and incubated over night at 4°C with anti- γH2AX antibody. After washing in 3% milk/PBS, Alexa Fluor 488 goat-anti rabbit antibodies (1:1000) were added for 1h at 37°C. After washing in PBS and rinsing in ddH_2O, coverslips were mounted on slides with DAPI containing mounting solution (Vectashield) and visualized with CLSM SP5 microscope.

Flow Cytometry - Cells were seeded at a concentration of 3 x 10^5 cells/ml in a 6 cm dish one day before treatment. The next day cells were treated and irradiated as indicated above, fixed in 4% formaldehyde for 15 at room temperature (RT) and permeabilized in 0.1% Triton-X100/PBS for 10 min on ice. Upon washing with 1% BSA/PBS cells were resuspended in 1% saponin dissolved in 1% BSA/PBS buffer containing the primary antibody (rabbit anti γH2AX 1:250) for 2h at RT. Cells were washed with saponin/BSA/PBS and the secondary antibody (anti-rabbit Alexa Fluor 488 1:50) was added in the same buffer for 30 min at RT in the dark. Cells were washed with saponin/BSA/PBS followed by 1% BSA/PBS before resuspension in 1% BSA/PBS containing 0.1 mg/ml RNase and 1μg/ml DAPI at RT in the dark 30min. Alexa Fluor 488 and DAPI signals were acquired on 10'000 cells / sample using a CyAn ADP 9 flow cytometer (Dako) and analyzed with Summit 4.3 software. Data are represented as mean ± SEM.

Pulse-field gel electrophoresis – Sub-confluent cultures of U2OS were treated with vehicle alone (DMSO), camptothecin (CPT 1μM) or **Ru65** (50 μM) in the dark or

upon UV-A irradiation. Cells were harvested by trypsinization, and agarose plugs of 10^6 cells were prepared in a disposable plug mold (BioRad). Plugs were incubated in lysis buffer (100 mM EDTA, 1% (w/v) sodium lauryl sarcosyl, 0.2% (w/v) sodium deoxycholate, 1mg/ml proteinase K) at 37 ºC for 72h and washed four times in 20 mM Tris-HCl pH 8.0, 50 mM EDTA before loading onto an agarose gel. Electrophoresis was performed for 23h at 14 ºC in 0.9% (w/v) Pulse Field Certified Agarose (BioRad) containing Tris-borate/EDTA buffer according to the conditions described in [70] and adapted to a BioRad CHEF DR III apparatus. The gel was finally stained with ethidium bromide (EtBr) and analyzed using an Alpha Innotech Imaging system.

Alkaline comet assay – Alkaline comet assays were performed using the CometAssay Reagent Kit (Trevigen), according to the manufacturer's instructions. Briefly, U2OS cells were seeded at a concentration of 3 x 10^5 cells/ml in a 6 cm dish one day before treatment. The next day cells were treated and irradiated as indicated above and let recover for 30min or 16h. After resuspension in PBS at a concentration of 1 x 10^5 cells/ml and combined with LM Agarose at a ratio of 1:10 (v/v), 50 μl of the mixture was loaded onto CometSlide and placed at 4 °C for 30 min. Embedded cells were lysed in a bath at 4 °C for 30 min, slides were immersed in alkaline unwinding solution for 20 min at RT, prior to alkaline electrophoresis (21 V, 30 min, in alkaline electrophoresis solution). Following two baths in H_2O of 5 min and one of 70% EtOH of 5 min, samples were dried at 37 °C and stained with SYBR green for 30 min. A total of 60 cells were scored using Comet Assay IV analysis system (Perceptive Instruments, UK) and an epifluorescence microscope (Leica) with 20x magnification objective. Results are presented as mean values for % of DNA in tail.

3. Discussion and Outlook

Advantages of using photo-activatable metal-based anticancer agents over conventional anticancer drugs.

3.1. ADVANTAGES OF PDT OVER CONVENTIONAL CHEMOTHERAPY

Research in the field of light-activated prodrugs is rapidly expanding since this strategy offers the possibility of overcoming several drawbacks of traditional chemotherapeutics. The advantages of photoactivatable prodrugs consist in:

(i) Spatial and temporal control of drug activity

The fact that the generated toxicity does not originate from the drug itself, but from the ROS produced upon a specific light, is crucial to overcome systemic toxicity and side effects (nausea, nephrotoxicity, ototoxicity); since the toxicity is sequestered to the irradiated area.

(ii) Light as a trigger

- Light is easily applicable and economically affordable in the clinic.

- The use of optic fibres allows reaching internal areas located in cavities or colorectal and oesophageal areas. Such fibres can also treat solid cancer located in the core of organs by incisions and insertions into the organ. Therefore, PDT could potentially substitute removal surgery in the case of cancers located in areas that are easily reachable with fibres (cavities) or in areas where esthetical outcome matters (i.e. head and neck cancer). As an example, TOOKAD, a photosensitizer, currently in clinical trials, accumulates preferentially into prostate cancer tissues. The local treatment of the tumor with fibres permits to avoid total resection of the prostate, as currently performed in the clinic.[73]

- Porphyrin photosensitizers absorb light in the red (600-800 nm), allowing light to penetrate the dermis of the skin.[74] Research to tune molecules for near infra-red (NIR)(>800 nm) absorbance are ongoing, since such wavelengths penetrate deeper into the skin, and will allow for treatment of cancer located deeper in the tissue without surgery. According to the location of the cancer, it may be of interest to modulate the light penetrability of the skin, and thereby the activation of the drug. Indeed, if the layer of skin underlying the tumor is at risk or need to be protected, the use of a topical or short skin entrance (UV-A) is relevant (optical properties of the skin in Figure 8)

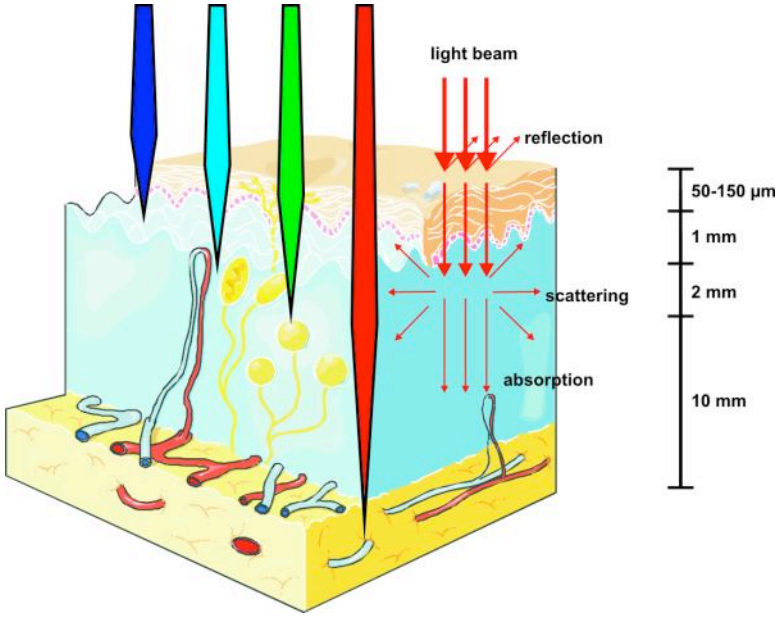

Figure 16. Propagation of light in the tissue according to its wavelength. Taken from ref [74].

(iii) Photodynamic Therapy and Photodiagnosis

5-Aminolevulinic acid (ALA), is metabolized *via* the heme biosynthetic pathway and results in the endogenous photosensitizer protoporphyrin IX (PpIX). The latter photosensitizer can also be used as a fluorescence cancer marker for the detection of cancer, combining PDT and photodiagnosis.[75] The advantage of such a molecule is that combined to surgery, remaining cancer tissue can be visualized and treated.

(iv) Substitute to surgery

For safety reasons, during removal surgery of a solid tumor, a large surrounding area, mostly composed of healthy tissue is also sacrificed. The use of PDT would be aesthetically preferable, where removal of large skin areas, for example, on the head, will lead to bad esthetical outcomes or skin difficulty to reattach. As mentioned above, the use of fibres in an organ to locally treat tumor tissues instead of the total ablation could benefit to the patient, as illustrated by the prostate case.

3.2. Advantages of Ru complexes over traditional porphyrin based photosensitisers

Nowadays, most of the photosensitizers clinically used in PDT are porphyrins-based. However, they suffer several drawbacks that non-porphyrin based Ru complexes could tackle.

(i) Poor solubility

The poor water solubility of porphyrins makes them difficult to synthesize, mostly because of the purification step. The same is true in biological solution, raising the issue for bloodstream administration. Research towards increasing solubility is on going with the so-called 2nd PS generation. To this end, one of the strategies examined is the insertion of a metal fragment, such as Zn or Ru, to *inter alia* increase the solubility of the conjugated porphyrin.[30]

(ii) Extended photosensitivity in patient skin

An other important drawback from with patients suffer, is the prolonged photosensitivity of current PS like Photofrin.[54] Therefore, using PS with non-porphyrin structure could be a way to reduce photosensitivity.

3.3. ADVANTAGES OF THE CAGING AND TRIGGERED-RELEASE STRATEGY IN CANCER THERAPY

(i) Reduced systemic toxicity

In the field of targeted therapy, the selective and located delivery of biologically active compounds into living cells is highly attractive. The control derived from such a strategy permits to concentrate the action of the drug at a given location, reducing though the systemic toxicity of the latter molecule. The availability of existing cages permit the use of internal or external trigger, the latter one offering additional temporal control on the drug activity.

(ii) Use of endogenous and exogenous triggers

Are considered endogenous trigger, all the events derived from diseased cellular tissues, such as ROS level, specific pH change or presence of a tissue-specific enzyme. More appealing is the use of an external trigger to activate the release of the molecule, since it offers complete control on the release. Different sort of cages exist. They respond to specific events such as light, magnetic field or temperature. The most interesting trigger is light, since, as explained earlier, it is cheap and the range of wavelength allows for tuning the skin permeability.

3.4. FUTURE DIRECTION

The next step in this research field would be to increase the targeting efficiency of PDT agents. Although the enhanced permeability and retention effect of PS in cancer tissues favors the accumulation of the latter in tumor over healthy cells,[76] this feature could be improved by the attachment of a targeting molecule to the PS. As example, a specific biomolecule could be used as a targeting moiety since it is known that several receptors at the surface of cancer cells are overexpressed.

More work needs also to be done in order to find efficient PS complexes with absorption in the near-IR, to targets tumors localized deeper in the skin without surgery.

4. Appendix

Supplementary informations of [43-45].

Supplementary Data:

Molecular and Cellular Characterization of the Biological Effects of Ruthenium(II) Complexes Incorporating 2-Pyridyl-2-Pyrimidine-4-Carboxylic Acid

Vanessa Pierroz,[a,b] Tanmaya Joshi,[c] Anna Leonidova,[a] Cristina Mari,[a] Julia Schur,[d] Ingo Ott,[d] Leone Spiccia,[c,] Stefano Ferrari[b,*] and Gilles Gasser[a,*]*

[a]Institute of Inorganic Chemistry, University of Zurich, Winterthurerstrasse 190, CH-8057 Zurich, Switzerland; [b]Institute of Molecular Cancer Research, University of Zurich, Winterthurestrasse 190, CH-8057 Zurich, Switzerland; [c]ARC Centre of Excellence for Electromaterials Science and School of Chemistry, Monash University, Melbourne, Victoria 3800, Australia; Institute of Medicinal and Pharmaceutical Chemistry, Technische Universität Braunschweig, Beethovenstrasse 55, 38106 Braunschweig, Germany.

* Corresponding authors: Email: leone.spiccia@monash.edu; Fax: +61 3 9905 4597; Tel: +61 3 9905 4526 ; WWW: www.chem.monash.edu.au/staff/spiccia/. Email: sferrari@imcr.uzh.ch; Fax: +41 44 635 3484; Tel: +41 44 635 3471; WWW: www.imcr.uzh.ch/research/Ferrari.html. Email: gilles.gasser@aci.uzh.ch; Fax: +41 44 635 6803; Tel: +41 44 635 4630; WWW: www.gassergroup.com.

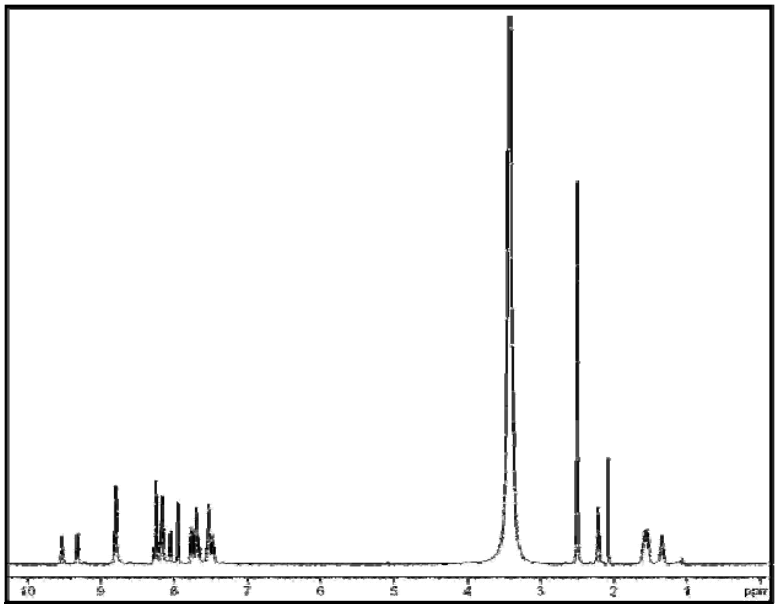

Figure S1. ^{1}H NMR spectrum of **[Ru(bipy)$_2$(Cpp-L-OH)](PF$_6$)$_2$ (2)** in DMSO-d$_6$.

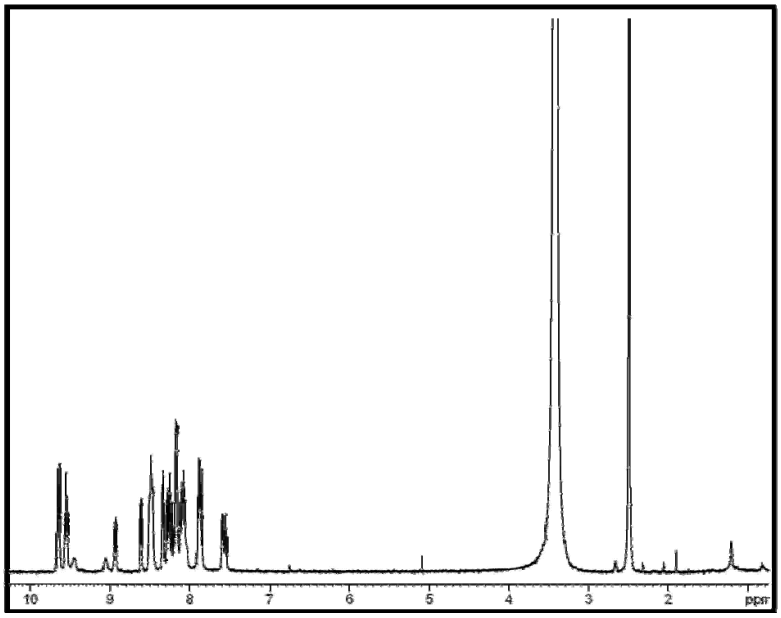

Figure S2. ^{1}H NMR spectrum of **[Ru^{II}(dppz)$_2$(CppH)](PF$_6$)$_2$ (3)** in DMSO-d$_6$**.**

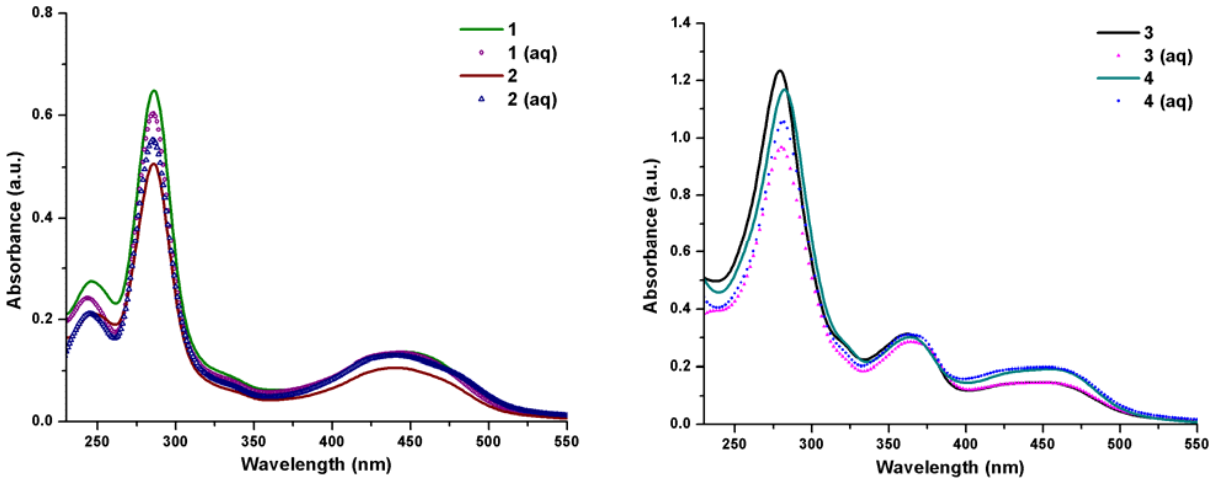

Figure S3. Absorption spectra for 10 μM solutions of Ru(II) complexes. Solid traces represent the spectrum in acetonitrile and dotted traces show spectra in H_2O/0.2% DMSO solutions.

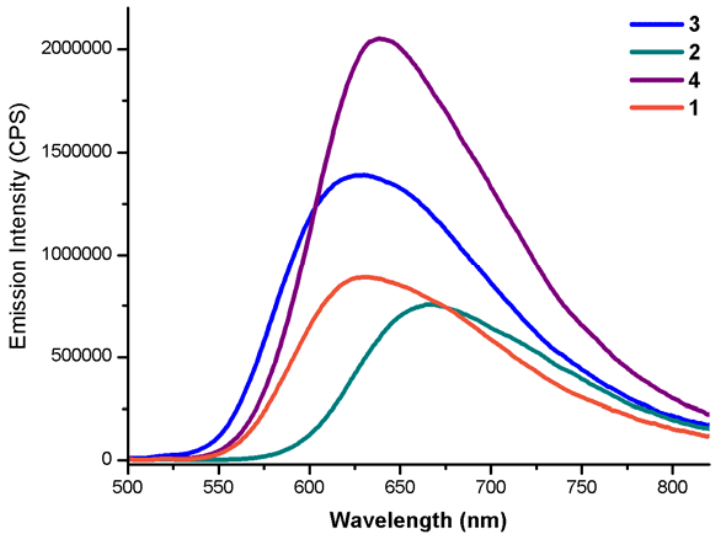

Figure S4. Emission spectra recorded on excitation of 10±1 μM acetonitrile solutions of **1-4** at 450 nm.

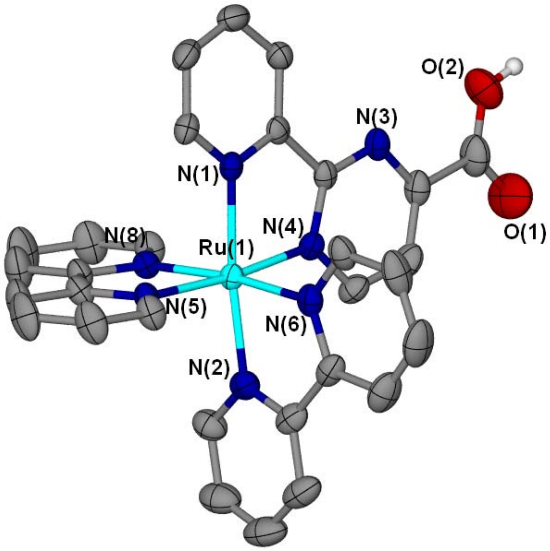

Figure S5. Thermal ellipsoid representation of the cationic unit $[Ru(bipy)_2(CppH)]^{2+}$, in **1** (probability ellipsoids drawn at 50%; selected hydrogen atoms, counter PF_6^- anions and water molecules omitted for clarity).

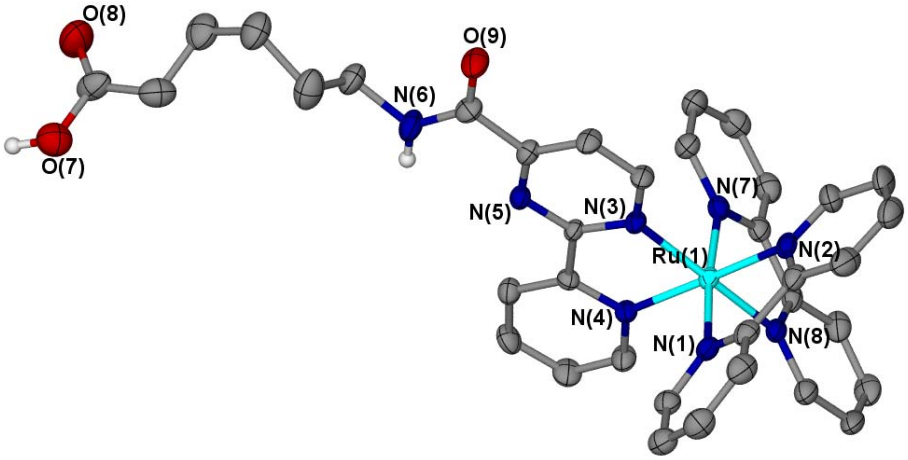

Figure S6. Thermal ellipsoid representation of a cationic unit, $[Ru(bipy)_2(Cpp\text{-}NH\text{-}Hex\text{-}COOH)]^{2+}$, of **2** (probability ellipsoids drawn at 50%; selected hydrogen atoms, counter ClO_4^- anions and water molecules omitted for clarity).

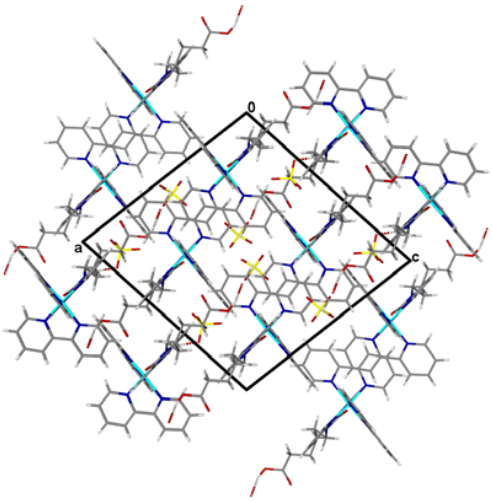

Figure S7. Molecular packing diagram for $[Ru(bipy)_2(Cpp\text{-}NH\text{-}Hex\text{-}COOH)](ClO_4)_2$ (**2**) showing hydrogen-bonding interactions (shown in dashed bonds) and C-H….π interactions present in the crystal lattice, as viewed along the 'b' axis.

Table S1. Selected bond lengths [Å] and angles [°] for **1** and **2**.

1		**2**	
Ru(1)-N(4)	2.048(3)	Ru(1)-N(4)	1.947(4)
Ru(1)-N(6)	2.051(4)	Ru(1)-N(2)	1.951(4)
Ru(1)-N(5)	2.054(3)	Ru(1)-N(3)	2.053(3)
Ru(1)-N(2)	2.058(4)	Ru(1)-N(8)	2.058(4)
Ru(1)-N(8)	2.057(3)	Ru(1)-N(7)	2.178(4)
Ru(1)-N(1)	2.069(4)	Ru(1)-N(1)	2.184(4)
C(30)-O(1)	1.239(7)	C(36)-O(7)	1.340(7)
C(30)-O(2)	1.261(7)	C(36)-O(8)	1.268(6)
		C(30)-O(9)	1.193(5)
N(4)-Ru(1)-N(6)	88.54(13)	N(4)-Ru(1)-N(2)	174.10(15)
N(4)-Ru(1)-N(5)	173.85(13)	N(4)-Ru(1)-N(3)	78.88(14)
N(6)-Ru(1)-N(5)	95.40(13)	N(2)-Ru(1)-N(3)	96.76(14)
N(4)-Ru(1)-N(2)	95.65(14)	N(4)-Ru(1)-N(8)	96.45(14)
N(6)-Ru(1)-N(2)	78.60(15)	N(2)-Ru(1)-N(8)	88.28(14)
N(5)-Ru(1)-N(2)	89.77(14)	N(3)-Ru(1)-N(8)	172.63(15)
N(4)-Ru(1)-N(8)	97.60(14)	N(4)-Ru(1)-N(7)	87.05(14)
N(6)-Ru(1)-N(8)	172.29(14)	N(2)-Ru(1)-N(7)	97.34(16)
N(5)-Ru(1)-N(8)	78.89(13)	N(3)-Ru(1)-N(7)	94.93(14)
N(2)-Ru(1)-N(8)	96.07(15)	N(8)-Ru(1)-N(7)	79.03(14)
N(4)-Ru(1)-N(1)	78.75(13)	N(4)-Ru(1)-N(1)	97.07(15)
N(6)-Ru(1)-N(1)	97.64(14)	N(2)-Ru(1)-N(1)	78.70(16)
N(5)-Ru(1)-N(1)	96.01(13)	N(3)-Ru(1)-N(1)	87.90(13)
N(2)-Ru(1)-N(1)	173.40(14)	N(8)-Ru(1)-N(1)	98.40(14)
N(8)-Ru(1)-N(1)	88.18(13)	N(7)-Ru(1)-N(1)	175.40(13)
O(1)-C(30)-O(2)	124.8(5)	O(8)-C(36)-O(7)	123.1(6)

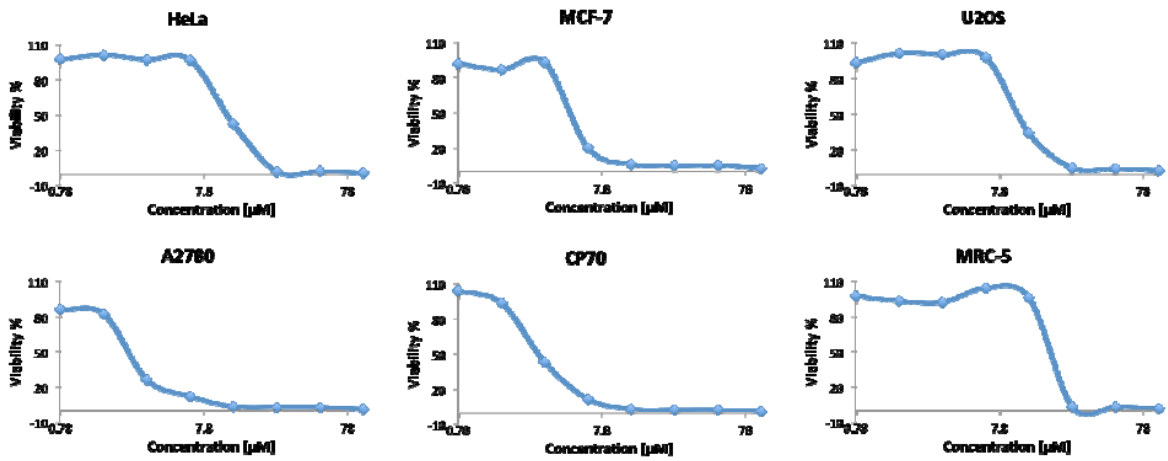

Figure S8. Cytotoxicity of **3** on HeLa, MCF-7, U2OS, A2780, CP-70 and MRC-5 cells measured by the resazurin assay.

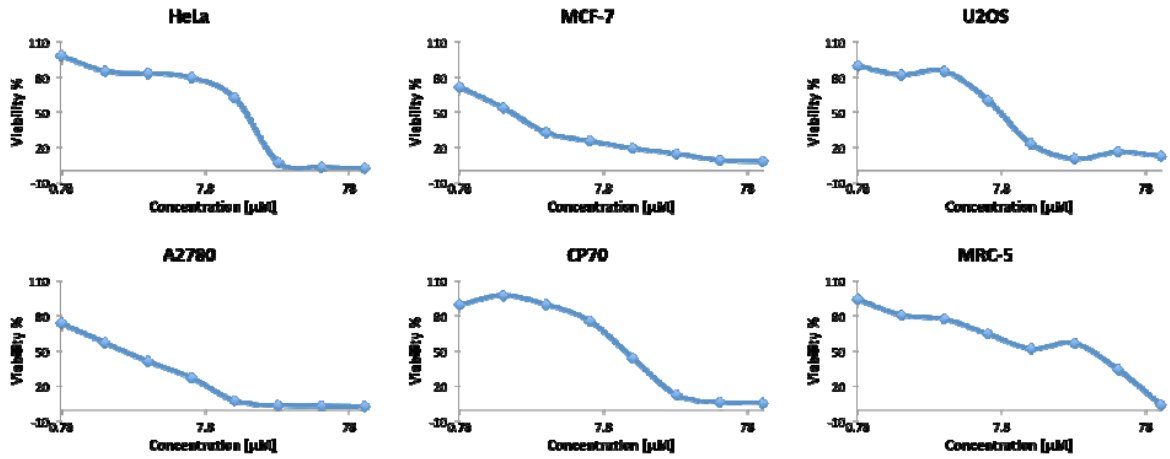

Figure S9. Cytotoxicity of Cisplatin on HeLa, MCF-7, U2OS, A2780, CP-70 and MRC-5 cells measured by the resazurin assay.

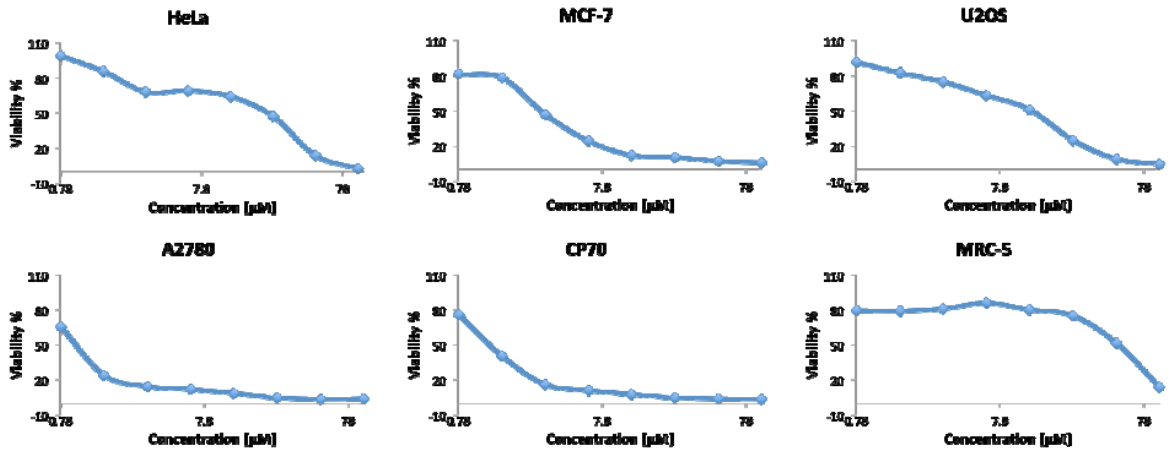

Figure S10. Cytotoxicity of dequalinium choride hydrate on HeLa, MCF-7, U2OS, A2780, CP-70 and MRC-5 cells measured by the resazurin assay.

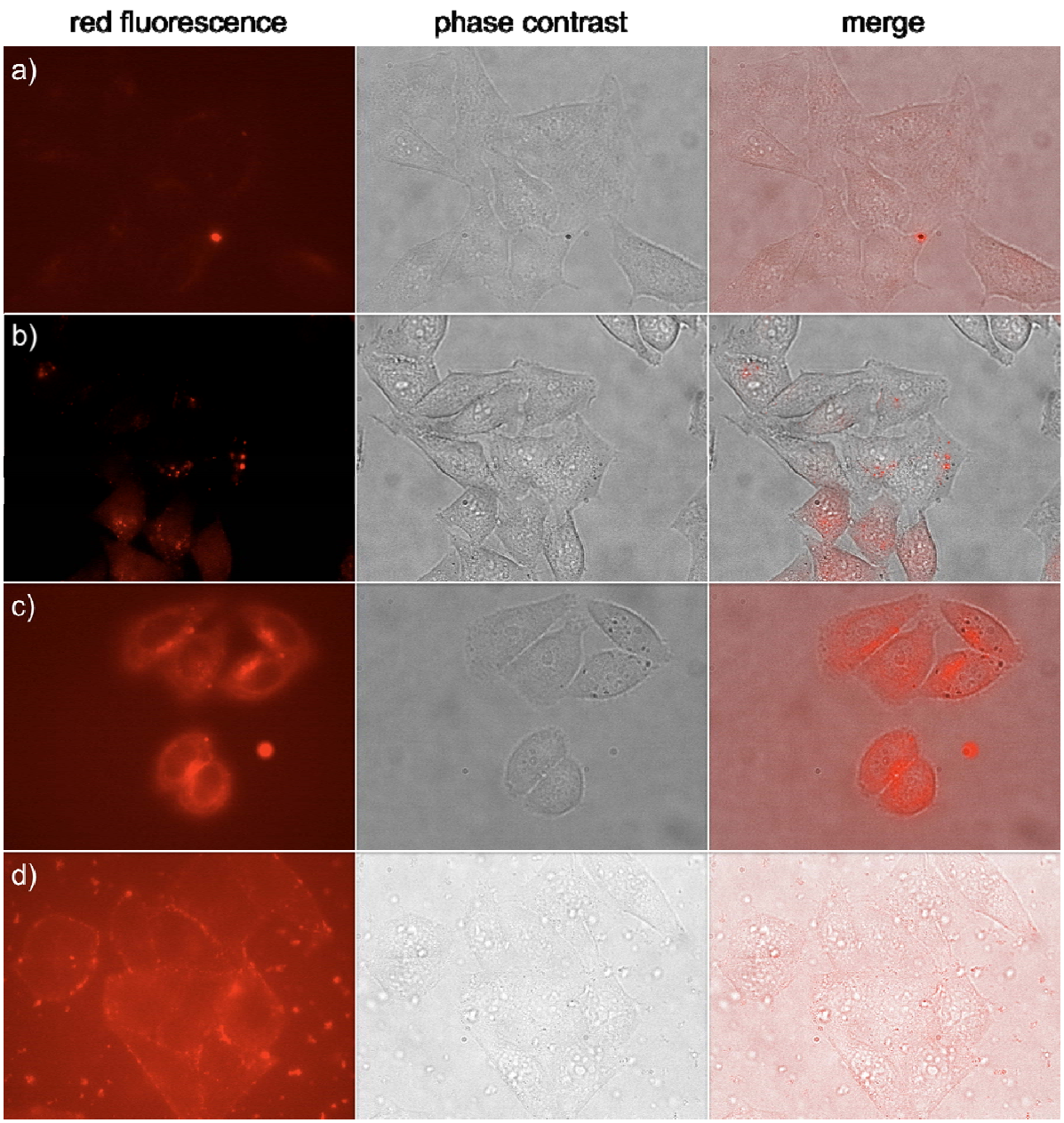

Figure S11. Fluorescence microscopy images of living HeLa cells incubated with: a) **1** (100 μM, 2 h); b) **2** (15 μM, 4 h); c) **3** (20 μM, 2 h) and d) **4** (70 μM, 15 min). Images show cellular staining of ruthenium compounds, phase contrast and the overlay.

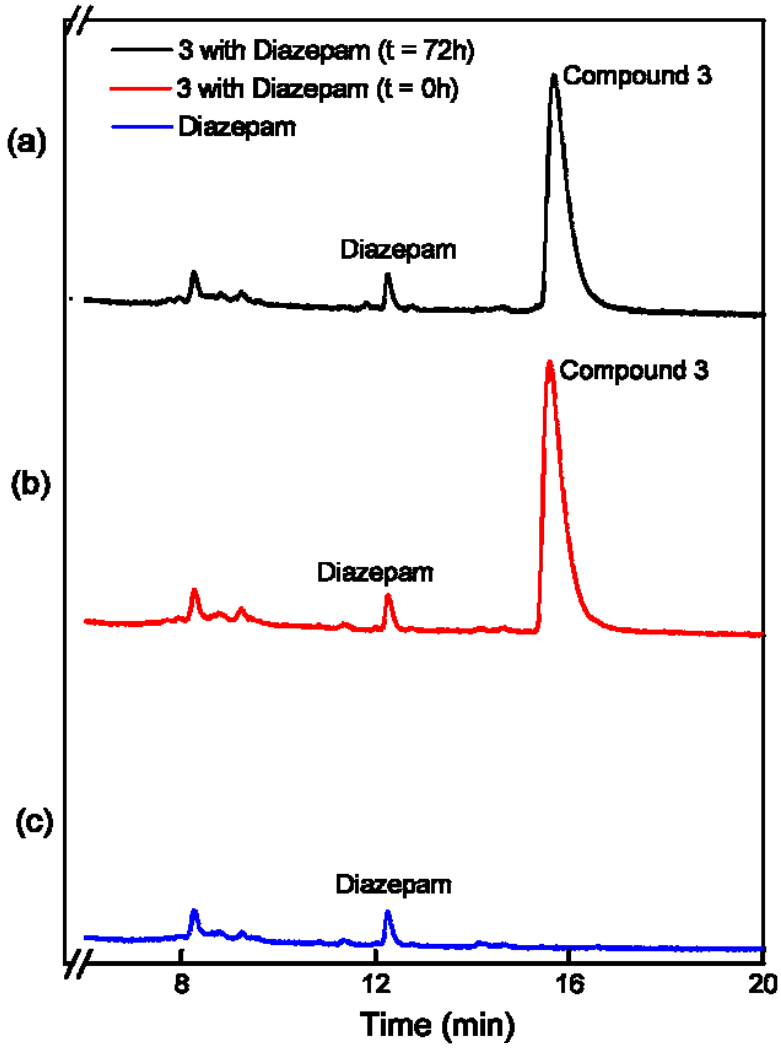

Figure S12. UV traces (300 nm) for LC-MS analysis of human blood plasma incubated with **3** (20 μM) at t = 0 and 72 h (Diazepam was used as internal standard).

Table S2. Ratio of peak areas of **3**/diazepam at t = 0 and 72 h.

Time (h)	Ratio of peak area (**3**/Diazepam)
0	21.54
72	20.17

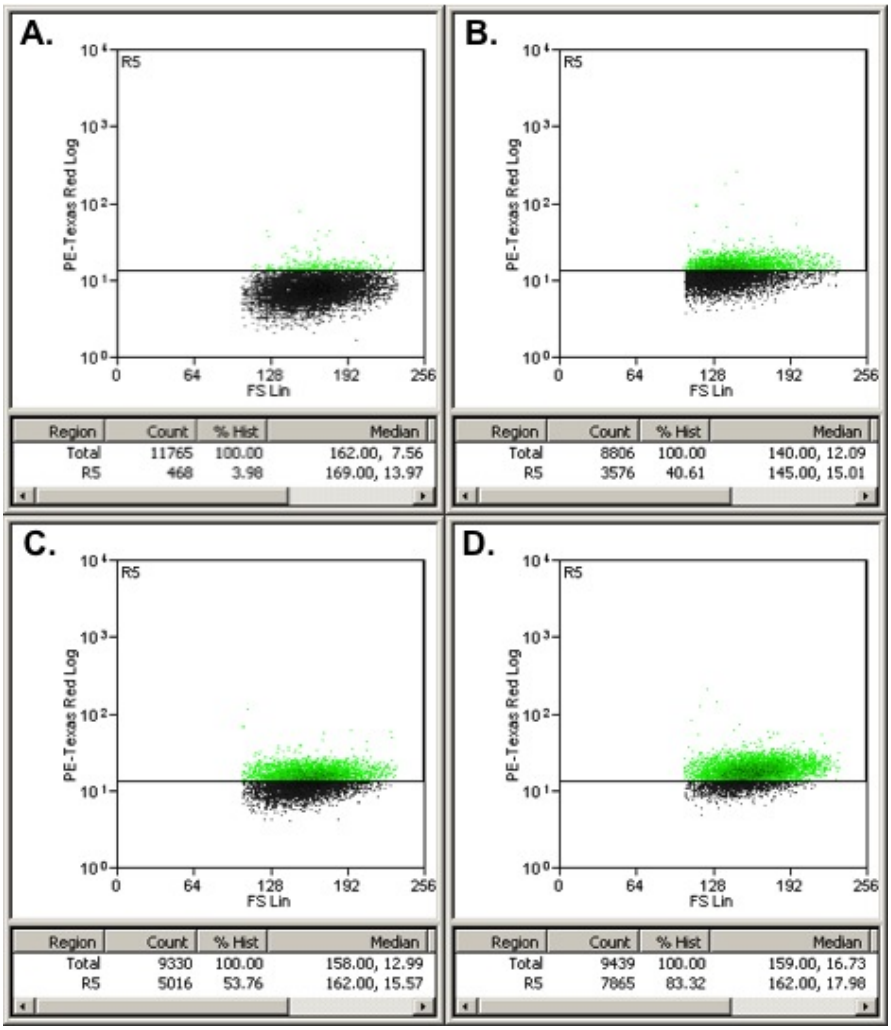

Figure S13. Flow cytometry dot plots showing the effect of the temperature on the uptake of **3** (20 μM) after 6 h in HeLa cells. Green spots represent cells that have taken up **3** in **A)** control untreated cells or cells treated at **B)** 4 °C, **C)** 23 °C, and **D)** 37 °C.

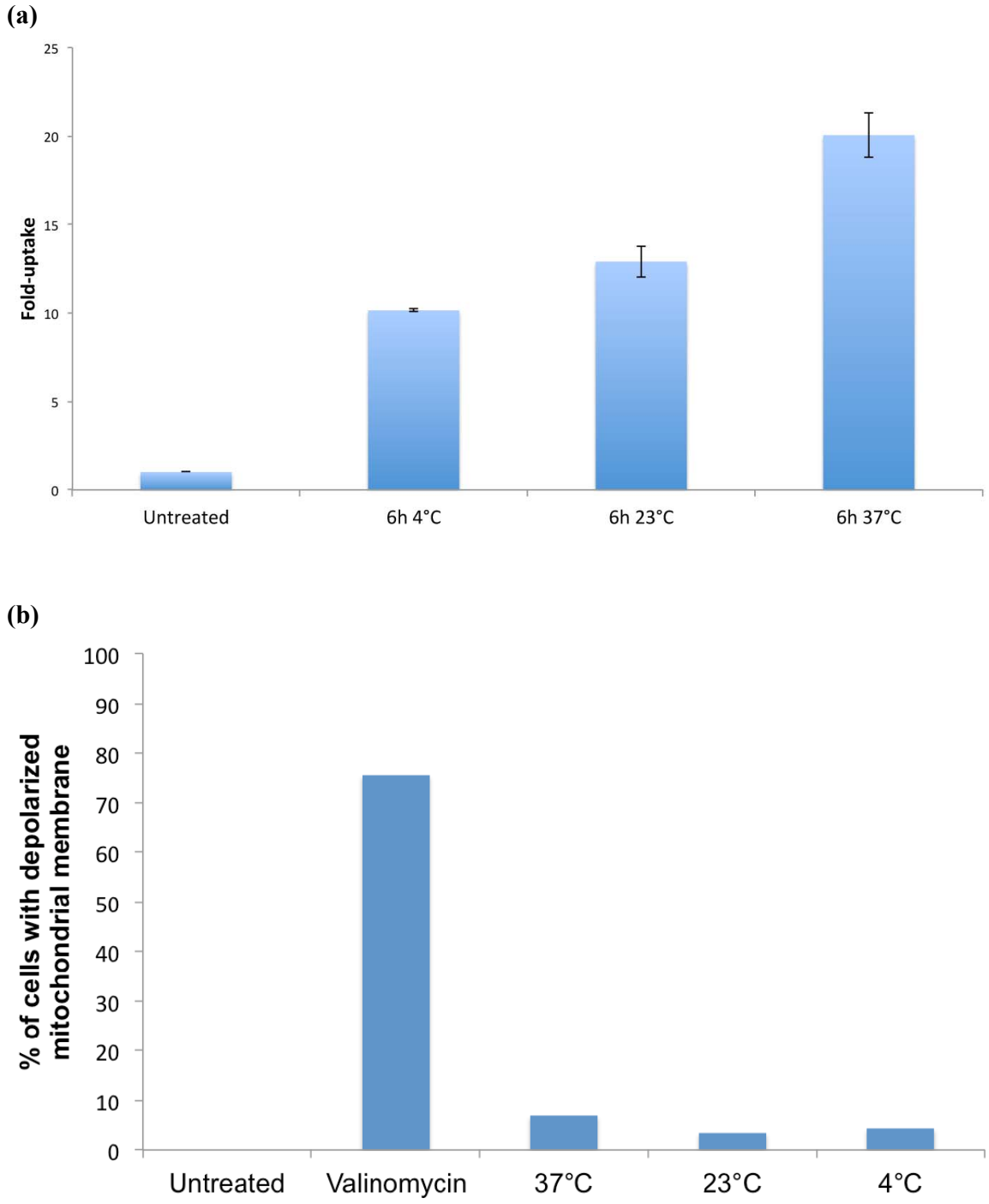

Figure S14. Effect of temperature on: **(a)** uptake of **3** {HeLa cells were incubated with **3** (20 μM, 6h) at 4 °C, 23 °C or 37 °C and the amount of compound taken up was determined by flow cytometry}; **(b)** mitochondrial membrane potential of untreated HeLa cells incubated for 6 h at 4 °C, 23 °C or 37 °C {Valinomycin was used a positive control (6 h at 37 °C)}.

Table S3. Cyclic voltammetric data obtained as a function of scan rate (v) at a glassy carbon electrode from the oxidation of **2-4** (1.0 mM) in MeCN (0.1 M nBu_4NPF_6) at (20 ± 2) ºC.

Complex	N (mVs^{-1})	E_p^{ox} (mV)[a,b]	E_p^{red} (mV)[a,b]	ΔE_p (mV)[a,b]	E_m (mV)[a,b]	$\lvert i_p^{ox}/i_p^{red}\rvert$[a,c]	Diffusion coeff (cm^2s^{-1}) ($x10^{-5}$)[d]
2	100	1010	930	80	970	1.09	1.03±0.1
	200	1010	930	80	970	1.07	
	300	1010	930	80	970	1.07	
	400	1020	930	90	975	1.06	
	500	1020	930	90	975	1.05	
	700	1020	930	90	975	1.04	
	1000	1020	930	90	975	1.02	
3	100	1130	1070	60	1100	0.91	1.05±0.1
	200	1140	1070	70	1105	0.92	
	300	1140	1070	70	1105	0.93	
	400	1140	1070	70	1105	0.93	
	500	1140	1070	70	1105	0.93	
	700	1140	1070	70	1105	0.94	
	1000	1140	1070	70	1105	0.95	
4	100	1100	1030	70	1065	0.92	1.12±0.1
	200	1100	1030	70	1065	0.93	
	300	1100	1020	80	1060	0.94	
	400	1100	1020	80	1060	0.95	
	500	1100	1020	80	1060	0.93	
	700	1100	1020	80	1060	0.93	
	1000	1100	1020	80	1060	0.93	

[a]Oxidation peak potential = E_p^{ox}; reduction peak potential = E_p^{red}; $E_m = (E_p^{ox}+E_p^{red})/2$ versus the $Fc^{0/+}$ couple; oxidation peak current = i_p^{ox}; reduction peak current = i_p^{red}. [b]Measured peak potentials have an error of ±5 mV versus $Fc^{0/+}$. [c]The ratios of peak currents associated with the oxidation and reduction of the complexes were calculated according to the empirical method derived by Nicholson.[1] [d]Diffusion coefficient data obtained from the linear plot of i_p^{ox} versus $\nu^{1/2}$, employing the Randles-Sevcik equation.[2-4]

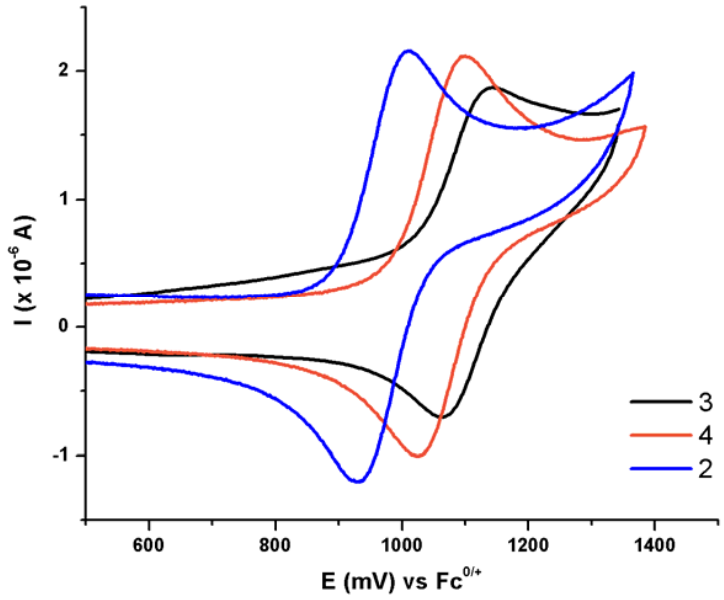

Figure S15. Cyclic voltammograms obtained at a glassy carbon electrode using a scan rate of 100 mV s^{-1} for the oxidation of 1 mM Ru(II) complexes in MeCN (0.1 M nBu_4NPF_6).

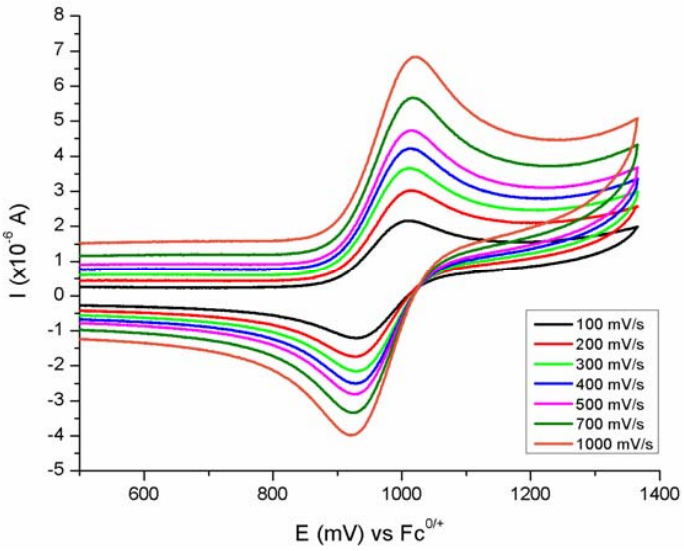

Figure S16. Cyclic voltammograms obtained at a glassy carbon electrode for the oxidation of 1 mM **2** in MeCN (0.1 M nBu_4PF_6) as a function of scan rate.

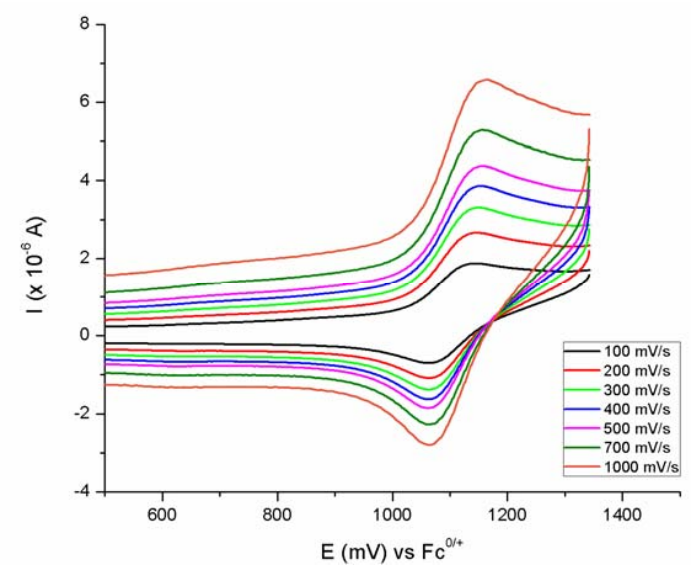

Figure S17. Cyclic voltammograms obtained at a glassy carbon electrode for the oxidation of 1 mM **3** in MeCN (0.1 M nBu_4PF_6) as a function of scan rate.

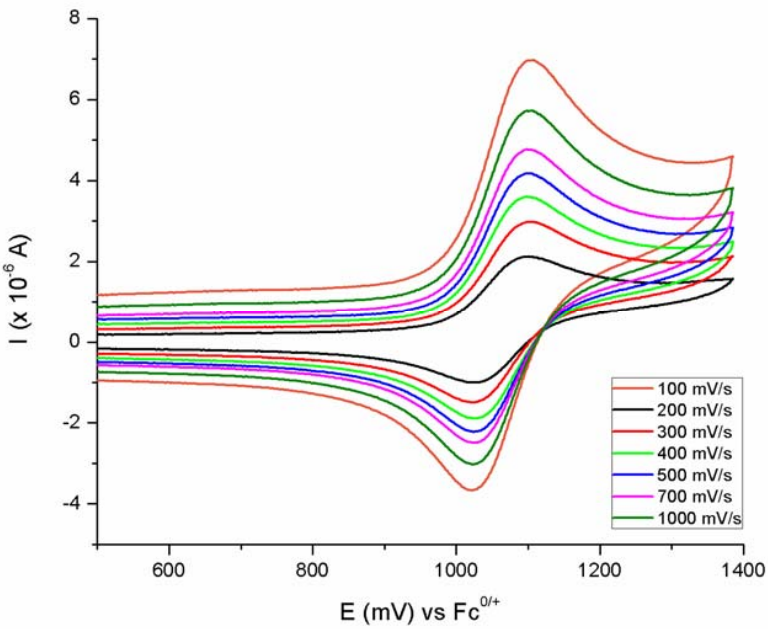

Figure S18. Cyclic voltammograms obtained at a glassy carbon electrode for the oxidation of 1 mM **4** in MeCN (0.1 M nBu_4PF_6) as a function of scan rate.

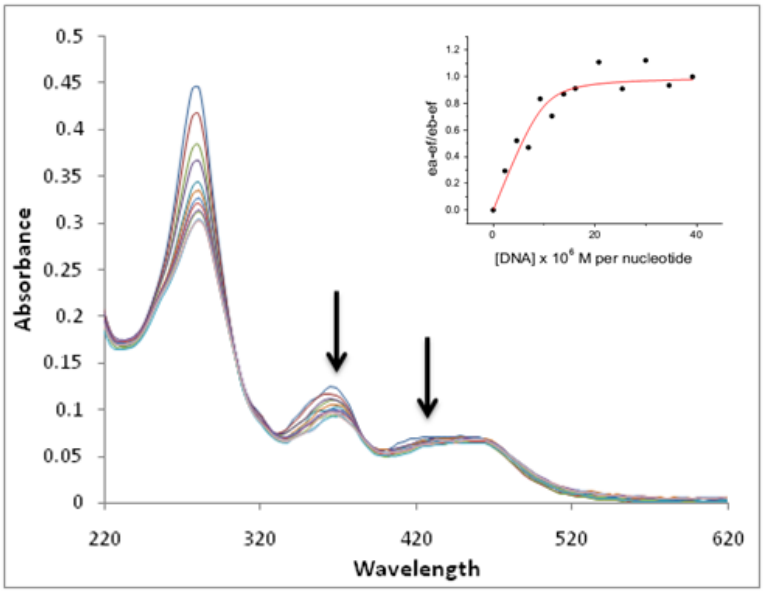

Figure S19. Changes in absorption spectra of **3** (3.96 μM) in 10 mM phosphate buffer (pH = 7.01, 50 mM NaCl) with increasing concentrations of CT-DNA until [DNA]/[Ru] = 4. Arrows show spectral changes upon increasing DNA concentrations. In the inset: plot of $(\varepsilon_a - \varepsilon_f)/(\varepsilon_b - \varepsilon_f)$ vs [DNA] and the non-linear fit of the titration data.

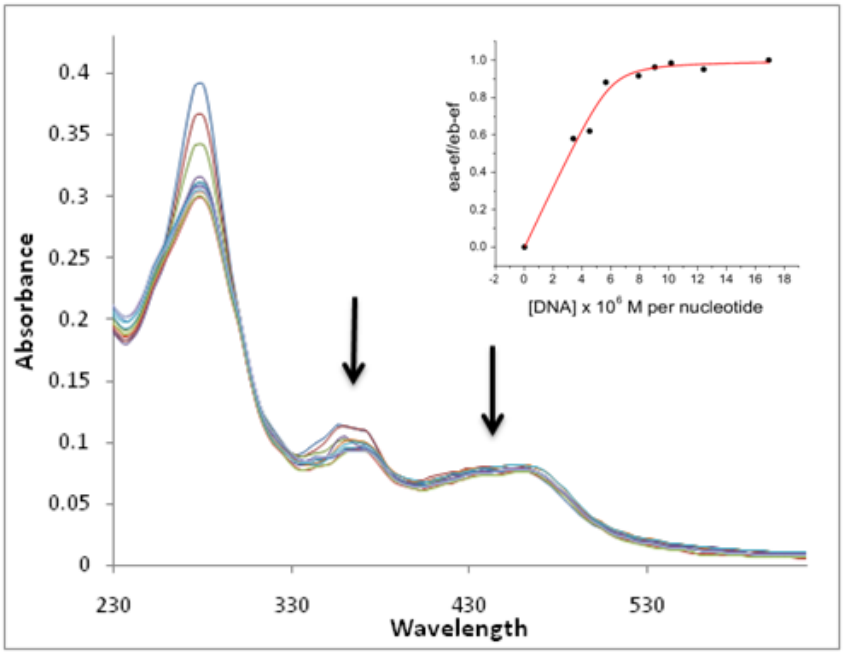

Figure S20. Changes in absorption spectra of **4** (4.62 μM) in 10 mM phosphate buffer (pH = 7.01, 50 mM NaCl) with increasing concentrations of CT-DNA until [DNA]/[Ru] = 3. Arrows show spectral changes upon increasing DNA concentrations. In the inset: plot of $(\varepsilon_a - \varepsilon_f)/(\varepsilon_b - \varepsilon_f)$ vs [DNA] and the non-linear fit of the titration data.

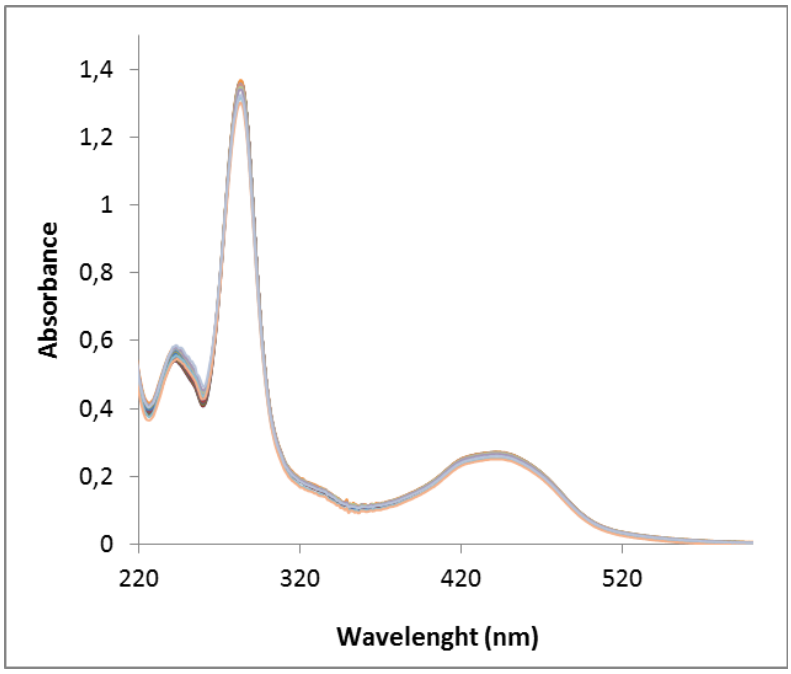

Figure S21. Changes in absorption spectra of **1** (20 μM) in 10 mM phosphate buffer (pH = 7.01, 50 mM NaCl) with increasing concentrations of CT-DNA until [DNA]/[Ru] = 6.

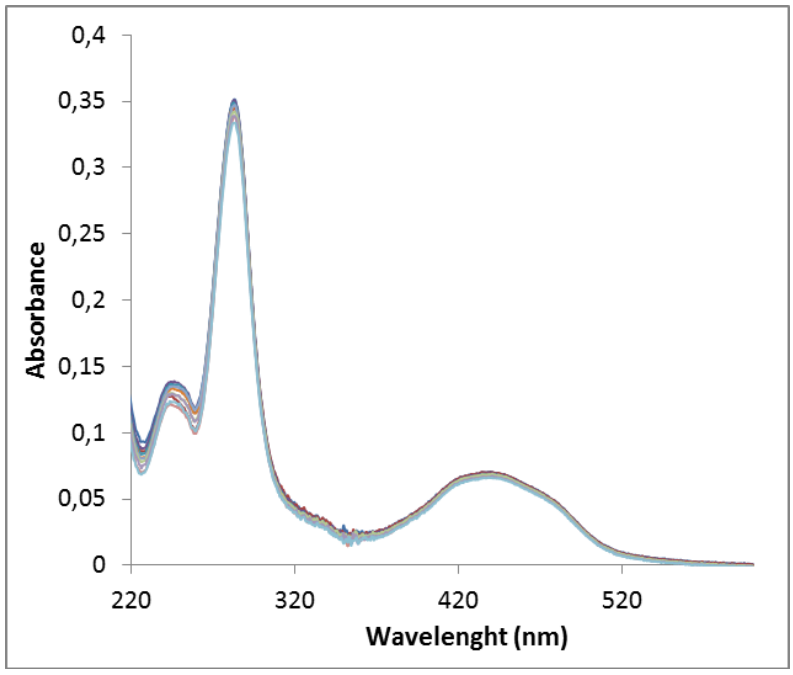

Figure S22. Changes in absorption spectra of **2** (5.48 μM) in 10 mM phosphate buffer (pH = 7.01, 50 mM NaCl) with increasing concentrations of CT-DNA until [DNA]/[Ru] = 9.

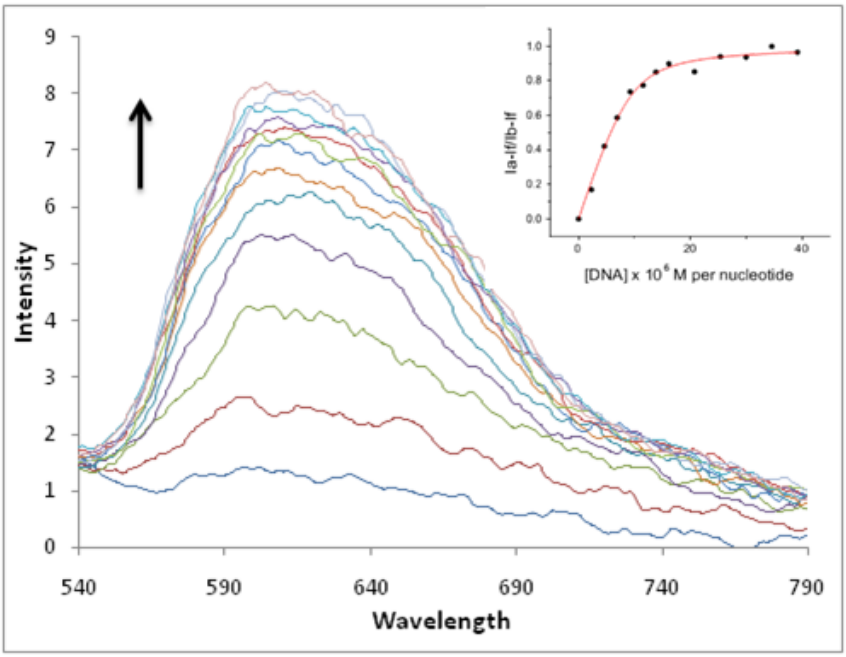

Figure S23. Changes in emission spectra (λ_{ex} = 440 nm) of **3** (3.96 μM) in 10 mM phosphate buffer (pH = 7.01, 50 mM NaCl) with increasing concentrations of CT-DNA until [DNA]/[Ru] = 4. Arrows show spectral changes upon increasing DNA concentrations. In the inset: plot of $(I_a - I_f)/(I_b - I_f)$ vs [DNA] and the non-linear fit of the titration data.

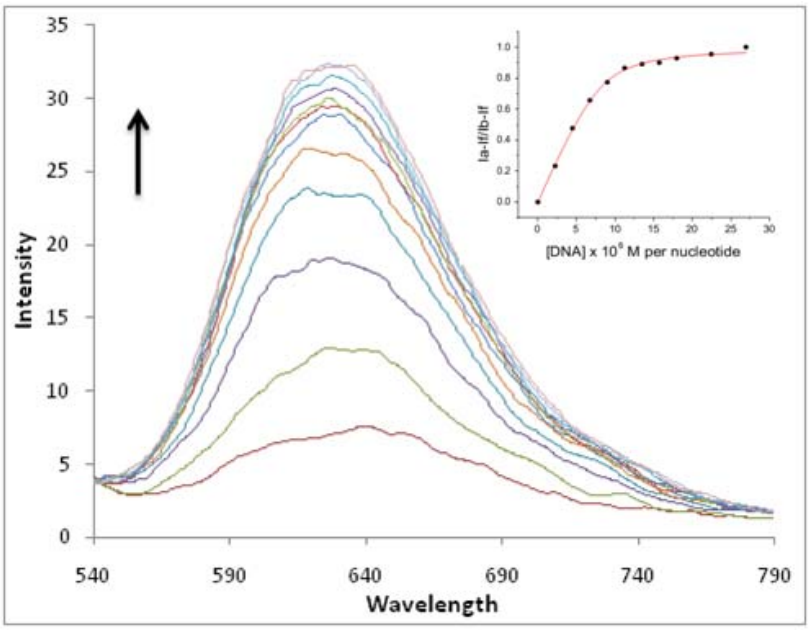

Figure S24. Changes in emission spectra (λ_{ex} = 440 nm) of **4** (4.62 μM) in 10 mM phosphate buffer (pH = 7.01, 50 mM NaCl) with increasing concentrations of CT-DNA, until [DNA]/[Ru] = 3. Arrows show spectral changes upon increasing DNA concentrations. In the inset: plot of $(I_a - I_f)/(I_b - I_f)$ vs [DNA] and the linear fit of the titration data.

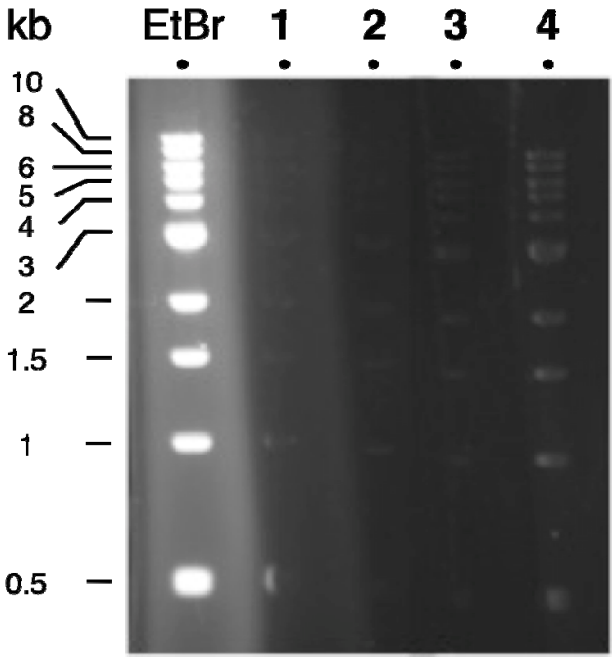

Figure S25. Slices of a 1% agarose gel containing 0.5 μg of 1kb DNA ladder were incubated with ruthenium compounds (2.5 μM) for 40 minutes and visualized by UV (365 nm). Ethidium bromide was taken as positive control.

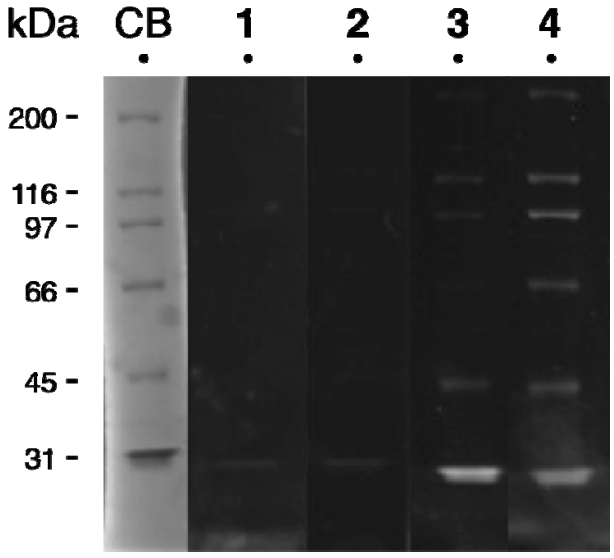

Figure S26. Slices of a 8% SDS-gel containing 5 μL of Bio-Rad Broad Range Protein Markers (0.25 μL) were resolved on a 8% SDS-gel and individual lanes were incubated with ruthenium compounds (2.5 μM) for 40 minutes, analyzed with ethidium bromide colorimetric filter. Coomassie blue was taken as positive control.

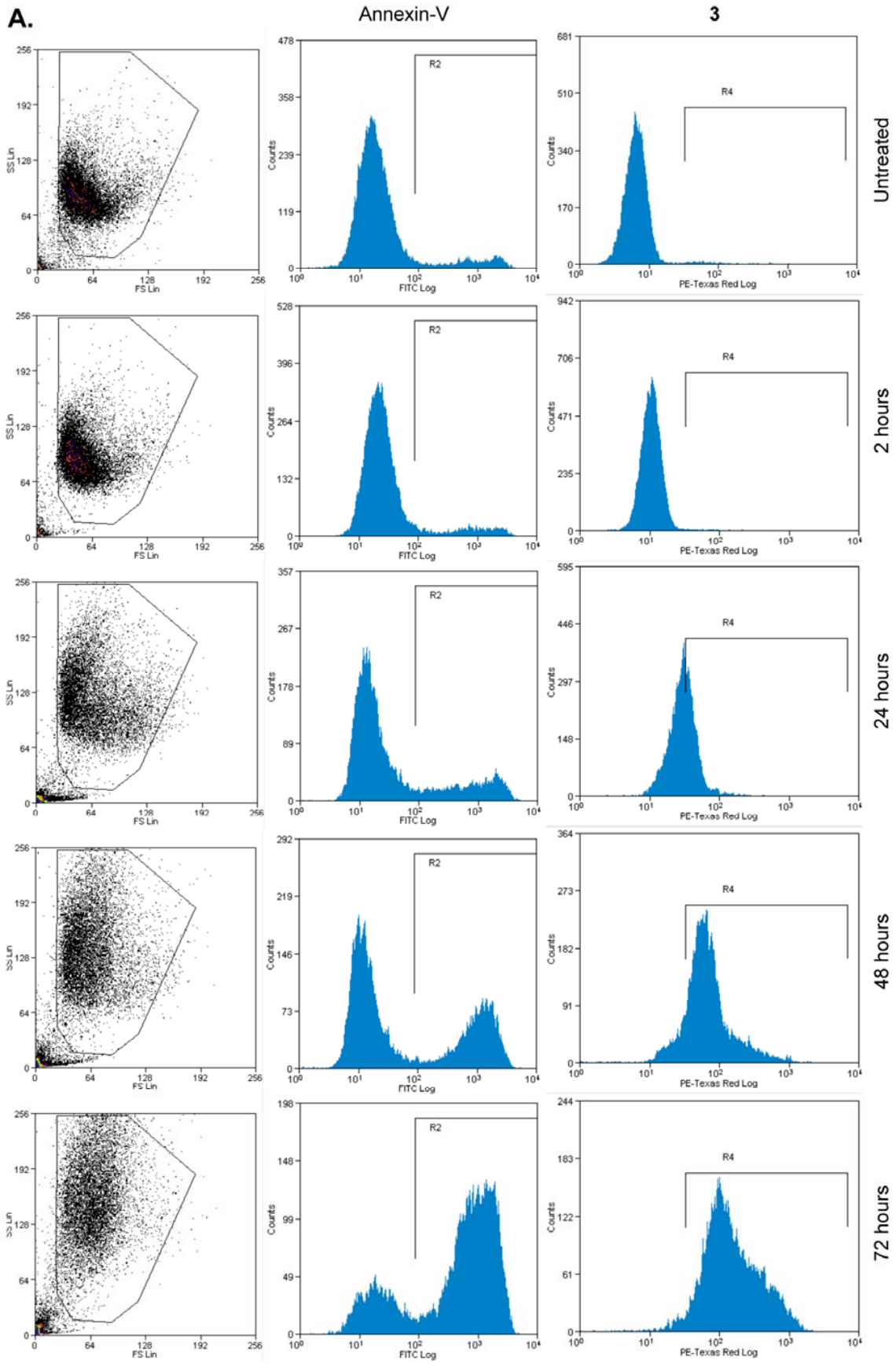
A.
Annexin-V
3
Untreated
2 hours
24 hours
48 hours
72 hours
SS Lin
FS Lin
Counts
FITC Log
PE-Texas Red Log
R2
R4

B.

	Annexin (%)	**3** (%)
Untreated	10.28	2.1
2 h	10.49	0.81
24 h	23.41	42.26
48 h	38.55	87.85
72 h	77.59	96.58

Figure S27. Apoptosis assay. (A) Scattergrams of HeLa cells (forward vs. side scatter; left panels), histograms of cells stained with annexin V-FITC after treatment with **3** (20 μM) for 2, 24, 48 or 72 h: annexin-positive cells are shown in the R2 gate (middle panels) and cells stained with **3** in the R4 gate (right panels). FITC and Ruthenium fluorescence were analyzed in the FITC and in the PE-Texas Red channels, respectively. (B) Quantification table of apoptotic cells.

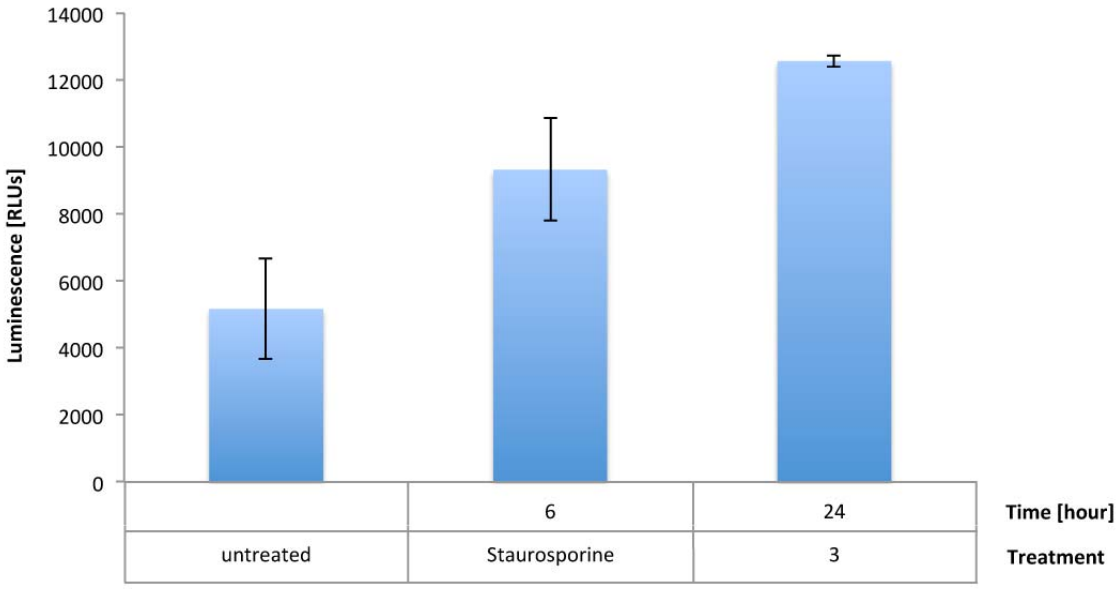

Figure S28. Caspase 3/7 activity measurements. HeLa cells were incubated with **3** (20 μM, 24 h) or staurosporin (150 nM, 6 h) at 37 °C and the extent of substrate cleavage by caspase 3/7 was determined.

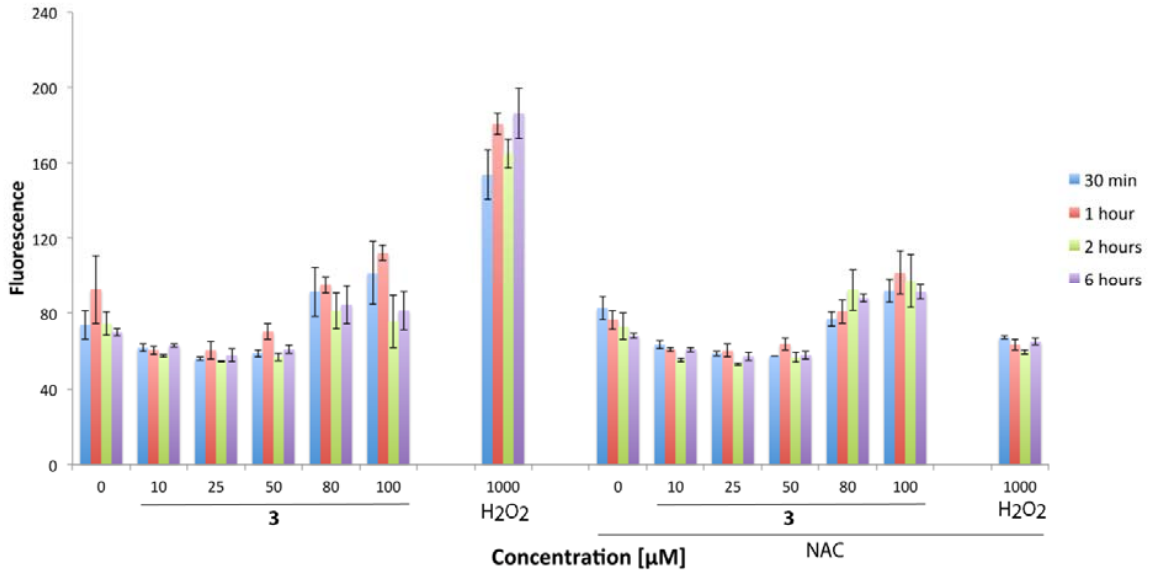

Figure S29. ROS production measurements. HeLa cells were incubated with **3** for 30 min, 1 h, 2 h or 6 h at 37 °C in presence or absence of NAC (10 mM).

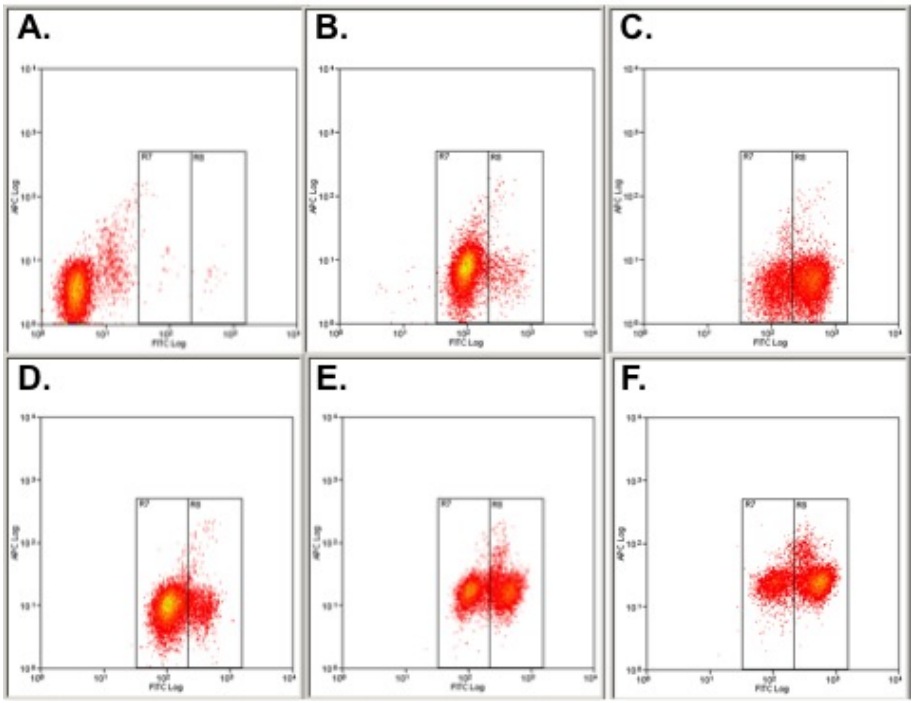

Figure S30. Flow cytometry dot plots showing the effect of **3** (20 µM) on the mitochondrial membrane potential (MMP) in HeLa cells. **A)** control unstained cells, **B)** untreated cells displaying normal MMP, **C)** cells treated with valinomycin, **D)**, **E)** and **F)** cells treated with **3** for 2 h, 24 h or 48 h, respectively.

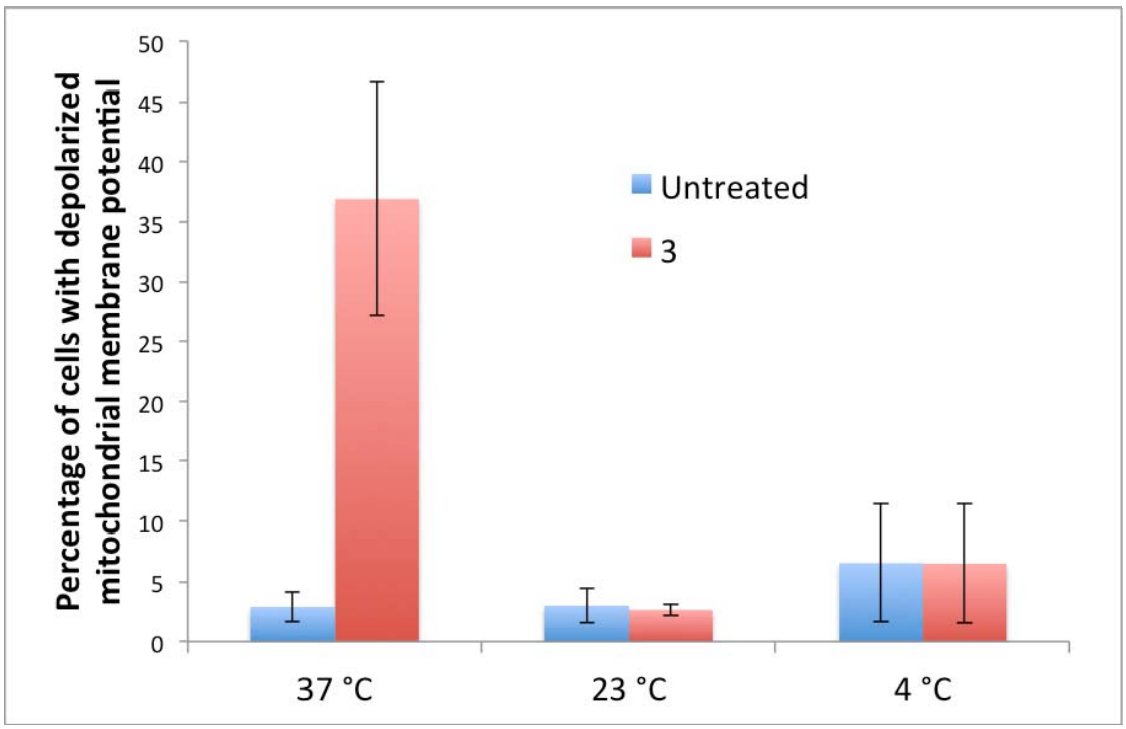

Figure S31. Effect of temperature on the mitochondrial membrane potential of HeLa cells incubated with **3** (20 μM). Cells were incubated for 6 h at 4 °C, 23 °C or 37 °C and the percentage of cells with depolarized mitochondrial membrane was determined.

Table S4. Crystallography collection and refinement data of **1** and **2**.

Compound	1	2
empirical formula	$C_{30}H_{23}F_{12}N_7O_4P_2Ru$	$C_{36}H_{34}Cl_2N_8O_{13}Ru$
M/g mol^{-1}	936.56	958.68
crystal system	Monoclinic	Monoclinic
space group	$P2_1/c$	$P2_1/c$
a/Å	11.6446(6)	15.8449(7)
b/Å	24.0079(11)	14.7672(8)
c/Å	13.3326(6)	16.7863(9)
β/deg	99.087(2)	99.325(3)
V/Å^3	3680.5(3)	3875.8(3)
Z	4	4
T/K	173(2)	173(2)
λ/Å	0.71073	0.71073
D_{alcdc}/g cm^{-3}	1.690	1.643
M(Mo Kα)/mm^{-1}	0.620	0.620
no. data measured	26656	36905
unique data (R_{int})	6440 (0.0421)	6850 (0.0611)
observed data [I > 2(σ)I]	5389	5149
final R1, wR2 (obsd data)	0.0488[a], 0.1309[b]	0.0529[a], 0.1321[b]
final R1, wR2 (all data)	0.0598, 0.1401	0.0760, 0.1445
ρ_{min}, ρ_{max}/*e* Å^{-3}	-0.768, 1.202	-0.630, 0.770

[a] $R = \Sigma(|F_o| - |F_c|)/ \Sigma |F_o|$. [b] $R' = [\Sigma w(|F_o| - |F_c|)^2/ \Sigma F_o^2]^{1/2}$, where $w = [\sigma^2(F_o)]^{-1}$.

References

(1) Nicholson, R. S. *Anal. Chem.* **1966**, *38*, 1406.
(2) Bard, A. J.; Faulkner, L. R. *Electrochemical Methods, Fundamentals and Application*; Second ed. Brisbane, Australia, 2001.
(3) Sevcik, A. *Collect. Czech. Chem. Commun.* **1948**, *13*, 349-377.
(4) Randles, J. E. B. *Trans. Faraday Soc.* **1948**, *44*, 322-327.

CHEMMEDCHEM
Chemistry & Drug Discovery

Supporting Information

Bis(dipyridophenazine)(2-(2′-pyridyl)pyrimidine-4-carboxylic acid)ruthenium(II) Hexafluorophosphate: A Lesson in Stubbornness

Tanmaya Joshi,*[a] Vanessa Pierroz,[a, b] Stefano Ferrari,[b] and Gilles Gasser*[a]

cmdc_201400029_sm_miscellaneous_information.pdf

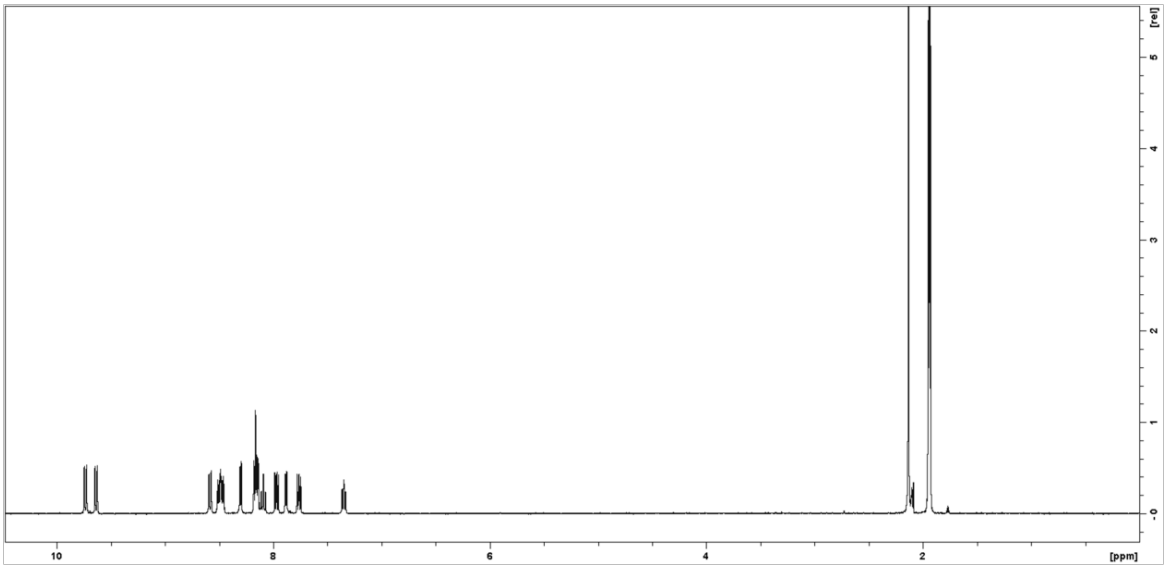

Figure S1. ^{1}H NMR spectrum of **2** in CD_3CN.

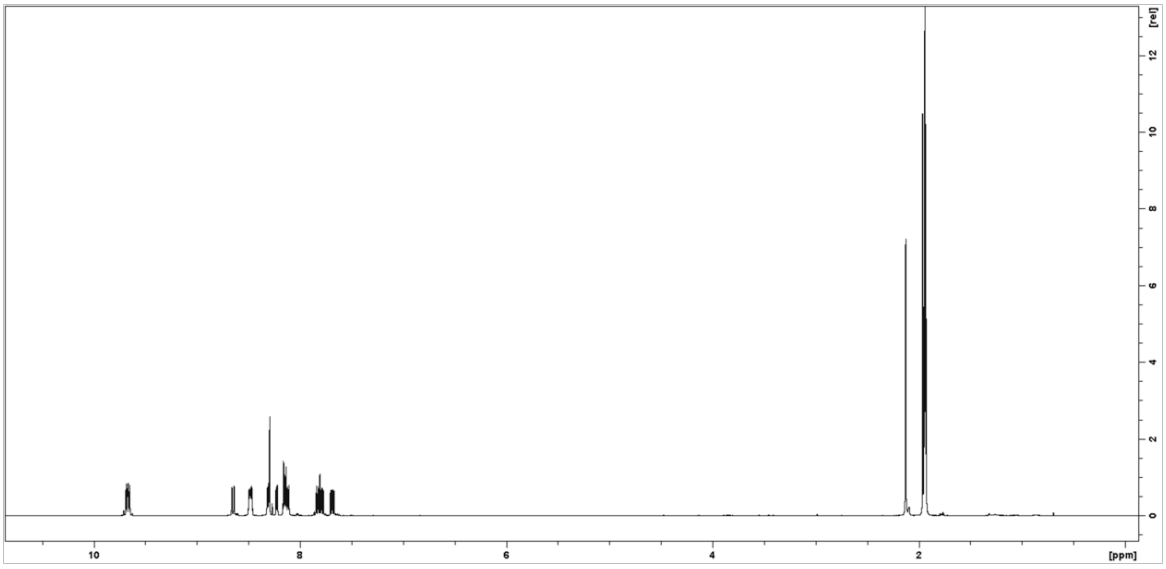

Figure S2. ^{1}H NMR spectrum of **3** in CD_3CN.

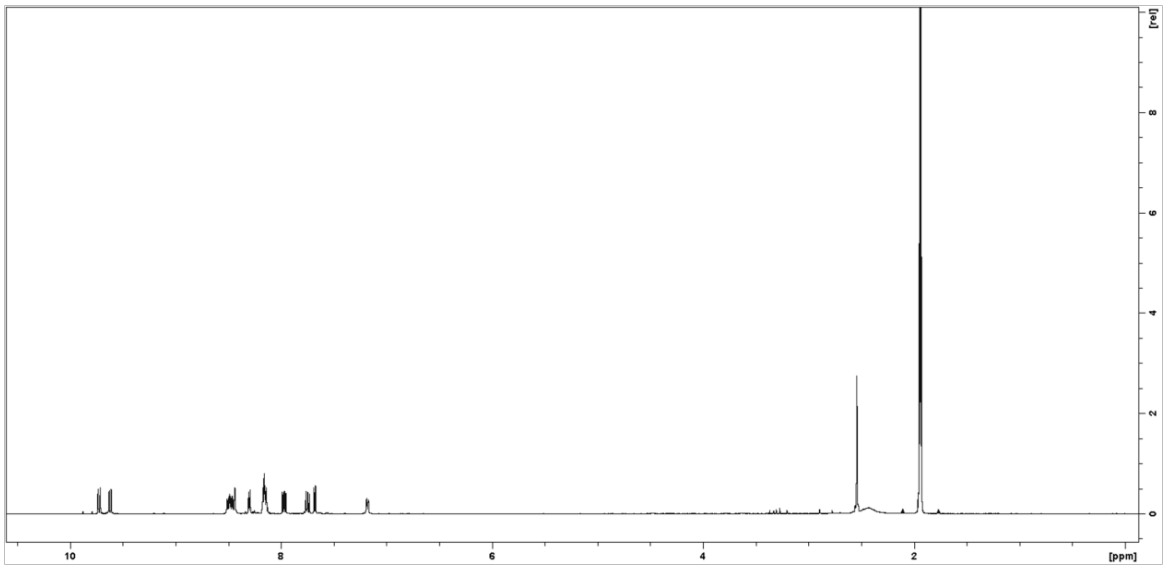

Figure S3. ^{1}H NMR spectrum of **4** in CD_3CN.

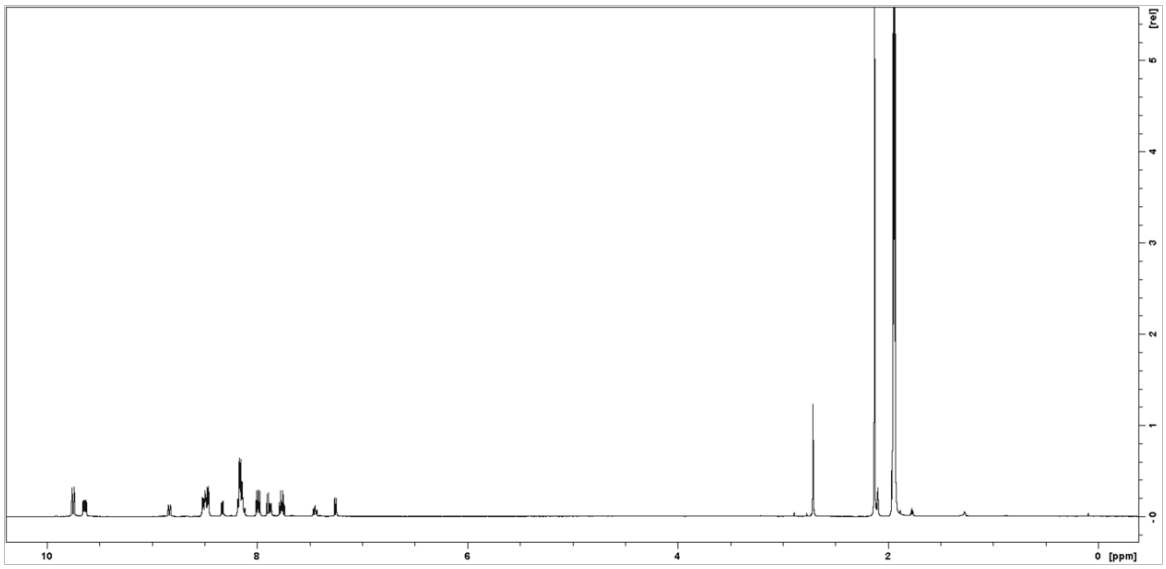

Figure S4. ^{1}H NMR spectrum of **6** in CD_3CN.

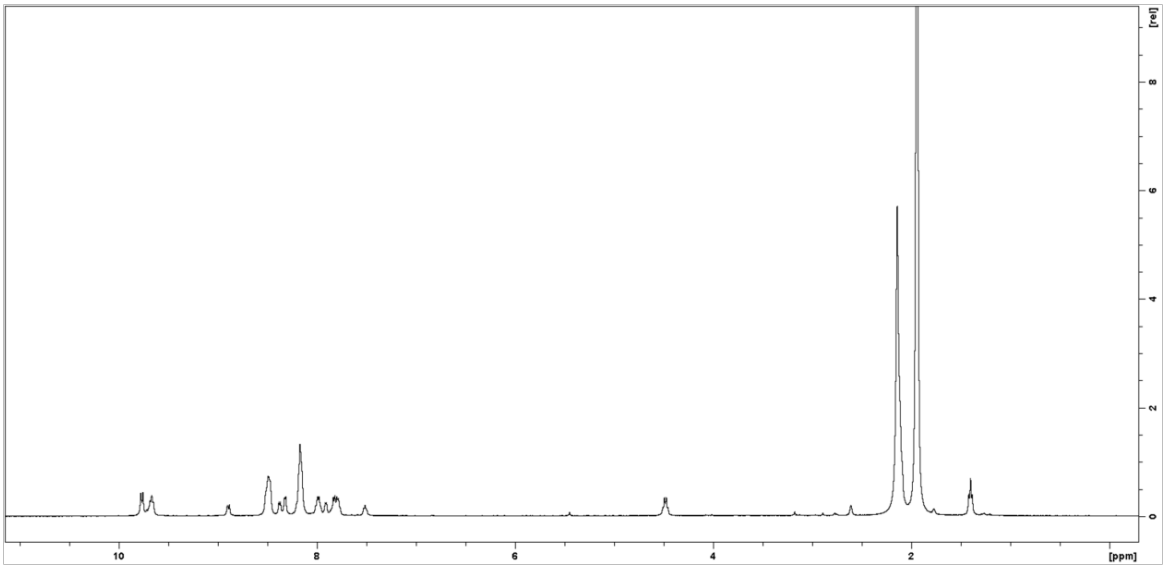

Figure S5. ^{1}H NMR spectrum of **7** in CD_3CN.

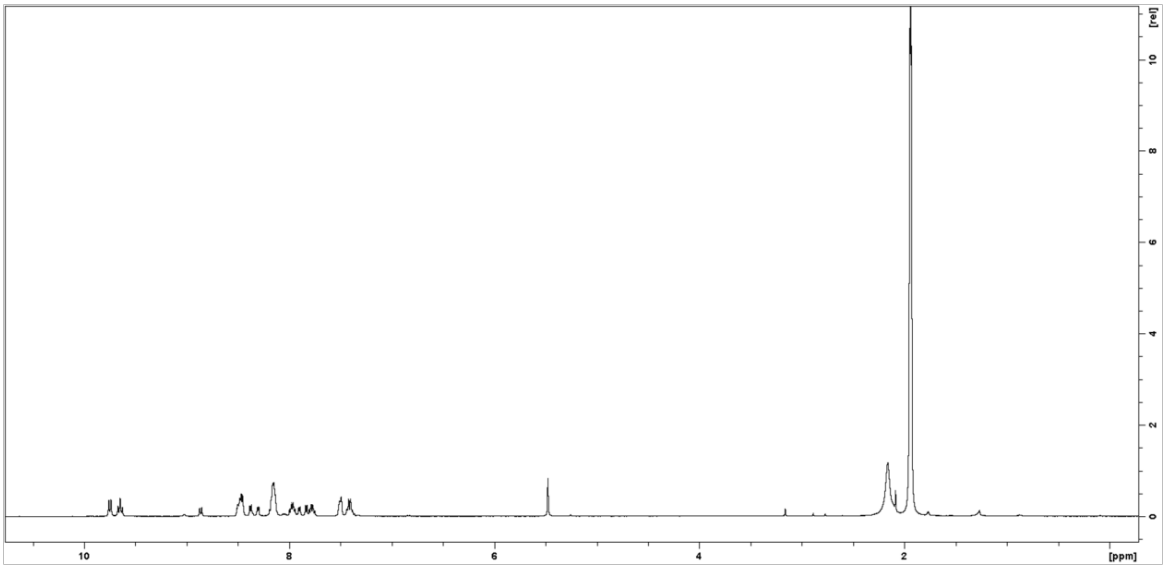

Figure S6. ^{1}H NMR spectrum of **8** in CD_3CN.

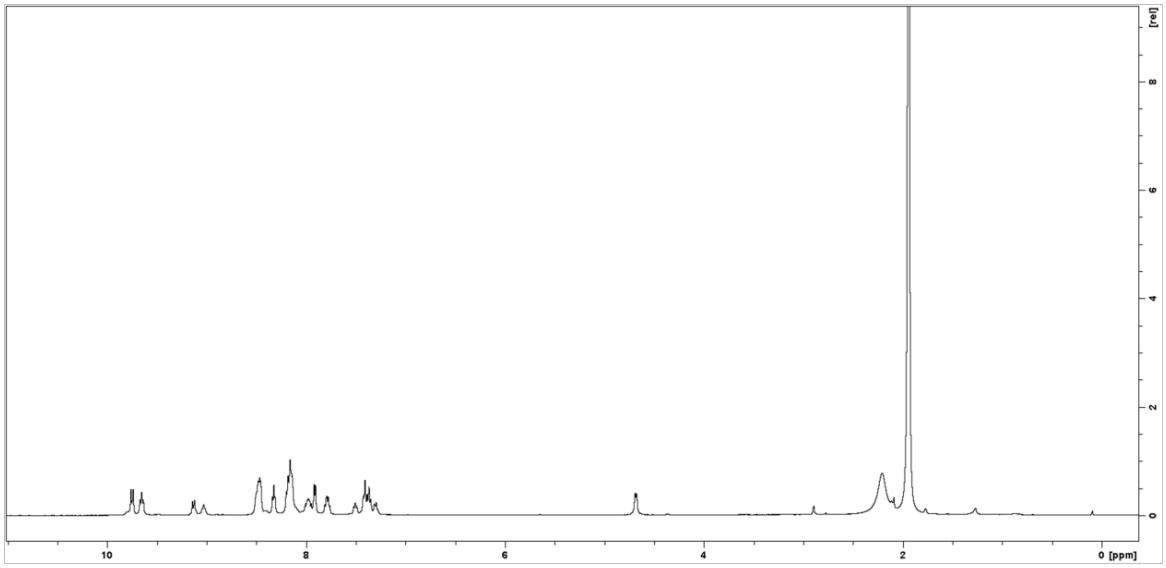

Figure S7. ^{1}H NMR spectrum of **9** in CD_3CN.

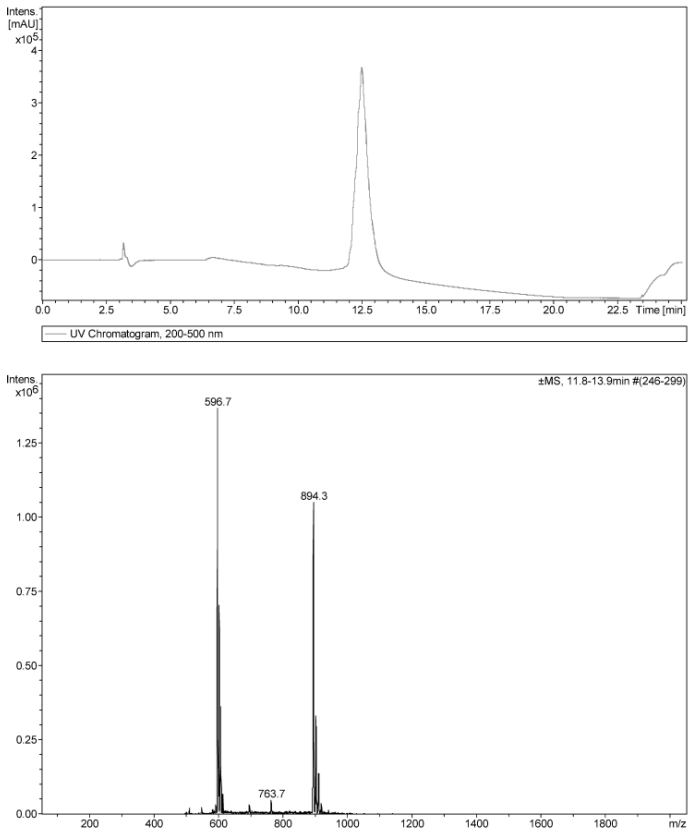

Figure S8. LC-MS spectrum of **11.**

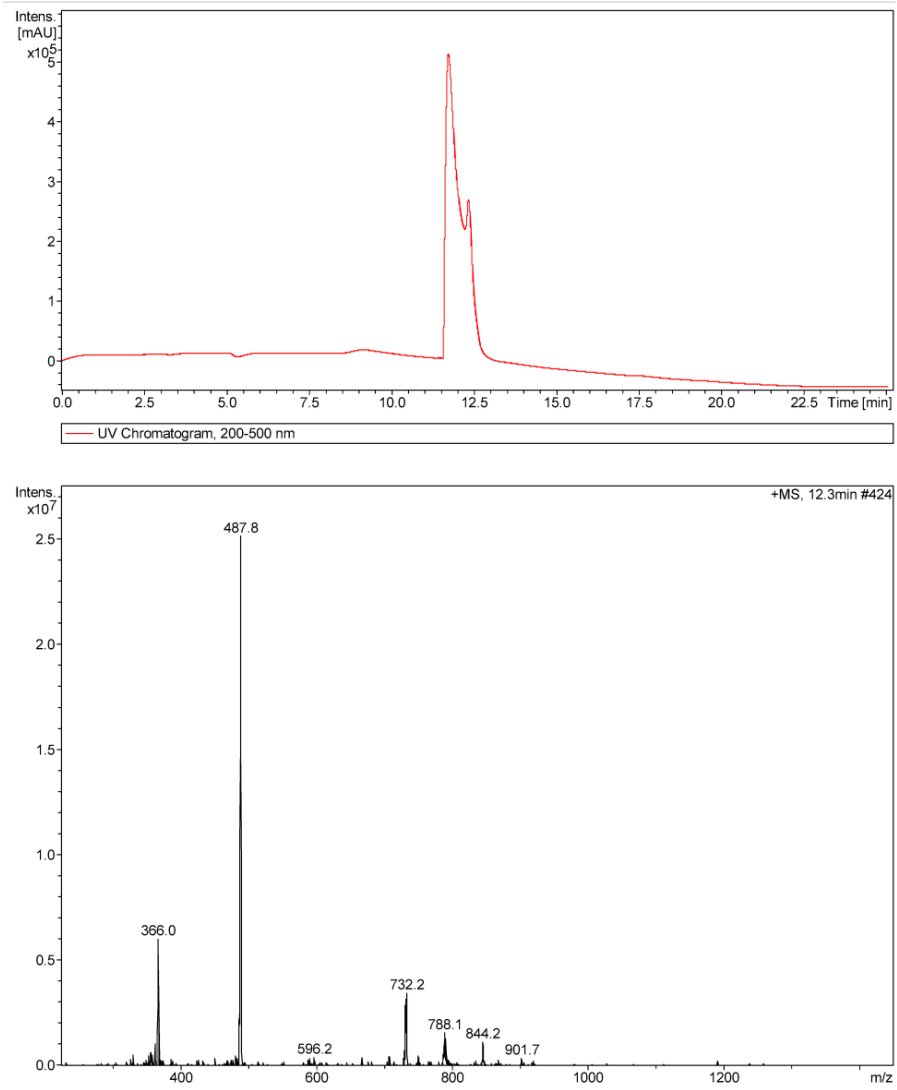

Figure S9. LC-MS spectrum of **12** (two major peaks in the LC spectrum show a similar MS pattern).

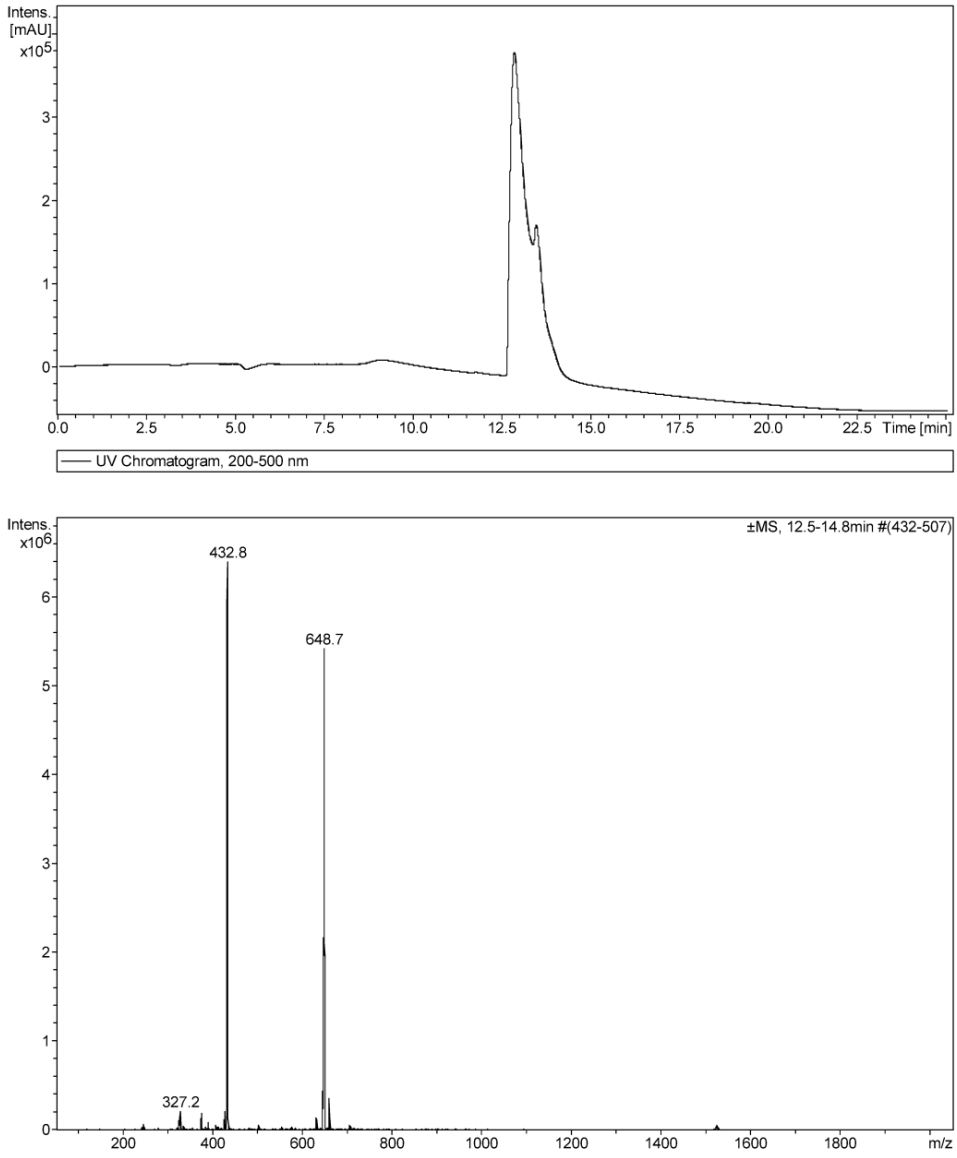

Figure S10. LC-MS spectrum of **13** (two major peaks in the LC spectrum show a similar MS pattern).

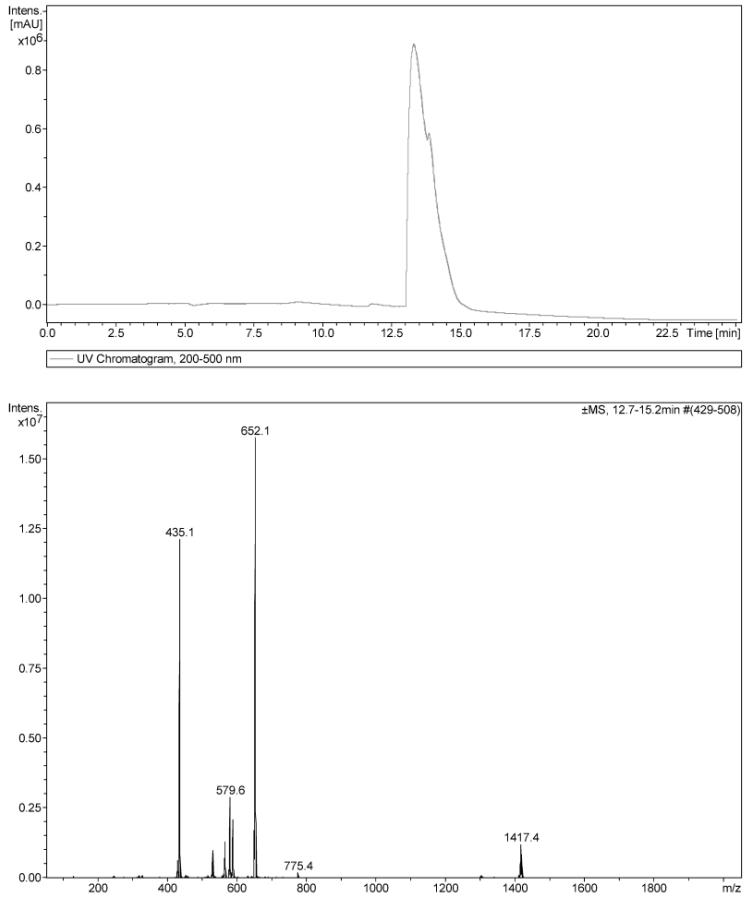

Figure S11. LC-MS spectrum of **14.**

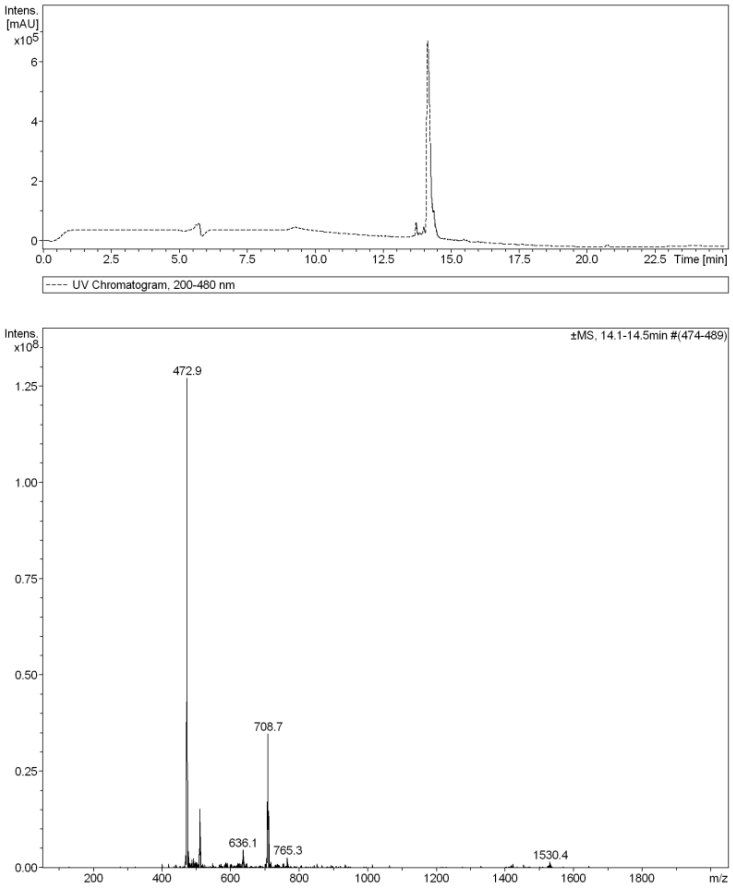

Figure S12. LC-MS spectrum of **15.**

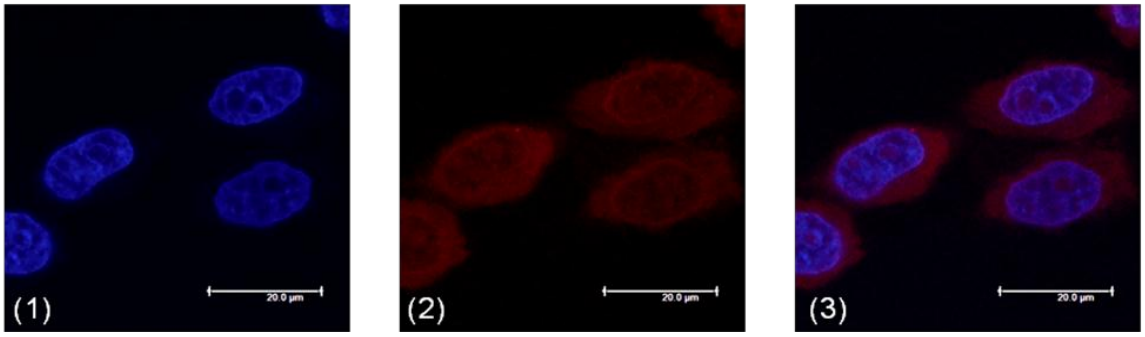

Figure S13. Fluorescence confocal microscopy images showing cellular staining patterns for HeLa cells incubated with **2** (60 μM) for 2 h. Images show (1) DAPI staining, (2) cellular staining of ruthenium compounds, and (3) the overlay.

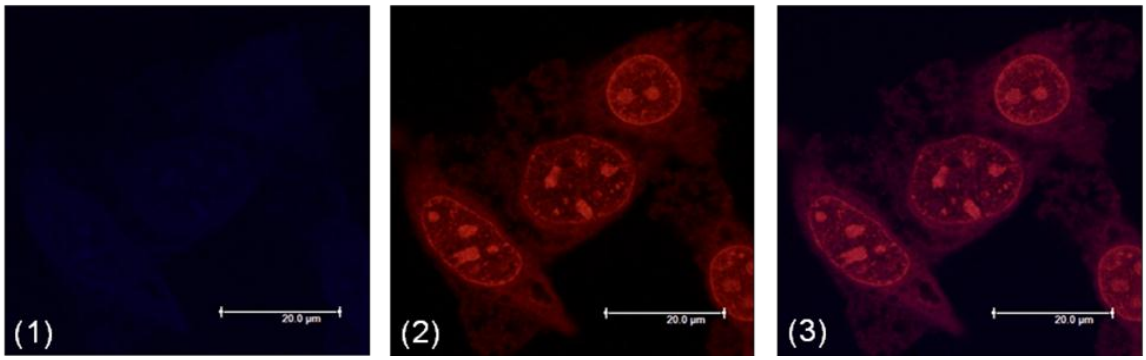

Figure S14. Fluorescence confocal microscopy images showing cellular staining patterns for HeLa cells incubated with **3** (60 μM) for 2 h. Images show (1) DAPI staining, (2) cellular staining of ruthenium compounds, and (3) the overlay.

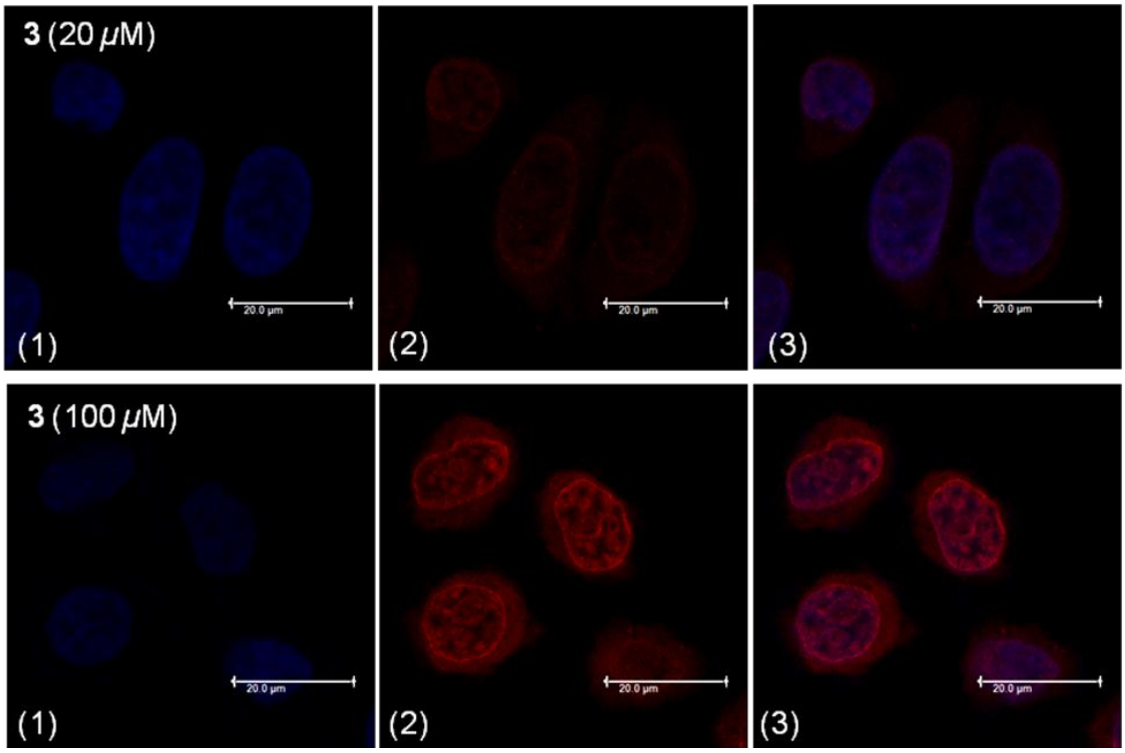

Figure S15. Fluorescence confocal microscopy images showing cellular staining patterns for HeLa cells incubated with **4** for 2 h. Images show (1) DAPI staining, (2) cellular staining of ruthenium compounds, and (3) the overlay.

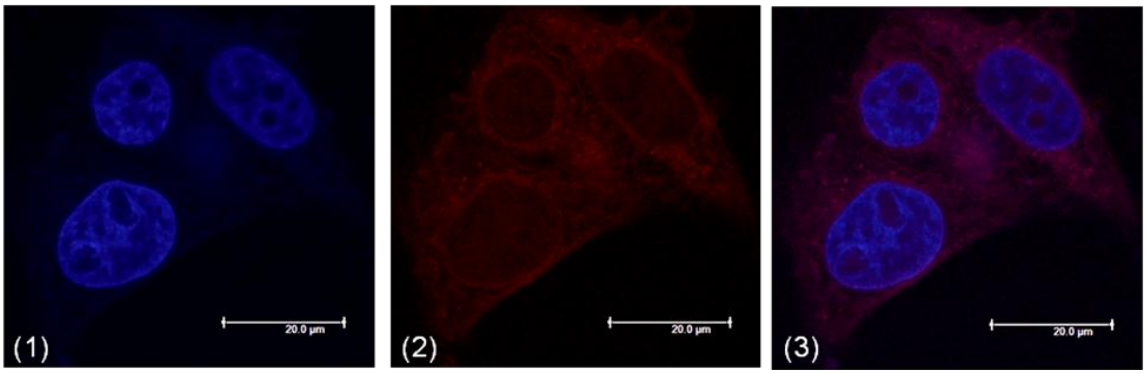

Figure S16. Fluorescence confocal microscopy images showing cellular staining patterns for HeLa cells incubated with **5** (40 μM) for 2 h. Images show (1) DAPI staining, (2) cellular staining of ruthenium compounds, and (3) the overlay.

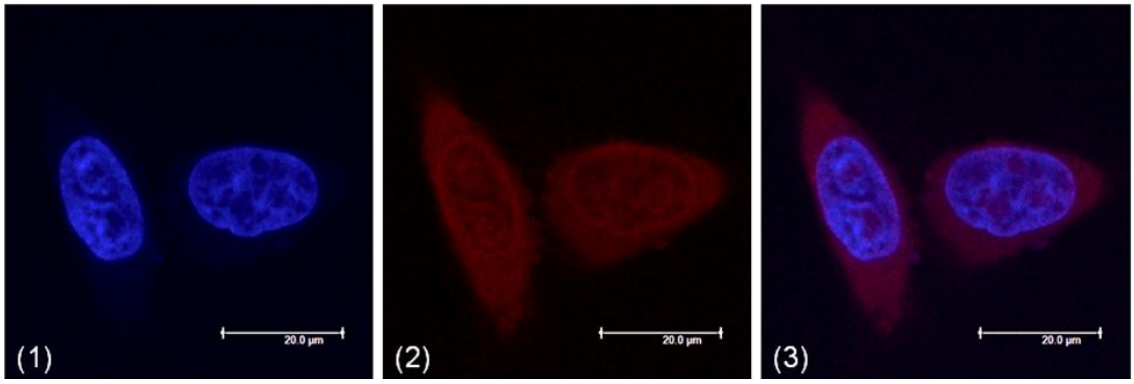

Figure S17. Fluorescence confocal microscopy images showing cellular staining patterns for HeLa cells incubated with **6** (100 μM) for 2 h. Images show (1) DAPI staining, (2) cellular staining of ruthenium compounds, and (3) the overlay.

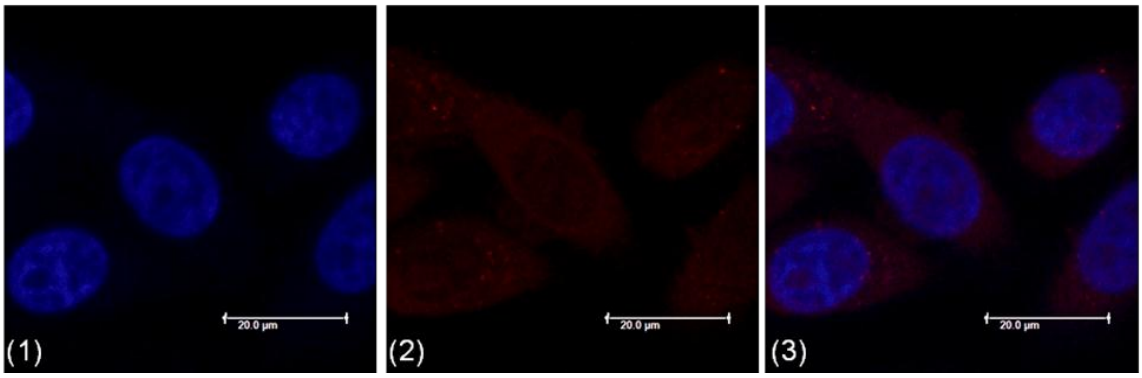

Figure S18. Fluorescence confocal microscopy images showing cellular staining patterns for HeLa cells incubated with **7** (30 μM) for 2 h. Images show (1) DAPI staining, (2) cellular staining of ruthenium compounds, and (3) the overlay.

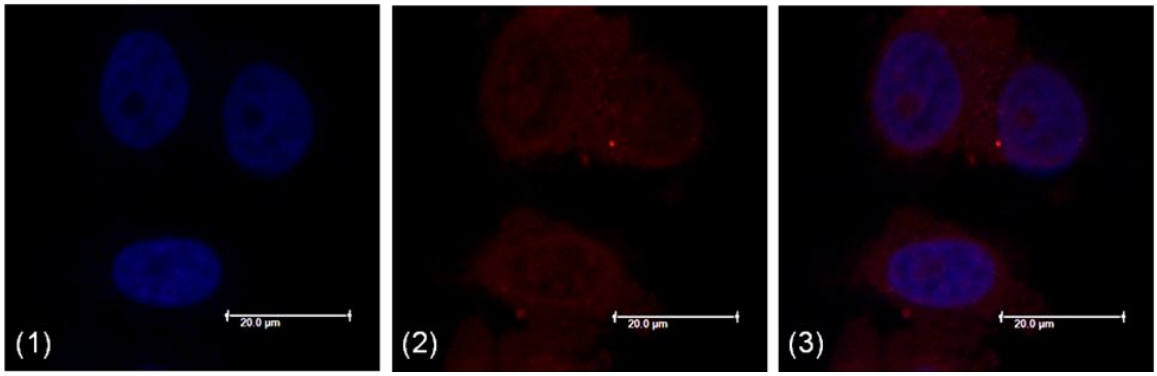

Figure S19. Fluorescence confocal microscopy images showing cellular staining patterns for HeLa cells incubated with **8** (30 μM) for 2 h. Images show (1) DAPI staining, (2) cellular staining of ruthenium compounds, and (3) the overlay.

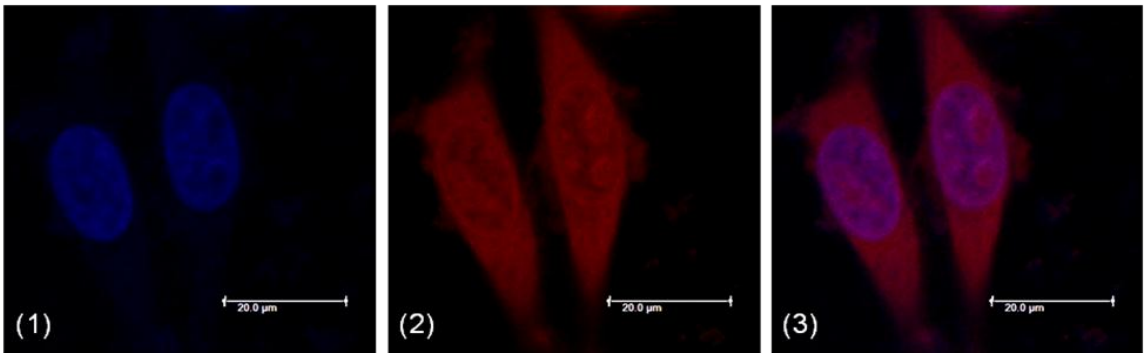

Figure S20. Fluorescence confocal microscopy images showing cellular staining patterns for HeLa cells incubated with **9** (70 μM) for 2 h. Images show (1) DAPI staining, (2) cellular staining of ruthenium compounds, and (3) the overlay.

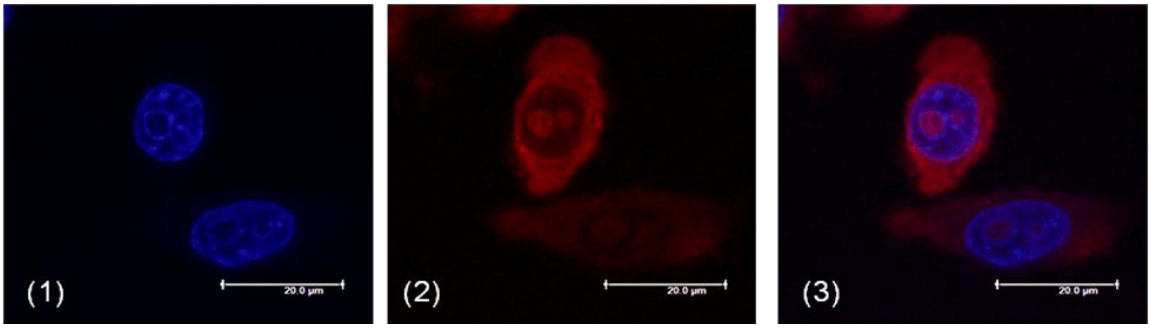

Figure S21. Fluorescence confocal microscopy images showing cellular staining patterns for HeLa cells incubated with **12** (40 μM) for 2 h. Images show (1) DAPI staining, (2) cellular staining of ruthenium compounds, and (3) the overlay.

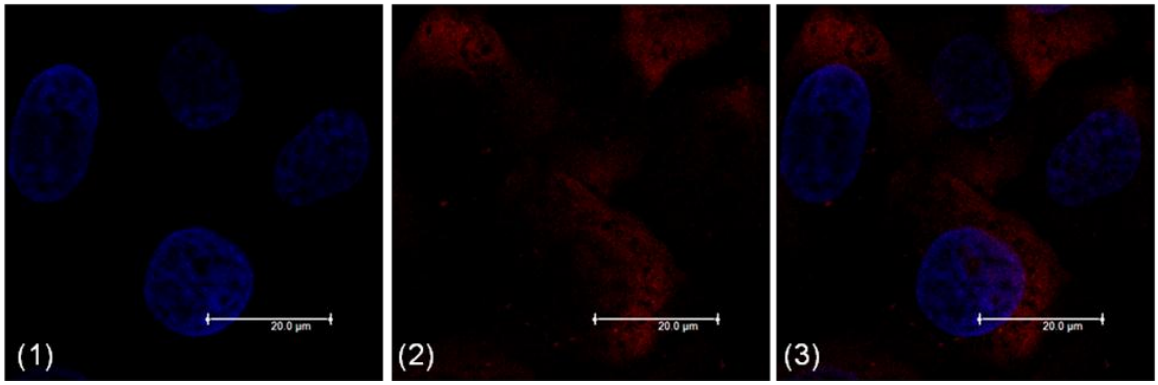

Figure S22. Fluorescence confocal microscopy images showing cellular staining patterns for HeLa cells incubated with **13** (100 μM) for 2 h. Images show (1) DAPI staining, (2) cellular staining of ruthenium compounds, and (3) the overlay.

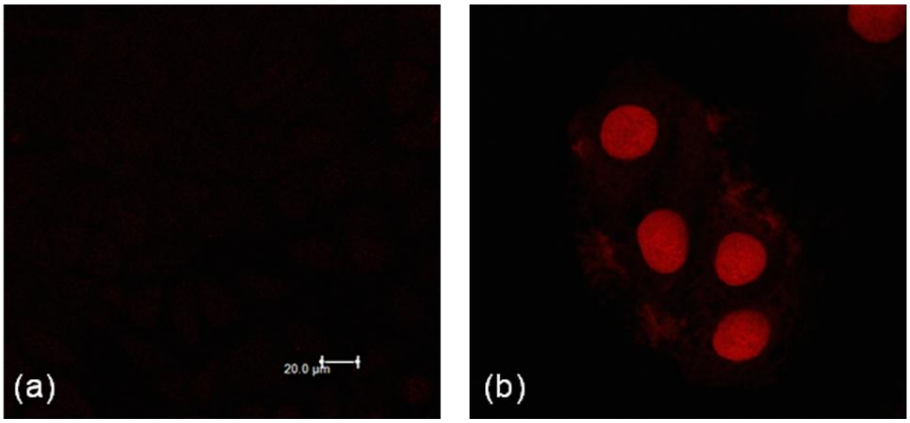

Figure S23. Fluorescence confocal microscopy images showing cellular staining patterns for HeLa cells incubated with (a) **14** (100 μM), and (b) **15** (100 μM) for 2 h.

Angewandte Chemie
Eine Zeitschrift der Gesellschaft Deutscher Chemiker

Supporting Information

69451 Weinheim, Germany

A Bis(dipyridophenazine)(2-(2-pyridyl)pyrimidine-4-carboxylic acid)ruthenium(II) Complex with Anticancer Action upon Photodeprotection**

Tanmaya Joshi, Vanessa Pierroz, Cristina Mari, Lea Gemperle, Stefano Ferrari, and Gilles Gasser**

anie_201309576_sm_miscellaneous_information.pdf

Supplementary Information

[a] Institute of Inorganic Chemistry, University of Zurich, Winterthurerstrasse 190, CH-8057 Zurich, Switzerland

[b] Institute of Molecular Cancer Research, University of Zurich, Winterthurestrasse 190, CH-8057 Zurich, Switzerland.

# These authors have contributed equally to the work.

* Corresponding authors: Email: tanmaya.joshi3@uzh.ch; gilles.gasser@aci.uzh.ch; Fax: +41 44 635 6803; Tel: +41 44 635 4630; WWW: www.gassergroup.com.

Experimental Section

Materials. All chemicals were of reagent grade quality or better, obtained from commercial suppliers and used without further purification. Solvents were used as received or distilled using standard procedures. Deionised water was used for all reactions in aqueous solution. *Thin layer chromatography (TLC)* was performed using silica gel 60 F-254 (Merck) plates with detection of spots being achieved by exposure to iodine or UV light. *Column chromatography* was done using Silica gel 60 (0.040-0.063 mm mesh, Merck) or activated neutral alumina (Brockmann l, Sigma-Aldrich). Eluent mixtures are expressed as volume to volume (v/v) ratios.

Instrumentation and methods. A vacuum line and Schlenk glassware were employed when reactions had to be carried out under an atmosphere of dry, oxygen-free nitrogen and assemblies were protected from light if necessary by wrapping them with aluminium foil. *^{1}H and $^{13}C\{^{1}H\}$ NMR spectra* were measured on Bruker DRX 400 and 500 spectrometers, at room temperature. The chemical shifts, δ, are reported in parts per million (ppm), using the signal of the deuterated solvent as an internal standard.[1] The abbreviations for the peak multiplicities are as follows: s (singlet), d (doublet), dd (doublet of doublets), t (triplet), q (quartet), m (multiplet), and br (broad). *ESI mass spectrometry* was performed using a Bruker Esquire 6000 spectrometer. In the assignment of the mass spectra, the most intense peak is listed. *Microanalysis* was performed on a LecoCHNS-932 elemental analyser.

Synthesis.

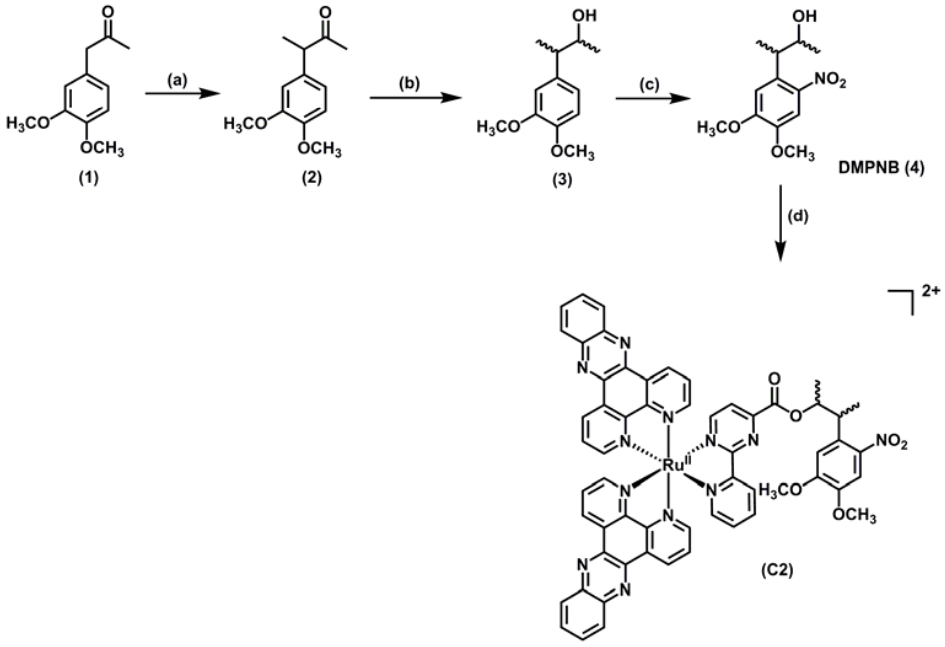

Scheme S1. Synthetic route for preparation of the prodrug candidate **C2** (racemic mixture). Reagents and conditions: **(a)** NaH, dry THF, MeI, 0 °C–rt, 2 h, 96%; **(b)** $NaBH_4$, THF/isopropanol (1:2 v/v), rt, 1 h, 98%; **(c)** $Cu(NO_3)_2$•$3H_2O$, Ac_2O, rt, o/n, 68%; **(d)** HATU, Et_3N, DMF, DMAP, 65 °C, 18 h, 76%.

Compound 3-(3,4-dimethoxyphenyl)-butan-2-ol **(3)** [2] (isolated as a mixture of erythro/threo isomers) and **[Ru(dppz)$_2$(CppH)](PF$_6$)$_2$ (C1)**[3] were synthesised according to the literature procedure. The characterisation data were in agreement with the published data.

3-(4,5-dimethoxy-2-nitrophenyl)butan-2-ol (DMPNB, 4). A mixture of 3-(3,4-dimethoxyphenyl)-butan-2-ol (0.476 g, 2.27 mmol) and $Cu(NO_3)_2$•$3H_2O$ (0.657 g, 2.72 mmol) in 20 mL acetic anhydride was stirred under nitrogen for 12 h. The reaction mixture was diluted with water (20 mL) and aqueous solution was extracted with dichloromethane (3 × 60 mL). The combined organics were washed with 2 N NaOH (2 × 30 mL), water and

brine, dried over Na_2SO_4, filtered and concentrated under reduced pressure. Purification of the crude product by silica gel column chromatography using ethylacetate/hexane (3:7 v/v) as eluent, yielded an erythro-threo isomeric mixture of **4** as a yellow solid. Yield: 0.395 mg (68%). R_f = 0.43 in ethylacetate/hexane (2:3 v/v). The characterisation data for **4** was found to be in agreement with that earlier reported.[2]

[Ru(dppz)$_2$(Cpp-ODMPNB)](PF$_6$)$_2$ (C2). The reaction was performed under the exclusion of light. HATU (0.013 g, 0.035 mmol), DMAP (0.06 g, 0.044 mmol), triethylamine (0.006 mL, 0.044 mmol) and **4** (0.010 g, 0.040 mmol) were added to a solution of **[Ru(dppz)$_2$(CppH)](PF$_6$)$_2$** (0.025 g, 0.022 mmol) in dimethylformamide (5 mL), and the reaction solution was heated at 65 °C under a nitrogenous atmosphere for 18 h. After removal of the solvent under reduced pressure, the residue was purified using column chromatography (SiO_2, eluent gradually changed from 100% EtOAc to CH_3CN/H_2O/sat. KNO_3 (16:3:1)). The bright orange band was collected and evaporated to dryness. The concentrate was suspended in minimum chloroform and filtered to remove insoluble KNO_3 salt. The filtrate was evaporated to dryness, and the residue was resuspended in saturated aqueous solution of NH_4PF_6, sonicated for 2 min and stored (2 h) at 2 °C for complete precipitation of the product. The precipitate was collected by filtration, washed with water and ether, and dried in vacuo. This yielded the desired complex **C2** as an orange solid. Yield: 0.023 g (76%). Anal. calcd. for $C_{58}H_{42}F_{12}N_{12}O_6P_2Ru$ (%): C, 49.97; H, 3.04; N, 12.06. Found: C, 50.06; H, 2.97; N, 11.99. ^{1}H NMR (400 MHz, CD_3CN): δ 1.26–1.45 (m, 6H), 3.61–3.86 (m, 7H), 5.46–5.54 (m, 1H), 6.97–7.06 (m, 1H), 7.22 (min) and 7.30 (maj) (s, 1H), 7.43–7.59 (m, 2H), 7.76–7.82 (m, 2H), 7.87–7.91 (m, 1H), 7.94–8.02 (m, 2H), 8.13–8.22 (m, 7H), 8.27–8.31 (m, 2H), 8.41–8.43 (m, 1H), 8.46–8.52 (m, 4H), 8.79–8.81 (m, 1H), 9.64–9.68 (m, 2H), 9.75–9.77 (m, 2H) ppm. MS (ESI$^+$): *m/z* 552.1 $[M\text{-}2PF_6]^{2+}$.

Photolysis evaluation. For photolysis measurements, 1 mL PBS (pH 7.2) solution of **C2** (50 μM) in a 1 cm quartz luminescence cuvette was irradiated at 350 nm, in a RPR100 Rayonet Chamber Reactor (Southern New England Ultraviolet Company), equipped with 6 lamps. UV-Vis spectra were recorded after different irradiation times (t = 0, 5, 10, 15, 20 minutes) and 70 μL aliquots were collected to evaluate the photouncaging of the compound by UPLC-MS analysis. A total of 5 μL of the solution was injected into the UPLC (Acquity Ultra Performance LC, Waters) that was connected to a mass spectrometer (Bruker Esquire 6000) operated in ESI mode. The Waters ACQUITY UPLC ® BEH C18 1.7 mm (2.1 × 50 mm) reverse phase column was used with a flow rate of 0.6 mL min^{-1} and UV-absorption was recorded at 275 nm. The runs were performed with a linear gradient of A (acetonitrile (Sigma Aldrich HPLC-grade)) and B (distilled water containing 0.02% TFA and 0.05% HCOOH): t = 0−0.25 min, 5% A; t = 4.5 min, 100% A; t = 5.5 min, 100% A.

To obtain the quantum yield of photorelease (Φ), a solutions of **C2** (50 μM in PBS) and a reference compound, 1-(2-Nitrophenyl)ethyl phosphate (57 μM in PBS) with known quantum yield (Φ_{ref} = 54%)[4], were irradiated at 350 nm for different irradiation times, in a quartz luminescence cuvette in the Chamber Reactor equipped with 2 lamps. Samples were collected until 20% of the caged compound was decomposed, and 30 μL of the collected sample was injected into the VWR HITACHI Chromaster HPLC system. Reference sample was analyzed with a MACHEREY NAGEL EC 250/3 Nucleosil 100-5 C18 reverse phase column with a flow rate of 1 mL min^{-1}, with a linear gradient of A (acetonitrile (Sigma Aldrich HPLC-grade and B (distilled water containing 0.1% TFA): t = 0–3 min, 5% A; t = 3–15 min, 86.4% A; 15–16 min, 100% A; 16–17.5 min, 100% A; 17.5–18.5 min, 5% A. **C2** samples were analyzed with a MACHEREY NAGEL EC 150/3 Nucleosil 100-5 C18 reverse phase column with a flow rate of 1 mL min^{-1}, with a linear gradient of A (acetonitrile (Sigma Aldrich HPLC-grade

and B (distilled water containing 0.1% TFA): t = 0–3 min, 20% A; 3–7 min, 50% A; 7–17 min, 73.1% A; 17–18 min, 100% A. From the HPLC chromatograms recorded at 300 nm, the area of the uncaged products was evaluated and plotted against the irradiation time for both the reference and the complex. The data were fitted with linear regression to derive slope (S) (Figure S3).

The photorelease quantum yields (Φ_{sample}) were determined using the equation:

$$\Phi_{sample} = \Phi_{ref} (S_{sample} / S_{ref}) (I_{ref} / I_{sample})$$

where S_{sample} and S_{ref} are the slope for the linear fit of the absorbance vs. irradiation time plots for the sample and reference, respectively, and I_{sample} and I_{ref} are the integrated light absorption of the sample and reference, respectively, calculated as:

$$I = I_0 (1 - 10^{-A(\lambda)})$$

where, I_0 is the light intensity of the irradiation source in the irradiation interval and A_λ is the absorbance of the sample at wavelength λ.

Singlet Oxygen Evaluation. The singlet oxygen measurements were performed following our previously published procedure,[5] using two different methods.

Near-IR luminescence (direct evaluation): Luminescence measurements were performed on a Fluorolog-3 Spectrofluorometer (Jobin Yvon Horiba, Model FL3-11) with a 450 W xenon lamp light source and single-grating excitation and emission spectrometers. For high beam intensity, the excitation slits were set to a maximum value of 29.4 nm. A colored glass filter was placed between the sample and the detector to cut off the light below 695 nm. The emission signal between 1200–1350 nm was collected at right angle to the excitation path, with an IR-sensitive liquid nitrogen cooled germanium diode detector (Edinburgh Instruments, Model EI-L). The detector was biased at -160 V. The signal-to-noise ratio of the

detected signals was improved with a lock-in amplifier (Stanford Research Systems, model SR510) referenced to the chopper frequency of 126 Hz, and the data-acquisition was done with DataMax. Samples in aerated acetonitrile were prepared at an optical density of 0.4 at the irradiation wavelength (365 nm), in 1 cm luminescence quartz cuvette. Four different transmittance filters were used to vary the intensity of the irradiation beam. Integrated area of the singlet oxygen luminescence was plotted against the intensity of irradiation (Figure S4), and slope for the linear fit was calculated (S_{sample}).

N,N-dimethyl-4-nitrosoaniline/histidine assay (indirect evaluation): Air-saturated PBS buffer solution containing the complex (OD = 0.15 at the irradiation wavelength), *p*-nitrosodimethyl aniline (RNO) (20 μM), histidine (10 mM) was irradiated in a 1 cm luminescence quartz cuvette at 350 nm, in a RPR100 Rayonet Chamber Reactor (Southern New England Ultraviolet Company) with 12 lamps, for different time intervals. For each sample, the absorbance of the irradiated solution was recorded and variation in the absorbance at 440 nm (A_0-A, where A_0 is the initial absorbance before irradiation) was plotted against the total irradiation time (Figure S5). Slope for the linear fit was calculated (S_{sample}) and used for quantum yield determination.

For both methods, phenalenone ($\Phi_{ref}(^1O_2)$ = 95%) was used as a reference compound to obtain S_{ref}.

The singlet oxygen quantum yields (Φ_{sample}) were determined using the equation:

$$\Phi_{sample} = \Phi_{ref} (S_{sample} / S_{ref}) (I_{ref} / I_{sample})$$

where S_{sample} and S_{ref} are the slope for the linear fit of the absorbance vs. irradiation time plots for the sample and reference, respectively, and I_{sample} and I_{ref} are the integrated light absorption of the sample and reference, respectively, calculated as:

$$I = I_0 (1 - 10^{-A(\lambda)})$$

where, I_0 is the light intensity of the irradiation source in the irradiation interval and A_λ is the absorbance of the sample at wavelength λ.

Cell Culture. Human cervical carcinoma cells (HeLa) were cultured in DMEM (Gibco) supplemented with 5% fetal calf serum (FCS, Gibco), 100 U/mL penicillin, 100 μg/mL streptomycin. The human osteosarcoma cell line (U2OS) was maintained in DMEM (Gibco) supplemented with 10% FCS (Gibco), penicillin (100 U/mL), and streptomycin (100 μg/mL). The normal human fetal lung fibroblast cell line (MRC-5) was grown in F-10 medium (Gibco) supplemented with 10% FCS (Gibco), penicillin (100 U/mL), and streptomycin (100 μg/mL). The cells were cultured at 37 °C and in 5% CO_2 humidified atmosphere.

Cytotoxicity Determination. The toxicity of the Ru(II) complexes to HeLa, U2OS and MRC-5 cells, in the dark and upon light (350 nm) irradiation, was evaluated using Resazurin based fluorometric cell viability assay. Stock solutions of the Ru(II) complexes (20 mM) were prepared in DMSO, and stored in the dark. The respective stock solutions were further diluted with complete medium to the desired working concentrations. For a typical experiment, 100 μL aliquots of cells in growth medium were seeded in 96-well plates (density of 4×10^3 cells/well for HeLa and U2OS, and 7.5×10^3 cells/well for MRC-5) and incubated at 37°C and 5% CO_2. After 24 h of incubation, cells were treated with different concentrations (0.8–100 μM, 200 μL final well volume) of the test compound and incubated for 4 h or 48 h, in the dark, as required. For experiments with compounds, cells were treated for 4 h, the medium was replaced thereafter, followed by incubation for additional 48 h. For light irradiation experiments, cells were exposed to light (350 nm) for 10 min (2.58 J cm^{-2}) prior to their 48 h incubation (for calculation purposes, the light dose intensity delivered was corrected for absorption by the 96-well plate lids). Thereafter, for all experiments, the medium was removed, 100 μL of freshly prepared resazurin containing complete medium (0.2 mg/mL final

concentration) was added, and cells were incubated at 37 ^{o}C for additional 4 h. At the end of the incubation period, fluorescence of the highly red fluorescent resorufin product (λ_{ex} = 540 nm), at 590 nm, was quantified using a SpectraMax M5 microplate Reader. The reported cytotoxicity data is an average of at least two independent experiments, with triplicate determinations for each drug concentration. Final DMSO concentration in the wells was less than 0.5% (v/v). Control experiments on cells treated with same amount of DMSO in culture medium showed no cytotoxic effect (results not shown).

In vitro **Fluorescence Evaluation.** Cellular localization of luminescent ruthenium(II) complexes was assessed by confocal microscopy. As for the cytotoxicity assays, stock solutions of the Ru(II) complexes (20 mM) were prepared in DMSO and diluted to the desired concentrations with culture medium. HeLa cells were grown on 18 mm Menzel-gläser coverslips at a density of 1 × 10^5 cells/mL in cell culture medium. Cells were incubated with ruthenium(II) complexes at defined incubation concentration (either IC_{50} values or at 100 μM for the non-toxic complexes) for 2 h, at 37 °C under 5% CO_2. The medium was removed, cells were fixed with a 4% formaldehyde solution in PBS and mounted on slides for viewing by confocal microscopy. For light irradiation experiments, the cells were exposed to light (350 nm) for 10 min (2.58 J cm^{-2}), in fresh complete cell culture medium, prior to their fixation. Co-staining of cell nuclei with DAPI was performed by using a mounting solution containing DAPI (λ_{ex} = 402 nm, λ_{em} > 420 nm). Fixed cells were imaged on a Leica SP5 confocal laser scanning microscope, using the red wavelength selection (λ_{ex} = 458 nm, λ_{em} = 600–650 nm).

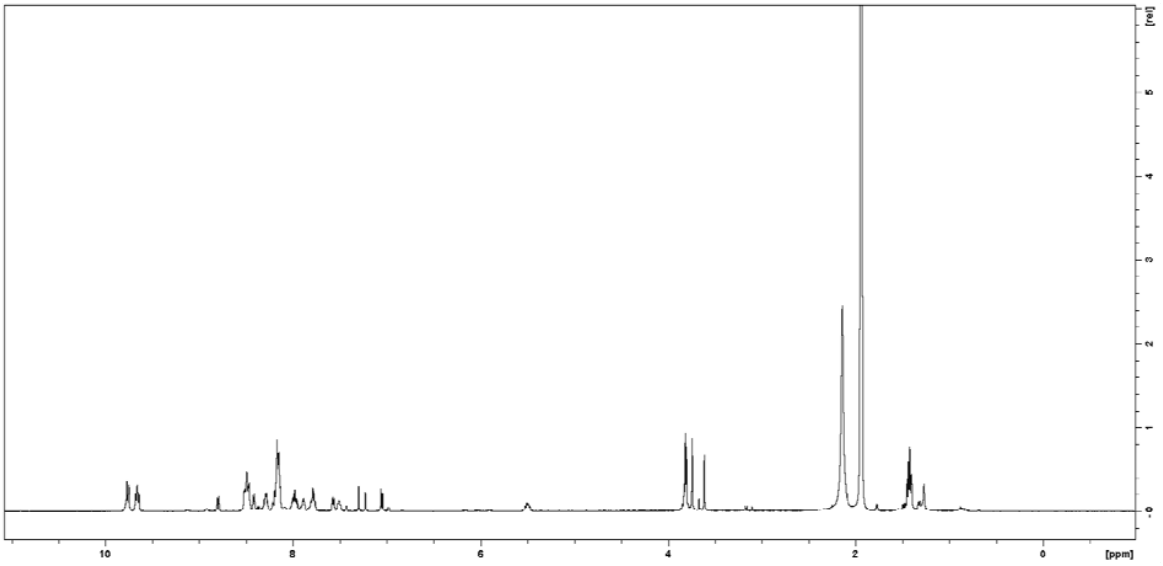

Figure S1. ^{1}H NMR spectrum of **C2** in CD_3CN.

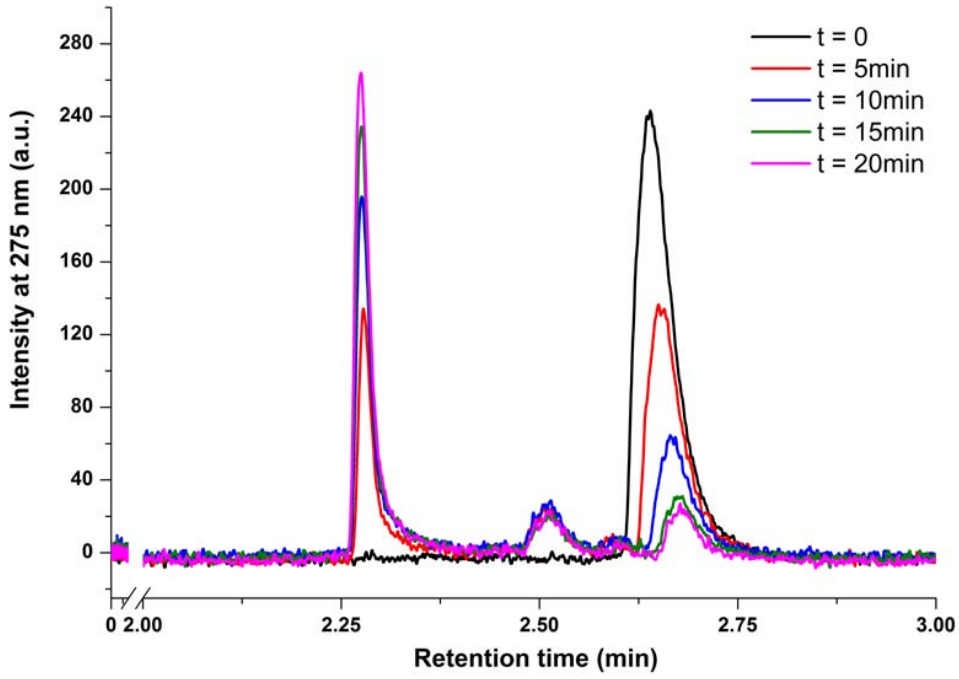

Figure S2. UPLC chromatograms for photolysis of **C2** upon irradiation for different time intervals.

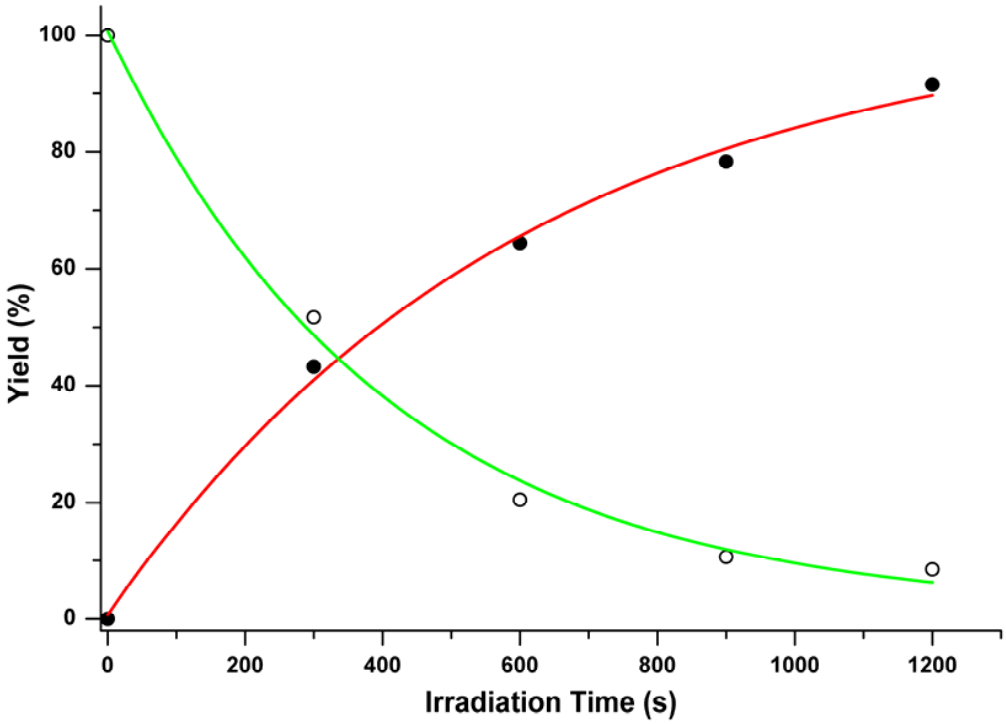

Figure S3. Exponential fit for photorelease of **C1**(●) from the prodrug **C2** (○).

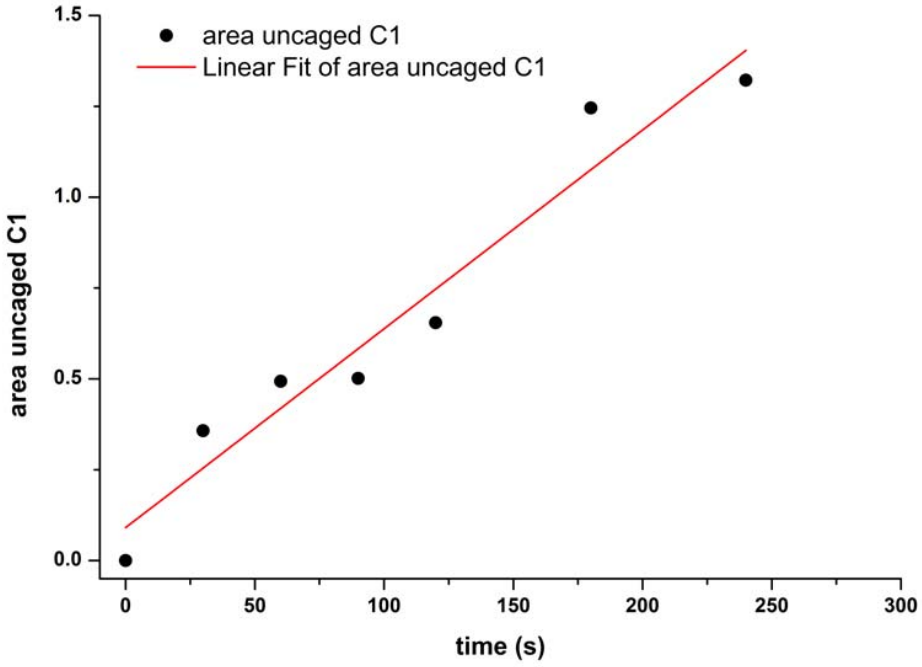

Figure S4. Linear fitting of the photorelease of **C1** for the calculation of the quantum yield.

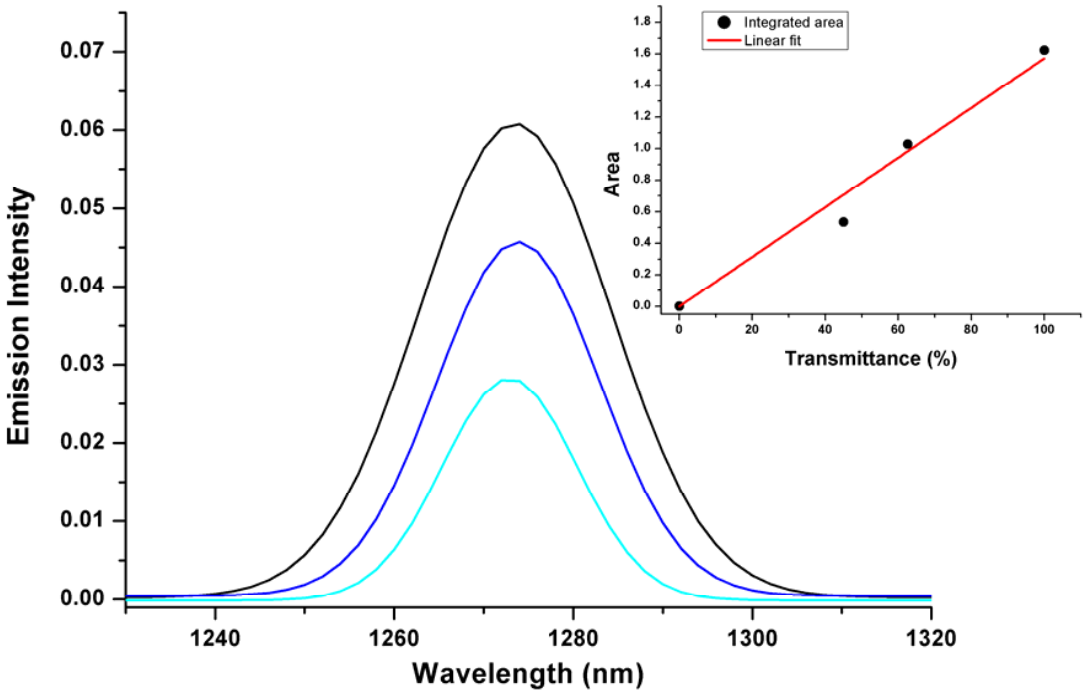

Figure S5. Near-IR luminescence spectra for singlet oxygen production from **C1** in acetonitrile (inset shows integrated area of the singlet oxygen luminescence with changing irradiation intensity).

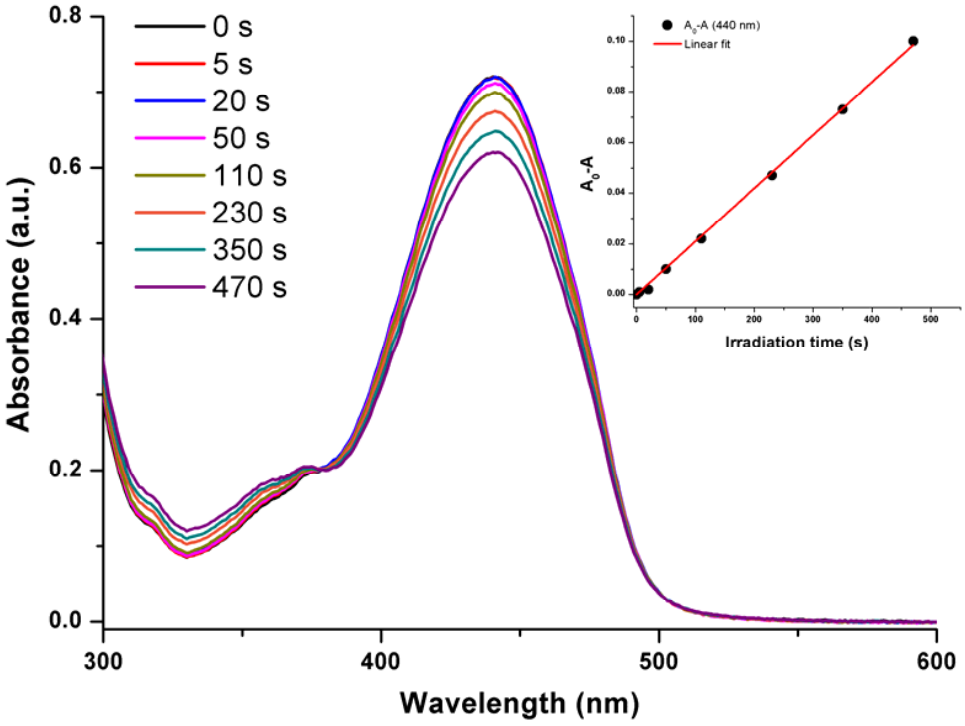

Figure S6. Absorption spectra for singlet oxygen production from **C1** in PBS buffer, as determined by RNO/histidine assay (indirect method), with the inset showing change in absorbance (440 nm) with increasing irradiation time.

Table S1. Singlet oxygen evaluation.

Complex	Acetonitrile[a]	PBS[b]
C1	81.1%	5.7%

[a]measured by near-IR luminescence (direct method). [b]measured by RNO/histidine assay (indirect method).

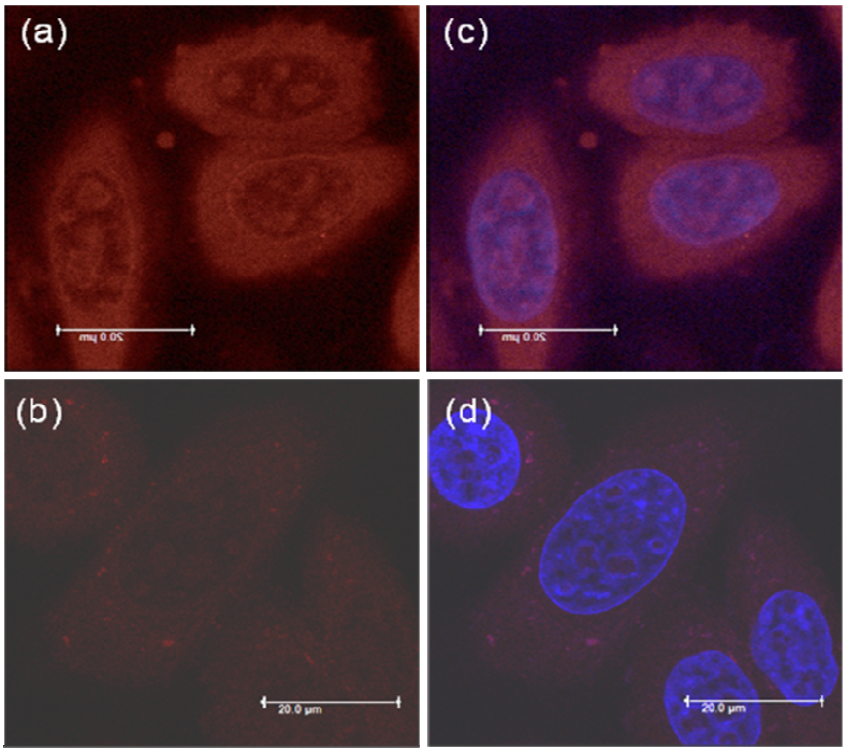

Figure S7. Fluorescence confocal microscopy images showing cellular staining patterns for HeLa cells incubated with **C2** (20 μM) for 2 h. Images show cellular staining in cells maintained in the dark **(a)**, and exposed to light irradiation **(b)**, and their respective overlays

with DAPI staining (**(c)** and **(d)**). For light irradiation experiments, the cells were irradiated at 350 nm for 10 min (2.58 J cm^{-2}) prior to confocal imaging.

References

[1] G. R. Fulmer, A. J. M. Miller, N. H. Sherden, H. E. Gottlieb, A. Nudelman, B. M. Stoltz, J. E. Bercaw, K. I. Goldberg, *Organometallics* **2010**, *29*, 2176-2179.

[2] A. Specht, J.-S. Thomann, K. Alarcon, W. Wittayanan, D. Ogden, T. Furuta, Y. Kurakawa, M. Goeldner, *ChemBioChem* **2006**, *7*, 1690-1695.

[3] V. Pierroz, T. Joshi, A. Leonidova, C. Mari, J. Schur, I. Ott, L. Spiccia, S. Ferrari, G. Gasser, *J. Am. Chem. Soc.* **2012**, *134*, 20376-20387.

[4] J. W. Walker, G. P. Reid, J. A. McCray, D. R. Trentham, *J. Am. Chem. Soc.* **1988**, *110*, 7170-7177.

[5] A. Leonidova, V. Pierroz, R. Rubbiani, J. Heier, S. Ferrari, G. Gasser, *Dalton Trans.* **2013**, DOI: 10.1039/C1033DT51817E

REFERENCES

1. Rosenberg, B.; VanCamp, L.; Krigas, T. Inhibition of cell division in Escherichia Coli by electrolysis products from a platinum electrode. *Nature* **1965,** 205, 698-699.
2. Rosenberg, B.; VanCamp, L.; Trosko, J. E.; Mansour, V. H. Platinum compounds: a new class of potent antitumour agents. *Nature* **1969,** 222, 385-386.
3. Yao, X.; Panichpisal, K.; Kurtzman, N.; Nugent, K. Cisplatin nephrotoxicity: a review. *Am. J. Med. Sci.* **2007,** 334, 115-124.
4. Bosl, G. J.; Motzer, R. J. Testicular germ-cell cancer. *N. Engl. J. Med.* **1997,** 337, 242-253.
5. Morris, M.; Eifel, P. J.; Lu, J.; Grigsby, P. W.; Levenback, C.; Stevens, R. E.; Rotman, M.; Gershenson, D. M.; Mutch, D. G. Pelvic radiation with concurrent chemotherapy compared with pelvic and para-aortic radiation for high-risk cervical cancer. *N. Engl. J. Med.* **1999,** 340, 1137-1143.
6. Rose, P. G.; Bundy, B. N.; Watkins, E. B.; Thigpen, J. T.; Deppe, G.; Maiman, M. A.; Clarke-Pearson, D. L.; Insalaco, S. Concurrent cisplatin-based radiotherapy and chemotherapy for locally advanced cervical cancer. *N. Engl. J. Med.* **1999,** 340, 1144-1153.
7. Hayes, D. M.; Cvitkovic, E.; Golbey, R. B.; Scheiner, E.; Helson, L.; Krakoff, I. H. High dose cis-platinum diammine dichloride: amelioration of renal toxicity by mannitol diuresis. *Cancer.* **1977,** 39, 1372-1381.
8. Trevisan, A.; Borella-Venturini, M.; Di Marco, L.; Fabrello, A.; Giraldo, M.; Zanetti, E.; Marzano, C.; Fregona, D. Erythrocyte aminolevulinic acid dehydratase inhibition by cis-platin. *Toxicol. Lett.* **2004,** 152, 105-110.
9. Keller, G. A.; Ponte, M. L.; Di Girolamo, G. Other drugs acting on nervous system associated with QT-interval prolongation. *Curr. Drug Saf.* **2010,** 5, 105-111.
10. Pratibha, R.; Sameer, R.; Rataboli, P. V.; Bhiwgade, D. A.; Dhume, C. Y. Enzymatic studies of cisplatin induced oxidative stress in hepatic tissue of rats. *Eur. J. Pharmacol.* **2006,** 532, 290-293.
11. Harrap, K. R. Preclinical studies identifying carboplatin as a viable cisplatin alternative. *Cancer Treat. Rev.* **1985,** 12 Suppl A, 21-33.
12. Jamieson, E. R.; Lippard, S. J. Structure, Recognition, and Processing of Cisplatin-DNA Adducts. *Chem. Rev.* **1999,** 99, 2467-2498.
13. de Gramont, A.; Figer, A.; Seymour, M.; Homerin, M.; Hmissi, A.; Cassidy, J.; Boni, C.; Cortes-Funes, H.; Cervantes, A.; Freyer, G.; Papamichael, D.; Le Bail, N.; Louvet, C.; Hendler, D.; de Braud, F.; Wilson, C.; Morvan, F.; Bonetti, A. Leucovorin and fluorouracil with or without oxaliplatin as first-line treatment in advanced colorectal cancer. *J. Clin. Oncol.* **2000,** 18, 2938-2947.
14. Sadzuka, Y.; Shoji, T.; Takino, Y. Effect of cisplatin on the activities of enzymes which protect against lipid peroxidation. *Biochem. Pharmacol.* **1992,** 43, 1872-1875.
15. Tacka, K. A.; Dabrowiak, J. C.; Goodisman, J.; Penefsky, H. S.; Souid, A. K. Effects of cisplatin on mitochondrial function in Jurkat cells. *Chem. Res. Toxicol.* **2004,** 17, 1102-1111.
16. Siddik, Z. H. Cisplatin: mode of cytotoxic action and molecular basis of resistance. *Oncogene.* **2003,** 22, 7265-7279.
17. Chu, G. Cellular responses to cisplatin. The roles of DNA-binding proteins and DNA repair. *J. Biol. Chem.* **1994,** 269, 787-790.

18. Zheng, H.; Wang, X.; Legerski, R. J.; Glazer, P. M.; Li, L. Repair of DNA interstrand cross-links: interactions between homology-dependent and homology-independent pathways. *DNA Repair* **2006,** 5, 566-574.
19. Kelland, L. R. New platinum antitumor complexes. *Crit. Rev. Oncol. Hematol.* **1993,** 15, 191-219.
20. Jung, Y.; Lippard, S. J. Direct cellular responses to platinum-induced DNA damage. *Chem. Rev.* **2007,** 107, 51387-1407.
21. Lippert, B. Cisplatin, Chemistry and Biochemistry of a Leading Anticancer Drug. *Verlag Helvetica Chimica Acta: Zürich; Wiley_VCH: Weinheim, germany* **1999**, 111-134.
22. Allardyce, C. S.; Dorcier, A.; Scolaro, C.; Dyson, P. J. Development of organometallic (organo-transition metal) pharmaceuticals. *Appl. Organomet. Chem.* **2005,** 19, 1-10.
23. Vock, C. A.; Ang, W. H.; Scolaro, C.; Phillips, A. D.; Lagopoulos, L.; Juillerat-Jeanneret, L.; Sava, G.; Scopelliti, R.; Dyson, P. J. Development of ruthenium antitumor drugs that overcome multidrug resistance mechanisms. *J. Med. Chem.* **2007,** 50, 2166-2175.
24. Hartinger, C. G.; Zorbas-Seifried, S.; Jakupec, M. A.; Kynast, B.; Zorbas, H.; Keppler, B. K. From bench to bedside--preclinical and early clinical development of the anticancer agent indazolium trans-[tetrachlorobis(1H-indazole)ruthenate(III)] (KP1019 or FFC14A). *J. Inorg. Biochem.* **2006,** 100, 891-801.
25. Guo, W.; Zheng, W.; Luo, Q.; Li, X.; Zhao, Y.; Xiong, S.; Wang, F. Transferrin serves as a mediator to deliver organometallic ruthenium(II) anticancer complexes into cells. *Inorg. Chem.* **2013,** 52, 5328-5338.
26. Sava, G.; Zorzet, S.; Turrin, C.; Vita, F.; Soranzo, M.; Zabucchi, G.; Cocchietto, M.; Bergamo, A.; DiGiovine, S.; Pezzoni, G.; Sartor, L.; Garbisa, S. Dual Action of NAMI-A in inhibition of solid tumor metastasis: selective targeting of metastatic cells and binding to collagen. *Clin. Cancer Res.* **2003,** 9, 1898-1905.
27. Rademaker-Lakhai, J. M.; van den Bongard, D.; Pluim, D.; Beijnen, J. H.; Schellens, J. H. A Phase I and pharmacological study with imidazolium-trans-DMSO-imidazole-tetrachlororuthenate, a novel ruthenium anticancer agent. *Clin. Cancer Res.* **2004,** 10, 3717-3727.
28. Koudinova, N. V.; Pinthus, J. H.; Brandis, A.; Brenner, O.; Bendel, P.; Ramon, J.; Eshhar, Z.; Scherz, A.; Salomon, Y. Photodynamic therapy with Pd-Bacteriopheophorbide (TOOKAD): successful in vivo treatment of human prostatic small cell carcinoma xenografts. *Int J Cancer*. **2003,** 104, 782-789.
29. Harris, A. L. Hypoxia--a key regulatory factor in tumour growth. *Nat. Rev. Cancer* **2002,** 2, 38-47.
30. Mari, C.; Pierroz, V.; Ferrari, S.; Gasser, G. Combination of Ru(II) complexes and light: new frontiers in cancer therapy. *Chem. Sci.* **2015**.
31. Lord, C. J.; Ashworth, A. The DNA damage response and cancer therapy. *Nature* **2012,** 481, 287-294.
32. Friedberg, E. C. How nucleotide excision repair protects against cancer. *Nat. Rev. Cancer* **2001,** 1, 22-33.
33. Sancar, A. DNA excision repair. *Annu. Rev. Biochem.* **1996,** 65, 43-81.
34. Shuck, S. C.; Short, E. A.; Turchi, J. J. Eukaryotic nucleotide excision repair: from understanding mechanisms to influencing biology. *Cell Res.* **2008,** 18, 64-72.
35. Legerski, R. J. Repair of DNA interstrand cross-links during S phase of the mammalian cell cycle. *Environ. Mol. Mutagen.* **2010,** 51, 540-551.

36. Huang, Y.; Li, L. DNA crosslinking damage and cancer - a tale of friend and foe. *Transl. Cancer Res.* **2013,** 2, 144-154.
37. Liu, Y.; Wilson, S. H. DNA base excision repair: a mechanism of trinucleotide repeat expansion. *Trends Biochem. Sci.* **2012,** 37, 162-172.
38. Markkanen, E.; Dorn, J.; Hübscher, U. MUTYH DNA glycosylase: the rationale for removing undamaged bases from the DNA. *Front. Genet.* **2013,** 4.
39. Yusaku, N. Cellular Levels of 8-Oxoguanine in either DNA or the Nucleotide Pool Play Pivotal Roles in Carcinogenesis and Survival of Cancer Cells. *Int. J. Mol. Sci* **2014,** 15, 12543-12557.
40. Zhu, G.; Lippard, S. J. Photoaffinity labeling reveals nuclear proteins that uniquely recognize cisplatin-DNA interstrand cross-links. *Biochemistry.* **2009,** 48, 4916-4925.
41. Rosenstein, B. S.; Ducore, J. M. Induction of DNA strand breaks in normal human fibroblasts exposed to monochromatic ultraviolet and visible wavelengths in the 240-546 nm range. *Photochem. Photobiol.* **1983,** 38, 51-55.
42. Piette, J.; Merville-Louis, M. P.; Decuyper, J. Damages induced in nucleic acids by photosensitization. *Photochem. Photobiol.* **1986,** 44, 793-802.
43. Pierroz, V.; Joshi, T.; Leonidova, A.; Mari, C.; Schur, J.; Ott, I.; Spiccia, L.; Ferrari, S.; Gasser, G. Molecular and cellular characterization of the biological effects of ruthenium(II) complexes incorporating 2-pyridyl-2-pyrimidine-4-carboxylic acid. *J. Am. Chem. Soc.* **2012,** 134, 20376-20387.
44. Joshi, T.; Pierroz, V.; Ferrari, S.; Gasser, G. Bis(dipyridophenazine) Ru(II)-(2-(2′-pyridyl)pyrimidine-4-carboxylic acid) complex: A Lesson in Stubbornness. *ChemMedChem.* **2013,** DOI: 10.1002/cmdc.201400029.
45. Joshi, T.; Pierroz, V.; Mari, C.; Gemperle, L.; Ferrari, S.; Gasser, G. Photocaged Bis(dipyridophenazine) Ru(II)-(2-(2′-pyridyl)pyrimidine-4-carboxylic acid) Complex: Light, Ruthenium, Anticancer Action. *Angew. Chem. Int. Ed.* **2014,** 53, 2960-2963.
46. Dobbelstein, M.; Moll, U. Targeting tumour-supportive cellular machineries in anticancer drug development. *Nat. Rev. Drug Discov.* **2014,** 13, 179-196.
47. Luo, J.; Solimini, N. L.; Elledge, S. J. Principles of cancer therapy: oncogene and non-oncogene addiction. *Cell* **2009,** 136, 823-837.
48. Shah, N. P.; Nicoll, J. M.; Nagar, B.; Gorre, M. E.; Paquette, R. L.; Kuriyan, J.; Sawyers, C. L. Multiple BCR-ABL kinase domain mutations confer polyclonal resistance to the tyrosine kinase inhibitor imatinib (STI571) in chronic phase and blast crisis chronic myeloid leukemia. *Cancer Cell* **2002,** 2, 117-125.
49. Hayata, Y.; Kato, H.; Konaka, C.; Ono, J.; Takizawa, N. Hematoporphyrin derivative and laser photoradiation in the treatment of lung cancer. *Chest.* **1982,** 81, 269-277.
50. McCaughan, J. S. J.; Hicks, W.; Laufman, L.; May, E.; Roach, R. Palliation of esophageal malignancy with photoradiation therapy. *Cancer* **1984,** 54, 2905-2910.
51. Taub, A. F. Photodynamic therapy: other uses. *Dermatol. Clin.* **2007,** 25, 101-109.
52. Castano, A. P.; Demidova, T. N.; Hamblin, M. R. Mechanisms in photodynamic therapy: part one-photosensitizers, photochemistry and cellular localization. *Photodiagnosis Photodyn, Ther.* **2004,** 1, 279-293.
53. Dolmans, D. E.; Fukumura, D.; Jain, R. K. Photodynamic therapy for cancer. *Nat. Rev. Cancer* **2003,** 3, 380-387.
54. Sibata, C. H.; Colussi, V. C.; Oleinick, N. L.; Kinsella, T. J. Photodynamic therapy in oncology. *Expert Opin. Pharmacother.* **2001,** 2, 917-927.

55. Mari, C.; Pierroz, V.; Rubbiani, R.; Patra, M.; Hess, J.; Spingler, B.; Oehninger, L.; Schur, J.; Ott, I.; Salassa, L.; Ferrari, S.; Gasser, G. DNA intercalating Ru(II) polypyridyl complexes as effective photosensitizers in photodynamic therapy. *Chemistry* **2014,** 20, 14421-14436.
56. Cooke, M. S.; Evans, M. D.; Dizdaroglu, M.; Lunec, J. Oxidative DNA damage: mechanisms, mutation, and disease. *FASEB J.* **2003,** 17, 1195-1214.
57. Gicquel, E.; Souchard, J. P.; Magnusson, F.; Chemaly, J.; Calsou, P.; Vicendo, P. Role of intercalation and redox potential in DNA photosensitization by ruthenium(II) polypyridyl complexes: assessment using DNA repair protein tests. *Photochem. Photobiol. Sci.* **2013,** 12, 1517-1526.
58. Forment, J. V.; Walker, R. V.; Jackson, S. P. A high-throughput, flow cytometry-based method to quantify DNA-end resection in mammalian cells. *Cytometry A.* **2012,** 81, 922-928.
59. Bologna, S.; Ferrari, S. It takes two to tango: Ubiquitin and SUMO in the DNA damage response. *Front. Genet.* **2013,** 4, 106.
60. Collins, A. R. The comet assay for DNA damage and repair: principles, applications, and limitations. *Mol. Biotechnol.* **2004,** 26, 249-261.
61. Olive, P. L.; Banáth, J. P. The comet assay: a method to measure DNA damage in individual cells. *Nat. Protoc.* **2006,** 1, 23-29.
62. Franken, N. A.; Rodermond, H. M.; Stap, J.; Haveman, J.; van Bree, C. Clonogenic assay of cells in vitro. *Nat. Protoc.* **2006,** 1, 2315-2319.
63. Gill, M. R.; Thomas, J. A. Ruthenium(II) polypyridyl complexes and DNA--from structural probes to cellular imaging and therapeutics. *Chem. Soc. Rev.* **2012,** 41, 3179-3192.
64. Stern, R. S. Psoralen and ultraviolet a light therapy for psoriasis. *N. Engl. J. Med.* **2007,** 357, 682-690.
65. Xie, H.; Yang, D.; Heller, A.; Gao, Z. Electrocatalytic oxidation of guanine, guanosine, and guanosine monophosphate. *Biophys. J.* **2007,** 92, L70-72.
66. Wallace, S. S.; Murphy, D. L.; Sweasy, J. B. Base excision repair and cancer. *Cancer Lett.* **2012,** 327, 73-89.
67. Stojic, L.; Mojas, N.; Cejka, P.; Di Pietro, M.; Ferrari, S.; Marra, G.; Jiricny, J. Mismatch repair-dependent G2 checkpoint induced by low doses of SN1 type methylating agents requires the ATR kinase. *Genes Dev.* **2004,** 18, 1331-1344.
68. Mari, C.; Pierroz, V.; Rubbiani, R.; Patra, M.; Hess, J.; Spingler, B.; Oehninger, L.; Schur, J.; Ott, I.; Salassa, L.; Ferrari, S.; Gasser, G. DNA Intercalating Ru(II) Polypyridyl Complexes as Effective Photosensitizers in Photodynamic Therapy. *Chemistry* **2014,** 20, 14421-36.
69. El-Shemerly, M.; Hess, D.; Pyakurel, A. K.; Moselhy, S.; Ferrari, S. ATR-dependent pathways control hEXO1 stability in response to stalled forks. *Nucleic Acids Res* **2008,** 36, 511-9.
70. Hanada, K.; Budzowska, M.; Davies, S. L.; van Drunen, E.; Onizawa, H.; Beverloo, H. B.; Maas, A.; Essers, J.; Hickson, I. D.; Kanaar, R. The structure-specific endonuclease Mus81 contributes to replication restart by generating double-strand DNA breaks. *Nat Struct Mol Biol* **2007,** 14, 1096-104.
71. Mori, T.; Nakane, M.; Hattori, T.; Matsunaga, T.; Ihara, M.; Nikaido, O. Simultaneous establishment of monoclonal antibodies specific for either cyclobutane pyrimidine dimer or (6-4)photoproduct from the same mouse immunized with ultraviolet-irradiated DNA. *Photochem Photobiol* **1991,** 54, 225-32.

72. Eid, W.; Steger, M.; El-Shemerly, M.; Ferretti, L. P.; Pena-Diaz, J.; Konig, C.; Valtorta, E.; Sartori, A. A.; Ferrari, S. DNA end resection by CtIP and exonuclease 1 prevents genomic instability. *EMBO Rep* **2010,** 11, 962-8.
73. Azzouzi, A. R.; Barret, E.; Moore, C. M.; Villers, A.; Allen, C.; Scherz, A.; Muir, G.; de Wildt, M.; Barber, N. J.; Lebdai, S.; Emberton, M. TOOKAD(®) Soluble vascular-targeted photodynamic (VTP) therapy: determination of optimal treatment conditions and assessment of effects in patients with localised prostate cancer. *BJU Int*. **2013,** 112, 766-774.
74. Agostinis, P.; Berg, K.; Cengel, K. A.; Foster, T. H.; Girotti, A. W.; Gollnick, S. O.; Hahn, S. M.; Hamblin, M. R.; Juzeniene, A.; Kessel, D.; Korbelik, M.; Moan, J.; Mroz, P.; Nowis, D.; Piette, J.; Wilson, B. C.; Golab, J. Photodynamic therapy of cancer: an update. *CA Cancer J. Clin*. **2011,** 61, 250-281.
75. Kennedy, J. C.; Marcus, S. L.; Pottier, R. H. Photodynamic therapy (PDT) and photodiagnosis (PD) using endogenous photosensitization induced by 5-aminolevulinic acid (ALA): mechanisms and clinical results. *J. Clin. Laser Med. Surg*. **1996,** 14, 289-304.
76. Greish, K. Enhanced permeability and retention (EPR) effect for anticancer nanomedicine drug targeting. *Methods Mol. Biol*. **2010,** 624, 25-37.

Vanessa **Pierroz**

Molecular Biologist

Infos

31.07.1986
single
swiss

Contact

Le Borgeaud 23
1921 Martigny-Croix
Switzerland

+41 (0)44 635 34 59
+41 (0)79 781 16 71

vanessa.pierroz@gmail.com
pierroz@imcr.uzh.ch

Languages

French mother tongue
English fluent
Spanish fair
German basic

Software Knowledge

Statistic software R,
Ethovision,
MS Office

Education // Experience

2011-Now **PhD** in Molecular Cancer research — University of Zurich

In vitro and In vivo Photo-Release of New Metal-Containing Bioconjugates: Towards Biological and Medicinal Application

During my PhD thesis I intend to identify new metal-based anticancer drug candidates, they will then be rendered innocuous by conjugation to a photolabile moiety and activated with light to kill cancer cells. // Cell culture, IC_{50} determination, confocal microscopy, FACS, ELISA and other molecular biological procedures

2009-2011 **Master** of Science in Medical Biology — University of Lausanne

Biochemical Studies on TNF Family Members: Proteolytic Maturation

In the course of my Master project, I was studying the proteolytic maturation of TWEAK, APRIL and BAFF, three TNF family members. // Cell culture, ELISA, FACS, PCR, Western Blot

Interindividual Vulnerability to Develop Alcohol Abuse in Rats

During this Pre-Master project, my role has been to train rats on a self-administration equipment and elevated plus maze device.

2006-2009 **Bachelor** of Science in Biology — University of Lausanne

2000-2006 Maturity — College of Saint-Maurice

Communication skills

Poster

2014 **Eurobic**
Zurich, Switzerland

2013 **Swiss Chemical Society Meeting**
Lausanne, Switzerland

Cancer Network Zurich Retreat
Grindelwald, Switzerland

2012 **9th Photodynamic Therapy and Photodiagnosis in Clinical Practice + 4th International Meeting of EPPM**
Brixen, Italy

Swiss Chemical Society Meeting
Zurich, Switzerland

Dorothy Crowfoot Hodgkin symposium
Zurich, Switzerland

Oral presentation

2014 **16th International Congress on Photobiology**
Cordoba, Argentina

2014 **Joint Cancer Meeting**
Zurich, Switzerland

2013 **5th International Meeting of EPPM**
Ustron, Poland

Contributions to PhD Program Zurich

2013 **Supervision of student for Summer Internship**
2012 **Supervision of students in BIO111**
2012-2014 **Supervision of students in BIO246**

Awards/Grants

2015 **2nd URPP on Translational Cancer Research (grant)**
2014 **SCNAT/SCS Chemistry Travel Award**
2012 **Poster prize: Dorothy Crowfoot Hodgkin symposium (Zurich)**

Referees

PhD

Gilles Gasser (gilles.gasser@chem.uzh.ch)
Department of Chemistry
University of Zurich
Winterthurerstrasse 190
CH-8057 Zurich
+41 (0)44 635 46 30

Stefano Ferrari (sferrari@imcr.uzh.ch)
Institute of Molecular Cancer Research
University of Zurich
Winterthurerstrasse 190
CH-8057 Zurich
+41 (0)44 635 34 71

Master

Pascal Schneider (Pascal.Schneider@unil.ch)
Department of Biochemistry, UNIL,
Ch. des Boveresses 155
CH-1066 Epalinges
+41 (0)21 692 57 09

Premaster

Benjamin Boutrel (Benjamin.Boutrel@unil.ch)
Neurosciences psychiatriques (CNP)
Site de Cery, Route du Mont
CH-1008 Prilly
+41 (0)21 643 69 47

Publications

2015 **Combination of Ru(II) Complexes and Light: New Frontiers in Cancer Therapy**
Mari C.*, **Pierroz V**.*, Ferrari S., Gasser G.
Chem. Sci.; DOI: 10.1039/C4SC03759F

2014 **DNA Intercalating Ru(II) Polypyridyl Complexes as Effective Photosensitizers in Photodynamic Therapy.**
Mari C., **Pierroz V**., Rubbiani R., Patra M., Hess J., Spingler B., Oehninger L., Schur J., Salassa L., Ferrari S., Gasser G.
Chemistry;20(44):14421-36.

Enhanced Cytotoxicity through Conjugation of a "Clickable" Luminescent Re(I) Complex to a Cell-Penetrating Lipopeptide.
Leonidova A., **Pierroz V**., Adams L. A., Barlow N., Ferrari S., Graham B., Gasser G.
ACS Med. Chem. Lett.;5(7):809-14.

Towards Matched Pairs of Porphyrin-Re^{I} /^{99m} Tc^{I} Conjugates that Combine Photodynamic Activity with Fluorescence and Radio Imaging.
Gianferrara T., Spagnul C., Alberto R., Gasser G., Ferrari S., **Pierroz V**., Bergamo A., Alessio E.
ChemMedChem.;9(6):1231-7.

Novel, mercury-free synthetic pathway for trifluoromethylthio-substituted metallocenes.
Hess J., Konatschnig S., Morard S., **Pierroz V**., Ferrari S., Spingler B., Gasser G.
*Inorg Chem.;*53(7):3662-7.

Bis(dipyridophenazine)(2-(2'-pyridyl)pyrimidine-4-carboxylic acid)ruthenium(II) Hexafluorophosphate: A Lesson in Stubbornness.
Joshi T.*, **Pierroz V**.*, Ferrari S., Gasser G.
ChemMedChem.;9(7):1419-27.

A Bis(dipyridophenazine)(2-(2-pyridyl)pyrimidine-4-carboxylic acid)ruthenium(II) Complex with Anticancer Action upon Photodeprotection.
Joshi T.*, **Pierroz V**.*, Mari C., Gemperle L., Ferrari S., Gasser G.
*Angew. Chem. Int. Ed. Engl.;*53(11):2960-3.

A Deadly Organometallic Luminescent Probe: Anticancer Activity of a Re^{I} Bisquinoline Complex.
Kitanovic I., Can S., Alborzinia H., Kitanovic A., **Pierroz V**., Leonidova A., Pinto A., Spingler B., Ferrari S., Molteni R., Steffen A., Metzler-Nolte N., Wölfl S., Gasser G.
Chemistry.;20(9):2496-507.

Towards cancer cell-specific phototoxic organometallic rhenium(I) complexes.
Leonidova A.*, **Pierroz V**.*, Rubbiani R., Heier J., Ferrari S., Gasser G.
Dalton Trans.;43(11):4287-94.

2013 **In vitro metabolic profile and in vivo antischistosomal activity studies of (η(6)praziquantel)Cr(CO)3 derivatives.**
Patra M., Ingram K., leonidova A., **Pierroz V**., Ferrari S., Robertson MN., Todd MH., Keiser J., Gasser G.
J. Med. Chem.;56(22):9192-8.

DMSO-Mediated Ligand Dissociation: Renaissance for Biological Activity of N-Heterocyclic-[Ru(η^6-arene)Cl_2] Drug Candidates.
Patra M., Joshi T., **Pierroz V**., Ingram K., Kaiser M., Ferrari S., Spingler B., Keiser J., Gasser G.
Chemistry.;19(44):14768-72.

Novel water-soluble (99m)Tc(I)/Re(I)-porphyrin conjugates as potential multimodal agents for molecular imaging.
Spagnul C., Alberto R., gasser G., Ferrari S., **Pierroz V**., Bergamo A., Gianferrara T., Alessio E.
J. Inorg. Biochem.;122:57-65.

[(η(6)-Praziquantel)Cr(CO)3] derivatives with remarkable in vitro anti-schistosomal activity.
Patra M., Ingram K., **Pierroz V**., Ferrari S., Spingler B., Gasser RB., Keiser J., Gasser G.
Chemistry.;19(7):2232-5.

2012 **Molecular and cellular characterization of the biological effects of ruthenium(II) complexes incorporating 2-pyridyl-2-pyrimidine-4-carboxylic acid.**
Pierroz V., Joshi T., Leonidova A., Mari C., Schur J., Ott I., Spiccia L**.,** Ferrari S., Gasser G.
J. Am. Chem. Soc.;134(50):20376-87.

Ferrocenyl derivatives of the anthelmintic praziquantel: design, synthesis, and biological evaluation.
Patra M., Ingram K., **Pierroz V**., Ferrari S., Spingler B., Keiser J., Gasser G.
J. Med. Chem.;55(20):8790-8.

***authors have contributed equally to the work.**